Università
Ca'Foscari
Venezia

Corso di Dottorato di ricerca

in

Scienza e Tecnologia dei Bio e Nanomateriali

XXXIV ciclo

Peptide engineering for the development of metalloprotease inhibitors by using yeast surface display technology

SSD: BIO/10

Coordinatore del Dottorato
ch. prof. Flavio Rizzolio

Supervisore
ch. prof. Alessandro Angelini

Supervisore cotutela
Devis Galesso

Dottorando
Stefano Pluda
Matricola 956455

Appendix

Acknowledgements

Abstract

Osteoarthritis (OA) is a degenerative disease of the joints leading to chronic pain and disability. It is the most common form of arthritis, affecting about 3% of the population, thus resulting in a major socioeconomic health burden. To date, there are no approved treatments for this disease. OA is characterized by the degeneration of the articular cartilage and intra-articular inflammation.(Zhang et al., 2016) These processes are caused by metalloproteinases, a large family of proteolytic enzymes whose catalytic activities involves a metal. Hence, metalloproteinases represent important drug targets for the prevention and treatment of OA.

The aim of this research is the development of inhibitors of two pivotal metalloproteases involved in OA: A-disintegrin and metalloproteinase with thrombospondin motifs-5 (ADAMTS-5) and A-disintegrin and metalloproteinase-17 (ADAM-17 or TACE). Rather than targeting these two proteins using small molecule-based and protein-based inhibitors, we decided to develop peptide-based inhibitors. Similar to protein-based inhibitors, peptides inhibitors are capable of binding the target with a surface of interaction large enough to obtain high efficiency and selectivity. Like small molecules, peptide-based inhibitors can be synthesised chemically, possess ease of modification, low toxicity, and reduced antigenicity. Their modular structure and the commercial availability of hundreds of amino acid building blocks simplifies the rapid development of peptides with tailored properties.

Yeast surface display technology, that enables quantitative screening of large combinatorial libraries of random peptide sequences, was applied for the development of peptide-based inhibitors. Two types of peptide libraries were explored. One library was designed to include solely canonical amino acids while the second one was conceived to bear a non-canonical amino acid to allow specific post-translational chemical modifications that could further tune the properties of the displayed peptides and greatly increase their chemical diversity.

In chapter 1, I provide you with an introduction of OA, ADAM and ADAMTS metalloproteases, peptide inhibitors against ADAM and ADAMTS metalloproteases, chemical modification of peptide via thiol-alkylation and copper-catalyzed Huisgen cycloaddition and yeast surface display technology.

In chapter 2, I presented the synthetic strategies of two classes of reactive hydroxamates, respectively thiol-alkylating agents and azido-click coupling agents. Hydroxamic moiety is a well-known metal chelating group used to increase the affinity of inhibitors to the active site of metalloproteases. Three novel di- alkylating agents (namely agents **2, 3** and **4**) and two click agents (namely agents **5** and **6**)

were obtained. Reactivity studies of hydroxamate derivatives with amino acid derivatives and peptides confirmed the potentialities of these functionalizing agents on high-throughput screening systems.

In chapter 3, I described the recombinant production of metalloprotease target ADAM-17. Firstly, expression and analysis of four constructs of ADAM-$17^{18\text{-}474}$ were performed in small scale to identify the most suitable protein for large scale production. ADAM-$17^{18\text{-}474}$-his_6-tag was selected as best construct, expressed, biotinylated and purified for further screening steps.

In chapter 4, I reported the expression and purification studies of metalloprotease target ADAMTS-5. ADAMTS proteins are challenging to purify, in a native or recombinant form, because of their large size, extensive glycosylation, intrinsic instability and tendency to form aggregates. As for ADAM-17, nine different constructs of ADAMTS-5 were expressed and characterized. The fusion mSA-ADAMTS-$5^{262\text{-}623}$-strept-tag was selected for further expression and cleavage/activity studies with its cognate active site mutant. Its overall low yield prevented the use of ADAMTS-5 as target for further high-throughput screening.

Finally, in chapter 5 I described the two strategies adopted for the discovery of peptide-based inhibitors of ADAM-17 using yeast surface display. Naïve yeast libraries of cyclic peptides made of solely canonical amino acids were tested, and binding properties of sorted libraries were investigated. Unfortunately, sorted library of ADAM-17 binders revealed issues of polyreactivity. The second strategy regards the use of yeast libraries of peptides with non-canonical amino acids chemically modified via click chemistry. Firstly, the conditions of post-translational chemical modification via copper-catalysed click coupling were optimized to maximize the coupling yield. Naïve yeast libraries of click-modified cyclic peptides were sorted, and binding properties investigated. Click agents afforded significant contribution on binding, however binding polyreactivity was again observed. Further studies are currently ongoing to decrease the polyreactivity and identify peptides capable of blocking ADAM-17 with high affinity and specificity.

Riassunto

L' Osteoartrite (OA) è una malattia degenerativa delle articolazioni che porta a dolore cronico e disabilità. È la forma più comune di artrite, colpisce circa il 3% della popolazione, determinando così un grave onere socioeconomico per la salute. Ad oggi, non ci sono trattamenti approvati per questa malattia. L'OA è caratterizzata dalla degenerazione della cartilagine articolare e dall'infiammazione intra-articolare. Questi processi sono causati dalle metalloproteasi, una grande famiglia di enzimi proteolitici la cui attività catalitica coinvolge un metallo. Pertanto, le metalloproteasi rappresentano importanti bersagli farmacologici per la prevenzione e il trattamento dell'OA.

Lo scopo di questa ricerca è lo sviluppo di inibitori di due cruciali metalloproteasi coinvolte nell'OA: A-disintegrina e metalloproteinasi con motivi trombospondinici-5 (ADAMTS-5) e A-disintegrina e metalloproteinasi-17 (ADAM-17 o TACE). Piuttosto che focalizzarci su queste due proteine utilizzando inibitori a base di piccole molecole e proteine, abbiamo deciso di sviluppare inibitori a base di peptidi. Analogamente agli inibitori proteici, gli inibitori peptidici sono in grado di legare il bersaglio con una superficie di interazione sufficientemente ampia da ottenere un'elevata efficienza e selettività. Come le piccole molecole, gli inibitori peptidici possono essere sintetizzati chimicamente, possedere facilità di modifica, bassa tossicità e ridotta antigenicità. La loro struttura modulare e la disponibilità commerciale di centinaia di amminoacidi, come elementi costitutivi, semplificano il rapido sviluppo di peptidi con proprietà personalizzate.

La tecnologia di espressione sulla superficie del lievito, che consente lo screening quantitativo di grandi librerie combinatoriali di sequenze peptidiche casuali, è stata applicata per lo sviluppo di inibitori a base peptidica. Sono stati esplorati due tipi di librerie di peptidi. Una libreria è stata progettata per includere esclusivamente amminoacidi canonici, mentre la seconda è stata concepita per contenere un amminoacido non canonico e consentire specifiche modifiche chimiche post-traduzionali che potrebbero modulare ulteriormente le proprietà dei peptidi espressi sulla superficie e aumentare notevolmente la loro diversità chimica.

Nel capitolo 1, fornisco un'introduzione di OA, metalloproteasi ADAM e ADAMTS, inibitori peptidici contro metalloproteasi ADAM e ADAMTS, modifica chimica di peptide tramite alchilazione della funzionalità tiolica e rame-catalizzata cicloaddizione di Huisgen e tecnologia di espressione sulla superficie del lievito.

Nel capitolo 2, ho presentato le strategie sintetiche di due classi di idrossammati reattivi, rispettivamente agenti alchilanti tiolici e agenti di accoppiamento click di gruppi azido. La componente idrossammica è un noto gruppo chelante dei metalli utilizzato per aumentare l'affinità degli inibitori con il sito attivo delle metalloproteasi. Sono stati ottenuti tre nuovi agenti dialchilanti

(agenti **2**, **3** e **4**) e due agenti di accoppiamento click (agenti **5** e **6**). Studi di reattività di derivati idrossammici con derivati di amminoacidi e peptidi hanno confermato le potenzialità di questi agenti funzionalizzanti con sistemi di screening ad alto rendimento.

Nel capitolo 3, ho descritto la produzione ricombinante della metalloproteasi bersaglio ADAM-17. In primo luogo, l'espressione e l'analisi di quattro costrutti di ADAM-$17^{18\text{-}474}$ sono state eseguite su piccola scala per identificare la proteina più adatta per la produzione su larga scala. ADAM-$17^{18\text{-}474}$-his_6-tag è stato selezionato come miglior costrutto, espresso, biotinilato e purificato per ulteriori fasi di screening.

Nel capitolo 4, ho riportato gli studi di espressione e purificazione della metalloproteasi bersaglio ADAMTS-5. Le proteine ADAMTS sono notoriamente difficili da purificare, in una forma nativa o ricombinante, a causa delle loro grandi dimensioni, glicosilazione puntuale, dell'instabilità intrinseca e della tendenza a formare aggregati. Come per ADAM-17, sono stati espressi e caratterizzati nove diversi costrutti di ADAMTS-5. La proteina di fusione mSA-ADAMTS-$5^{262\text{-}623}$-strept-tag è stata selezionata per ulteriori studi di espressione e studi di taglio/attività con il suo corrispettivo mutante al sito catalitico. La bassa resa complessiva ha impedito l'uso di ADAMTS-5 come obiettivo per un ulteriore screening ad alto rendimento.

Infine, nel capitolo 5 ho descritto le due strategie adottate per la scoperta di inibitori peptidici di ADAM-17 utilizzando la tecnologia di espressione sulla superficie del lievito. Sono state testate librerie di lievito di peptidi ciclici costituiti esclusivamente da amminoacidi canonici e sono state studiate le proprietà di legame delle librerie selezionate. Sfortunatamente, la libreria selezionata di leganti di ADAM-17 ha rivelato problemi di polireattività. La seconda strategia riguarda l'uso di librerie di peptidi di lievito con amminoacidi non canonici modificati chimicamente tramite click chemistry. Innanzitutto, le condizioni di modifica chimica post-traduzionale tramite accoppiamento click rame-catalizzato sono state ottimizzate per massimizzare la resa di reazione. Successivamente, le librerie di peptidi ciclici modificati con reazione di click sono state selezionate e le proprietà di legame studiate. Gli agenti di click apportano un contributo significativo al legame, tuttavia è stata nuovamente osservata la polireattività. Sono attualmente in corso ulteriori studi per diminuire la polireattività e identificare peptidi in grado di bloccare ADAM-17 con elevata affinità e specificità.

Chapter 1
Introduction

1.1 Osteoarthritis

Pathology

Osteoarthritis (OA) is a degenerative disease of the whole joints characterized by alteration of the articular cartilage, an intra-articular inflammation with formation of synovitis and changes in peri-articular and subchondral bone. **Fig. 1** (Goldring and Goldring, 2007). It is the most common form of arthritis with a leading cause of disability and source of societal cost in older adults. (Hunter and Bierma-Zeinstra, 2019). OA affects over 40 million people across the Europe and nearly 27 million in the USA (Woolf, 2015). Clinical diagnosis of OA is mainly based on symptoms and physical examination.

OA has a complex pathogenesis and multiple causes concur to its development, including joint injury, obesity, aging and genetic factors. However, the trigger and the progression mechanisms of OA remain fractionally understood and are still under investigation (Jiang, 2021). The active dynamic alteration of the joint tissues results in an imbalanced activity between catabolism and anabolism or so-called wear-and-tear disease (Abramoff and Caldera, 2020).

The most frequently affected sites are hands, knees, hips and spine and among them, the knee is the most common site of OA (Jones et al., 2019). Knee OA accounts for approximately 85% of the burden of this pathology worldwide.

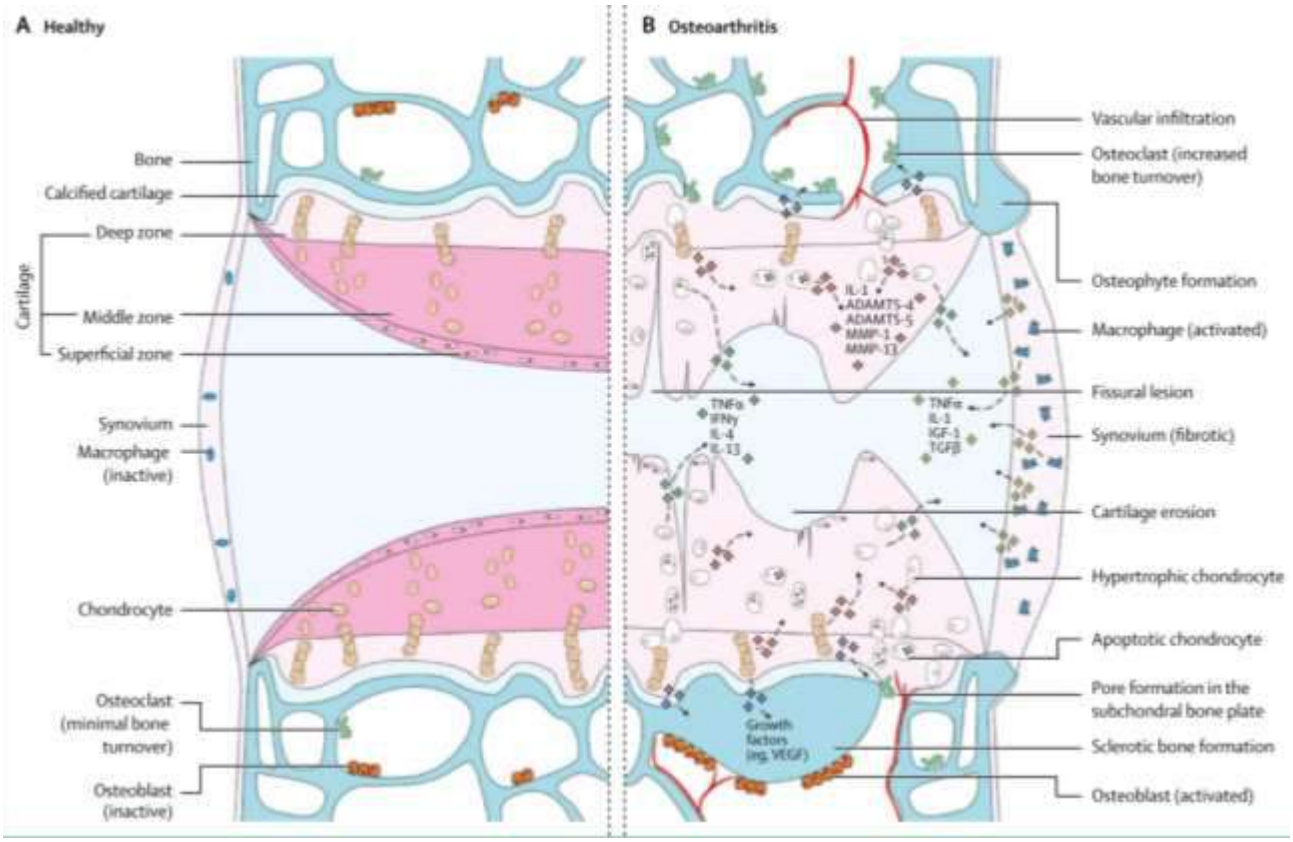

Fig. 1 Schematic rapresentation of healthy joint and with OA. Signalling pathways and structural changes in patology development (Hunter and Bierma-Zeinstra, 2019)

Risk factors

Risk factors are divided in systemic (age, bone density, ethnicity, race, genetics, diet) and local (obesity, injury, joint deformity). The incidence of this disease is strictly correlate with aging and obese incidence. Incidence of knee OA among adults is approximately three and five times as frequent as obese and morbidly obese individuals, respectively (Berenbaum et al., 2018). In the next future, OA will be the major cause of disability among individuals over the age of forty.

Today, obesity has doublet the risk of knee OA in roughly one out of four people over the age of fifty compared to a half-century ago (Berenbaum et al., 2018). A possible explanation is that an abnormal and constant loading environment for the joints is potentially hurtful for the cartilage (Griffin and Guilak, 2005). OA is considered both a mechano-inflammation and a metabolic disease. Mechano-inflammation is a process in which catabolic mediators are released by macrophages as a response of a release into the joint of matrix fragments. These include metalloproteinases, proteolytic enzymes produced by chondrocytes in response to a stimulus that are involved in degradation of the extracellular matrix (Berenbaum et al., 2018). OA is also considered a metabolic syndrome as it is associated with multiple metabolic factors, including central adiposity, dyslipidaemia, impaired fasting glucose levels and hypertension (Abramoff and Caldera, 2020). These alterations increase

systemic low-grade inflammation and could trigger joint cell activation in OA development (Hunter and Bierma-Zeinstra, 2019). Metabolic alterations such as hypertension correlate with subchondral bone ischemia, insulin resistance and increased risk of type 2 diabetes with matrix stiffness, muscle weakness, altered proprioception and subchondral bone loss, lipid abnormalities with activation of joint and muscle cells (Berenbaum et al., 2018). Moreover, a greater longevity over the century is a cause of increased prevalence of OA (Wallace et al., 2017).

Management

The approach towards management is centered on personalized treatments and specific needs with a focus on core treatments, including self-management and education, exercise, and weight loss as relevant (Hunter and Bierma-Zeinstra, 2019). Moreover, intra-articular treatments for knee osteoarthritis have been used for the past 20 years and include analgesics, glucocorticoids and hyaluronic acid (Jones et al., 2019). Finally, surgery is the ultimate choice for those who have not responded appropriately to less invasive methods.

Cartilage

Cartilage thickness and composition constantly modify during OA progress (Hunter and Bierma-Zeinstra, 2019). Pathology development is characterized by functional impairment, as well as signs and symptoms of inflammation, including pain, stiffness, and loss of mobility. Application of histopathological and imaging techniques help to define the OA stage with respect to cartilage alteration (Hunter and Bierma-Zeinstra, 2019).

During the early phase, cartilage erosion is superficial. Subsequently, cartilage fissures undergo local calcification. Successively, chondrocytes activation increases matrix degradation and production of proinflammatory mediators with stimulation of adjacent sinovium towards inflammatory response. (**Fig. 2**) This latest phase is often accompanied by tissue hypertrophy and increased vascularity (Hunter and Bierma-Zeinstra, 2019; Jiang, 2021).

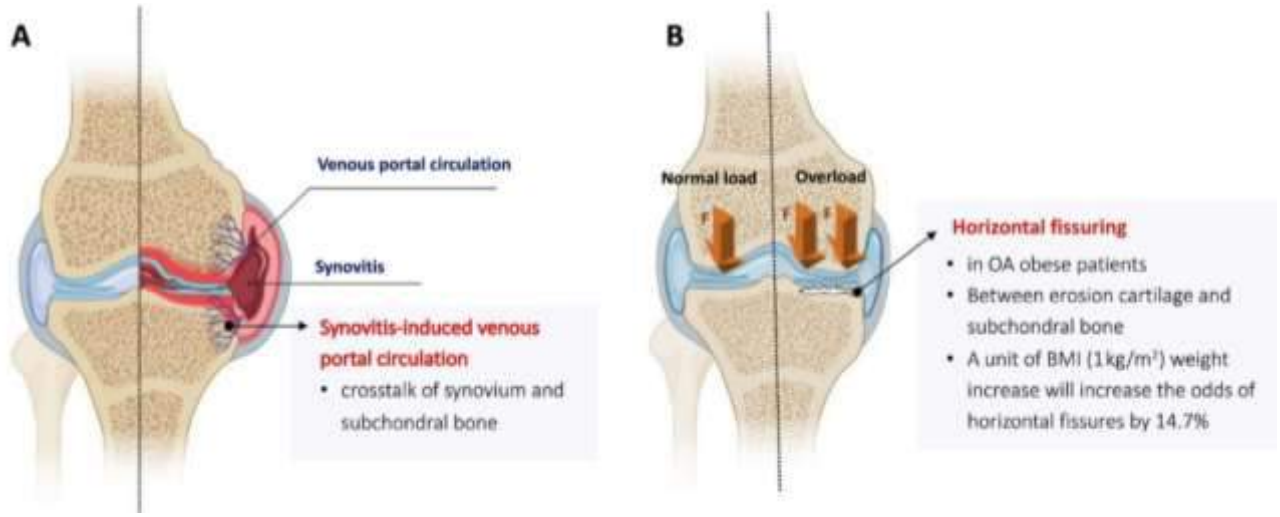

Fig. 2 Anatomy and pathology of OA (**A**) Synovitis-induced venous portal circulation (**B**) Horizontal fissures in obese OA patients (Jiang, 2021).

Articular cartilage is a highly specialized tissue with unique mechanical properties and low metabolic activity (Heinegård and Saxne, 2011). The tissue is mainly composed of extracellular matrix (collagen, proteoglycans) with a distribution of chondrocyte. Homeostasis of articular cartilage is the balance equilibrium between anabolic and catabolic processes. Type II collagen is the main collagen in cartilage with a triple helical structure (**Fig. 3A**). Aggrecan is the most preponderant proteoglycan, which is formed by a protein core with multiple glycosaminoglycan side chains (chondroitin sulphate and keratin sulphate). Finally, water binds effectively to hydrophobic polymers, realizing a low-friction compact tissue (Fosang and Little, 2008) (**Fig. 3B**). Aggrecan monomers bind to link protein and hyaluronic acid to form a large molecular weigh aggregates, which is able to immobilaze aggrecan at high concentrations within the tissue. Degradation of collagen and aggrecan is a clinical hallmark of degenerative joint disorders such as OA (Zhang et al., 2013; Yang et al., 2017) and rheumatoid arthritis (Fosang et al., 2008; Mead and Apte, 2018; Santamaria, 2020).

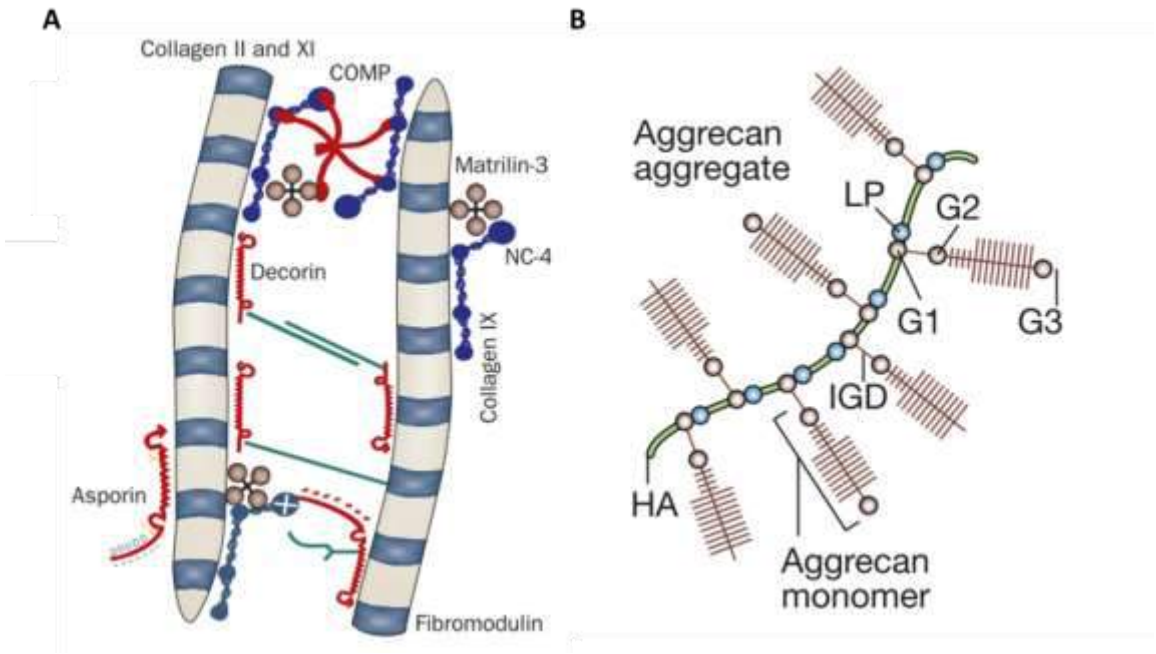

Fig. 3 Main components of articualar cartilage: collagen (**A**) and aggrecan aggrecate (**B**). Collagen interacts directly or indirectly with neighboring molecules: fibromodulin, decorin, cartilage oligomeric matrix protein (COMP), matrilins, heparin-binding nC-4 domain (NC-4). Different aggrecan monomers bound to hyaluronic acid (HA) and link protein (LP) to form stable trimeric complexes. The aggrecan core protein contains globular G1, G2 and G3 domains, with chondroitin sulfate and keratan sulfate glycosaminoglycans substituted between the G2 and G3 domains (Fosang et al., 2008; Heinegård and Saxne, 2011).

1.2 ADAM metalloproteases

ADAM (A Disintegrin and Metalloproteinase) proteins belong to the metzincin family of matrix metalloproteinases, so named for the conserved methionine residue and the presence of a zinc ion in the active site. ADAM proteins, with snake venom metalloproteinases (SVMP) and ADAMs with thrombospondin sequences (ADAMTS), form the adamalysin family (Seegar and Blacklow, 2019). In humans, 21 ADAMs have been identified, 13 of which encode a proteolytically active domain and share a common structure (ADAM8, -9, -10, -12, -15, -17, -19, -20, -21, - 28, -30, -33 and -DEC1), while 8 ADAMs (ADAM2, -7, -11, -18, -22, -23, -29 and -32) are catalytically inactive(Edwards et al., 2009; Seegar and Blacklow, 2019; Pluda et al., 2021). ADAM proteins are type-1 transmembrane and have a modular domain organization with signal sequence, prodomain, metalloproteinase, disintegrin-like, cysteine-rich, epidermal growth factor-like, transmembrane segment and a cytoplasmic tail. (**Fig. 4**) ADAM-17 and ADAM-10 are the only two members of ADAMs that lack the epidermal growth factor-like domain (Seegar and Blacklow, 2019).

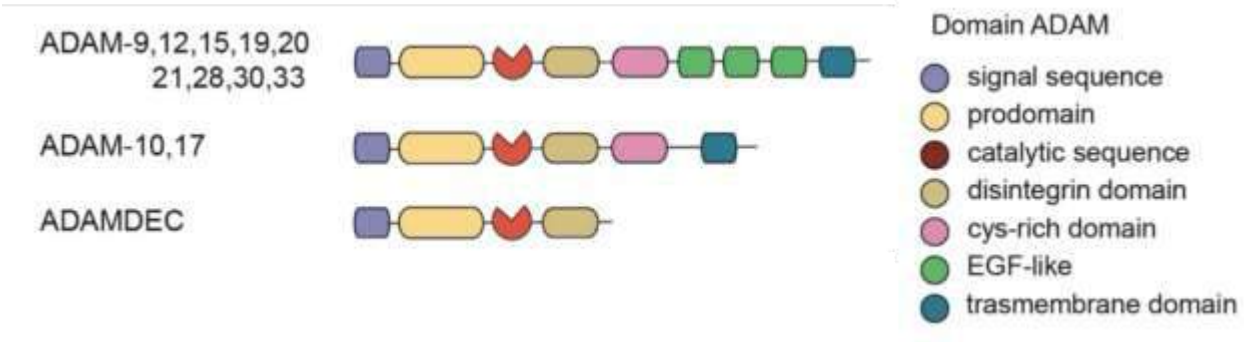

Fig. 4 Schematic representation of modular domain structure of human ADAM members (Pluda et al., 2021).

Moreover, ADAMDEC is the only family member secreted in soluble form, with a signal sequence, a prodomain, a catalytic domain and a short disintegrin domain. Proteins are expressed in an inactive from with a prodomain that act as inhibitor. Upon secretion and selective N-glycosylation, ADAMs undergo maturation and prodomain cleavage. ADAM-17 structure was determined in 1998 (Seegar and Blacklow, 2019) revealing a catalytic cleft between amino terminal and carboxyl terminal lobes along α-helix α4. Consensus HEXXHXXGXXH sequence of the catalytic site revealed the role of three histidine (H) residues that coordinate the zinc ion. Substrate hydrolysis is mediated by an activated water molecule that act together with a glutamate residue (E) (**Fig. 5**) Inactive members of ADAM family have mutations at the active site (Huovila et al., 2005).

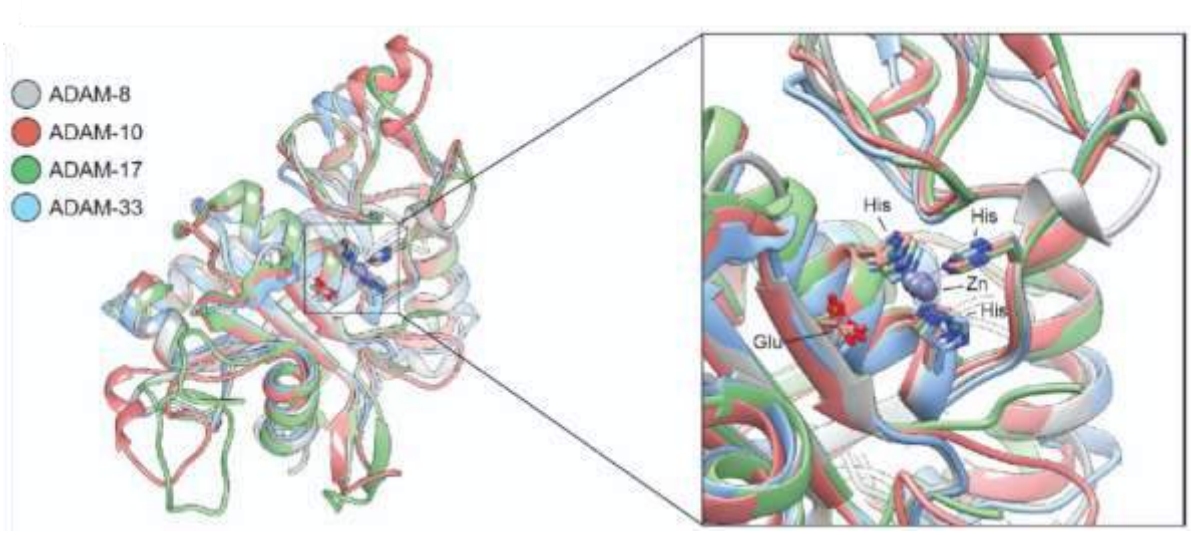

Fig. 5 Structural comparison of the tridimensional structures of the catalytic domains of ADAM proteins. Superimposed X-ray crystal structures of ADAM-8 (gray; PDB identification code 4DD4), ADAM-10 (red; PDB identification code 6BE6), ADAM-17 (green; PDB identification code 2DDF) and ADAM-33 (light blue; PDB identification code 1R55). (Pluda et al., 2021)

Zinc ion is located at the bottom of the groove between the subdomains and specificity for amino acid sequences $P_3P_2P_1P'_1P'_2P'_3$ is determined by subsides $S_3S_2S_1S'_1S'_2S'_3$. Substrate selectivity of ADAM proteins is strongly dependent on the flexibility of P3-P1 positions to fit into S3-S1 pocket with

extension of the side chain from P1' into S1' pocket. Depth of S1' pocket in ADAM-10 compared to ADAM-17 is the origin of substrate selectivity (Edwards et al., 2009; Seegar and Blacklow, 2019). Moreover, exosites of disintegrin and cysteine rich domains actively participate to substrate recognition (Seegar and Blacklow, 2019). Active ADAMs are involved in ectodomain release from a membrane-bound protein. Catalytically active ADAM proteins result in ectodomain shedding, the irreversible processing of a membrane-associated protein to release its ectodomain into the extracellular or luminal space. Some pharmacological agents affect ADAM activity by regulating the shedding properties, even though the underlying mechanisms are not well understood (Huovila et al., 2005). ADAMs are widely expressed in mammalian tissues and exhibit a wide range of different biological functions.

ADAM-17 and ADAM-10 are the most investigated. Shedding activity allow the release of cytokines, growth factors, membrane-bound precursors, or regulate receptor and cell surface proteins. Their regulation is essential for signalling pathways for the physiological development and pathological processes. Inhibition of sheddases activity of ADAM-17 and MMP-14, has been shown to restore the endocytic capacity and degradation (Yamamoto et al., 2017). Inhibition of ADAM-17 metalloprotease and soluble TNF-α result effective ways to control cartilage inflammation (Amin, 1999). Dysregulated activity of ADAMs have been associated to several other pathologies, such as cancer, neurodegenerative diseases, chronic immunity, Alzheimer's disease and arthritis (Moss et al., 2001; Duffy et al., 2009; Moss and Minond, 2017).

1.3 ADAMTS metalloproteases

ADAMTS (A Disintegrin and Metalloproteinase with Thrombospondin) proteins possess similar structural features of ADAM family, a variable number of C-terminal thrombospondin type-1 (TSP-1) motifs and the absence of a transmembrane domain (**Fig. 6**) (Apte, 2020).

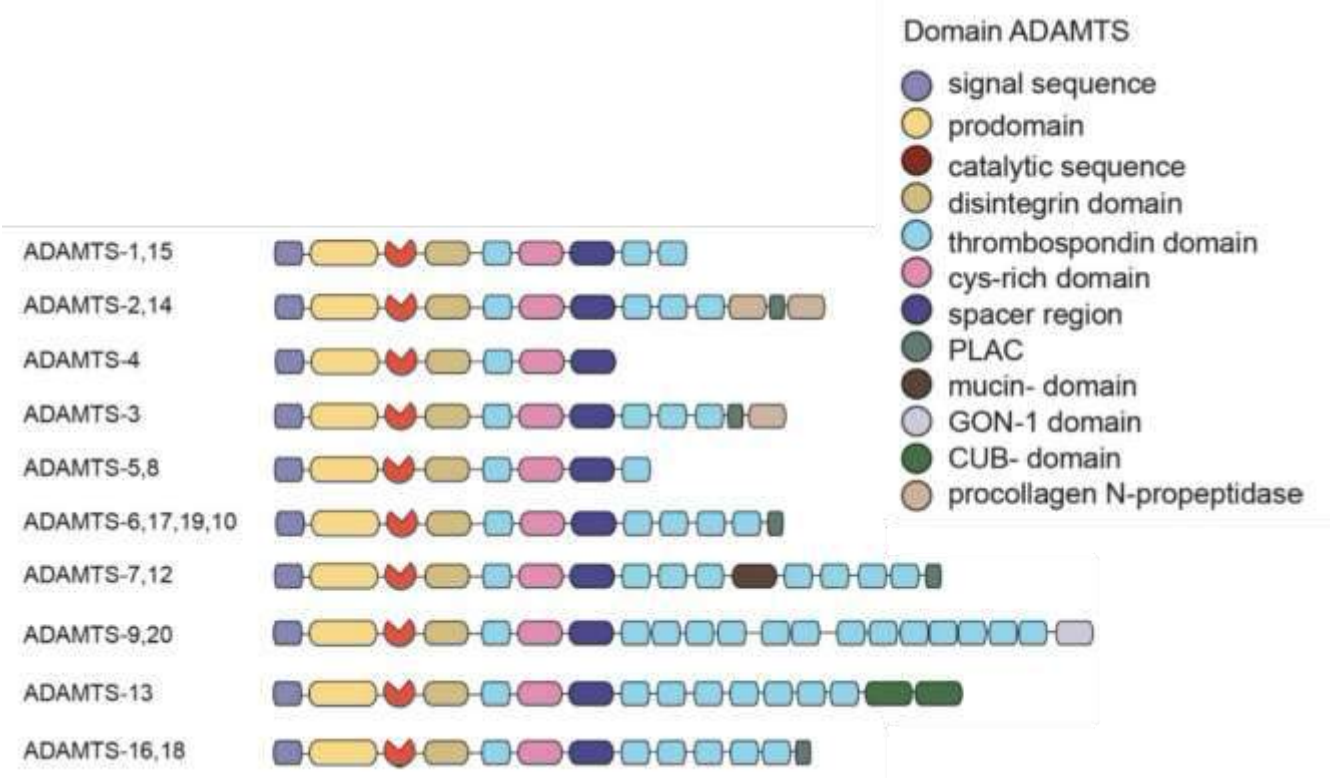

Fig. 6 Schematic representation of modular domain structure of human ADAMTS members (Pluda et al., 2021).

Active site of ADAMTSs is similar to that of ADAM family. Sequence HEXXHXXGXXH possess the histidine triad, which coordinate the zinc ion, and present a bulky apolar contribution from hydrophobic residues. The conserved methionine residue forms a turn, characteristic of the metzincin family (**Fig. 7**) (Fosang, 2008; Apte, 2020).

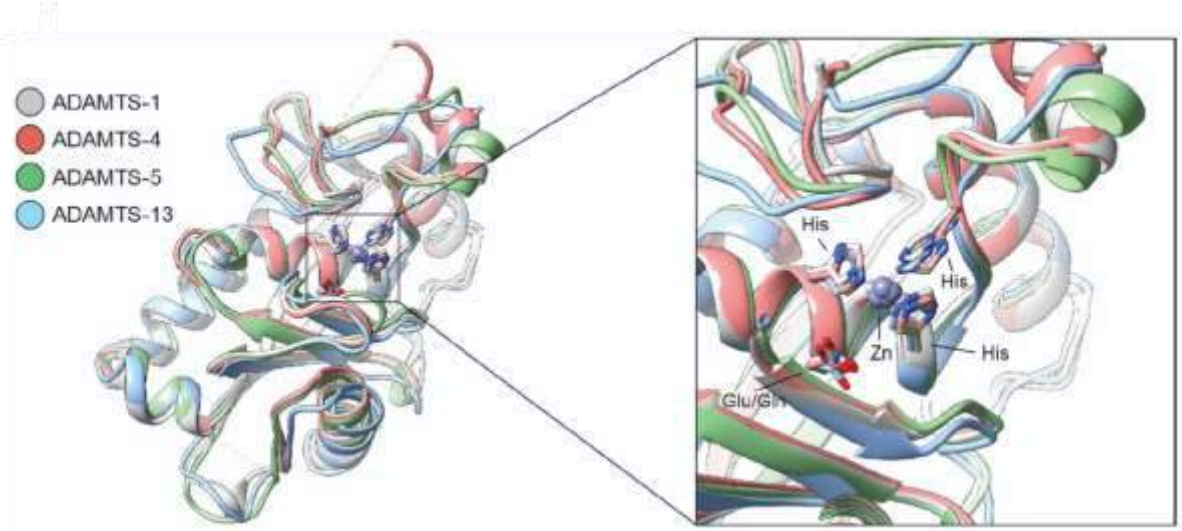

Fig. 7 Structural comparison of the tridimensional structures of the catalytic domains of ADAMTS proteins. Superimposed X-ray crystal structures of ADAMTS-1 (gray; PDB identification code 2V4B), ADAMTS-4 (red; PDB identification code 3B2Z), ADAMTS-5 (green; PDB identification code 3B8Z) and ADAMTS-13 (light blue; PDB identification code 6QIG). The zoomed-in view of the active sites of both ADAM and ADAMTS structures highlights

the similarities of the catalytic pockets including a glutamate (Glu) or glutamine (Gln) residue and three conserved histidine (His) residues that coordinate the zinc ion (light blue sphere). (Pluda et al., 2021)

ADAMTSs contribute to extracellular maintenance, tissue morphogenesis and remodelling (Kelwick et al., 2015; Apte, 2020). Nineteen members belong to ADAMTS family and are called aggrecanases or proteoglycanases (ADAMTS−1, −4, −5, −8, −9, −15 and −20), procollagen N-propeptidases (ADAMTS−2, −3 and −14), cartilage oligomeric matrix protein (also known as thrombospondin-5) cleaving proteinases (ADAMTS−7 and −12), von Willebrand factor (VWF) cleaving proteinase (ADAMTS-13) and a group of orphan enzymes (ADAMTS−6, −10, −16, −17, −18 and −19) (Kelwick et al., 2015; Apte, 2020). Since the discovery of the first member of ADAMTS family twenty-five years ago, the major number of studies is focused on few members of ADAMTS superfamily, specifically ADAMTS-13, ADAMTS-2, ADAMTS-4 and ADAMTS-5 (Apte, 2020).

ADAMTS-4 (aggrecanases-1) and ADAMTS-5 (aggrecanases-2) gained large attention as major targets in OA, in view of their key role in degradation of ECM type II collagen and aggrecan and raprensent a potential target for delay or prevent progressive cartilage erosion. They cleave proteoglycans, which play a structural role in many tissues (Fosang and Little, 2008). Cleavage of the Glu373–Ala374 bond in the interglobular domain of aggrecan complex induce the release of aggrecan from hyaluronan backbone (Fosang and Little, 2008). Several *in vivo* models of OA were developed to elucidate the contribution of aggrecanases to disease (Stanton et al., 2005; Santamaria, 2020). Significant protection against proteoglycan degradation was observed in *Adamts4/Adamts5* double knockout experiments (Majumdar et al., 2007). Moreover, many other ADAMTSs and ADAMs are expressed in cartilage and several show significantly altered expression in OA (Yang et al., 2017).

1.4 Peptide inhibitors of ADAM and ADAMTS metalloproteases

This chapter has been adapted from:

Pluda, S., Mazzocato, Y., & Angelini, A. (2021). Peptide-Based Inhibitors of ADAM and ADAMTS Metalloproteinases. *Frontiers in Molecular Biosciences*, *8*, 678.

Peptide inhibitors of ADAM metalloproteases

ADAM-8 and ADAM-17 are the only members of ADAM family that have been investigated as targets for the development of peptide inhibitors. ADAM-17 has been intensively studied during the last twenty years as it is involved in the maturation of TNF-α, a proinflammatory cytokine that plays a key role in inflammatory diseases, such as arthritis and Chron's disease (Feldmann and Maini, 2008). Furthermore, ADAM-8 is a sheddase and its upregulation is correlated with inflammatory diseases and development of cancer. In this chapter, the discovered peptide inhibitors and the development strategies against these two metalloproteinases are presented (**Fig. 8**) (Pluda et al., 2021).

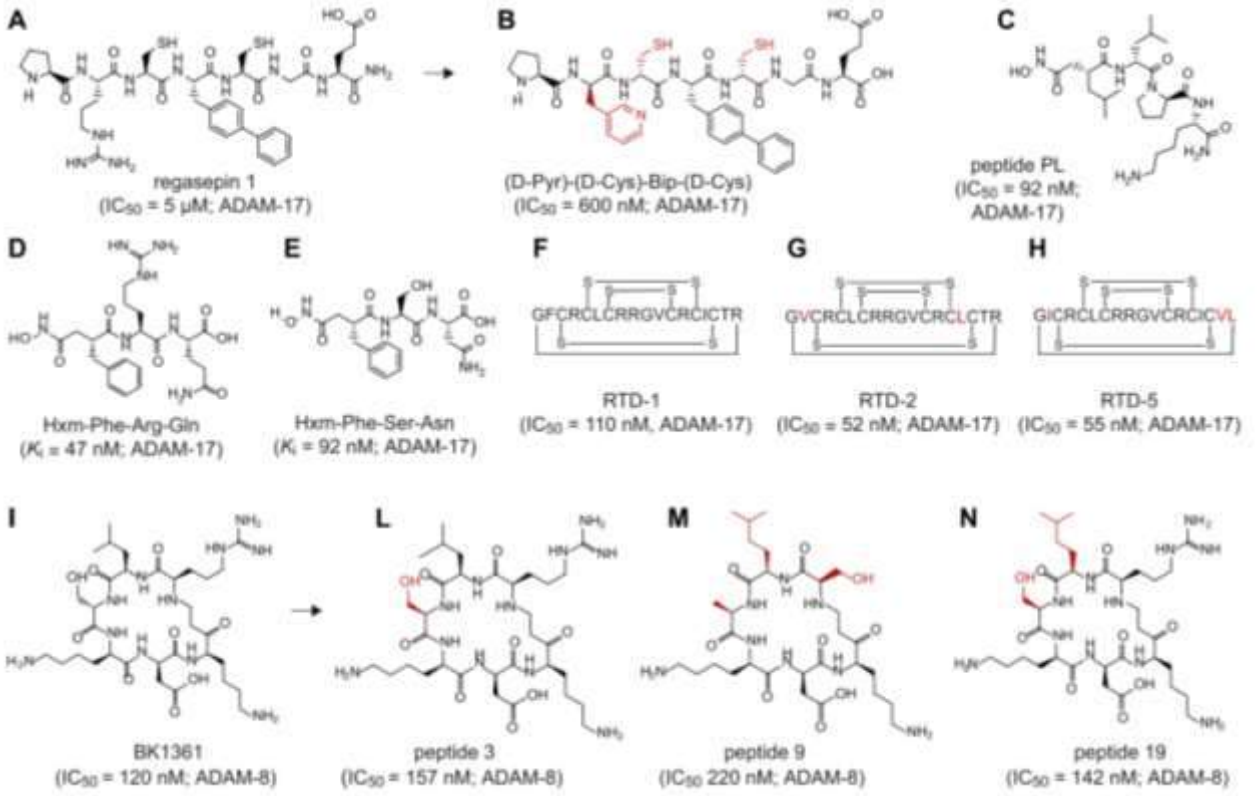

Fig. 8 Peptide inhibitors of ADAM proteins. (**A**) regasepin 1, (**B**) (D-Pyr)-(D-Cys)-Bip-(D-Cys), (**C**) PL, (**D**) Hxm-FRQ, (**E**) Hxm-FSN, (**F**) RTD-1, (**G**) RTD-2, (**H**) RTD-5, (**I**) BK1361, (**L**) peptide 3 (**M**) peptide 9 (**N**) peptide 19.

The development of the first peptide inhibitor of ADAM-17 was the result of a peptidomimetic study on sequence of collagen cleavable sites. This synthetic combinatorial screenings afforded ADAM-17 inhibitors at low micromolar range, called Regasepin 1 and 2, but unfortunately with no selectivity towards MMP-8 and MMP-9 (Qiu et al., 2012) (**Fig. 8A**).

A consecutive study for the potency improvement of Ragasepin 1 was performed on a 30-members small peptide library bearing D-amino acids in some preferred positions. (D-Pyr)-(D-Cys)-Bip-(D-Cys) (**Fig. 8B**) reached a stronger inhibition with IC_{50} in nM range, but no selectivity versus MMP-8 (Qiu et al., 2012). Geurink and co-workers reported an example of synthetic combinatorial strategy in which peptidomimetics with N-terminal zinc binding group were explored. Eight inhibitors were selected considering the potency and selectivity, and the inhibitory values spanned from sub-nanomolar to low micromolar range. Peptide PL showed the best results with a potency value of 92 nM and selectivity of 40 folds vs MMP-9 (Geurink et al., 2008) (**Fig. 8C**).

Two hydroxamate peptides, Hxm-Phe-Ser-Asn and Hxm-Phe-Arg-Gln (**Fig. 8D, E**), with nanomolar potency against ADAM-17 and good selectivity towards ADAM-10 were discovered from a combinatorial library of peptide hydroxamate compounds derived from natural inhibitor TAPI-2 (Wang et al., 2016). Most recently, from a class of natural 18-amino acid macrocyclic peptides, belonging to theta-defensins family, a potent inhibitor (RTD-1) of ADAM-17 and ADAM-10 was discovered (Schaal et al., 2017) (**Fig. 8F**). The efficacy was tested in a rodent model of rheumatoid arthritis, where treatment with RTD-1 was able to reverse joint disease. Then, natural RTD isoforms were tested on inhibitory activity against ADAM-17 and strongly correlated with suppression effects of TNF-α release *in vitro*. Next, five natural RTD isoforms were tested and their inhibitory activity against ADAM17 compared. The most potent macrocycles, RTD-2 and RTD-5, showed potency around 50 nM (Schaal et al., 2018) (**Fig. 8G,H**). Regarding peptide inhibitors of ADAM-8, cyclic peptide BK1361 (**Fig. 8I**) was discovered from a series of six-residue long cyclic peptides and generated via structural modelling of the disintegrin domain and a mimic study of the motif "RLSKDK" (Schlomann et al., 2015). D-amino acids were used to increase the stability and BK1361 shown remarkable inhibitory potency against ADAM-8 with more than 100 folds of selectivity towards other metalloproteases.

Based on the structure of BK1361, peptide 3, 9 and 19 (**Fig. 8L,M,N**) were selected from a synthetic library of peptidomimetics in a structure activity relationship study (Yim et al., 2016). The contribution of the polar side chain, arginine substitution and the role of the hydrophobic pocket on the peptide activity were identified. However, inhibitory potency against ADAM-8 had values comparable of the parent peptide.

Peptide inhibitors of ADAMTS metalloproteases

The interest on ADAMTS metalloproteases and their role in numerous pathologies have grown in the last twenty-five years, since the discovery of the first member, ADAMTS-1 (Apte, 2020). After the identification of ADAMTS-4 (aggrecanase-1), as a major target involved in cartilage degradation in OA, (Tortorella et al., 1999) multitude efforts for the development of small inhibitors able to control the aggrecanolytic activity have been investigated. However, few studies of peptide inhibitors against ADAMTS metalloproteases have been reported so far (**Fig. 9**)

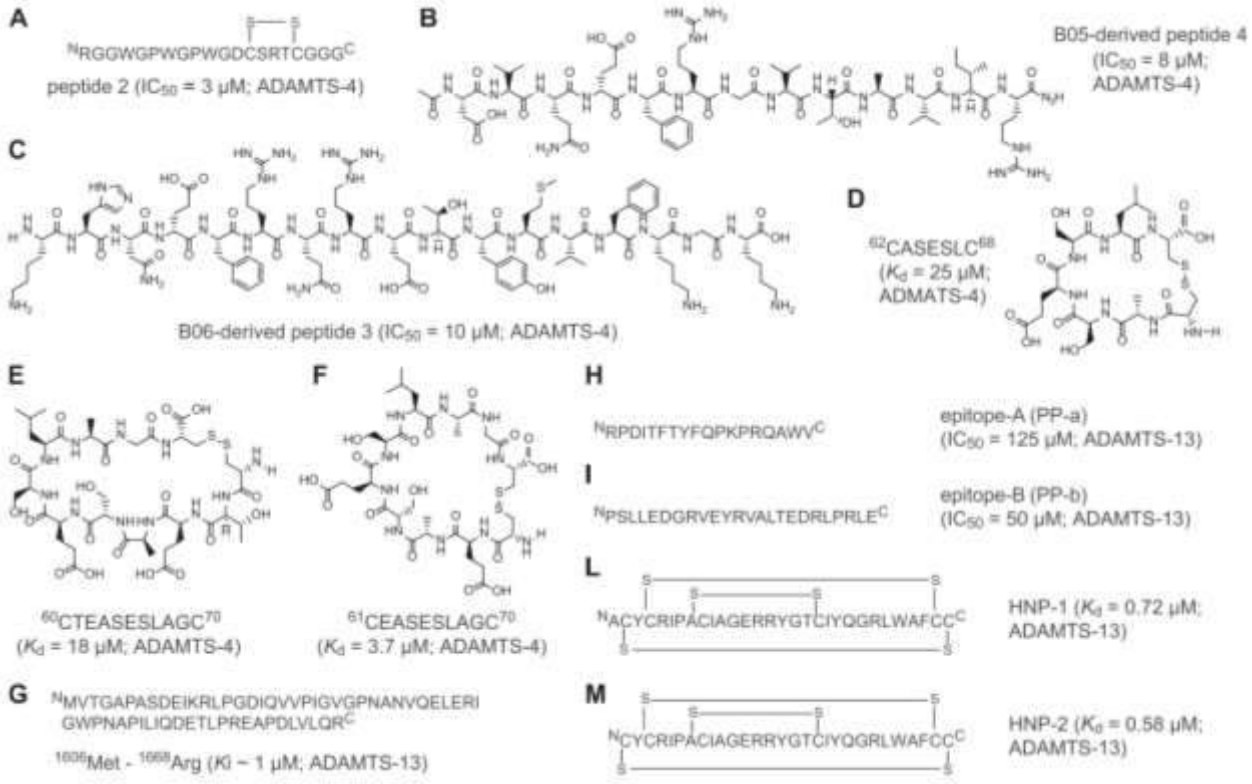

Fig. 9 Peptide inhibitors of ADAMTS proteins. (A) peptide 2, (**B**) B05-derived linear peptide 4, (**C**) B06-derived linear peptide 3, (**D**) ^{62}CASESLC^{68}, (**E**) ^{60}CTEASESLAGC^{70}, (**F**) ^{61}CEASESLAGC^{70}, (**G**) VWF-73, (**H**) PP-a, (**I**) PP-b, (**L**) HNP-1, (**M**) HNP-2.

The first peptide inhibitor against ADAMTS-4 was selected from sequences derived from the TSP-1 motif and tested for their ability to block the cleavage of bovine aggrecan at the Glu373/Ala374 site. Peptide 2 was the most potent peptide in blocking aggrecan cleavage, with a half inhibitory concentration with low micromolar value (Tortorella et al., 2000, Hills et al., 2007) (**Fig. 9A**). Peptide B05 and B06, with micromolar potency against ADAMTS-4 and good specificity against ADAMTS-5, were discovered using a *de novo* study of a phage display system (**Fig. 9B, C**). A random 13-mer peptide phage library allowed the determination of a 7-amino acid cleavage motif and insights on substrate recognition (Hills et al., 2007) From a computational modelling study of ADAMTS-4

structure in complex with its native inhibitory protein TIMP-3, peptide sequences were obtained and subsequently cyclized to reduce flexibility and increase stability. Cyclic peptides reported in **Fig. 9D, E,F** showed binding constants in the micromolar range, compared to the linear parent peptides (Zhang et al., 2018). Peptide inhibitors against ADAMTS-13 have been also explored because of its therapeutic potential in circulating and vascular system related diseases (South and Lane, 2018; Santamaria and de Groot, 2020). The first study reported a VWF-73 peptide, which was identified from the C-terminal region of von Willebrand factor (**Fig. 9 G**) and Inhibition mechanism of ADAMTS-13 was investigated and elucidated (Di Stasio et al., 2008). Moreover, from a study of VWF binding with phage display system, peptides PP-a and PP-b were discovered and showed inhibitory effects of ADAMTS-13 on the low micromolar range (Moriki et al., 2010). (**Fig. 9 H,I**) Finally, HNP-1 and HNP-2 were selected from a screening of polyicyclic human neutrophil peptides (**Fig. 9 L,M**). These peptides revealed effects on cleavage inhibition of peptide VWF-73 and multimeric VWF. Inhibitory potency in the low micromolar range were determined (Pillai et al., 2016).

1.5 Chemical modification of peptide using thiol-alkylation and copper-catalyzed Huisgen cycloaddition

Bioconjugation reactions are chemoselective modifications of biomolecules with functionalities that are not coded by genetic information. They represent an indispensable approach for life science research and the development of therapeutics (Ochtrop and Hackenberger, 2020). Constant endeavors allow advances in bioconjugation chemistry that are linked with selective targeting of amino acid for the precise engineering of proteins (DeGruyter et al., 2017). A bioconjugation reaction should be site-selective, robust and proceed under physiological or mild conditions (pH, temperature, pressure, solvent). Moreover, preservation of the structure and related activity are also important factors to take in consideration (DeGruyter et al., 2017; Pickens et al., 2018). The bioconjugation strategy is selected in consideration of the reactivity of the target amino acid residue (acid/base, electro/nucleophilicity, red-ox properties) and its environment (in-chain, terminal position, sequence specificity, accessibility) (Koniev and Wagner, 2015). Residues with polar side chains have been extensively investigated because they represent the most easily modified amino acids. Undoubtedly, cysteine residue is the most well-studied reactive group in the bioconjugation literature (Koniev and Wagner, 2015; DeGruyter et al., 2017).

Chemical modification of peptide using thiol-alkylation

Thiol-alkylation is a common bioconjugation strategy employed to chemical modify peptides bearing the canonical amino acid cysteine (DeGruyter et al., 2017). The side chain of cysteine includes a thiol moiety, an excellent nucleophile in aqueous conditions with a pKa value around 8-9. Thiol deprotonation generates a thiolate group, essential for the development of the thiol-ether bond (Peraro et al., 2016). A strategy to induce conformational restriction of linear peptides involves the cross-linking of two or more unprotected cysteines. Crosslinked peptides show reduced conformational flexibility and smaller entropic penalty upon binding (Derda and Jafari, 2018). Nonetheless, cyclization strategy increases the stability and resistance to proteolytic degradation towards degrading enzymes (Derda and Jafari, 2018). Alkylation reactions of synthetic peptides with di- and tri-bromo aryl derivative linkers was firstly reported by Timmerman and co-workers **(Fig. 10)** (Timmerman et al., 2005).

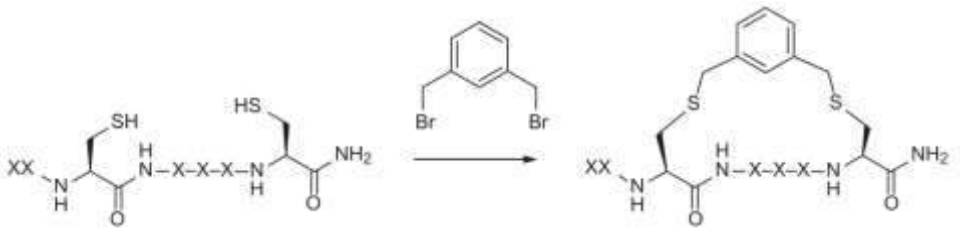

Fig. 10 Cross-linking reaction of two unprotected cysteines with m-dibromoxylene (Peraro et al., 2016)

The reaction showed excellent efficiency in buffer at pH 8 and was applied to generate conformational diversified peptide epitopes. This allowed rapid preparation and screening of a panel of peptide loops with constrain conformation and high binding affinity (Timmerman et al., 2005).

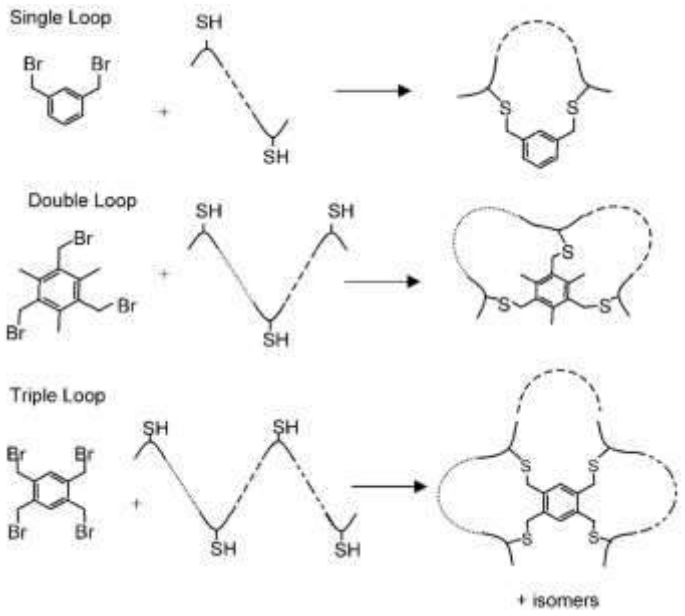

Fig. 11. Schematic representation of one-step cross-linking for single-, double-, and triple- loop peptide construction (Timmerman et al., 2005)

This chemistry was initially developed for introducing conformational constraints on libraries of synthetic peptides. Subsequently, it was further expanded for the modification of peptides expressed on the surface of phage particles (Heinis et al., 2009) and mRNA display libraries (Huang et al., 2019). Heinis and coworkers pave the way with the bicyclization of a trillion- member phage-display library containing three cysteines (**Fig. 12**) (Heinis et al., 2009).

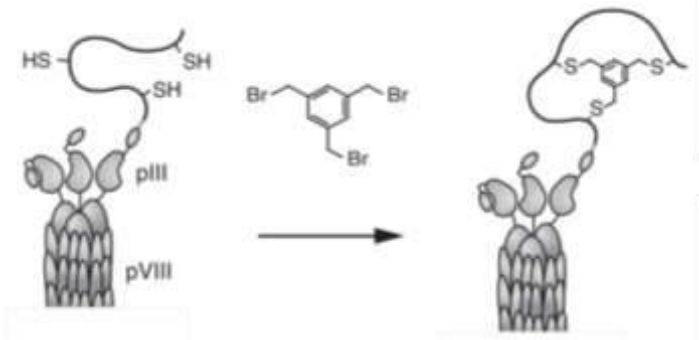

Fig. 12 Schematic representation of peptide bi-cyclization with tris-(bromomethyl)benzene on phage (Heinis et al., 2009)

This powerful technology for generating and screening DNA-encoded peptide/protein libraries allowed the development of several potent and selective inhibitors (Heinis and Winter, 2015; Zorzi et al., 2017). Furthermore, chemical modification to introduce topological constraints was expanded to increase the chemical diversity with the introduction of small molecule ligands, fluorophores and

photo-switchable compounds (Heinis and Winter, 2015). Thiol-alkylation chemistry was pushed even further by Suga and co-workers. Thioether-cyclization of peptide libraries of mRNA display system allowed the synthesis of cyclic peptides using flexizyme-assisted translation. By means of introduction of a chloroacetyl group in the side chain of peptide, a thioether bond is formed by intramolecular reaction with cysteine (Sako et al., 2008; Goto et al., 2011; Passioura and Suga, 2017).

Chemical modification of peptide using copper-catalyzed Huisgen cycloaddition

Twenty years ago, Sharpless and Meldal reported the formation of a regiospecific 1,4-substituted triazole under mild reaction with the use of catalytic amounts of copper (I) (Rostovtsev et al., 2002; Tornøe et al., 2002). Subsequently, the versatility and efficiency of this copper-catalyzed Huisgen cycloaddition (CuAA) elect it as the most famous reaction in the click chemistry toolbox. Copper is the catalyst and Cu (I) is more easily formed *in situ* with the action of a reducing agent, commonly sodium ascorbate, because it is readily oxidized to Cu (II). Moreover, unintended side reactions promoted by the metal, especially in cell-based assays, introduced the use of copper-stabilizing ligand. The site-specific functionalization of peptides relies on the high chemoselectivity of CuAA in presence of the functional groups of natural amino acid. Functionalization of synthetic peptide is relatively simple, because SPPS allow the introduction of commercially available non canonical amino acids (ncAA) bearing azide or alkyne functionalities. Furthermore, peptide CuAA represent an attractive way to cyclize with the imposition of conformational restriction and structure stabilization (**Fig. 13**) (White and Yudin, 2011).

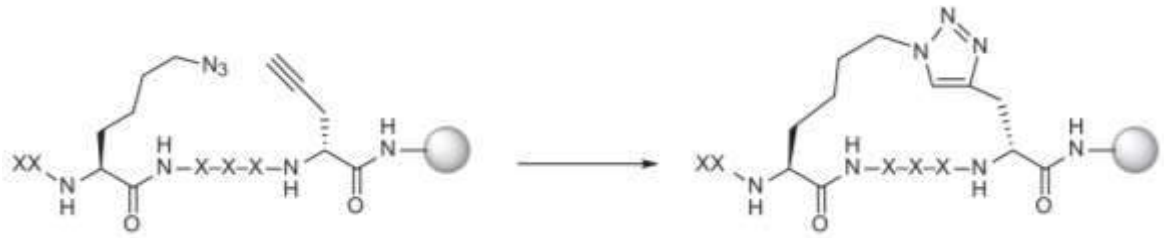

Fig. 13 Copper-catalyzed Huisgen cycloaddition reaction of azido and alkyne groups of side chains (Peraro et al., 2016)

The versatility of this CuAA-mediated macrocyclization reaction has been widely investigated with protected, deprotected and solid-supported SPPS peptides (White and Yudin, 2011). Nonetheless, 1,4-disubstituted 1,2,3-triazoles is a good substitute of trans-amide bond in crosslinking bridge and the peptidomimetic contribution is important for target recognition and binding affinity. Finally, the insertion of ncAA in expressed peptides or proteins is more challenging and achieved by means of the use of aminoacyl tRNA synthetases (Antonczak et al., 2011). In **Fig. 14** is reported an example

of yeast surface display system with incorporation of ncAA. Subsequent CuAA reaction with biotin-alkyne derivative is achieved on cell surface (Van Deventer et al., 2016).

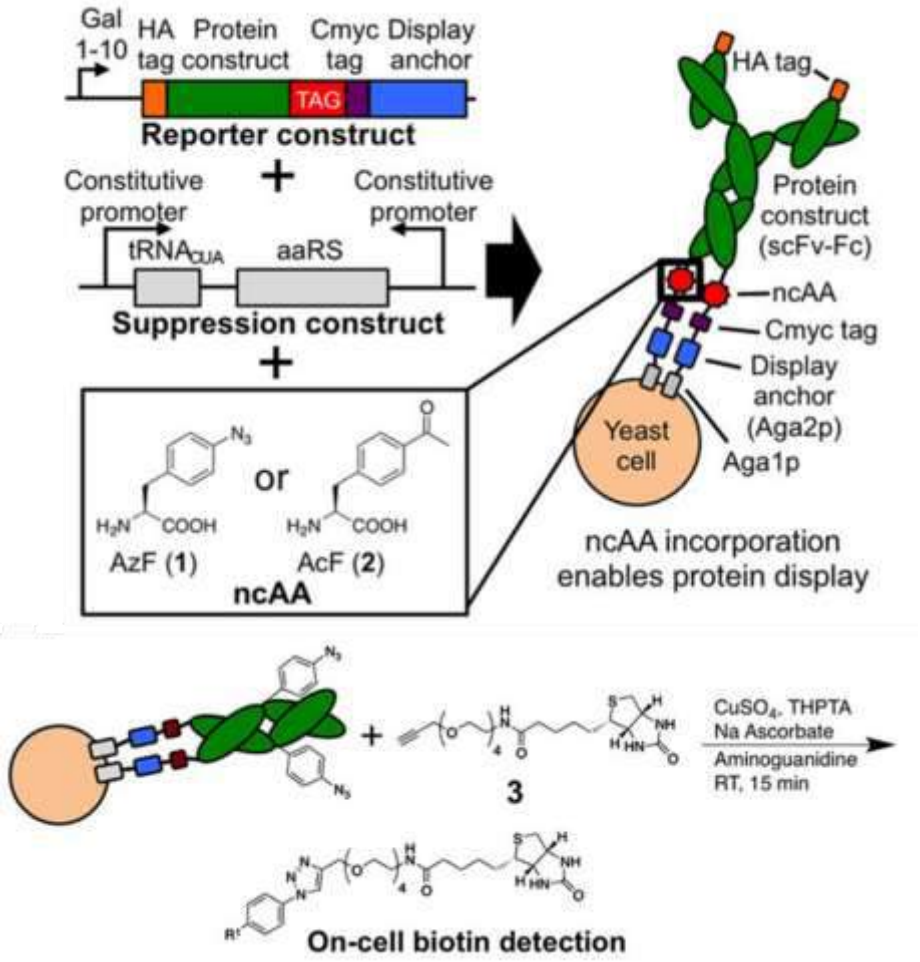

Fig. 14 Schematic representation of protein with ncAA on a yeast surface display system and CuAA reaction with biotin-alkyne derivative on cell surface (Van Deventer et al., 2016).

1.6 Yeast surface display technology

This chapter has been adapted from:

Linciano, S., Pluda, S., Bacchin, A., & Angelini, A. (2019). Molecular evolution of peptides by yeast surface display technology. *MedChemComm, 10*(9), 1569–1580.

Yeast surface display technique is twenty-five years old and is a popular tool for protein engineering and library screening applications. (Boder and Wittrup, 1997) This invention was first validated to increase the affinity of existing proteins, but subsequently proved its effectiveness for isolating *de novo* proteins from näive combinatorial libraries of multiple immunoglobulin and non-

immunoglobulin scaffolds, including some peptides (Angelini et al., 2015; Cherf and Cochran, 2015; Könning and Kolmar, 2018). In addition to improve the affinity and specificity of multiple proteins and peptides against a wide range of targets, yeast surface display technology has also been successfully employed for epitope mapping, to improve recombinant production and stability of protein of interest, as well as to engineer the function of different enzymes. (Farinas et al., 2001; Linciano et al., 2019) The greatest advantage of yeast display compared to other in vitro display technologies, is its compatibility with fluorescence-activated cell sorting (FACS) that allows high-throughput screening and biophysical characterization of large combinatorial libraries of proteins and peptides (**Fig. 15**). (Angelini et al., 2015; Tizei et al., 2016; Linciano et al., 2019)

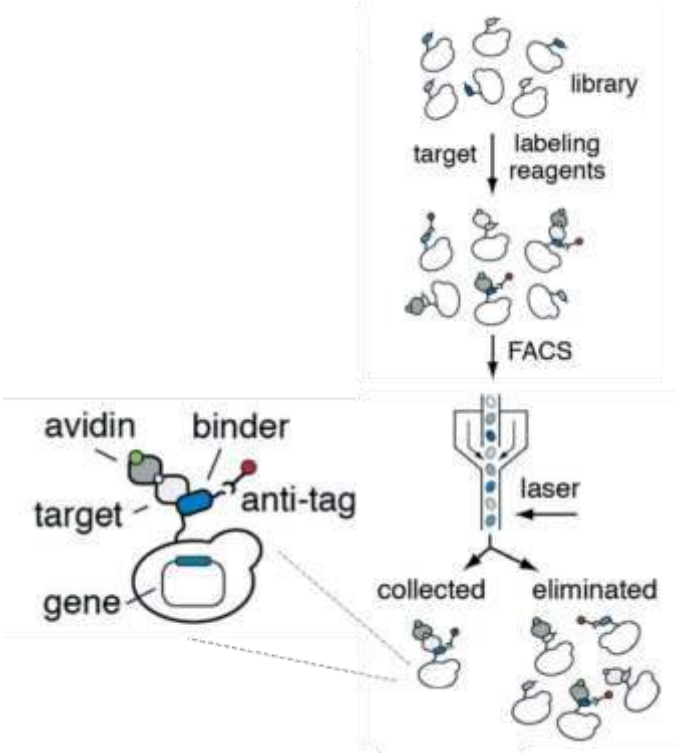

Fig. 15 Schematic representation of binder selection from a yeast display library by using fluorescence-activated cell sorting (Linciano et al., 2019).

Although diverse yeast strains and various cell wall anchors have been used to display a large variety of protein and peptide scaffolds, (Lim et al., 2017; Andreu and del Olmo, 2018; Mcmahon et al., 2018) the *Saccharomyces cerevisiae* Aga1– Aga2 system remains the most commonly used. In this arrangement, the molecule of interest is expressed as fusion to the Aga2 protein that is linked to the membrane anchored a-agglutinin Aga1 protein through two disulfide bridges, resulting in a covalent complex on the surface of the yeast cell. Proteins and peptides of interest can be displayed on the yeast surface as either C- or N-terminal fusions to the Aga2 protein (**Fig. 16**). (Orcutt and Wittrup, 2010; Angelini et al., 2015)

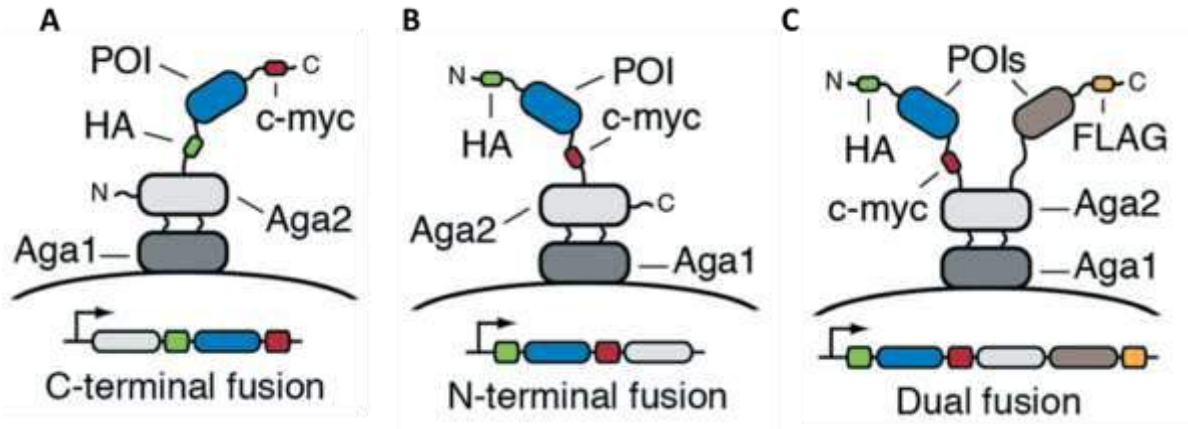

Fig. 16 Schematic representation of the yeast display technology based on Aga1–Aga2 system. (**A**) The protein or peptide of interest (POI) is displayed as a C-terminal fusion to the Aga2 protein, flanked by two tags for immunofluorescent detection: the hemagglutinin (HA) epitope tag at the N-terminus and the c-myc epitope tag at the C-terminus. The Aga2 protein forms two disulfide bonds with the membrane-anchored Aga1 protein (**B**) the POI is displayed as a N-terminal fusion to the Aga2 protein (**C**) co-expression of two different POIs fused at the N- and at the C-terminus of the Aga2 protein (Linciano et al., 2019)

The epitope tags located at the N- and at the C-terminus of the molecule of interest fused to Aga2 allow quantification of the full-length fusion expression and normalization of function to surface expression by flow cytometry. Similarly, binding to the target of interest can be determined by incubating yeast cells with the labeled target. By using a two-color labeling scheme, with one fluorescent probe for expression and another for target binding, proteins and peptides of interest can be engineered for affinity, specificity and stability concomitantly.

Flow cytometry can also be used for the biophysical and quantitative characterization of individual variants as cell-surface fusions without the need for sub-cloning, soluble expression and purification. By applying different labeling approaches, including equilibrium binding and kinetic competition, yeast display combined with flow cytometry allows quantitative and fine discrimination between variants with different binding affinities for the target.(VanAntwerp and Wittrup, 2000) By normalizing the median fluorescence intensity from the binding signal to the median fluorescence intensity from the display signal, as a function of protein concentration, is possible to determine the equilibrium dissociation constant (K_D) of each individual selected clone. Importantly, previous studies have demonstrated that the K_D values determined using yeast surface display are in agreement with those measured using alternative techniques such as fluorescence polarization, surface plasmon resonance and biolayer interferometry.(Angelini et al., 2015) However, the yeast display technology is not without its limitations. First, the library size diversity ($\sim 10^7$–10^9) is usually a few orders of magnitude lower than that obtained with other systems. Second, the presence of multiple copies of a displayed protein or peptide on the surface of yeast could lead to undesired polyvalent interactions

that synergize to enhance the apparent binding affinity.(Mammen et al., 1998) Each yeast cell displays approximately 10^5 copies of the Aga2 fusion on its surface, although individual expression levels may vary depending on the stability and solubility of the displayed molecule. This effect is commonly referred to as 'avidity' and can occur only when the soluble target is multivalent, and its binding sites are sufficiently close together to be simultaneously recognized by multiple copies of proteins or peptides present on the surface of yeast. Such polyvalent interactions lead to increases in the residence time and in the local concentration of the target thus favoring its binding and rebinding and ultimately resulting in often undesired higher binding affinities. Third, the technique is still hampered by the low flow rate ($\sim 10^7$ cells per hour) of the majority of flow cytometry instruments currently available. However, while these drawbacks are crucial for large proteins, they are in general less critical for short peptides for which the diversity to be covered is smaller and the high avidity beneficial when working with weak peptide binders or substrates otherwise undetectable. Moreover, if necessary, multivalent binding can be overcome by applying kinetic strategies in the presence of large amounts of a competitive target able to interfere in a concentration-dependent manner. Using such approach, the yeast cells displaying the protein or peptide of interest are initially incubated with the labeled target and the unbound fraction removed by washing. The labeled cells are following incubated with a large excess of unlabeled target to prevent rebinding of the labeled one after dissociation. Hence, protein or peptide variants displayed on the surface of yeast cells can be discriminated based on their dissociations rate constants (k_{off}) with variants having the higher affinity retaining the largest percentage of initially bound labeled target. Considering all these factors, yeast display represents a versatile and suitable tool for the design and engineering of a wide variety of peptides.

Chapter 2
Chemical modifying agents with hydroxamic moiety

2.1 Introduction

The zinc(II) ion plays a crucial role in the catalytic and structural functions of a plethora of zinc-containing proteins involved in numerous key physiological processes whom misregulation can lead to the onset and the progression of a variety of human diseases (Coleman, 1992). Relevant zinc-dependent proteins that have been implicated in numerous pathologies include as histone deacetylases, carbonic anhydrases, metzincin members (Yang et al., 2015, 2019; Mishra et al., 2020; Lenci et al., 2021). The development of inhibitors targeting zinc-dependent proteins has traditionally involved the use of a zinc binding groups such as hydroxamic acids, carboxylates, thiols, and phosphonic acids (Georgiadis and Yiotakis, 2008; Murumkar et al., 2010; El Bakali et al., 2014; Li et al., 2020). Of these, bidentate hydroxamic acids emerged as the preferred chelator for zinc-containing proteins due to their relative ease of synthesis and potent/high binding affinity (Whittaker et al., 1999; Georgiadis and Yiotakis, 2008; Yiotakis and Dive, 2009; Gilbert et al., 2011). Though potent hydroxamate-based inhibitors have been developed over the years, most of them had limited success in the clinic (Fisher and Mobashery, 2006; Jacobsen et al., 2010). Failures have often been attributed to off-target side effects due to structural similarities among the active sites of the different zinc-containing proteins and the consequent toxicities associated (Yiotakis and Dive, 2009). As a result, there is a great interest in developing novel inhibitors targeting zinc-dependent proteins that can selectively recognize a single member of each family. Such specificity could be achieved by exploring binding sites located outside of the highly conserved active site pocket. Unlike small organic molecules, peptides can cover larger surface of interaction and reach unexplored areas of the protein surface otherwise inaccessible, ultimately leading to high potency and selectivity. Like small molecules, peptides can be synthesized chemically and possess ease of modification thus enabling incorporation of hydroxamic acid-containing functional groups in their structure that confer strong binding to the catalytic cavity.

Toward this goal, we envision the development thiol-reactive linkers bearing a hydroxamic chemical group. While the zinc-binding hydroxamic acid group has the potential to direct/anchor the peptide to the protein target active site, the linker bearing two thiol-reactive group selectively 29yclized the linear peptide containing two cysteine residues thus reducingthe entropic penalty upon binding to the target. Linkers have been designed to i) include different geometries that might impose different conformations on the backbones of 29yclized peptides, ii) bear polar chemical groups that could potentially form intra- or inter-molecular polar interactions and iii) be compatible with an aqueous solvent.

2.2 Results and Discussion

Synthesis and reactivity of di-thiol-alkylating agents

The synthesis of three new thiol-reactive linkers containing a hydroxamic acid group has been described and their chemical reactivities and selectivities assessed (**Fig.17**).

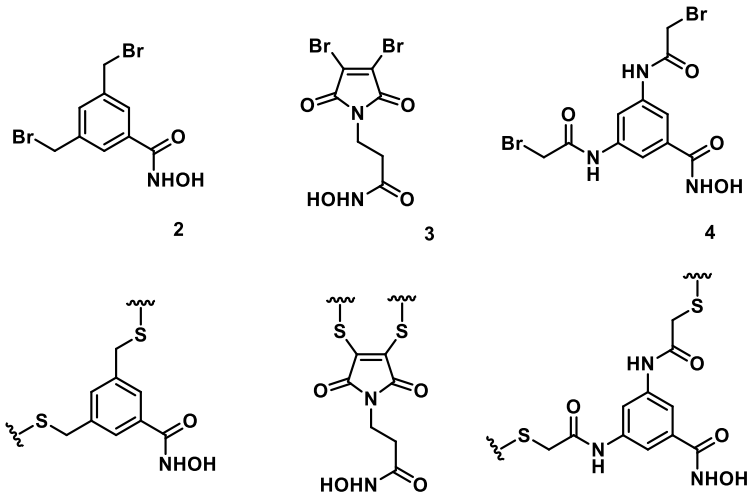

Fig. 17 Chemical structures of di-thiol-alkylating agents: 3,5-bis(bromomethyl)-N-hydroxybenzamide (**2**), 3-(3,4-dibromo-2,5-dioxo-2,5-dihydro-1H-pyrrol-1-yl)-N-hydroxypropanamide (**3**) and N,N'-(5-(hydroxycarbamoyl)-1,3-phenylene)bis(2-bromoacetamide) (**4**) and alkylated products.

Di-alkylating agents (**2, 3, 4**) were designed to have a C2-symmetry with two alkyl bromide or alkenyl bromide moieties and one hydroxamic moiety in order to avoid isomers formation upon peptide cyclization. Common approaches applied in the synthesis hydroxamate involve the activation of carboxylic acid through the use of acid chlorides, anhydrides or esters (Mohammad A. Alam, 2019). However, initial attempts involving the use of benzotriaole derivatives (PyBOP, HATU, HBTU) as carboxylic acid activators yielded several side products, because of the nucleophiles-sensitive moieties. While the further use of ethyl chloroformate for the generation of anhydrides (Reddy et al., 2000) under neutral conditions yielded the expected product it also promoted the Lossen rearrangement with aniline formation (Ohtsuka et al., 2016).

Firstly, mono-alkylating agent **1** was synthesized and the reactivity tested in order to assess the strategy for the novel di-alkylating agents (**2, 3, 4**) (**Fig.18**).

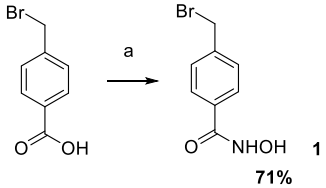

(a) i) $SOCl_2$, reflux, 4 h ii) NH_2OH. HCl, NaOH/Et_2O 1/4 v/v, 30 min, r.t.

Fig. 18 Synthesis of thiol-alkylating agent **1**

Reactivity towards thiol moiety and stability of the hydroxamic group were tested with an alkylation assay under conditions reported by Peraro and coworkers (Peraro et al., 2016). (**Fig. 19**)

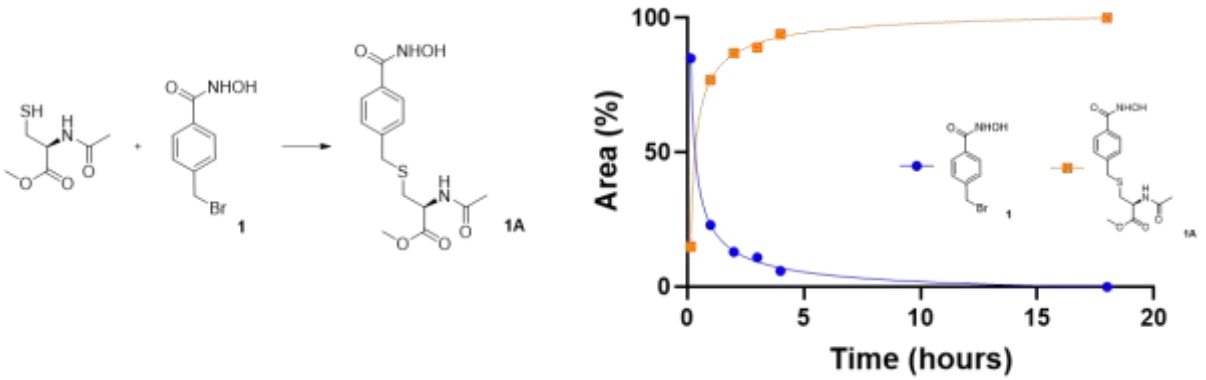

Fig. 19 Alkylation assay of **1** with methyl acetyl-D-cysteinate and reaction kinetics via LC-MS

Reaction kinetics of the mono-alkylating agent **1** showed excellent reactivity, reaching completeness in few hours, and good stability of the hydroxamic group. Product **1A** was further purified and characterized to confirm the structure.

Finally, di-alkylating agents (**2, 3, 4**) were obtained via acyl chloride in a biphasic reaction mixture, following the procedure reported by Amitai and coworkers (Amitai et al., 2016) **Fig. 20.**

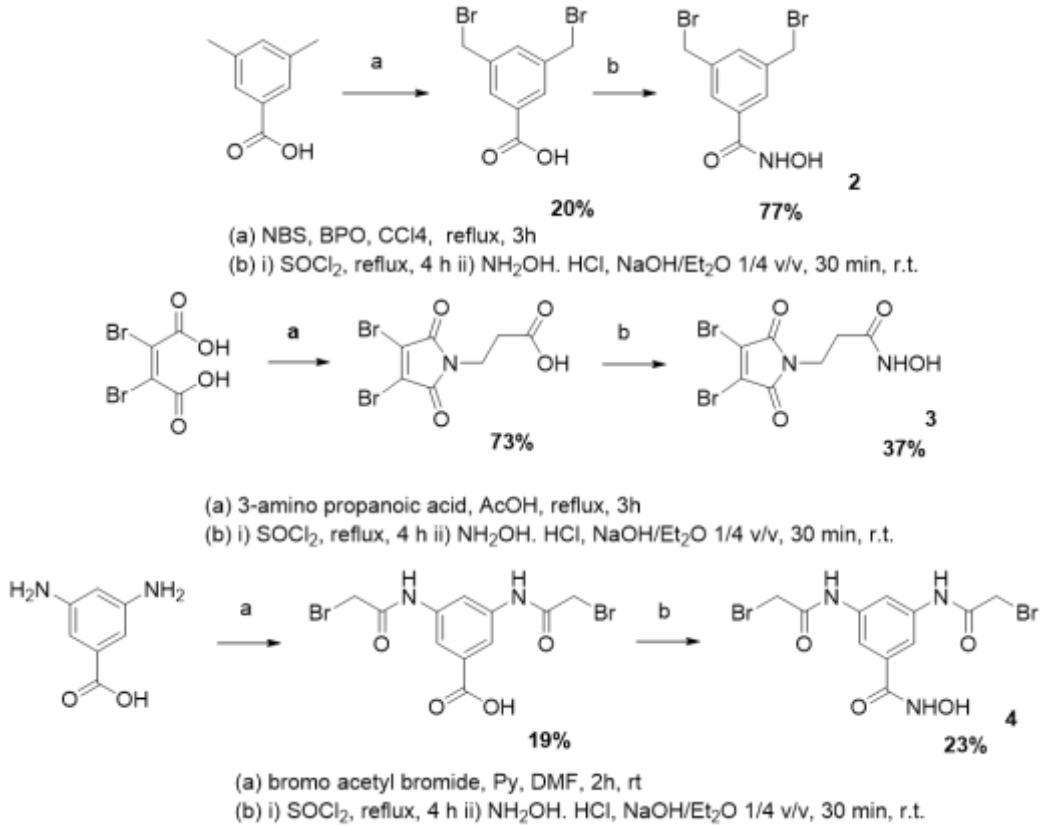

Fig. 20 Synthesis of di-alkylating agents **2**, **3** and **4**

Bromination of dimethylbenzoic acid was carried out using N-bromosuccinimide, according to Lawson and coworkers (Lawson et al., 2003). Precipitation was effective for compound **2**, and compound **3** and **4** required final purification step. Product **3** was obtained via succinimide ring closure, according to the protocol reported by Morais and coworkers (Morais et al., 2017), and subsequent amidation of carboxylic acid. Product **4** was obtained via bis-amidation with acyl bromide (Wong et al., 1998) and subsequent amidation of carboxylic acid.

Reactivity of di-thiol-alkylating agents **2,3,4** was tested with peptide **P4** in a cyclization assay via LC-MS analysis (**Fig. 21**)

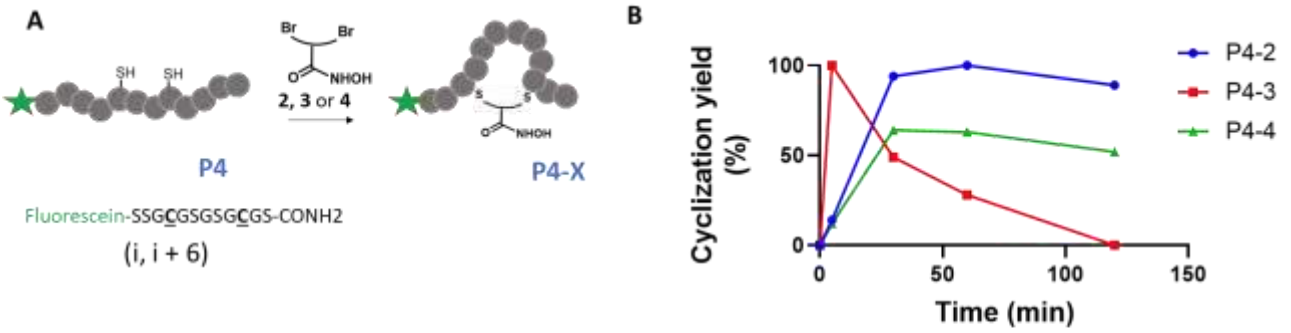

Alkylating agent	Cyclic peptide P4-X			
	Id.	Calc m/z $[M+2H]^{2+}$	Obs m/z $[M+2H]^{2+}$	r.t.
2	P4-2	732,2	732,2	20,0; 20,4
3	P4-3	741,5	741,4	19,0; 20,0
4	P4-4	775,2	775,1	17,2

Fig. 21 (**A**) Schematic representation of cyclization assay (**B**) Reaction kinetics and product identification via LC-MS

Peptide **P4** was synthesized via SPPS with two cysteine residues at position (i, i +6) and non-reactive residues (Gly, Ser) on a rink amide resin in order to obtain a terminal carboxamide group (**Tab. 1** Experimental Methods). Fluorescein was coupled at the N-terminal as a chromophore to increase detectability. All three alkylating agents enabled peptide cyclization though with different yields and kinetics. Di-thiol-alkylating agent **2** afforded a quantitative yield in less than an hour, while agent **3** showed a total conversion in few minutes, followed by a fast hydrolysis of succinimide ring (Morais et al., 2017). Di-thiol-alkylating agent **4** reached a maximum yield of around 60% in 30 minutes. Interestingly, di-thiol-alkylating agents **2** and **3** yielded two peptide isomers, as a consequence of conformational restriction.

In conclusion, the di-thiol-alkylating agent **2** showed the highest yield, stability, and solubility in different solvents (ACN, MeOH, DMF). Next the reactivity of di-alkylating agent **2** was tested in presence of reducing agent TCEP, often applied to avoid disulfide bridge formation in basic aqueous environment (**Fig. 22A**).

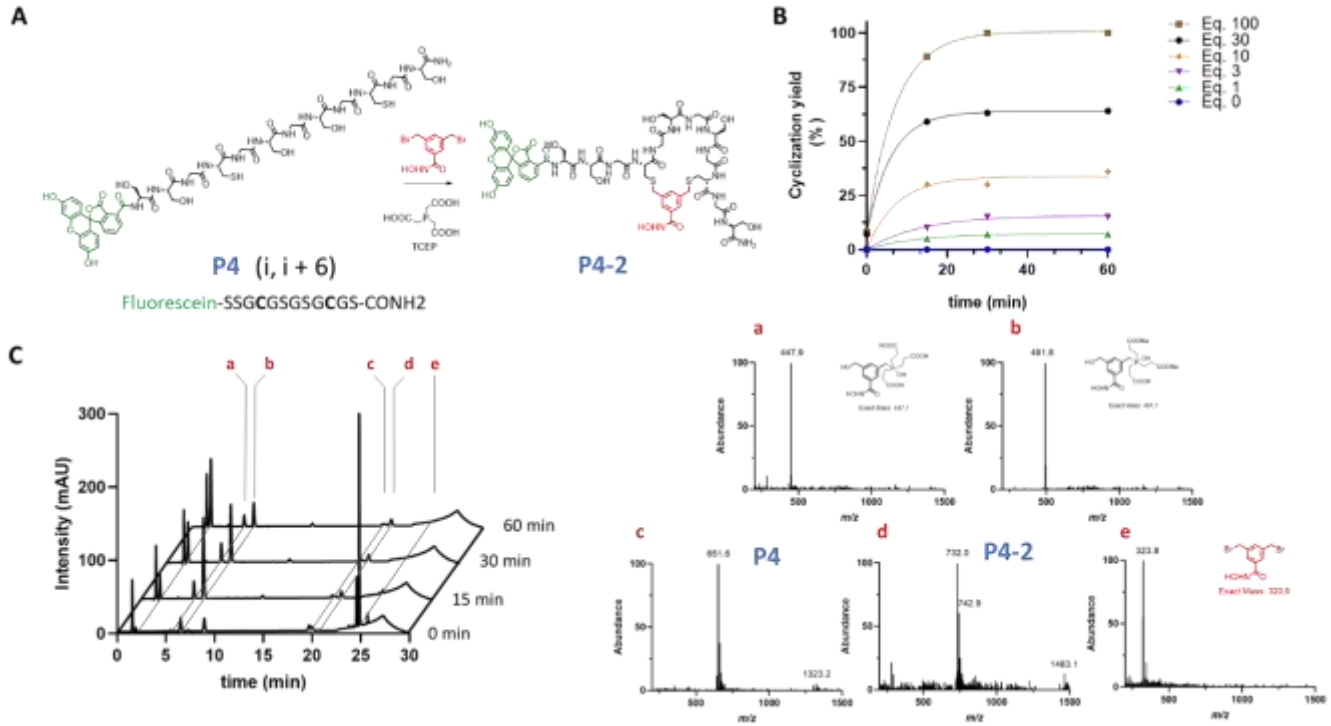

Fig. 22 (**A**) Schematic representation of cyclization assay with TCEP (**B**) Reaction kinetics with different equivalent of di-alkylating agent **2** (**C**) Chromatograms and mass spectra of cyclization assay with 30 Eq. of di-alkylating agent **2**

LC-MS analysis revealed that TCEP reacted with alkylating agent ultimately affecting with the cyclization yield (**Fig. 22C**). Quantitative peptide cyclization was achieved only by using a large excess of di-alkylating agent (100-fold molar excess) 10-fold molar excess of **2** over reducing agent. Interestingly, all the kinetics fitted well with exponential plateau curves reaching plateaus in 30 min (**Fig. 22B**). Furthermore, good stability of hydroxamate product was observed under the tested conditions.

Reaction kinetics of **2** towards thiol moiety was investigated with an alkylation assay of single amino acid. (**Fig. 23**)

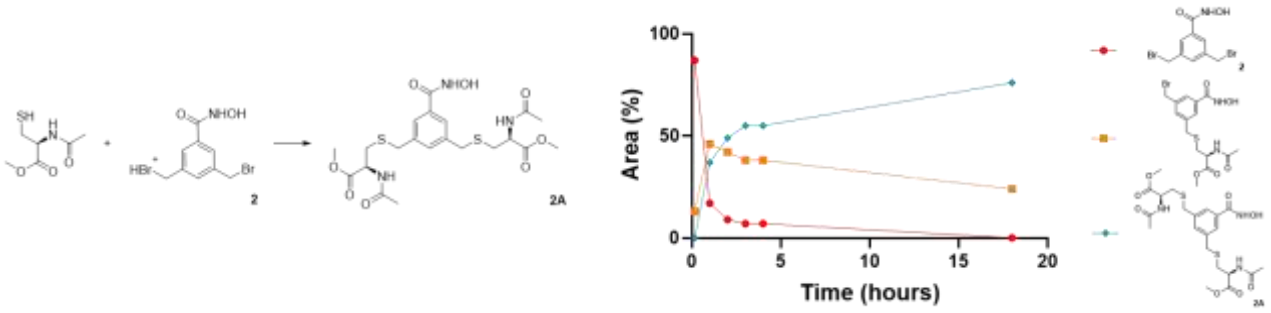

Fig. 23 Alkylation assay of **2** with methyl acetyl-D-cysteinate and reaction kinetics via LC-MS

Product **2A** was isolated and characterized to confirm the structure. The fast disappearance of alkylating agent confirmed its good reactivity and the formation of mono-alkylated intermediate and di-alkylated product **2A** was followed.

Moreover, reactivity of di-alkylating agent **2** towards peptides containing a single nucleophilic residue was tested (**Fig. 23**).

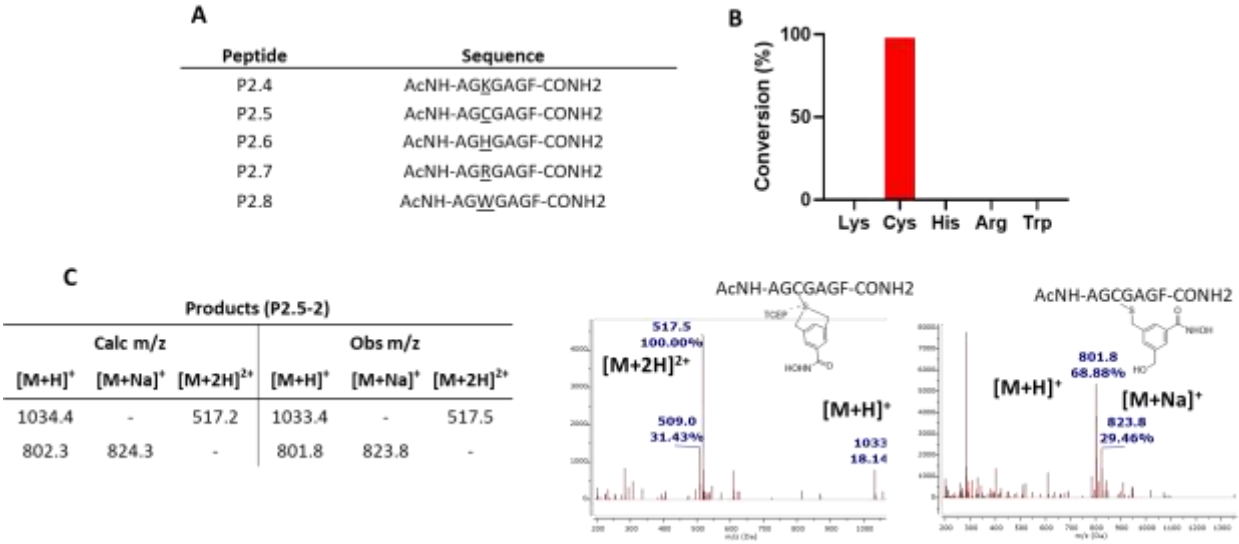

Fig. 23 (**A**) Tested peptides with single nucleophilic residue (**B**) Conversion yield of peptides with nucleophilic residue with di-alkylating agent **2** (**C**) Mass data and mass spectra of **P2.5-2** products

Peptides were synthesized via SPPS in good yields and purity without HPLC purification with a C and N-terminus protected, and with a Phe residue to increase detectability (**Tab. 1** Experimental Methods). Peptide with thiol moiety (**P2.5)** reacted completely with di-alkylating agent **2** while no reaction occurred with primary amine, imidazolium, guanidinium and indole moieties (**Fig. 23B**). Importantly, no dimer formation was observed. However, masses corresponded to di-alkylated peptides (lacking bromine plus the mass of TCEP) and hydrolysed mono-alkylated peptide were identified (**Fig. 23C**). This is in agreement with previous results reported by Peraro and co-workers (Peraro et al., 2016).

Finally, reactivity of di-alkylating agent **2**, towards peptides with two nucleophilic residues (Cys, Lys) at different space length was tested to explore the cyclization efficiency (**Fig. 24A**)

A

Peptide	Sequence	Nu position
P1.2	FmocNH-GGGCGCGGG-CONH2	(i, i + 2)
P1.3	FmocNH-GGCGGGCGG-CONH2	(i, i + 4)
P1.4	FmocNH-GCGGGGGCG-CONH2	(i, i + 6)
P1.5	FmocNH-GCGGGGGKG-CONH2	(i, i + 6)

B

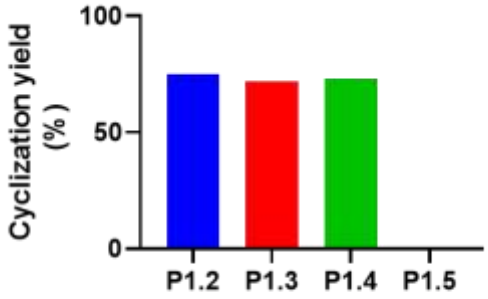

C

Id.	Calc m/z		Obs m/z	
	$[M+H]^+$	$[M+Na]^+$	$[M+H]^+$	$[M+Na]^+$
P1.2-2	1006.3	1028.3	1005.7	1027.7
P1.3-2	1006.3	1028.3	1005.6	1027.6
P1.4-2	1006.3	1028.3	1005.8	1027.7

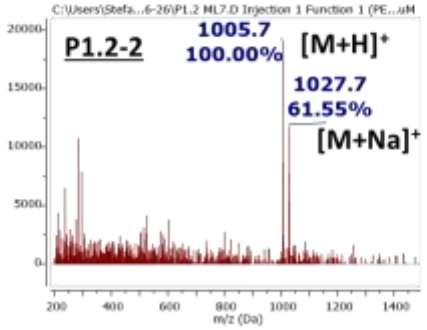

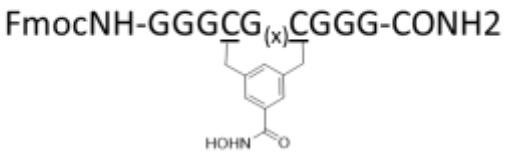

Fig. 24 (**A**) Tested peptides with two nucleophilic residues (**B**) Cyclization yield of peptides with two nucleophilic residues with di-alkylating agent **2** (**C**) Table of mass data of **P1.2-2**, **P1.3-2**, **P1.4-2** products and mass spectrum of **P1.2-2** products

Peptides were synthesized via SPPS in good yields and purity (**Tab. 1** Experimental Methods). Expected cyclic products were observed as isomers (**Fig. 24C**). Replacement of a cysteine with a lysine residue did not yield cyclisation, furthermore highlighting the selectivity of di-alkylating agent **2** to produce conformationally constrained cyclic peptides functionalized with an hydroxamic group (**Fig. 24B**). In conclusion, this strategy takes advantage of cysteine alkylation reaction and might be applied for the development of cyclic peptide with increased chemical diversity.

Synthesis and reactivity of click agents

The strategy for the introduction of the hydroxamic group via click-coupling, as zinc binding group of metallo enzymes, was previously reported by Suzuki and coworkers (Suzuki et al., 2012).
Terminal alkyne group is necessary in click chemistry for the triazole synthesis via CuAA. Toward this goal, we envision the development click agents bearing a hydroxamic group that can selectively modify and tune the properties of the displayed peptides on yeast surface and greatly increase their chemical diversity.
Molecules **5** and **6** with a terminal alkyne moiety and an hydroxamic acid group were synthesized and characterized (**Fig. 25**).

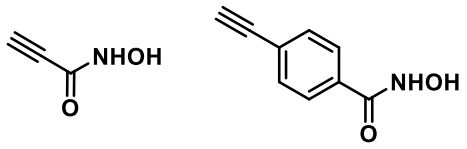

5 6

Fig. 25 azido-click coupling agents with hydroxamic moiety

They were synthesized following the strategy reported in **Fig. 26**.

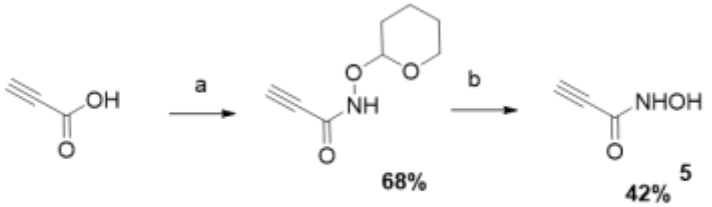

(a) NH_2OTHP, DCC, DCM, 0°C to rt (b) p-TsOH.H_2O, MeOH, rt

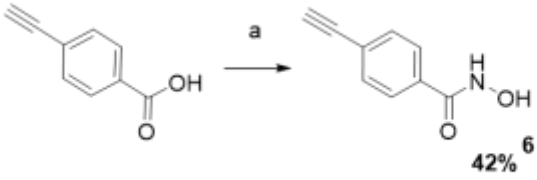

(a) i) $SOCl_2$, reflux, 4 h ii) NH_2OH. HCl, NaOH/Et_2O 1/4 v/v, 30 min, r.t.

Fig. 26 Synthesis of azido-click coupling agents **5** and **6**

Synthesis of agent **5** started with the coupling of propiolic acid and protected hydroxyl amine (NH_2OTHP) in the presence of DCC to yield the corresponding protected hydroxamate. Next, deprotection of the THP group with p-toluenesulfonic acid afforded **5**. For the synthesis of **6**, we employed a coupling in biphasic solution via acyl chloride in order to avoid a protecting group for the hydroxylamine. Similar yields were reported in literature with the protection-deprotection strategy (Suzuki et al., 2012).

Reactivity of azido-click coupling agents **5** and **6** was assessed using non canonical amino acid bearing azido group (**Fig. 27**). P-azido-L-phenylalanine and p-azidomethyl-L-phenylalanine (AzM) can be genetically incorporated into proteins using yeast (Supekova et al., 2018).

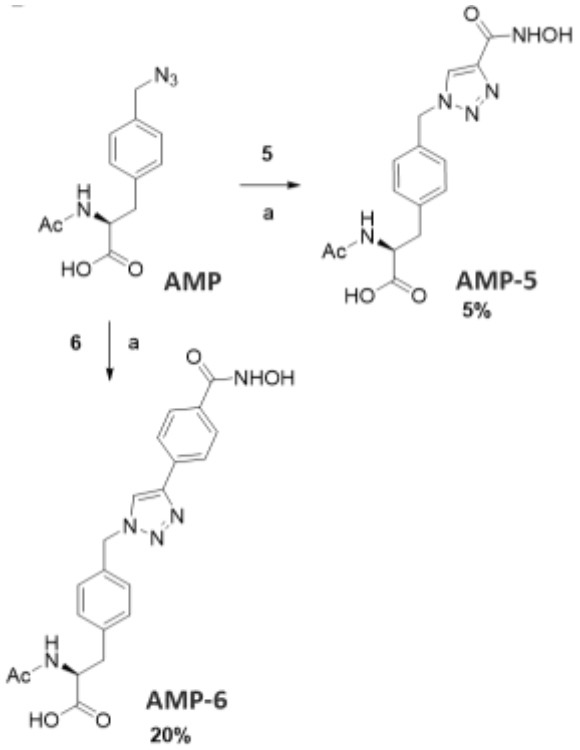

Fig. 27 Synthesis of click p-azidomethyl-L-phenylalanine derivatives

Initially, alkyne hydroxamate agents **5** and **6** were reacted with protected AMP (Acetyl p-azide-L-methyl phenylalanine) to yield product **AMP-5** and **AMP-6** (**Fig. 27**). Next, click agents were reacted with a azido group located at the N-terminus of chemically synthesized peptide, named **P3** (**Fig. 28A**).

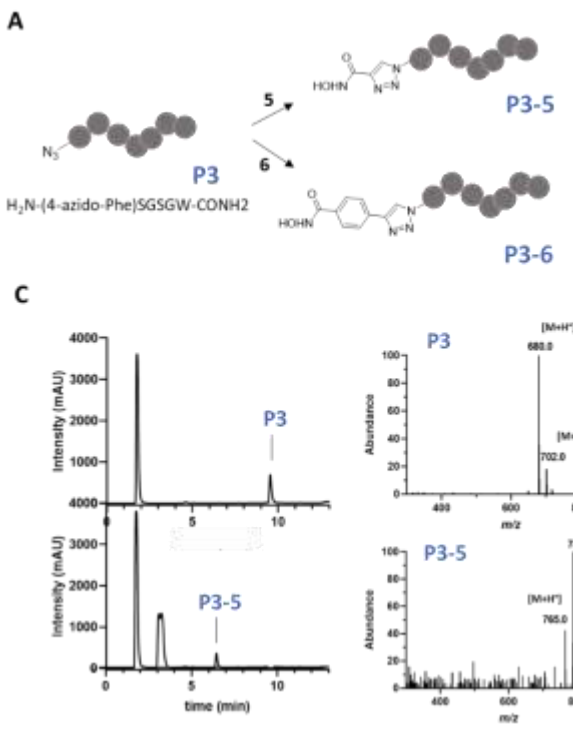

Product	Azide peptide (P3)	Click agent	Cu (II)	ascorbate	Conversion yield
Id.	Eq.	Eq.	Eq.	Eq.	%
P3-5	1	1	0.1	0.4	15
P3-5	1	50	40	70	100
P3-6	1	1	0.1	0.4	0
P3-6	1	25	40	70	100

Fig. 28 (**A**) Schematic representation of click-coupling assay with azido peptide **P3 (B**) Table with reaction stoichiometry and conversion yield of products **P3-5** and **P3-6** (**C**) Chromatograms and mass spectra of **P3** and **P3-5** (**D**) Chromatograms and mass spectra of **P3** and **P3-6**

Peptide **P3** was synthesized via SPPS with a terminal azido residue and a Trp residue to increase detectability. High purity of peptide **P3** is appreciable from reported chromatogram and protonic NMR spectrum (**Appendix**). Click-chemistry reactions of agents **5** and **6** were performed with different stoichiometries and yielded quantitative yields after few minutes of reaction (**Fig. 28B**).

2.3 Conclusions

In this chapter, the synthesis of two hydroxamate classes, thiol-alkylating agents and azido-click coupling agents, have been investigated. Based on the structure of known dithiol bis-alkylating agents, three novel di-alkylating agents bearing hydroxamic moiety (**2, 3, 4**) have been obtained and tested. Cyclizing agents showed interesting and different reactivities. Di-alkylating agent **2** was selected as the most promising functionalizing agent for reactivity and stability. Further studies investigated its reactivity in presence of a reducing agent showing a feasible one-pot strategy for a cyclization/functionalization approach under reducing conditions. Moreover, chemoselectivity towards common nucleophilic residues allows functionalization of non-protected peptide and comparable cyclization efficiency with different spacer length highlighted no ring size effect. These results showed the strength and versatility of di-alkylating agent **2** to produce cyclic peptides functionalized with hydroxamic moiety.

Finally, azido-click coupling agents were synthesized and showed good functionalizing abilities for azido amino acids and azido peptides. Click agents **5** and **6** were previously used for the generation of synthetic libraries (Suzuki et al., 2012) and here we explored their reactivity towards non-canonical amino acids and synthetic peptide for the site-specific coupling of an hydroxamic moiety. Quantitative coupling yields of azido peptides expanded their use for chemical modification via click chemistry of yeast libraries of peptides with ncAAs.

2.4 Materials and methods

Materials and instruments

All reagents were purchased from Merck and used without further purification.

Proton and carbon NRM spectra were recorded with a Bruker Avance 300 and Ascend 400 spectrometers, working at 300-400 MHz and 75-100 MHz respectively. LC-MS chromatograms and mass spectra were acquired on single quadrupole spectrometer (Agilent 6120 ESI-LC/MS Quadrupole mass) coupled to UV-Vis detector a 1260 VWD (Infinity II LC system, Agilent). System was equipped with a Zorbax Eclipse C18 column (Agilent Eclipse XDB-C18, 4.6 x 150 mm) and mobile phase was composed of eluant A (99.9% v/v H2O, 0.1% v/v TFA) and eluant B (99.9% v/v acetonitrile, 0.1% v/v TFA) with a flow rate of 1 mL/min.

LC-MS Method A: eluant A from 90 to 30 % in 26 min, detector UV at 210 nm

LC-MS Method B: eluant A from 90 to 80 % in 20 min, from 80 to 30 % in 5 min, from 30 to 90 % in 5 min, detector UV at 238 nm, inj. 20 µL, Scan 200-1500 m/z, Frag. 150.

LC-MS Method C: eluant A from 95 to 5 % in 7 min, from 5 to 95 % in 3 min, detector UV at 210 nm, inj. 20 µL, Scan 200-1000 m/z, Frag. 100.

LC-MS Method D: eluant A from 90 to 70 % in 10 min, from 70 to 30 % in 1 min, from 30 to 90 % in 2 min, detector UV at 220 nm, inj. 10 µL, Scan 300-900 m/z, Frag. 100

Preparative HPLC was performed on a 2695 HPLC coupled to UV-Vis detector a VWD (Waters 2487 Dual Dual) and an automated fraction collector. System was equipped with a Waters C18 column (OBD Prep Column, 100Å, 5 µm, 30 mm X 250 mm) and mobile phase was composed of eluant A (99.9% v/v H2O, 0.1% v/v TFA) and eluant B (99.9% v/v acetonitrile, 0.1% v/v TFA) with a flow rate of 20 mL/min.

Method: eluant A from 90 to 30 % in 16 min, detector UV at 210 nm, 20 mL/min

Synthetic procedures and characterization

4-(bromomethyl)-N-hydroxybenzamide (1)

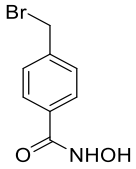

From a modified procedure reported by Amitai and co-workers (Amitai et al., 2016), thionyl chloride (5 mL, 69 mmol) was added under nitrogen atmosphere to 4-(bromomethyl)benzoic acid (1 g, 4.6 mmol) at room temperature and the suspension was refluxed for 4 h. Excess thionyl chloride was removed by vacuum distillation and the acyl chloride was used for the next step without further purification. A solution of hydroxylamine hydrochloride (0.65 g, 9.2 mmol) in NaOH 2 N (5 mL) was slowly added to a solution of acyl chloride in diethyl ether (20 mL) at 0°. Then, the reaction mixture was stirred at room temperature for 30 min, then cooled to 0 °C and 2 N HCl (4 mL) was added. The obtained solid was filtered, washed with water and dried in vacuum to give 1.06 g of a white solid (71%)

1H NMR (400 MHz, Acetone-d6) δ 10.81 (s, 1H), 8.38 (s, 1H), 7.83 (d, J = 8.4 Hz, 2H), 7.55 (d, J = 8.4 Hz, 2H), 4.68 (s, 2H). 13C NMR (101 MHz, Acetone) δ 165.39, 142.64, 133.06, 130.15, 128.24, 33.33. LRMS (ESI) m/z calcd. for $C_8H_8BrNO_2$ $[M+H]^+$: 230.0, 232.0 found $[M+H]^+$: 229.9.0, 232.0

3,5-bis(bromomethyl) benzoic acid

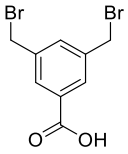

To a solution of 3,5- dimethylbenzoic acid (2.0 g, 13.3 mmol) in DCM (20 ml), N-bromo succinimide (3.556 g, 20 mmol) was added. A catalytic amount of benzoyl peroxide (0.140 g) was added and the solution stirred under reflux for 3 hours. Solid was filtered off and the solvent was removed under vacuum. The product was purified via flash silica gel chromatography (95/5/5 ciclohexane/ethyl acetate/acetic acid) and after solvent removal a white solid was obtained (0.804 g, 20%).

1H NMR (400 MHz, Acetone-d6) δ 8.06 (s, 2H), 7.82 (s, 1H), 4.74 (s, 4H). 13C NMR (101 MHz, Acetone) δ 166.61, 140.52, 134.94, 132.60, 130.94, 32.97. GC-MS: m/z calcd. for $C_9H_8Br_2O_2$: 305.9 found : 305.8

3,5-bis(bromomethyl)-N-hydroxybenzamide (2)

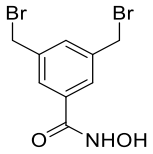

Under nitrogen, thionyl chloride (2.5 mL, 35 mmol) was added to 3,5-bis(bromomethyl) benzoic acid (0.3 g, 0.974 mmol) at room temperature and the suspension was refluxed for 4 h. Excess thionyl chloride was removed by vacuum and the acyl chloride was used for the next step without further purification. A solution of hydroxylamine hydrochloride (0.2 g, 2.878 mmol) in NaOH 2 N (2 mL) was slowly added to a solution of acyl chloride in diethyl ether (15 mL) at 0°. Then, the reaction mixture was stirred at room temperature for 30 min, then cooled to 0 °C and 2 N HCl (2.5 mL) was added. The obtained solid was filtered, washed with water and dried in vacuum to give 0.243 g of a white solid (77% yield)

1H NMR (400 MHz, Acetone-d6) δ 10.91 (s, 1H), 8.31 (s, 1H), 7.85 (d, J = 1.7 Hz, 2H), 7.72 (t, J = 1.7 Hz, 1H), 4.69 (s, 4H). 13C NMR (101 MHz, Acetone) δ 163.87, 139.47, 133.59, 132.56, 127.60, 32.21. LRMS (ESI) m/z calcd. for C9H9Br2NO2 $[M+H]^+$: 323.9 ; $[M+Na]^+$: 345.9 ; found $[M+H]^+$: 323.9 $[M+Na]^+$: 345.9.

3-(3,4-dibromo-2,5-dioxo-2,5-dihydro-1H-pyrrol-1-yl)propanoic acid

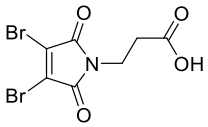

A solution of 3,4-dibromomaleic acid (0.5 g, 1.83 mmol) in acetic acid (7 mL) was refluxed for 1 hour. Then, 3-Aminopropanoic acid (0.180 g, 2.02 mmol) was added to the solution and the mixture was stirred for 3 h under reflux. Acetic acid was removed under vacuum and the product was purified by flash silica gel chromatography (9/1/0.1 DCM/MeOH/Acetic Acid) to give a white solid (0.434 g, 73%).

1H NMR (400 MHz, Acetone-d6) δ 3.87 (dd, J = 7.7, 7.0 Hz, 2H), 2.70 (dd, J = 7.7, 7.0 Hz, 2H). 13C NMR (101 MHz, Acetone) δ 171.13, 163.71, 129.23, 35.15, 31.67.

3-(3,4-dibromo-2,5-dioxo-2,5-dihydro-1H-pyrrol-1-yl)-N-hydroxypropanamide (3)

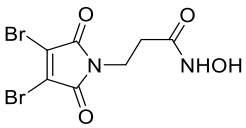

Under nitrogen, thionyl chloride (5 mL, 69 mmol) was added to 3-(3,4-dibromo-2,5-dioxo-2,5-dihydro-1H-pyrrol-1-yl)propanoic acid (0.25 g, 0.764 mmol) at 0°C and the suspension was refluxed for 2 h. Excess thionyl chloride was removed by vacuum and the acyl chloride was used for the next

step without further purification. A solution of hydroxylamine hydrochloride (0.106 g, 1.525 mmol) in NaOH 2 N (1 mL) was slowly added to a solution of acyl chloride in diethyl ether (5 mL) at 0°C. Then, the reaction mixture was stirred at room temperature for 30 min, then cooled to 0 °C and 2 N HCl (1.5 mL) was added. The obtained solid was vacuum dried and purified by flash silica gel chromatography (90/5/0.1 DCM/MeOH/acetic acid) to give a pink solid (0.098 g, 37 % yield).
1H NMR (400 MHz, Acetone-d6) δ 10.07 (s, 1H), 8.08 (s, 1H), 3.87 (t, J = 7.2 Hz, 2H), 2.48 (t, J = 6.8 Hz, 2H). 13C NMR (101 MHz, Acetone) δ 166.64, 163.69, 129.23, 35.82, 30.71. LRMS (ESI) m/z calcd. for C7H6Br2N2O4 $[M+H]^+$:342.9 $[M+Na]^+$: 364.9; found $[M+H]^+$:342.8 $[M+Na]^+$: 365.8.

3,5-bis(2-bromoacetamido)benzoic acid

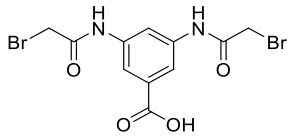

To a solution of 3,5-Diaminobenzoic acid (0.5 g, 3.3 mmol) in dry DMF (50 ml), bromoacetyl bromide (1.459 g, 7.2 mmol) and pyridine (0.572 g, 7.23 mmol) were added at at 0°C and let stir for 2 hours at room temperature. The solvent was removed under vacuum and product was purified by flash silica gel chromatography (5:5:0.2 Ethyl Acetate : Cyclohexane : Acetic Acid) to give a white solid (0.250 g, 19%).
1H NMR (400 MHz, Acetone-d6) δ 9.77 (s, 2H), 8.28 (t, J = 2.1 Hz, 1H), 8.10 (d, J = 2.0 Hz, 2H), 4.07 (s, 4H). 13C NMR (101 MHz, Acetone) δ 167.05, 165.85, 140.33, 132.67, 116.92, 115.18, 30.25 LRMS (ESI) m/z calcd. for C11H10Br2N2O4 [M+H]+: 394.9; found [M+H]+: 394.7

N,N'-(5-(hydroxycarbamoyl)-1,3-phenylene)bis(2-bromoacetamide) (4)

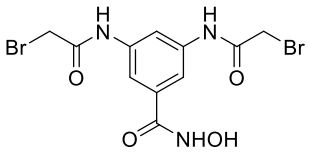

Under nitrogen, thionyl chloride (15 mL, 207 mmol) was added to 3,5-bis(2-bromoacetamido)benzoic acid (0.25 g, 0.6 mmol) at 0°C and the suspension was refluxed for 4 h. Excess thionyl chloride was removed by vacuum and the acyl chloride was used for the next step without further purification. A solution of hydroxylamine hydrochloride (0.5 g, 0.7 mmol) in NaOH 2 N (4 mL) was slowly added to a solution of acyl chloride in diethyl ether (20 mL) at 0°C. Then, the reaction mixture was stirred at room temperature for 30 min, then cooled to 0 °C and 2 N HCl (3.5

mL) was added. The obtained solid was vacuum dried and purified by flash silica gel chromatography (8/2/1 DCM /methanol /acetic acid) to give a pink solid (60 mg, 23%).

1H NMR (300 MHz, methanol-d4) δ 8.07 (s, 1H), 7.73 (s, 2H), 3.98 (s, 4H). LRMS (ESI) m/z calcd. for C11H11Br2N3O4 [M+H]+: 409.9 ; [2M+H]+: 818.8 ; found [M+H]+: 409.7; [2M+H]+: 818.3

methyl N-acetyl-S-(4-(hydroxycarbamoyl)benzyl)-D-cysteinate (1A)

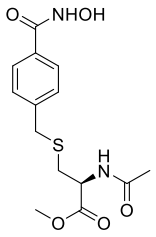

A solution of 4-(bromomethyl)-N-hydroxybenzamide **(1)** (20 mL, 500 µM) in ACN and a solution of methyl acetyl-D-cysteinate (20 mL, 500 µM) in NH_4HCO_3 buffer 30 mM pH 8 were mixed and let react at room temperature for 3 hours. Solvent was removed by lyophilization and purification by preparative RP-HPLC (Symmetry C18; Method A) followed by freeze-drying afforded 3 mg (93 %) of product as a white solid.

1H NMR (400 MHz, Acetone-d6) δ 7.80 (d, J = 7.9 Hz, 2H), 7.61 – 7.47 (m, 1H), 7.44 (d, J = 7.8 Hz, 2H), 4.69 (td, J = 7.7, 5.3 Hz, 1H), 3.84 (s, 2H), 3.67 (s, 3H), 2.93 – 2.70 (m, 2H), 1.96 (s, 3H). 13C NMR (101 MHz, Acetone) δ 171.98, 170.46, 165.67, 143.07, 131.81, 129.98, 128.00, 52.76, 52.51, 36.24, 33.65, 22.62. LRMS (ESI) m/z calcd. for C14H18N2O5S [M+H]+: 327.1; [M+Na]+: 349.1; found [M+H]+:327.1 ; [M+Na]+: 349.1

dimethyl 3,3'-(((5-(hydroxycarbamoyl)-1,3-phenylene)bis(methylene))bis(sulfanediyl))(2S,2'S)-bis(2-acetamidopropanoate) (2A)

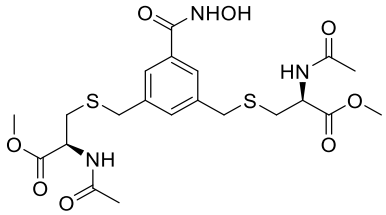

A solution of 3,5-bis(bromomethyl)-N-hydroxybenzamide **(2)** (40 mL, 300 µM) in ACN and a solution of methyl acetyl-D-cysteinate (40 mL, 500 µM) in NH_4HCO_3 buffer 30 mM pH 8 were mixed and let react at room temperature for 4 hours. Solvent was removed by lyophilization and purification by preparative RP-HPLC (Symmetry C18; Method A) followed by freeze-drying afforded 3.7 mg (60 %) of product as a white solid.

1H NMR (400 MHz, Acetone-d6) δ 7.70 (s, 2H), 7.60 (d, J = 7.6 Hz, 2H), 7.50 (s, 1H), 4.67 (td, J = 7.7, 5.9 Hz, 2H), 3.84 (s, 4H), 3.68 (s, 6H), 2.91 – 2.68 (m, 4H), 1.97 (s, 6H). 13C NMR (101 MHz,

Acetone) δ 171.94, 170.65, 165.45, 140.09, 133.65, 133.45, 127.33, 52.83, 52.55, 36.12, 33.43, 22.71. LRMS (ESI) m/z calcd. for C21H29N3O8S2 [M+H]+: 516.1; [M+Na]+: 538.1; found [M+H]+:516.2.1 ; [M+Na]+: 538.2

N-((tetrahydro-2H-pyran-2-yl)oxy)propiolamide

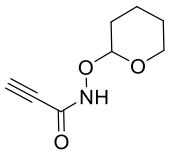

A solution of propiolic acid (300 mg; 4.28 mmol) in DCM (6 mL) was treated with tetrahydro-2H-pyran-2-yl) hydroxylamine (552 mg; 4.71 mmol) and a solution of DCC (970 mg; 4.71 mmol) in DCM at 0 ° C. The reaction mixture was kept under stirring for 3 hrs at room temperature. Then, filtration was carried out on celite and solution concentrated under vacuum. The product was purified with FSGC (EtOAc /Petroleum ether 2/3) as a yellow oil (493.3 mg, 68% yield).
1H NMR (400 MHz, Chloroform-d) δ 9.28 (s, 1H), 5.02 – 4.93 (m, 1H), 4.01 – 3.86 (m, 1H),3.70 – 3.56 (m, 1H), 2.89 (s, 1H), 1.86 – 1.71 (m, 3H), 1.69 – 1.46 (m, 3H). 13C NMR (101 MHz, CDCl3) δ 149.97, 102.85, 76.07, 74.66, 62.72, 27.91, 24.93, 18.45. LRMS (ESI) m/z calcd. for C8H10NNaO3 $[M+H]^+$: 192.1 found $[M+H]^+$: 192,1

N-hydroxypropiolamide (5)

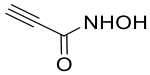

p-toluenesulfonic acid monohydrate (51.63 mg; 0.30 mmol) was added to a solution of N-((tetrahydro-2H-pyran-2-yl)oxy)propiolamide (457 mg; 2.70 mmol) and MeOH (20 mL). The reaction was kept under stirring for 4 hrs at room temperature. Then, the product was purified with FSGC (EtOAc / Petroleum ether 3/1 v/v) as a pale yellow solid (110 mg; yield 48%).
1H NMR (400 MHz, Acetone-d6) δ 10.59 (s, 1H), 8.57 (s, 1H), 3.63 (s, 1H). 13C NMR (101 MHz, Acetone) δ 149.83, 75.78, 75.27. LRMS (ESI) calcd. for C3H3NO2 $[M+H]^+$: 86,02 m/z, found $[M+H]^+$: 86,1 m/z.

4-ethynyl-N-hydroxybenzamide (6)

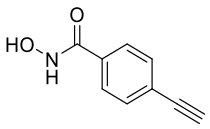

The procedure has been adapted from the literature (doi.org/10.1021/jm300837y). In a reaction flask containing 4-ethynylbenzoic acid (500 mg; 3.4 mmol) with ice bath, was added thionyl chloride (5

mL). The reaction was kept under reflux for 2 hours. The solvent was removed under vacuum and diethylether (50 mL) was added. At 0 ° C, a solution of hydroxylamine hydrochloride (475 mg; 6.8 mmol) in NaOH (2 M; 5 mL) was added and mixed for 30 min at room temperature. Then, a cold solution of HCl (2 M, 4 mL) was added and the product filtration off and dried under vacuum. The product was purified with FSGC (DCM / MeOH 9/1 v /v 1% acetic acid) and a red solid was obtained (231 mg; yield 42%).

1H NMR (400 MHz, DMSO-d6) δ 11.28 (s, 1H), 9.08 (s, 1H), 7.74 (d, J = 7.4 Hz, 2H), 7.54 (d, J = 7.6 Hz, 2H), 4.34 (s, 1H). 13C NMR (101 MHz, DMSO) δ 163.33, 132.87, 131.70, 127.14, 124.36, 82.82, 82.75. LRMS (ESI) calcd. for C9H7NO2 $[M+H]^+$: 162,0 m/z, found $[M+H]^+$: 162,0 m/z.

(S)-2-acetamido-3-(4-(azidomethyl)phenyl)propanoic acid (AMP)

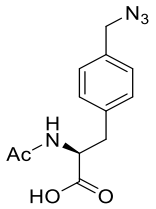

(S)-2-amino-3-(4-(azidomethyl)phenyl)propanoic acid (250 mg, 1.13 mmol) in a 2 mL solution (1 mL DMF and 1 mL H_2O) was treated with acetic anhydride (139 mg, 1.36 mmol) and triethylamine (137 mg, 1.35 mmol) were added. The solution was stirred at room temperature overnight. Then, DMF was removed under reduced pressure and the water removed by lyophilization.

LRMS (ESI) Calcd. for C12H14N4O3, $[M+Na]^+$: 285,1 *m/z*; found $[M+Na]^+$: 285,1 *m/z*.

(S)-2-acetamido-3-(4-((4-(hydroxycarbamoyl)-1H-1,2,3-triazol-1-yl)methyl)phenyl)propanoic acid (AMP-5)

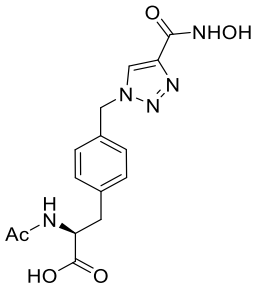

To a solution of (S)-2-acetamido-3-(4-(azidomethyl)phenyl)propanoic acid (161 mg, 0.614 mmol), N-hydroxypropiolamide (52 mg, 0.322 mmol), and BTTES (30 mg, 10 mol %) in MeOH (5 mL) was added a solution of $CuSO_4 \cdot 5H_2O$ (15 mg, 10 mol %) and sodium ascorbate (62 mg, 50 mol %) in water (5 mL). The reaction mixture was stirred for 4 h at room temperature. MeOH was removed under reduced pressure and the water removed by lyophilization. Purification by preparative RP-

HPLC (Symmetry C18; Method A: 5.2 min) and freeze-dry gave 42 mg (21 %) of product as a pale-green solid.

1H NMR (400 MHz, DMSO-d6) δ 11.25 (s, 1H), 8.57 (s, 1H), 8.16 (s, 1H), 8.14 (s, 1H), 7.30 – 7.15 (m, 4H), 5.60 (s, 2H), 4.39 (td, J = 8.8, 4.9 Hz, 1H), 3.07 – 2.78 (m, 2H), 1.77 (s, 3H). 13C NMR (101 MHz, DMSO) δ 173.48, 169.71, 138.37, 134.17, 129.95, 128.39, 126.78, 53.79, 53.26, 36.83, 22.79. LRMS (ESI) m/z calcd. for $C_{15}H_{17}N_5O_5$ $[M+H]^+$: 348.1; $[M+Na]^+$: 370.1; $[2M+Na]^+$: 717.2; found $[M+H]^+$: 348,1; $[M+Na]^+$: 370.2; $[2M+Na]^+$: 717.1

(S)-2-acetamido-3-(4-((4-(4-(hydroxycarbamoyl)phenyl)-1H-1,2,3-triazol-1-yl)methyl)phenyl)propanoic acid (AMP-6)

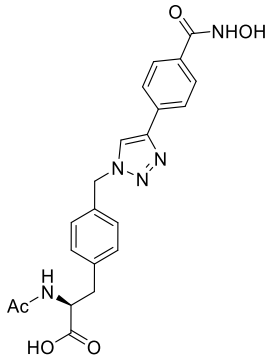

To a solution of (S)-2-acetamido-3-(4-(azidomethyl)phenyl)propanoic acid (81 mg, 0.31 mmol), 4-ethynyl-N-hydroxybenzamide (50 mg, 0.31 mmol), and BTTES (15 mg, 10 mol %) in MeOH (4 mL) was added a solution of $CuSO_4 \cdot 5H_2O$ (7.7 mg, 10 mol %) and sodium ascorbate (31 mg, 50 mol %) in water (4 mL). The reaction mixture was stirred for 4 h at room temperature. MeOH was removed under reduced pressure and the water removed by lyophilization. Purification by preparative RP-HPLC (Symmetry C18; Method A: 8.4 min) and freeze-dry gave 6 mg (5 %) of product as a pale-pink solid.

1H NMR (400 MHz, DMSO-d6) δ 11.24 (s, 1H), 8.71 (s, 1H), 8.17 (s, 1H), 8.15 (s, 1H), 7.87 (dd, J = 42.9, 8.0 Hz, 4H), 7.34 – 7.16 (m, 4H), 5.62 (s, 2H), 4.39 (ddd, J = 9.3, 7.9, 4.9 Hz, 1H), 3.09 – 2.77 (m, 2H), 1.77 (s, 3H). 13C NMR (101 MHz, DMSO) δ 173.51, 169.71, 146.33, 138.30, 134.42, 133.71, 129.96, 128.30, 125.43, 122.76, 53.82, 53.32, 36.84, 22.80. LRMS (ESI): m/z calcd. for $C_{21}H_{21}N_5O_5$ $[M+H]^+$: 424.2; $[M+Na]^+$: 446.1; $[2M+Na]^+$: 869.3; found $[M+H]^+$: 424.2; $[M+Na]^+$: 446.1; $[2M+Na]^+$: 869.2

P3

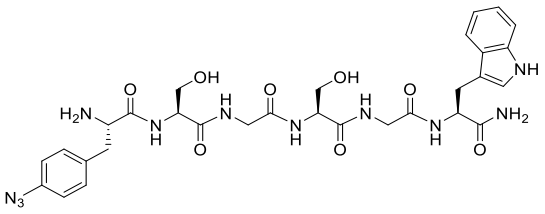

Synthesis was performed according to the SPPS procedure. Purification was conducted by preparative RP-HPLC (Symmetry C18; Method A: 9.4 min) and freeze-dry gave 4,4 mg (0,0065 mmol; yield 22%) of product as a white solid.

1NMR (400 MHz, Deuterium Oxide) δ 7.57 (dt, *J* = 8.0, 1.1 Hz, 1H), 7.41 (dt, *J* = 8.1, 1.0 Hz, 1H), 7.23 – 7.03 (m, 5H), 7.00 – 6.86 (m, 2H), 4.56 (dd, *J* = 8.0, 6.0 Hz, 1H), 4.44 (t, *J* = 5.6 Hz, 1H), 4.37 (t, *J* = 5.2 Hz, 1H), 4.14 (t, *J* = 7.2 Hz, 1H), 4.02 – 3.79 (m, 3H), 3.78 – 3.68 (m, 5H), 3.28 – 3.05 (m, 2H), 3.03 (d, *J* = 7.3 Hz, 2H).

LRMS (ESI) calcd. for C30H37N11O8 $[M+H]^+$: 680,3 *m/z,* found $[M+H]^+$: 679,9 *m/z.*

Solid phase Peptide synthesis

Peptides were synthesized on the MultiPep RSi synthesizer (Intavis, Germany) by standard Fmoc solid-phase chemistry on a Rink Amide AM resin (batch size 0.01 mmol scale, 100 - 200 mesh loading 0.52 mmol/g). Fmoc-protected amino acids, Rink Amide AM resin and PyBOP were purchased from Novabiochem (Merck millipore, Italy). Coupling step was carried out twice for each amino acid (6 eq., 0.4 M solution in DMF) using PyBOP (5.5 eq, 0.4 M solution in DMF)-NMM (9 eq, 4 M solution in DMF) coupling system. Fmoc groups were removed using a 20% (v/v) solution of piperidine in DMF. The final peptide was deprotected and cleaved from the resin using a TFA/thioanisole/water/anisole/octanditiol mixture (90/2.5/2.5/2.5/2.5 v/v) for 3 hours at room temperature under vigorous shacking. The peptide was precipitated with cold diethyl ether (40 ml), resuspended and washed with diethyl ether (20 ml x 2). Finally, the purity of the crude peptide was analysed by analytical RP-HPLC using a Vydac C18 column, a linear gradient with a mobile phase composed of eluant A (99.9% v/v H2O, 0.1% v/v TFA) and eluant B (99.9% v/v acetonitrile, 0.1% v/v TFA) and a flow rate of 1 mL/min.

If necessary, crude peptides were dissolved in acetonitrile/water (1:1) and purified by preparative reversed-phase HPLC (Method A) on Waters Prep LC 4000 system with eluant A (99.9% v/v H2O, 0.1% v/v TFA) and eluant B (99.9% v/v acetonitrile, 0.1% v/v TFA) with a linear gradient from 0 to 50% over 30 min flow rate of 20 mL/min. Finally, the peptides were freeze-dried.

Name	Sequence (N-C)	Mass Calcd. (Da)	Mass obs. (Da)	Mass (mg)	Yield (%)	Purity (%)
P4	Fluorescein-SSGCGSGSGCGS-CONH2	1301.4	651.6$[M+2H]^+$	15	65	>95
P2.4	AcNH-AGKGAGF-CONH2	647.3	648.3$[M+H]^+$	6	90	>95
P2.5	AcNH-AGCGAGF-CONH2	622.3	623.2$[M+H]^+$	9	88	>95
P2.6	AcNH-AGHGAGF-CONH2	656.3	657.3$[M+H]^+$	9	85	>95
P2.7	AcNH-AGRGAGF-CONH2	675.3	676.3$[M+H]^+$	9	92	>95
P2.8	AcNH-AGWGAGF-CONH2	705.3	706.3$[M+H]^+$	10	93	>95
P1.2	FmocNH-GGGCGCGGG-CONH2	844.3	844.7$[M+H]^+$	20	80	>95
P1.3	FmocNH-GGCGGGCGG-CONH2	844.3	844.7$[M+H]^+$	21	80	>95
P1.4	FmocNH-GCGGGGGCG-CONH2	844.3	844.7$[M+H]^+$	21	80	>95
P1.5	FmocNH-GCGGGGGKG-CONH2	869.3	870.2$[M+H]^+$	24	85	>95
P3	H_2N-(p-AFN)SGSGW-CONH2	679.3	680.0$[M+H]^+$	4	22	>95

Tab. 1 Name and properties of synthetic peptide via SPPS

Reactivity assays

Cyclization assay

Alkylating agent 2, 3 or 4 (final conc. 150 µM, 3 Eq.) was solvated in MeOH and mixed with di-thiol peptide P4 (final conc. 50 µM, 1 Eq) in 90% v/v NH_4HCO_3 buffer 50 mM pH 8, 5mM EDTA, 10 % v/v MeOH, rt. Reaction progress was monitored via RP-HPLC-MS (Method B) at time points 0, 30, 60, 120 minutes and cyclization yield was calculated on normalized area of identified products.

Alkylating agent	Cyclic peptide			
	Id.	Calc m/z $[M+2H]^{2+}$	Obs m/z $[M+2H]^{2+}$	r.t. (min)
2	P4-2	732,2	732,2	20,0; 20,4
3	P4-3	741,5	741,4	19,0; 20,0
4	P4-4	775,2	775,1	17,2

Alkylation assay

A solution of 4-(bromomethyl)-N-hydroxybenzamide **(1)** (final conc. 500 µM) or 3,5-bis(bromomethyl)-N-hydroxybenzamide **(2)** (final conc. 300 µM) in ACN was mixed with a solution of methyl acetyl-D-cysteinate (final conc. 500 µM) in NH_4HCO_3 buffer 30 mM pH 8 1/1 v/v.

Reaction progress was monitored via RP-HPLC-MS (Method C) at time points 0, 1, 2, 3, 4, 18 hours and yield was calculated as ratio percent of product area and the sum of all peak areas.

Cyclization assay with reducing agent

Reaction of peptide P4 (10 µM, 1 Eq) with alkylating agent **2** (0, 1, 3, 10, 30, 100 Eq.) and TCEP (100 µM, 10 Eq) was performed in 90% v/v NH_4HCO_3 buffer 50 mM pH 8, 5mM EDTA, 10 % v/v ACN, rt. Reaction mixture (100 µL) was quenched with 10 µL HCl 1 M and analysed via RP-HPLC-MS (Method B) at time points 0, 15, 30, 60 minutes and cyclization yield was calculated on normalized area of identified product. Points were fitted with an exponential plateau curve: Y= YM – (YM-Y0)*exp (-K*x)

Reactivity assay with single nucleophilic residue

Peptide P2.X (300 µM, 1 Eq), TCEP (300 µM, 1 Eq), alkylating agent **2** (750 µM, 2.5 Eq.) were let react in 90% v/v NH_4HCO_3 buffer 30 mM pH 8, 10 % v/v ACN, at room temperature for 1h. Then, reaction mixtures were analysed via RP-HPLC-MS (Method B) and conversion yield was calculated on normalized area of starting peptide.

Reactivity assay with two nucleophilic residues

Peptide P1.X (300 µM, 1 Eq), TCEP (300 µM, 1 Eq) alkylating agent **2** (750 µM, 2.5 Eq.) were let react in 90% v/v NH_4HCO_3 buffer 30 mM pH 8, 10 % v/v ACN, at room temperature for 1h. Then, reaction mixtures were analysed via RP-HPLC-MS (Method B) and cyclization yield was calculated on normalized area of identified product.

Click-coupling assay with azido peptide

To a solution of peptide **P3** (650 µM, 1 Eq.) in MilliQ water, a freshly prepared solution of **5** in MilliQ water (1 or 50 Eq.) or **6** in DMSO (1 or 25 Eq.) was added. Then, solutions of freshly prepared $CuSO_4 \cdot 5H_2O$ and sodium ascorbate in MilliQ water were added and mixed. Reaction kinetics was monitored via LC-MS analysis (Method D).

P3-5 LRMS (ESI) Calcd. C33H40N12O10 $[M+Na]^+$: 787,3 m/z, ; found $[M+Na]^+$: 786,9 m/z.

P3-6 LRMS (ESI) Calcd. C39H44N12O10 $[M+Na]^+$: 840.3 m/z, ; found $[M+Na]^+$: 840.9 m/z.

Chapter 3
Production of ADAM-17

3.1 Introduction

ADAM-17 is the most investigated member of ADAM family because it is involved in the ectodomain shedding activity (Arribas and Borroto, 2002) of several cytokines, such as tumor necrosis factor- α (TNF-α), a key player in inflammatory diseases (Feldmann and Maini, 2008; Georgiadis and Yiotakis, 2008). Indeed ADAM-17 was originally identified as TNF-α Converting Enzyme, or TACE (Moss et al., 1997). ADAM-17, like other members of the family, is expressed as inactive precursor. Further maturation occurs via secretory pathway with concomitant furin cleavage. Its structure is composed of multiple domains. From N- to C-terminal, ADAM-17 includes a prodomain, metalloproteinase, disintegrin-like, cysteine-rich, transmembrane and a cytoplasmic tail (**Fig. 29**).

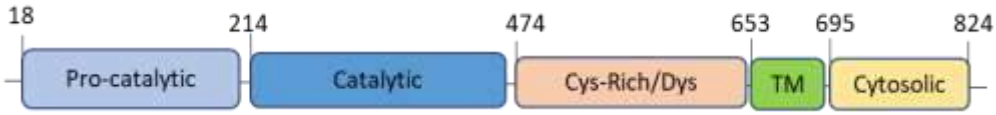

Fig. 29 Schematic representation of human ADAM-17 domains

Its structure was first determined in 1998 revealing that the catalytic cleft is characteristic of metzincin family (Maskos et al., 1998). Between the amino terminal and carboxyl terminal lobe along α-helix α4, there is a consensus HEXXHXXGXXH sequence. Zinc ion is coordinated by three histidine residues. A glutamate residue is involved, together with a water molecule, to the hydrolysis mechanism. Moreover, a conserved loop, called Met-turn, is present at level of carboxyl terminal lobe (Seegar and Blacklow, 2019). ADAM-17 is a sheddase of an extremely broad range of substrates: Pro-TNF- α, Pro-TGF- α, Pro-Amphiregulin, Pro-HB-EGF, Pro-epiregulin, Neuregulin, Epigen, P75 TNF Receptor, P55 TNF Receptor, IL-1 Receptor-II, Amyloid precursor protein, Delta-like ligand-1 Notch1,TRANCE/RANKL, Kit ligand-1 and -2 L-selectin, Neurotrophin receptor p75NTR, TrkA neurotrophin receptor ErbB4/HER4, CD44, CD40, CD30, Growth hormone receptor, L1-CAM,VCAM-1, IL6 Receptor, Cellular prion protein, CX3CL1/Fractalkine, LAG-3, Colony stimulating factor-1, Nectin-4, ALCAM, Desmoglein-2 Klotho, Vacuolar protein sorting Vps10-p, N-CAM, PTP-LAR Collagen XVII, Pre-adipocyte factor-1, ACE2/ SARS-CoV Receptor, Semaphorin 4D, neuronal pentraxin receptor, MHC-class I-related chain A/B. Furthermore, ADAM-17 is linked to EGFR signalling (Edwards et al., 2009). It is an upstream regulator of one of the most important signalling pathways in vertebrates, since EGF and related ligands (HB-EGF, TGF-α, epiregulin, amphiregulin and betacellulin) are all membrane-associated molecules (Seegar and Blacklow, 2019). ADAM-17 is a vital enzyme that carry out critical functions in mammalian

development, coordinating immune and inflammatory responses. From knockout mice experiments, effects of perinatal lethality were observed as a cause of heart defects and insufficient epithelial tissue maturation (Edwards et al., 2009).

In this chapter, the evaluation of different ADAM-17 constructs, their expression and characterization are presented and discussed.

3.2 Results and Discussion

Construct evaluation

Four constructs (M-114, M-115, M-116, M-117), encoding the procatalytic and catalytic domains of human ADAM-17 (18-474) were generated to evaluate the expression levels and catalytic activity of the expressed proteins (**Fig. 30**). Expression yield and activity are necessary parameters to produce the active target in a large scale for screening purpose.

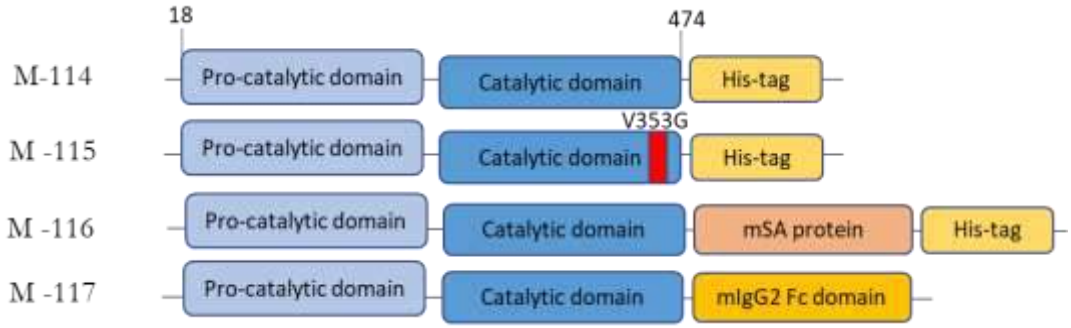

Fig. 30 Schematic representation of expression constructs encoding of human ADAM-17: pro catalytic, catalytic domain, HysTag (M-114), pro catalytic, catalytic domain with mutation V353G, HysTag (M-115), pro catalytic, catalytic domain, mouse serum albumin, HysTag (M-116), pro catalytic, catalytic domain, monoclonal Anti-Human IgG2 Fc receptor (M-117).

Pro-catalytic domain is essential for the secretion and activation of functional ADAM-17. Activation and maturation occur via the secretory pathway with concomitant furin cleavage between pro-catalytic and catalytic domain. Furthermore, prodomain includes a consensus cysteine switch motif (PKVCGY[186]), which act as an inhibitor by ligating the zinc ion in the catalytic site (Milla et al., 1999). To limit the metalloprotease autoproteolysis that spontaneously occurs at the Y352–V353 site present within the flexible loop located in close proximity to the P-side of the active site, we generated the mutant (M-115, V353G) (Ingram et al., 2006). All the constructs include an affinity tag in order to allow the purification via affinity column. Finally, constructs bearing foreign protein domains, such as serum albumin or Fc antibody fragments for construct M-116 and M-117, respectively, were generated to enhance solubility and stability.

Conditioned media of transfected CHO cells after four days were analysed with SDS-PAGE, **Fig. 31B**, and activity assay (**Fig. 31C**)

A

construct	MW	Epsilon
-	KDa	M^{-1} cm $^{-1}$
M-114	53,5	54968
M-115	53,5	54968
M-116	119,9	94373
M-117	79,4	84668

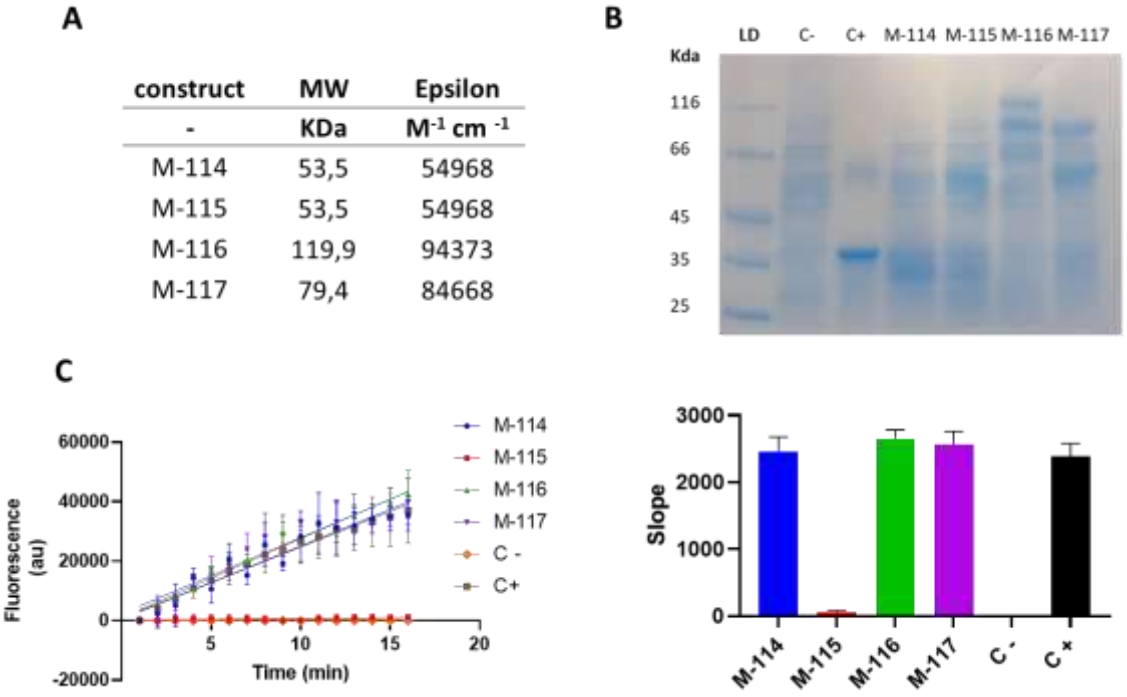

Fig. 31 (**A**) Molecular weights and molar attenuation coefficient of expression constructs (**B**) comassie-stained SDS-PAGE of conditioned media (**C**) FRET-based catalytic activity and slope of conditioned media

Slightly appreciable bands for all the constructs at the expected molecular weights were detected (**Fig. 31B**). Except of mutant of M-115, all the clones M-114, M-116, M-117 showed comparable activity (**Fig. 31C**). Construct M-114 was selected as a candidate to produce the target in a larger scale.

Kinetics of protein expression

The kinetics of ADAM-17 expression (construct M-114) was evaluated from zero to six days post-transfection in CHO cells. Expression levels in the media were evaluated via SDS-PAGE (**Fig.32 A**) and FRET-based catalytic assay (**Fig. 32B)**.

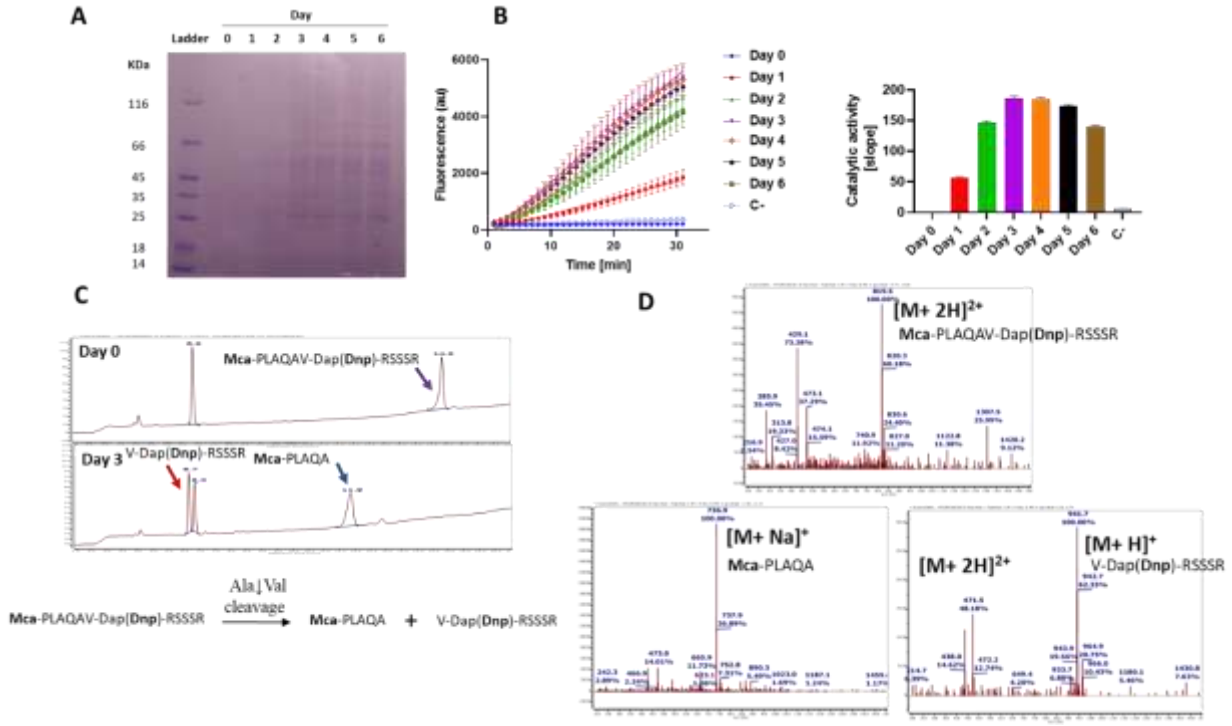

Fig. 32 (**A**) Coomassie-stained SDS-PAGE of conditioned media at different time points (**B**) FRET-based catalytic activity and slope of conditioned media at different time points (**C**) LC-MS chromatograms and (**D**) mass spectra of conditioned media at day 0 and day 3.

Activity assay of cell media containing M-114 at different time points revealed differences on the hydrolysis rate of the fluorogenic substrate. (**Fig. 32B**) Medium of non-transfected cells (negative control) confirmed absence of cleavage. Interestingly, the activity plot showed the fluorescence slope reached a maximum at day three. Assuming that the catalytic activity is directly dependent on the enzyme concentration, we observed a maximum of expression levels. However, the activity reduction can be explained by events of enzyme spontaneous inactivation or degradation.

Finally, samples of activity assay, at day zero and day three post-transfection, were analyzed by mass analysis confirming that cleavage products were formed only in the presence of the metalloprotease (**Fig. 32C**). Moreover, the substrate was appropriately cleaved at the Ala-Val bond of the fluorogenic peptide, confirming the proteolysis site of pro TNF-α (**Fig. 32D**). Proteolysis of Ala76-Val77 peptide bond is specific and necessary for TNF-α release of 26-kDa membrane-bound pro TNF-α by ADAM-17 metalloprotease (Hoth et al., 2007).

Large scale production of ADAM-17$^{18-474}$

DNA construct M-114, encoding ADAM-17 (18-474) plus the C-terminal linker Gly-Ser-$(His)_6$, was used to produce the recombinant protein, according to the protocol of Maskos and colleagues (Maskos et al., 1998).

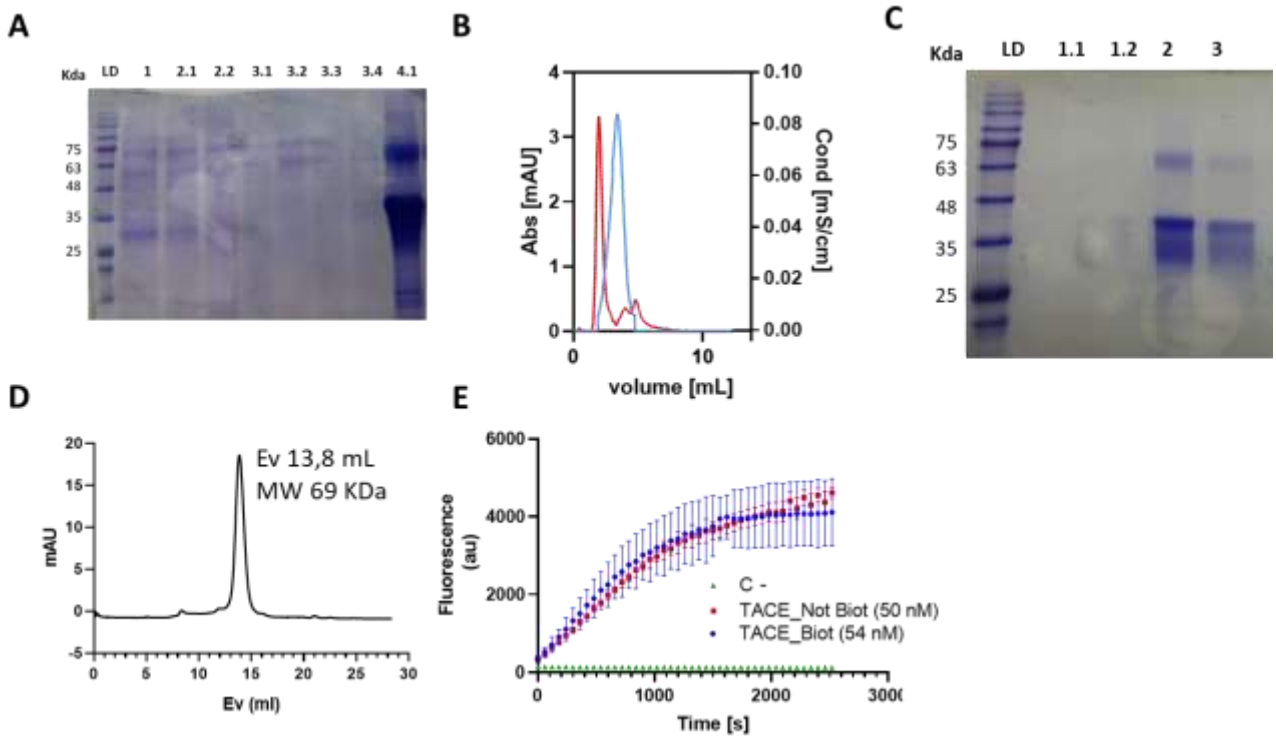

Fig. 33 (**A**) Coomassie-stained SDS-PAGE of affinity purification steps: (1) supernatant (2) flow through (3) wash (4) eluate (**B**) desalting chromatogram (**C**) d) Coomassie-stained SDS-PAGE of (1) flow through via concentrator (2) after biotinylation (3) after SEC (**D**) SEC chromatogram (E) Activity assay of biotinylated and non-biotinylated protein

The metalloprotease was expressed in CHO cells and purified using metal-affinity chromatography (**Fig. 33A**). The fractions were visualised by SDS-PAGE and eluate fractions afforded the full-length (65 kDa) and the cleaved protein (39 kDa). Observed molecular weights are in accordance with theorical 55 kDa plus glycosylation and 30 kDa plus glycosylation, as previously reported (Milla et al., 1999).

Then, desalting step was performed to remove the excess of imidazole (**Fig. 33B**) and the biotinylating step was performed using a 25-fold molar excess of biotinylating reagent followed by size exclusion gel chromatography. Protein biotinylation is essential for enzyme immobilization on magnetic beads during the screening assay. The protein was concentrated with a concentrator affording a total of 12 mg and a good expression yield of 12 mg/L, in accordance with Hoth and coworkers (Hoth et al., 2007). Finally, final product conserved the expected molecular weight (**Fig. 33C**), however, as indicate by analytical gel permeation chromatography, the protein in solution appeared in a dimeric form (**Fig. 33D**). More importantly, we observed no alteration of catalytic activity subsequently at the biotinylating step (**Fig. 33E**). The obtained biotinylated ADAM-17 (18-474) target will be further used for screening assays.

3.3 Conclusions

In this chapter, the recombinant production of metalloprotease target ADAM-17$^{18-474}$ has been described. Firstly, expression and analysis of four constructs were performed in small scale to identify the most suitable protein for large scale production.

Construct M-114, encoding for procatalytic and catalytic domains, was selected and its kinetics of protein expression was further explored to maximize the yield. Moreover, catalytic activity showed the correct folding of the active site, an important parameter for the screening study, and mass analysis confirmed the specific cleavage site of peptide substrate.

Finally, target protein was expressed, biotinylated and purified in a large scale affording the desired amount for yeast display assays. A satisfactory expression yield was obtained and protein biotinylation was necessary for further enzyme immobilization on magnetic beads during the screening steps.

3.4 Materials and methods

Small scale protein expression

The expression constructs encoding for human ADAM-17 (18-474):

- pro catalytic, catalytic domain, His-Tag (M-114),
- pro catalytic, catalytic domain with mutation V353G, His-Tag (M-115),
- pro catalytic, catalytic domain, mouse serum albumin, His-Tag (M-116),
- pro catalytic, catalytic domain, human Fc receptor (M-117)

were transfected in ExpiCHO cells (Thermo Fisher Scientific). The culture media (10 mL) was incubated at 30°C for four days. Then, cells were harvested by centrifugation (6000 g, 20 min at 4 °C), removed by filtration (0,2 µm, RC filter), the medium freezed and stored at -80 °C until further processing. Conditioned media were analysed with SDS-PAGE analysis and FRET-based assay.

Activity assay

From a modified method reported by Wong and coworkers (Wong et al., 2016), catalytic domain of ADAM-17 was used as positive control (42 nM). Conditioned media from un-transfected cells was used as a negative control. The enzymatic activity of media was evaluated in the presence of fluorogenic peptide substrate (Mca-Pro-Leu-Ala-Gln-Ala-Val-Dap(Dnp)-Arg-Ser-Ser-Ser-Arg-NH_2, 48 µM, 4031302, Bachem) in 96 well plates (Nunc maxisorp) with a plate reader (Tecan Infinite

M200). The assay was run in triplicate in 25 mM Tris pH 8, 2.5 μM $ZnCl_2$, and 0.1% v/v Brij-35. Substrate solution was added to the 1:10 diluted solution of cell media, and the plate was read every minute for 15 min at 37 °C. Excitation and emission wavelengths were 355 and 405 nm, correspondingly.

Kinetics of protein expression

Transfected CHO cells were grown in ExpiCHO™ Expression Medium (Thermofisher) for 6 days, and aliquots (1 mL) were taken every day for SDS-PAGE analysis and FRET-based assay. Secreted ADAM-17 was detected using coomassie-stained SDS-PAGE analysis. Activity assay was performed following the conditions reported above. Furthermore, sample solutions (10 μL, day 0 and day 3) of activity assay were analysed via RP-HPLC on an Agilent 1260 Infinity pump at 1/mL with a ZORBAX Eclipse XDB-C18 column and UV detector (220 nm) and Quadrupole LC/MS 6120. Method A: H_2O/TFA (0.1%)– CH_3CN/TFA (0.1%) from 90 to 50 % in 15 min.

Large scale expression, biotynilation, purification and characterization

ExpiCHO™ cells were grown in 1 L of ExpiCHO™ Expression Medium at 31 °C and 5% CO_2 and shacked at 180 rpm. The culture was transfected with PEI MAX (15 ug/mL) and plasmid DNA (3 ug/mL). After 4 days, the cells were removed by centrifugation (6000 g, 20 min at 4 °C) and filtration (0.2 μm). Supernatant was diluted 1/10 v/v with buffer (50 mM HEPES, 0.3 M NaCl, pH 8) and loaded on nickel Sepharose column (Excel GE Healthcare) which was first equilibrated against buffer A (50 mM HEPES, 0.3 M NaCl, pH 8). First, the column was washed with buffer B (50 mM HEPES, 300 mM NaCl, 25 mM imidazole, pH 8) in order to remove unspecific proteins. Then, the protein was eluted with buffer C (50 mM HEPES, 300 mM NaCl, 250 mM imidazole, pH 8). The excess of imidazole was removed with a desalting column (Hiprep 26/10 Desalting) on ÄKTA pure chromatography system previously equilibrated with 50 mM HEPES, 300 mM NaCl, 2.5 uM ZnCl2, 0,005% Brij-35 (v/v), pH 8. Fractions containing the protein were collected and stored overnight with Complete Mini EDTA-free Protease Inhibitor Cocktail (Roche). The product was concentrated to a final concentration about 1 mg/ml with centrifugal filter (Amicon, 10KDa, Millipore). ADAM-17 (46 μM; 39 kDa) in 15 mL HEPES buffer 50 mM 300 mM 2.5 μM ZnCl2 0.005% Brij-35 pH 8 was incubated with EZ-link NHS-LC-Biotin (925 μM) for 1 hr at 4 °C. Final purification was performed by SEC column (HiLoad® 16/600 Superdex® 75 pg) using HEPES buffer 50 mM 300 mM 2.5 μM ZnCl2 0.005% Brij-35 pH 8 and the protein was concentrated with ultrafiltration (Amicon 10KDa,

Millipore) and the concentration was determined spectrophotometrically at 280 nm (11,6 mg, 4,67 mg/mL).

Chapter 4
Production of ADAMTS-5

4.1 Introduction

ADAMTS-5 was discovered twenty-three years ago from a team of scientists at the pharmaceutical company DuPont. Looking for a major responsible enzyme of aggrecan cleavage, they cloned and identified a target for articular cartilage degradation (Tortorella et al., 1999). Extracellular matrix function is severally affected by aggrecan degradation and differnt OA models confirmed the correlation (Santamaria, 2020). ADAMTS-5 possesses several domains: a large pro-catalytic domain, a zinc-dependent catalytic domain, a disintegrin, a thrombospondin, a cysteine-rich and a spacer followed by a C-terminal thrombospondin domain (**Fig. 34**).

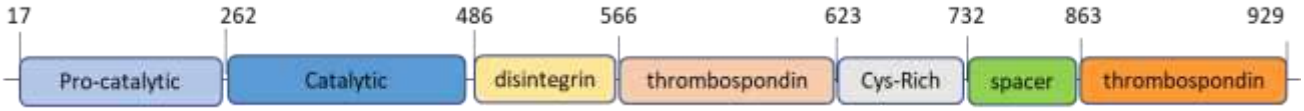

Fig. 34 Schematic representation of domain architecture of ADAMTS-5

The characteristic metalloproteinase catalytic domain belongs to the metzincin family, in which three histidine residues coordinate a zinc atom and a glutamate residue exerts the hydrolytic role. A conserved methionine residue forms a Met-turn with constrain role and exosite mediate the binding activity to the substrate. ADAMTS-5 is one of the major targets in OA, in view of their key role in degradation of extracellular matrix type II collagen and aggrecan. It is identified as aggrecanases, because it able to cleave the E373A374 bond of aggrecan interglobular domain. Moreover, in vitro studies have shown that ADAMTS-5 is more potent than ADAMTS-4 (Santamaria, 2020). Since its discovery from articular explant, its pivotal role in cartilage turnover is reinforced (Abbaszade et al., 1999; Tortorella et al., 1999). From *in vitro* studies in human chondrocytes, inhibition of ADAMTS-5 significantly reduces aggrecan degradation and cartilage loss in arthritis models was reduced in knockout mice (Stanton et al., 2005). Moreover, ADAMTS-5 activity is connected to a broad range of physiological functions, and due to its quite strict substrate specificity is investigated for several pathological treatments. Due to the role of proteoglycans in cardiovascular system, more recently aggrecanase-2 was connected to aneurysms and atherosclerosis treatments. Furthermore, its role in immune system, cancer development, steatosis, glucose metabolism in liver and wound healing are under investigation (Santamaria, 2020).

In this chapter, the evaluation of different ADAMTS-5 constructs, protein expression and characterization are discussed.

4.2 Results and Discussion

Construct evaluation

According to Colige , ADAMTS proteins are challenging to purify, in a native or recombinant form, because of their large size, extensive glycosylation, autocatalytic truncation and tendency to form aggregates (Apte, 2020). Moreover, Tomasselli and coworkers used site-directed mutagenesis, high pressure refolding, and thermal unfolding to achieve the preparation of active catalytic domain of ADAMTS-5 (Shieh et al., 2008). Reported studies of expression and purification of the human ADAMTS-5 and its domain deletion mutants elucidated the role of different domains on the extracellular matrix interaction and proteolytic activities (Zeng et al., 2006; Gendron et al., 2007; Fushimi et al., 2008).

Of the nine generated constructs (M-118, M-119, M-120, M-121, M-122, M-123, M-124, M-125, M-126) including a catalytic domain (262-486), disintegrin domain (486-566), thrombospondin domain (566-623) of human ADAMTS-5, only one (M-126) afforded good expression yield and catalytic activity (**Fig.35).**

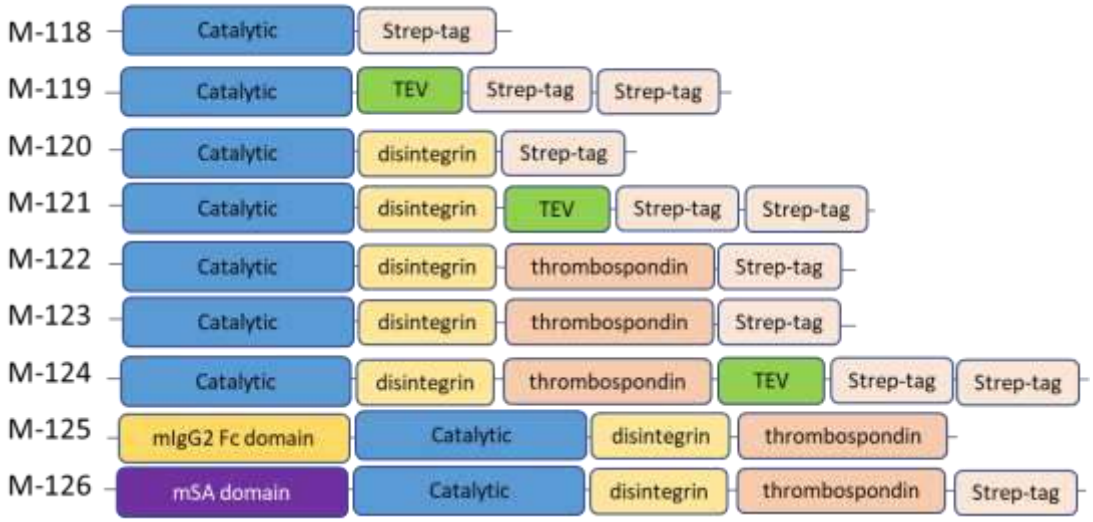

Fig.35 Schematic representation of expression constructs encoding for human ADAMTS-5 domains: catalytic (262-486), disintegrin (486-566) and trombospondin (566-623). Encoded sequences for Strep-tag (GSAWSHPQFEK), TEV (ENLYFQG), mouse serum albumin (mSA) and monoclonal Anti-Human IgG2 Fc receptor (mIgG2 Fc) were used.

A

construct	MW	Epsilon
-	KDa	M^{-1} cm^{-1}
M-118	28.4	33710
M-119	31.1	40700
M-120	37.1	45420
M-121	39.8	52410
M-122	44.0	66577
M-123	44.0	66577
M-124	46.8	73567
M-125	70.2	85277
M-126	110.9	100482

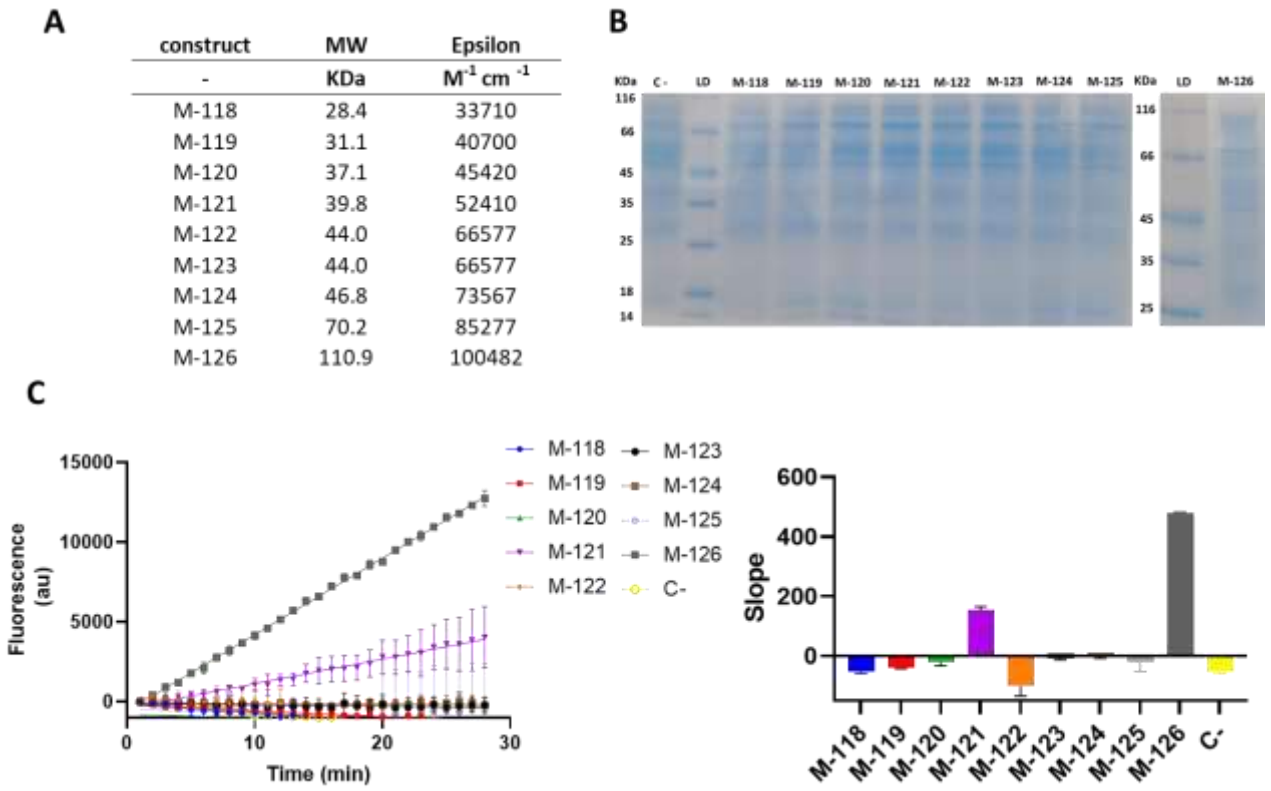

Fig. 36 (**A**) Molecular weights and molar attenuation coefficient of expression constructs (**B**) comassie-stained SDS-PAGE of conditioned media (**C**) FRET-based catalytic activity and slopes

Protein of M-126 construct was slightly visible at the corresponding molecular weight (**Fig. 36B**). Moreover, Positive slope values of catalytic activity were observed only in the conditioned media of M-121 and M-126 constructs (**Fig. 36C**) without aspecific cleavage (control). Surprisingly, albumin fusion protein afforded superior expression yield and activity. This might be explained by the proximity effect of albumin domain to catalytic domain. It is known that absence of pro-catalityc domain can influence protein expression, folding and extracellular release (Zeng et al., 2006). In conclusion, M-126 construct was selected for further expression and purification of recombinant protein mSA-ADAMTS-5 $^{262\text{-}623}$-Strept-tag.

3.5 Expression and purification of mSA-ADAMTS-5$^{262\text{-}623}$ and active site mutant

Vector M-157, encoding for active site mutant E411Q, was produced from vector M-126. According to Wyeth's Researcher (Zeng et al., 2006), E411Q active site mutant possess increased stability against autoproteolytic and TEV cleavage allows the generation of ADAMTS-5 $^{262\text{-}623}$ by elimination of albumin domain and affinity tag.

Recombinant protein mSA-ADAMTS-5 $^{262-623}$-Strept-tag and E411Q mutant were expressed in a medium scale (125 mL) and a good expression yield at high degree of purity were obtained using a single step purification protocol.

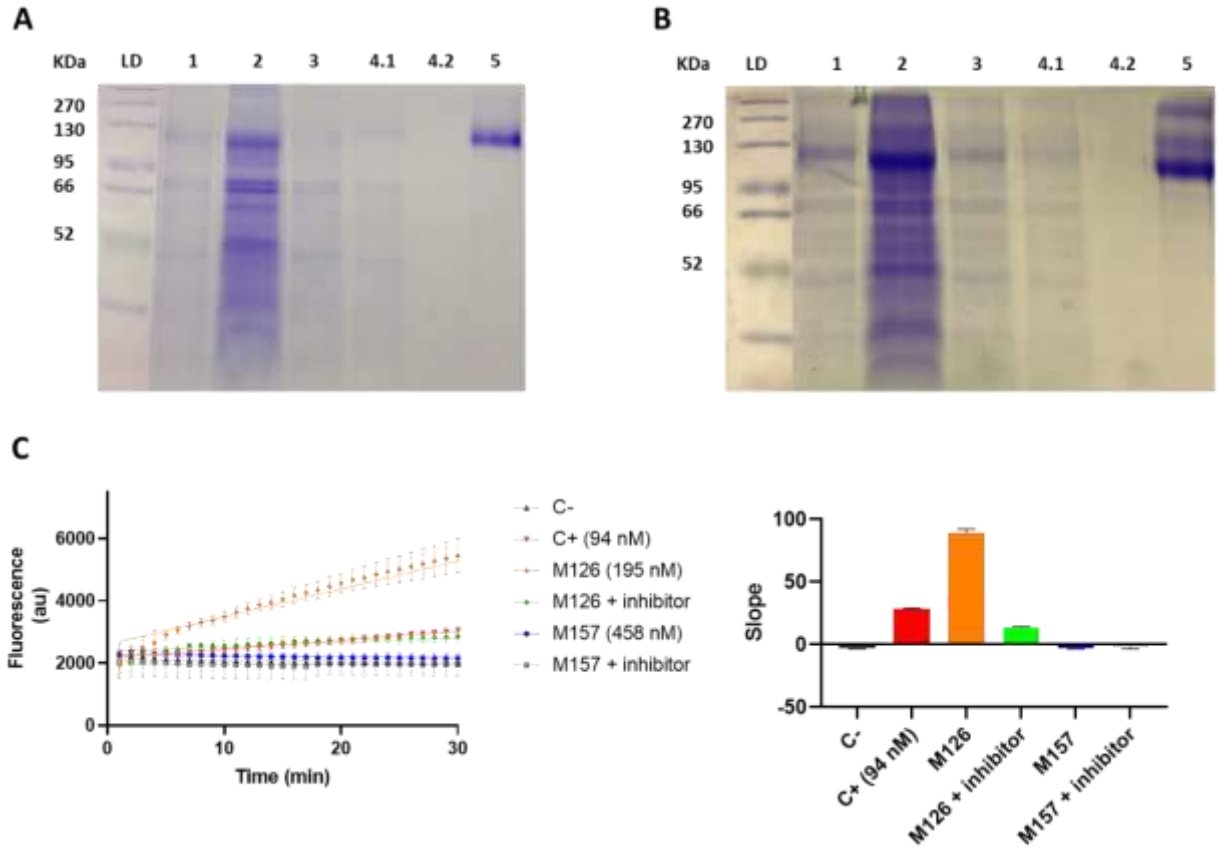

Fig. 37 (**A**) Coomassie-stained SDS-PAGE of affinity purification steps: (1) supernatant (2) supernatant conc. (3) flow through (4) wash (5) eluate of mSA-ADAMTS-5 $^{262-623}$-Strept-tag and (**B**) active site mutant E411Q (**C**) Activity assay of purified proteins encoded by M-126 and M-157 vectors.

The proteins were purified from conditioned media via Strep-tactin affinity column affording a good recovery from the eluate fractions (**Fig. 37A, B**) The proteins were concentrated affording a total of 240 µg and 650 µg of mSA-ADAMTS-5 $^{262-623}$-Strept-tag and mutant, respectively, with corresponding expression yields of 1.9 mg/L and 5.2 mg/L. The values were remarkable comparing the expression yields reported in literature (Apte, 2020). The highest expression yield was reported by Brebion and coworkers with a value of 1.5 mg of ADAMTS-5 $^{262-567}$ protein per liter (Brebion et al., 2021). Activity of purified proteins was tested by FRET-based assay (**Fig. 37C**) and albumin fusion protein confirmed a good activity. Surprisingly, point mutation at the catalytic site was performed to reduce the catalytic activity of the proteinase, however it was obtained a complete enzyme inactivation. Finally, inhibition was tested with a broad-range protease inhibitor affording a

strong activity reduction of the active metalloproteinase. The stability and the ability to generate ADAMTS-5 $^{262-623}$ under TEV digestion was tested using an engineered protease on two proteins.

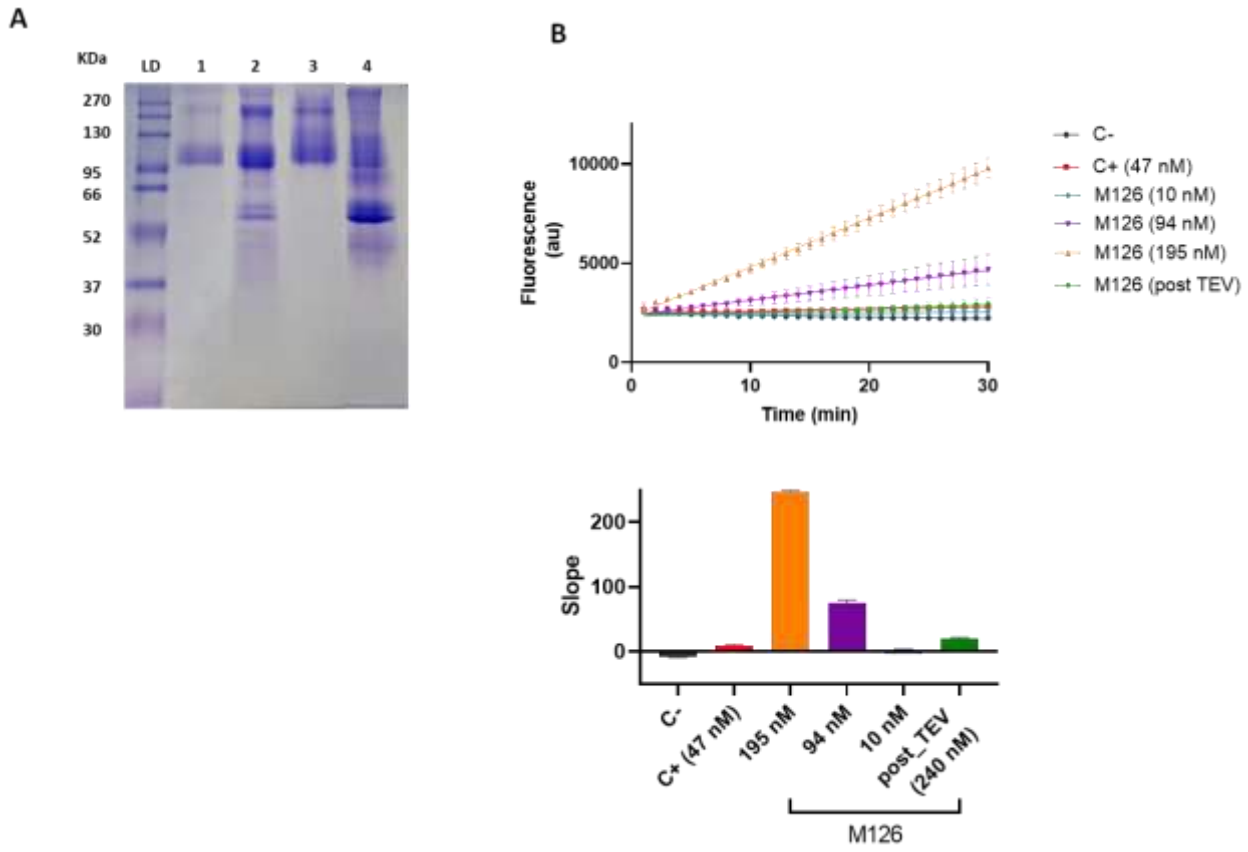

Fig.38 (**A**) Coomassie-stained SDS-PAGE of (1) mSA-ADAMTS-5 $^{262-623}$-Strept-tag, (2) TEV-treated mSA-ADAMTS-5 $^{262-623}$-Strept-tag (3) mutant E411Q (4) TEV-treated mutant E411. (**B**) Activity assay of purified protein before and after TEV treatment.

Before digestion, native proteins showed comparable molecular weights, in accordance with their theoretical weights of 108 kDa and 112 kDa (**Fig. 38A**). After cleavage, the mutant afforded bands in 50-60 kDa range, in accordance with the expected molecular weights of albumin (60 kDa) and ADAMTS-5 $^{262-623}$ (50 kDa) (**Fig. 38A line 4**). Finally, as expected the activity rates of albumin fusion protein were concentration dependent (**Fig. 38B**). However, cleavage treatment drastically reduced the activity of purified protein.

Despite the successful production and purification of target metalloproteinase at medium scale, the value of expression yields (1.9 mg/L) was not sufficiently high to obtain the required amount even at large scale production. In conclusion, its overall low yield prevented the use of ADAMTS-5 as target for further yeast display screening.

4.3 Conclusions

In this chapter, the production of metalloprotease target ADAMTS-5 has been described.
Yeast display screening steps require several milligrams of purified protein, and a correct folding of the active site for binding recognition and inhibitor development.
Nine different constructs were expressed in a small scale, in order to explore the contribution of protein domains to expression and catalytic activity. Albumin fusion protein afforded superior expression yield and activity compared to the other proteins. This outcome has been explained by the proximity effect of albumin domain to catalytic domain. All the constructs were designed without the procatalitic domain and this region effects protein expression, folding and extracellular release.
Furthermore, active site mutant E411Q was generated to increase the protein stability against autoproteolytic. However, the mutation ended in a complete enzyme inactivation, but the cleavage study confirmed the correct molecular weight of the protein.
In conclusion, despite the successful production of mSA-ADAMTS-5 $^{262-623}$-Strept-tag protein, the overall expression yield of the metalloprotease target forbade the use of ADAMTS-5, even at large-scale production, as target for further yeast display screening.

4.4 Materials and methods

Protein expression

ADAMTS-5 recombinant proteins spanned from catalytic domain to thrombospondin (262-623) domains. Affinity tags were added at the C-terminus and TEV sites were added for a cleavage strategy. Albumin and Fc fragment were integrated as a fusion protein to improve the stability and solubility.
Expression constructs encoded for the following sites and domains:

- catalytic domain, Strep-Tag (M-118),
- catalytic domain, TEV site, double Strep-Tag (M-119),
- catalytic domain, disintegrin domain, Strep-Tag (M-120),
- catalytic domain, disintegrin domain, TEV site, double Strep-Tag (M-121),
- catalytic domain, disintegrin domain, thrombospondin domain, Strep-Tag (M-122),
- catalytic domain, disintegrin domain, thrombospondin domain, Strep-Tag (M-123),
- catalytic domain, disintegrin domain, thrombospondin domain, TEV site, double Strep-Tag (M-124),

- monoclonal human Fc fragment, catalytic domain, disintegrin domain, thrombospondin domain (M-125),
- mouse serum albumin, catalytic domain, disintegrin domain, thrombospondin domain, Strep-Tag (M-126),
- mouse serum albumin, TEV site, catalytic domain (E411Q), disintegrin domain, thrombospondin domain, TEV site, Strep-Tag (M-157)

ADAMTS-5 constructs were transfected in ExpiCHO cells (Thermo Fisher Scientific). Strep-tag sequence corresponds to GSAWSHPQFEK and TEV sequence corresponds to ENLYFQG. All the constructs were encoded in pMP-PB plasmid, except for M-123 which was encoded in gWiz plasmid. The cultures (10 mL) were incubated at 30°C for four days. Then, cells were harvested by centrifugation (6000 g, 20 min at 4 °C), removed by filtration (0,2 µm, RC filter), the media freezed and stored at -80 °C until further processing. Conditioned media were analysed by SDS-PAGE analysis and FRET-based assay.

Catalytic activity

FRET-based assay was performed as reported by Deng and coworkers (Deng et al., 2012). As a negative control, conditioned medium of not transfected cells was used. The enzymatic activity of media was evaluated in the presence of FRET Substrate (25 µM, WAAG - 3R, Aggrecanase Substrate, AS-60431-1, Anaspec) in 96 well plates (Nunc maxisorp) and read with a plate reader (Tecan Infinite M200). The assay was run in triplicate in 50 mM HEPES, pH 7.5, 100 mM NaCl, 5 mM $CaCl_2$, 0.1% CHAPS, and 5% glycerol. Substrate solution was added to the 1:10 diluted solution of cell media and the plate was read every minute for 30 min at 37 °C. Excitation and emission wavelengths were 340 and 420 nm, respectively.

Mutagenesis

A mutant at the active site of recombinant protein mSA-ADAMTS-5 $^{262-623}$-Strept-tag was produced by point mutation (E411Q) in order to reduce the catalytic activity and increase the stability against autoproteolytic processes. Following the protocol reported by Wyeth's Researcher (Zeng et al., 2006) (US7223858B2) QuickChange Site Directed Mutagenesis Kit (Stratagene) was used. Mutant was obtained by consecutive PCR reactions using a High-fidelity DNA Polymerase (PfuUltra II Fusion). Single clones of TOP10 Chemically Competent E. coli were selected.

Medium scale expression, purification and TEV cleavage

ExpiCHO™ cells were grown in ExpiCHO™ Expression Medium (125 mL) at 31 °C and 5% CO_2 and mixed at 180 rpm. The culture was transfected with PEI MAX (15 ug/mL) and plasmid DNA of construct M-126 (3 ug/mL). After 4 days, the cells were removed by centrifugation (6000 g, 20 min at 4 °C) and filtration (0.2 µm). Supernatant was diluted 1/4 v/v with buffer (80mM Tris-HCL pH8, 20 mM CaCl2, 40 µM ZnCl2, 200 mM NaCl) and loaded on Strep-Tactin®XT Superflow column (IBA Lifescience) which was first equilibrated against buffer A (20 mM Tris-Cl (pH 8.0), 5 mM CaCl2, 10 µM ZnCl2, 50 mM NaCl). First, the column was washed with buffer A in order to remove unspecific proteins. Then, the protein was eluted with buffer B (100 mM Tris-HCl pH 8, 150 mM NaCl, 50 mM biotin). The protein was concentrated with centrifugal filter (Amicon, 3 KDa, Millipore) and the concentration was determined spectrophotometrically at 280 nm (240 µg, 1.6 mg/ml). Catalytic activity was tested with a FRET-based assay. Sample without enzyme was used a negative control, and rh-ADAMTS-5 (2198-AD, R&D system) was used a positive control. cOmplete™ Protease Inhibitor Cocktail (11697498001, Merck) was used as metalloproteinase inhibitor. Concentration of FRET substrate and analysis conditions were used as described above.

Digestion was performed using an engineered protease (ProTEV plus, Promega) able to cleave protein fusion with the ENLYFQ(G/S) sequence following the manufacturer protocol. Protein cleavage (250 µg) was performed with 1,5 U of TEV protease at 4°C for 16 hours in PROTEV buffer with 1 mM DTT. Then, proteins were concentrated to a conc. 20 µM via centrifugal concentration (Amicon 3KDa).

Chapter 5
Screening peptide binders of ADAM-17
via yeast surface display

5.1 Results and Discussion

In this chapter, two strategies for the discovery of peptide binders of ADAM-17 via yeast surface display with canonical and ncAAs (non-canonical amino acids) are presented. Naïve yeast libraries of cyclic peptides were selected via magnetic activated cell sorting and fluorescent activated cell sorting achieving high throughput screenings. Finally, binding properties and specificity of selected libraries were investigated.

In the second strategy, yeast libraries of peptides with ncAAs were chemically modified via click chemistry in order to expand the chemical diversity and introduce the hydroxamic moiety. Firstly, the conditions of post-translational chemical modification via copper-catalysed click coupling were investigated in a parameter study in order to maximize the coupling yield with click agents **5** and **6**. Finally, the effects of click agents and derivatives on ADAM-17 binding and inhibition were studied.

Yeast display screening and sorting of peptides with canonical amino acids

Yest surface display is a powerful tool for the high throughput screening of binders of a target via an in vitro directed evolution approach. Specifically, in this study the screen of large combinatorial libraries of cyclic peptides was explored in order to select binders with enhanced affinity and specificity for the metalloproteinase target. If the binding occurs at the level of catalytic site, hindering the substrate recognition or enzyme mechanism, the binder act as a metalloproteinase inhibitor. Constrained cyclic peptides were preferred to linear peptides because are well suited for targeting protein-protein interaction and benefit from lower entropic penalty upon binding and increased stability (Simonetti and Ivarsson, 2020). Cyclic peptides can be genetically encoded and used in yeast display system because linear peptides containing two or more cysteine residues undergo of spontaneous oxidation forming disulfide bridge (Linciano et al., 2019).

The strategy of yeast display screening and sorting of peptides with canonical amino acids is represented in **Fig. 39A** with a focus on genotype-phenotype correlation of directed evolution technique. The approach is composed of consecutive steps: construction of yeast genomic library, surface display of peptide library, binder selection, DNA and peptide characterization. LB1, LB6, LB13, LB14 and LB15 libraries were sorted with two rounds of magnetic activated cell sorting (MACS) steps achieving the library SB2, which was subsequently sorted with two rounds of fluorescent activated cell sorting (FACS) (**Fig. 39B**).

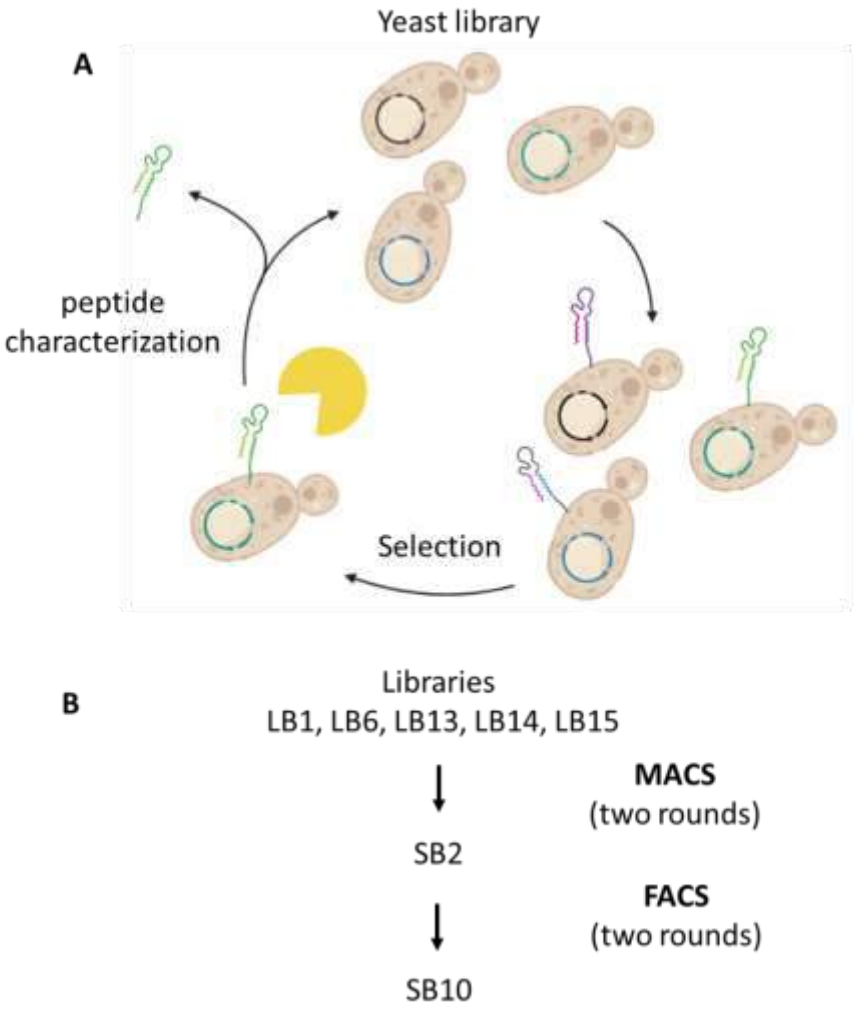

Fig. 39 (**A**) Schematic representation for selection of peptide ADAM-17 binders from a naïve yeast display library with canonical amino acids. Steps of peptide expression, display, sorting, DNA and peptide characterization are represented. (**B**) Screening strategy of a naïve yeast library with rounds of magnetic-activated and fluorescence-activated cell sorting.

The construction of a random naïve yeast library was allowed by incorporation of library DNA inserts in vector backbone in order to obtain cyclic peptide, with loops of 5, 8, 9, 11 amino acid residues (Benatuil et al., 2010). Degenerated sequences of DNA inserts (paragraph Primers in Appendix) coding for peptide sequences were incorporated with an efficient yeast transformation method obtaining high values of diversity for LB1, LB6, LB13, LB14 and LB15 libraries varying in length from 9 to 15 amino acids. (**Tab. 2**)

Peptide library	Yeast strain	Peptide Sequence	Theoretical Diversity	Experimental Diversity
LB1	EBY100	CX_7C	1.10^9	4.10^8
LB6	EBY100	CX_9C	5.10^{11}	2.10^9
LB13	EBY100	CX_3CX_9C	4.10^{15}	6.10^8
LB14	EBY100	CX_6CX_6C	4.10^{15}	3.10^8
LB15	EBY100	CX_9CX_3C	4.10^{15}	5.10^8

Tab. 2 Peptide libraries used in yeast display screening of peptides with canonical amino acids

Experimental diversities were not sufficient to cover the theoretical values (residue permutation), however represent an improvement on typical size of yeast libraries ($\sim 10^7$).

Aga1– Aga2 is the most used display system with *Saccharomyces cerevisiae*, and proteins or peptide of interest can be displayed on the yeast surface as either C- or N-terminal fusions to the Aga2 protein. However, we used Stalk system (Mcmahon et al., 2018)(Mcmahon et al., 2018) instead of Aga1-Aga2 display system because it lacks disulfide bridges, allowing the generation of a stable display system in reducing conditions. Moreover, display system was flanked by the hemagglutinin (HA) epitope tag for immunofluorescent detection and quantification of peptide display on yeast surface.

LB1, LB6, LB13, LB14 and LB15 libraries were unified and screened with two rounds of positive MACS towards metalloproteinase ADAM-17. Positive selection was performed with ADAM-17 bounded to magnetic beads at conc. 1µM and induced cells were placed in contact and washed. After two rounds of selection, binders were replicated and identified as SB2 library, affording a diversity of 10^3-10^4. Library size decreased of 5 orders of magnitude from the parent naïve yeast library.

SB2 library was titrated at different concentrations of metalloprotease to confirm the affinity for the target. (**Fig. 40**)

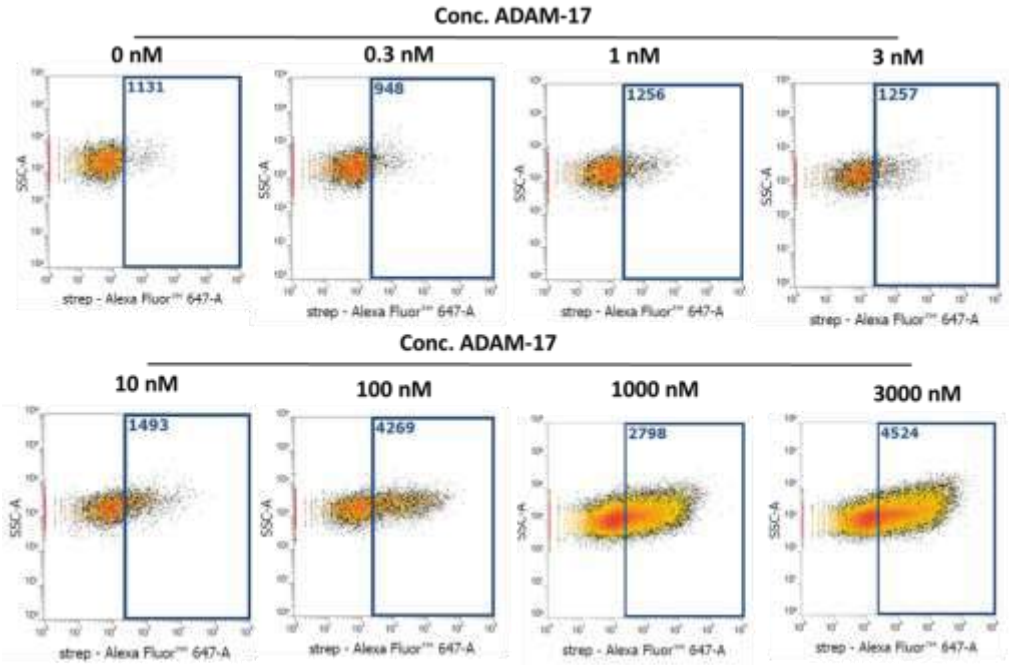

Fig. 40 Flow cytometry plots (Strep-647 fluorescence vs side scattering) of SB2 library titrated with ADAM-17 at different concentrations (0 nM, 0.3 nM, 1 nM, 3 nM, 10 nM, 100 nM, 1000 nM, 3000 nM).

Flow cytometry plots of target binding vs side scattering show that ADAM-17 binding is concentration dependent. Furthermore, two rounds of FACS were performed on SB2 library at ADAM-17 conc. 300 nM and 30 nM, respectively (**Fig. 41**)

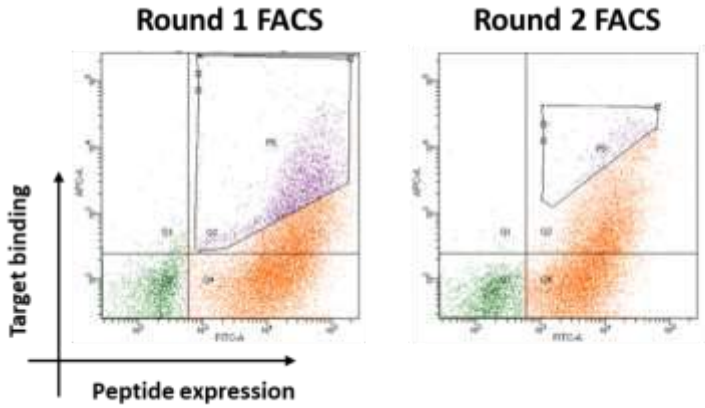

Fig. 41 FACS plots of SB2 library at first and second round of selection

Double staining was performed for immunofluorescent detection of peptide display and target binding. Two rounds of enrichment were performed selecting the gated population on the upper part of the diagonal. Finally, sorted SB10 library was characterized with flow cytometry analysis to investigate the binding ability and specificity of selected population towards other zinc metalloproteinases (PSMA and ACE) and RecA protein. (**Fig. 42**)

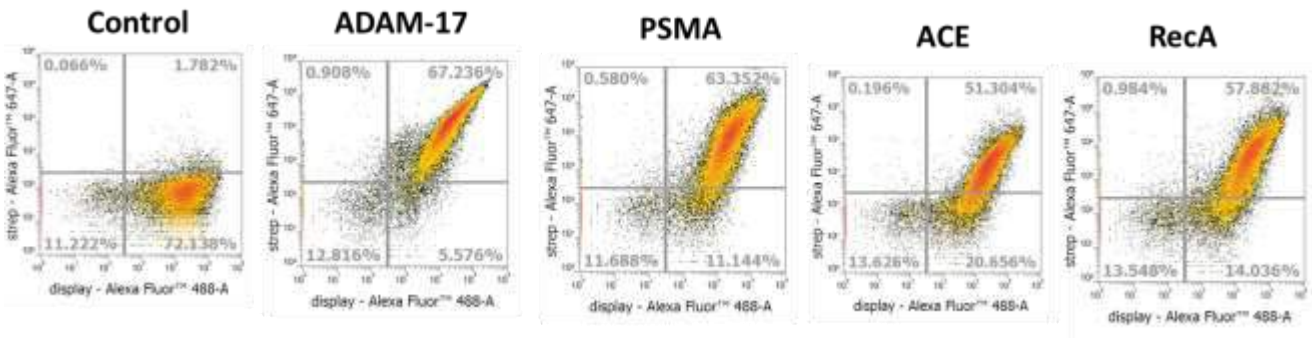

Fig. 42 Flow cytometry plots (Alexa Fluor 488 fluorescence vs Strep-647 fluorescence) of SB10 library treated with no protein (control), ADAM-17, PSMA, ACE and RECA protein.

Library SB10 showed good binding of metalloprotease target compared to control (no target), but unfortunately, no selectivity towards other tested proteins. Selectivity issues might be the result of an ineffective enrichment and sorting towards the selected protein target. Binding may occur between the components of yeast cell surface or peptide display system and protein. Moreover, selection may be driven by some structural features of the protein of interest or with incorrect folding, resulting in an aspecific enrichment.

Library was further characterized with DNA extraction and sequence analysis in order to identify the nature of sorted peptide and parent library. DNA isolation, digestion, transformation in E.Coli. and plating allowed to obtain different clones. Five random clones were selected for sequencing analysis and results are reported (**Tab. 3)**.

n.	peptide sequence	Loop scheme	parent library
1	CDRWIYYAGRYWFVC	$CX_{13}C$	-
2	CYLYCYINGNCFVKC	$CX_3CX_5CX_3C$	LB13 or LB15
3	CSDRFRNCPADEALC	CX_6CX_6C	LB14
4	CFWYNLYWVLC	CX_9C	LB6
5	CYLYCYINGNCFVKC	$CX_3CX_5CX_3C$	LB13 or LB15

Tab. 3 Peptide sequences, loop scheme and parent library of selected clones

DNA sequences coding for respective peptide sequences were identified for loop scheme and, considering the cysteine position, parent libraries were assigned. Analysis of sequence 1 revealed a probable mutation with a loss of a cysteine residue and a parent library assignment of libraries with three cysteine (LB13, LB14 or LB15). Moreover, sequence 2 and 5 were equal, representing a greater probability among peptide distribution.

Parameter study of post-translational chemically modified peptide on yeast cell via copper-catalysed click coupling

A strategy to expand the chemical diversity of biological systems and possibilities for high throughput discovery is the coupling of protein/peptide and ncAAs. Site-specific introduction of ncAA into displayed proteins and quantification of conjugates directly on yeast surface was recently applied and reported by Schultz and coworkers (Supekova et al., 2018) and Van Deventer and coworkers (Stieglitz et al., 2018). From a protocol of Van Deventer and coworkers (Van Deventer et al., 2016), conditions for copper-catalyzed Azide–Alkyne Cycloaddition of azido peptide on yeast surface were investigated in order to apply the protocol to post-translational chemically modified peptide libraries and introduce the hydroxamic moiety. Essential components for CuAA can be summarized: Cu (II) as a soluble form of copper, sodium ascorbate as a reducing agent for copper reduction, copper ligand and scavenging molecules to reduce the toxicity of catalyst.

In this study, reaction conditions were investigated for the CuAA of click agents **5** and **6** with azido peptide on the surface of yeast cells. p-azide-L-methyl phenylalanine is the ncAA incorporated on peptide sequence. CuAA efficiency is quantified as median fluorescence intensity of fluorescent streptavidin coupled to biotin on the surface of yeast cells and analyzed at flow cytometry. If azido peptide is firstly modified with click agents **5** or **6**, the second CuAA is performed with alkyne-biotin and CuAA efficiency is quantified by labelling with fluorescent streptavidin. (**Fig. 43**)

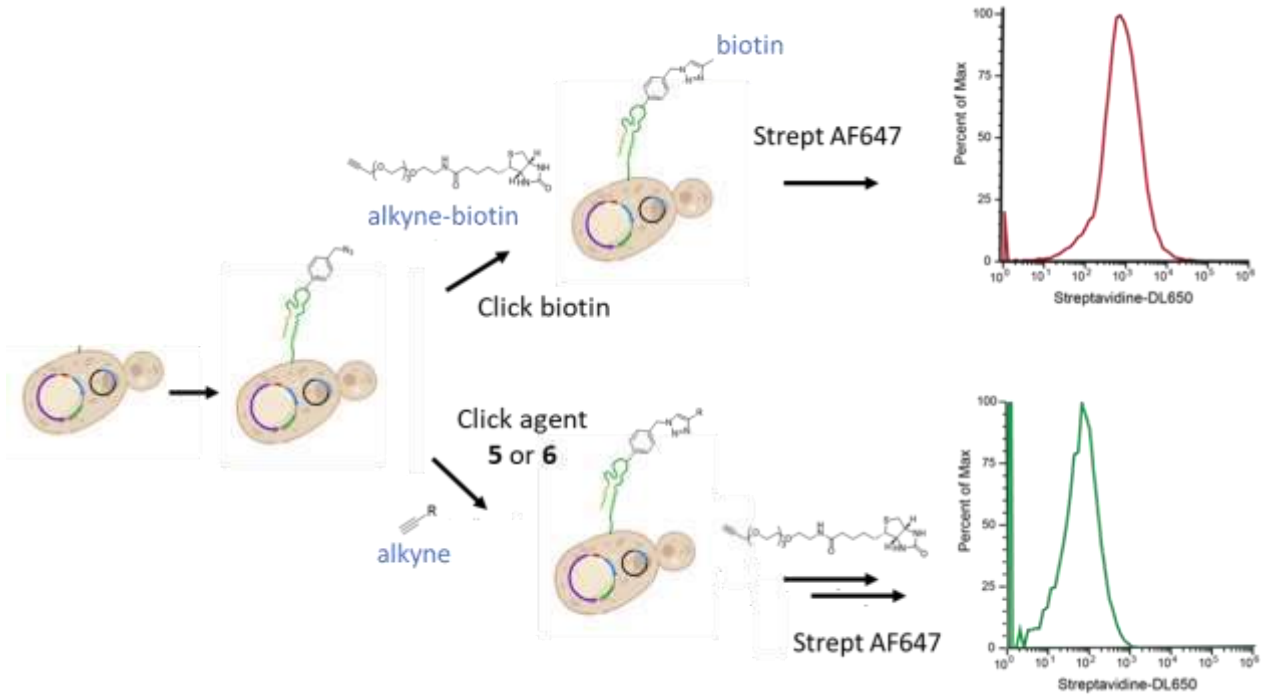

Fig. 43 Schematic representation of peptide display with ncAA on yeast surface and click modification with alkyne-biotin or click agent **5** or **6**. Staining of biotin derivative occurs with fluorescent streptavidin.

For this assay, the heptapeptide SSSZSSS (where Z is AzM) was displayed on the yeast surface via a stalk display system. The incorporation of ncAA took advantage of the engineered Leucine E. Coli tRNALeu/aatRNALeu pair developed by Shultz and coworkers (Chin et al., 2003).

AzM incorporation occurred in correspondence of an amber stop codon (TAG) and it is possible to quantify the incorporation by HA labelling. C-terminal HA tag (YPYDVPDYA) is translated only by means of AzM incorporation in peptide sequence.

For click agents **5** and **6** concentration, composition of reaction mixture and number of consecutive click reaction to maximize the click efficiency were determined. First, conditions for positive labelling with alkyne-biotin CuAA and streptavidin detection were set. Alkyne-biotin concentration and solvent effect were explored in order to investigate the effect on CuAA yield.

Efficiency of post-translational click modification on yeast surface was evaluated testing (**Fig. 44**):

- Alkyne-biotin concentration (0 μM, 1 μM, 3 μM, 10 μM, 30μM, 100 μM, 300 μM and 1000 μM)
- Solvent (PBS, 10% v/v ACN, 30% v/v MeOH, 20% v/v EtOH)
- Concentration of MeOH (0%, 5%, 10%, 20% and 30% v/v in PBS) and EtOH (0%, 5%, 10%, 20% v/v in PBS).
- Concentration of click agent, **5** and **6** (0 μM, 1 μM, 3 μM, 10 μM, 30μM, 100 μM, 300 μM, 1000 μM) in 0%, 5%, 10%, 20% v/v of MeOH in PBS.
- number of consecutive click reaction (0, 1, 2, 3, 4)

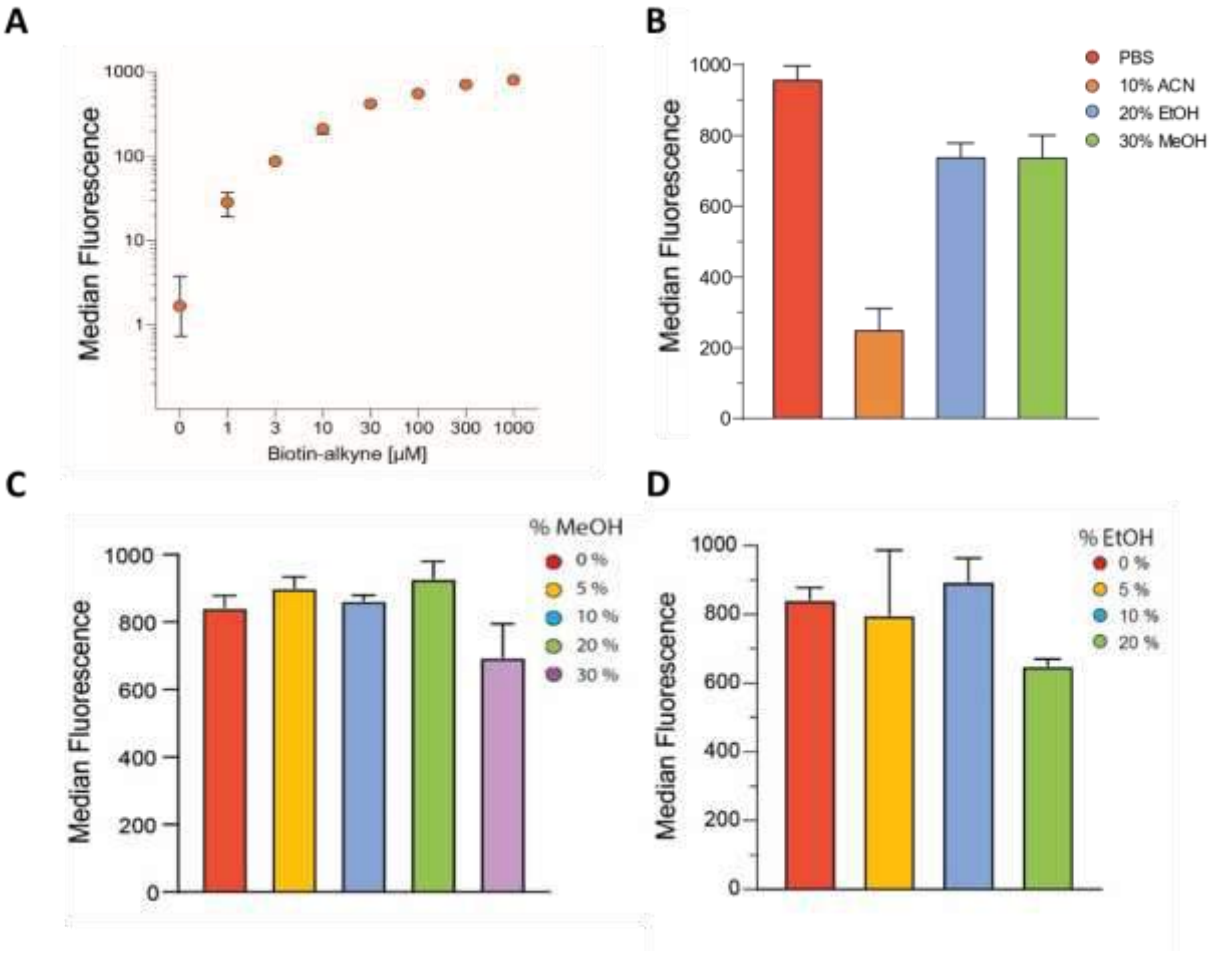

Fig. 44 Median fluorescence of labelled yeast cells after post-translational click modification (A) with different concentrations of alkyne-biotin (0 µM, 1 µM, 3 µM, 10 µM, 30µM, 100 µM, 300 µM and 1000 µM) (B) in different solvent (PBS, 10% v/v ACN, 30% v/v MeOH, 20% v/v EtOH) (C) in MeOH at conc. (0%, 5%, 10%, 20% and 30% v/v in PBS) (D) in EtOH at conc. (0%, 5%, 10%, 20% v/v in PBS).

Flow cytometry data showed that fluorescence intensity reached a plateau at around biotin concentration of 300 µM with a complete CuAA of azido peptide (**Fig. 44A**). This concentration was used for further experiments. Furthermore, considering the poor aqueous solubility of click agent **6**, mixtures of organic solvents were tested (**Fig. 44B**). Mixtures of organic solvent that allow good cell viability were chosen. CuAA yield was slightly reduced in presence of alcoholic mixtures, compared to the aqueous solvent, and represented a good compromise for further studies. Different concentrations of MeOH (**Fig. 44C**) and EtOH (**Fig. 44D**) in PBS were explored and concentrations up to 20% v/v of MeOH and up to 10% v/v of EtOH afforded no reduction in yield.

Click agent **5** and **6** were tested at different concentrations and percentages of MeOH in order to identify the optimal conditions to reach a maximum CuAA yield (**Fig. 45A, B**).

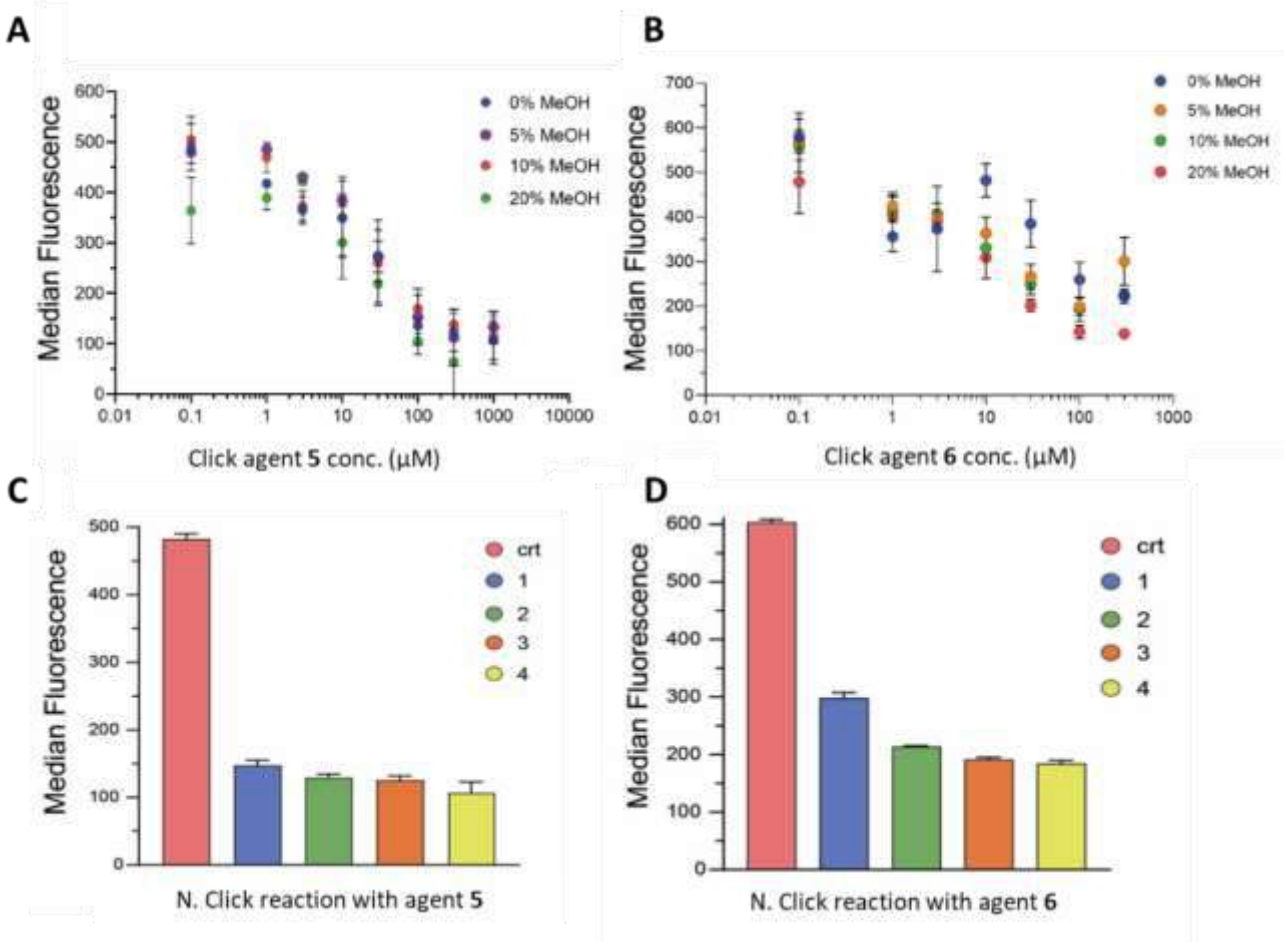

Fig. 45 Median fluorescence of labelled yeast cells after post-translational click modification with (**A**) click agent **5** and (**B**) click agent **6** at conc**.** (0 μM, 1 μM, 3 μM, 10 μM, 30μM, 100 μM, 300 μM, 1000 μM) in 0%, 5%, 10%, 20% v/v of MeOH in PBS. Median fluorescence of labelled yeast cells after consecutive click reaction (0, 1, 2, 3, 4) with click agent (**C**) **5** and (**D**) **6**.

Double click reaction assay (negative labeling) revealed a sigmoidal trend between fluorescence intensity and conc. of click agents **5** and **6**. No effect of solvent was appreciable for click agent **5** and reaction efficiency is affected only by the click agent **5** concentration. PBS and click agent **5** concentration of 300 μM were the selected conditions for further studies.

However, solvent effect on CuAA yield was appreciable for click agent **6** because solubility increased at higher percentages of MeOH. The use of 5% v/v MeOH and click agent **6** concentration of 300 μM were the selected conditions for further studies.

Finally, numbers of sequential CuAA were investigated for both click agents (**Fig. 45C, D**). The effect of the number of consecutive click reactions on post-translational chemical modification efficiency was appreciable. For click agents **5** and **6**, a total of two sequential CuAAs was selected for further studies considering the yield increase.

Yeast display screening and sorting of peptides with non-canonical amino acid

Using the conditions of the parameter study, large combinatorial libraries of peptides with ncAA were chemically modified with click agents **5** and **6** and sorted (**Fig. 46A**). Naïve yeast libraries of cyclic peptides (LB2, LB3, LB4, LB5) were selected via magnetic activated cell sorting and fluorescent activated cell sorting for enrichment and identification of ADAM-17 binders (**Fig. 46B**).

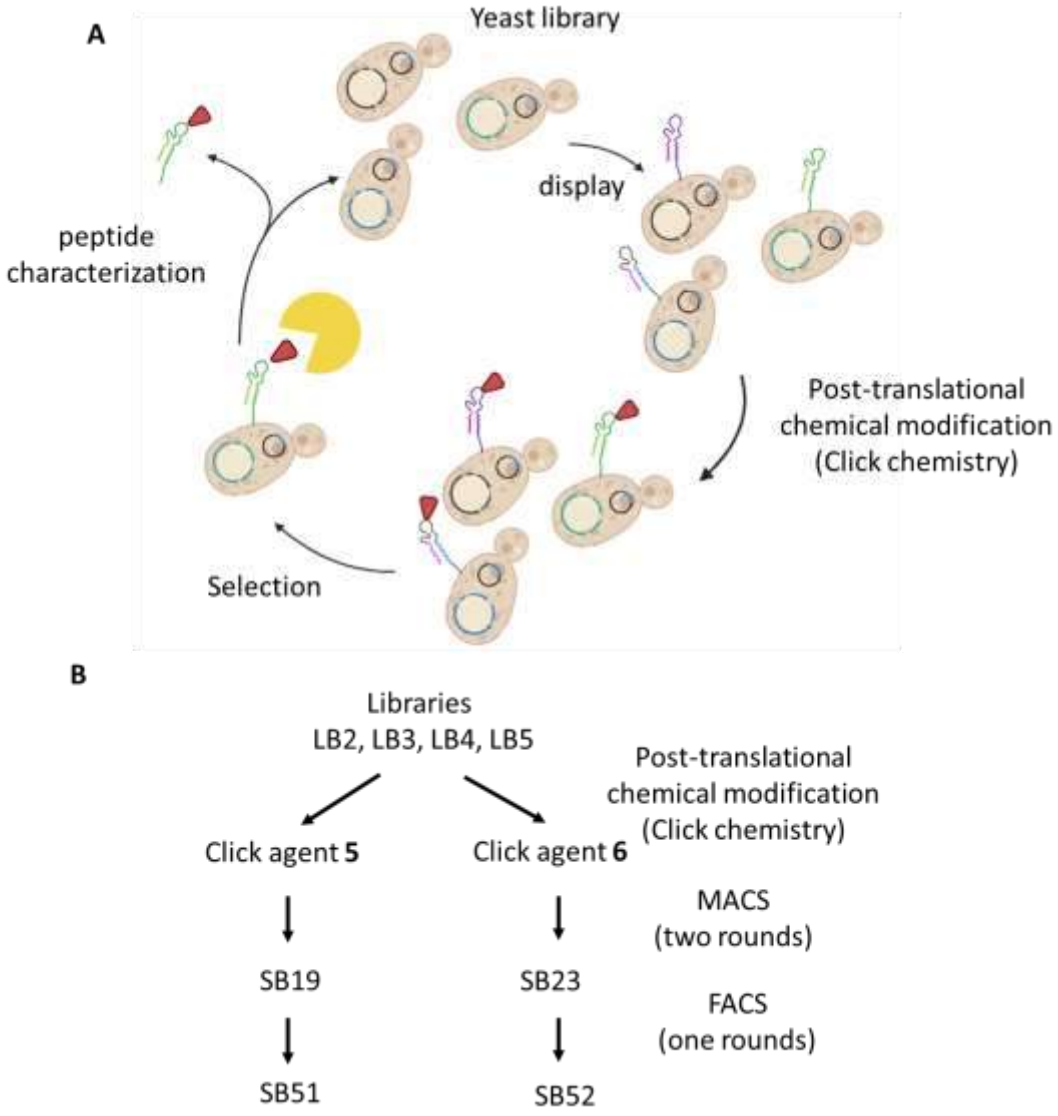

Fig. 46 (**A**) Schematic representation for selection of peptide ADAM-17 binders from a naïve yeast display library with ncAAs. Steps of peptide expression, display, post-translational chemical modification, sorting and characterization are represented. (**B**) Screening strategy of click-modified naïve yeast libraries with rounds of magnetic-activated and fluoresceence-activated cell sorting.

Hydroxamic moiety was coupled to cyclic peptides to introduce a metal chelating group and increase the affinity for the catalytic site of metalloprotease. ncAA was incorporated on peptide sequence following the same strategy of the parameter study, or rather, taking advantage of the engineered E.

Coli tRNALeu/aatRNALeu pair for AzM incorporation in correspondence of the amber stop codon (TAG).

Construction of four naïve yeast libraries was allowed by incorporation of DNA inserts in display vector backbone for the generation of cyclic peptides with loops of 9 amino acid residues. Degenerated sequences of DNA inserts (paragraph Primers in Appendix) were incorporated obtaining high values of diversity, comparable with theoretical values for LB2, LB3, LB4 and LB5 libraries. (**Tab. 4**)

Peptide library	Yeast strain	Peptide Sequence	Theoretical Diversity	Experimental Diversity
LB2	RJY100	$CX\underline{Z}X_5C$	6.10^7	2.10^8
LB3	RJY100	$CX_3\underline{Z}X_3C$	6.10^7	5.10^8
LB4	RJY100	$CX_5\underline{Z}XC$	6.10^7	5.10^8
LB5	RJY100	$\underline{Z}CX_7C$	1.10^9	5.10^8

Tab. 4 Peptide libraries used in yeast display screening of peptides with ncAA (Z: AzM)

LB2, LB3, LB4 and LB5 libraries were unified, induced, post-translational click modified and screened with two rounds of positive MACS and one round of FACS toward metalloproteinase ADAM-17. Positive MACS selections were performed with ADAM-17 bounded to magnetic beads at conc. 1µM and induced cells were first post-translational chemically modified and then placed in contact and washed. After two rounds of selection, binders were replicated and identified as SB19 and SB23 library for modification with click agent **5** and **6**, respectively.

Finally, double staining of display system and target was performed for FACS step. Post-translational chemically modified libraries SB19 and SB23 were enriched with a round of FACS. (**Fig. 47**)

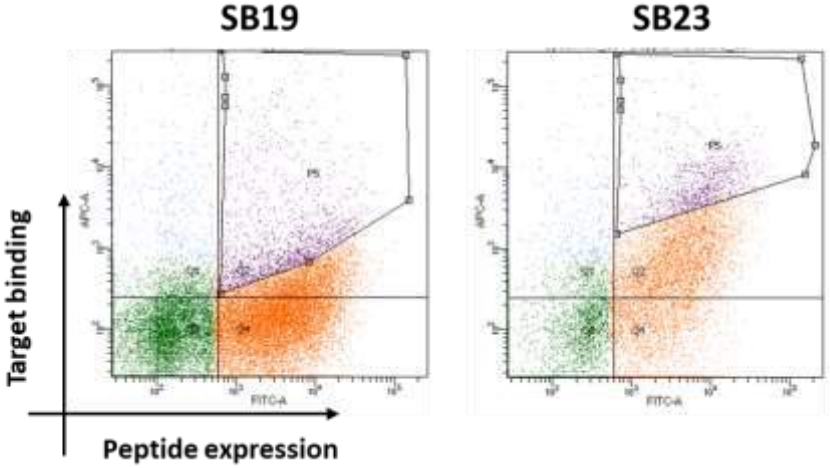

Fig. 47 FACS plots of SB19 and SB23 library

Gated populations were selected, revealing higher values of binding affinity for SB23 library than SB19 library.

Finally, affinity for ADAM-17 of sorted populations, SB51 and SB52, was characterized by flow cytometry analysis. Effect of metalloprotease target and click modification were evaluated on the selected populations (**Fig. 48A, B**).

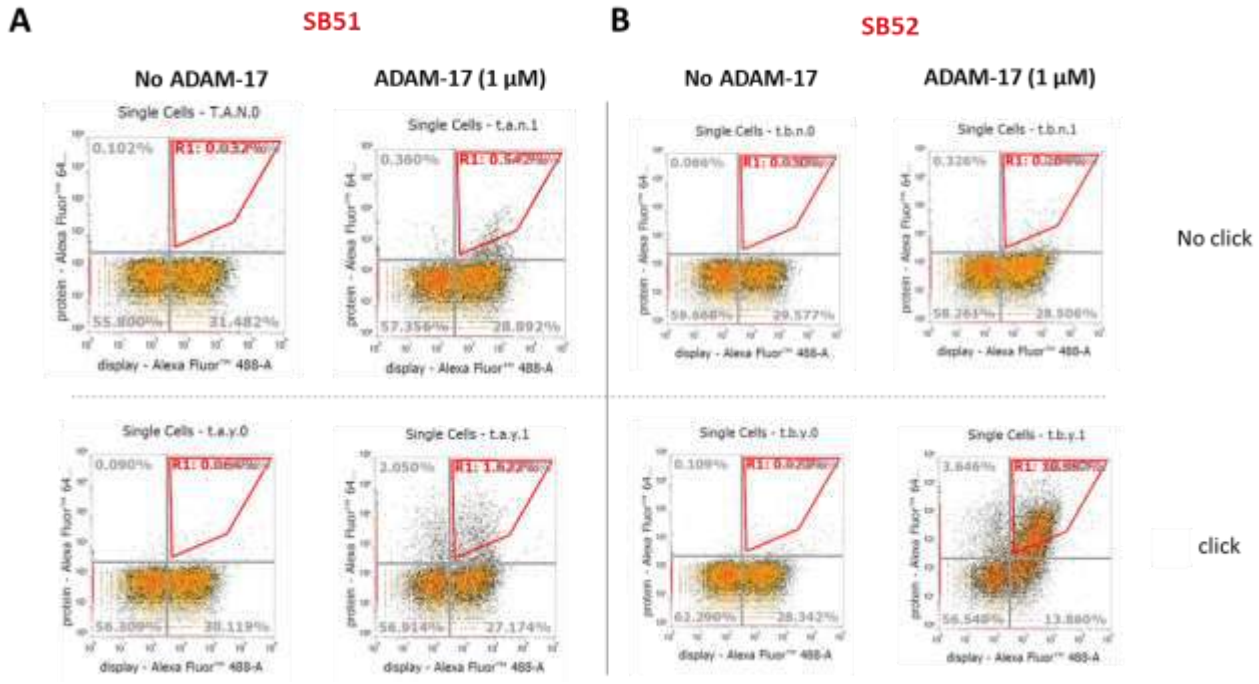

Fig. 48 (**A**) Flow cytometry plots (Alexa Fluor 488 fluorescence vs Strep-647 fluorescence) of SB51 library with and without post-translational modification with click reagent **5** and treatment with ADAM-17 (0 and 1 µM). (**B**) Flow cytometry plots (Alexa Fluor 488 fluorescence vs Strep-647 fluorescence) of SB52 library with and without post-translational modification with click reagent **6** and treatment with ADAM-17 (0 and 1 µM).

All populations confirmed a good peptide display (horizontal shift). Negative controls (without target) showed no effect of aspecific labelling, with and without click modification of peptides on yeast surface. Not modified population treated with metalloprotease revealed the peptide contribution on the target binding and SB51 population was slightly more effected than SB52. Finally, click-modified libraries induced a remarkable shift in the gated area (vertical shift). Effect of CuAA step on target binding was superior for SB52 population compared to SB51 library, showing the contribution of click agent scaffold. In other words, aromatic ring of azido click agent **6** greatly impact on ADAM-17 binding compared to click agent **5**.

The libraries were further characterized to investigate the binding ability and specificity via flow cytometry analysis. Metalloprotease ADAM-17 was compared with albumin, PSMA and NMD-1 at

conc. 100 nM. PSMA and NMD-1 are two zinc metalloproteinases and serum albumin was selected for its binding properties of hydrophobic molecules (**Fig. 49A**).

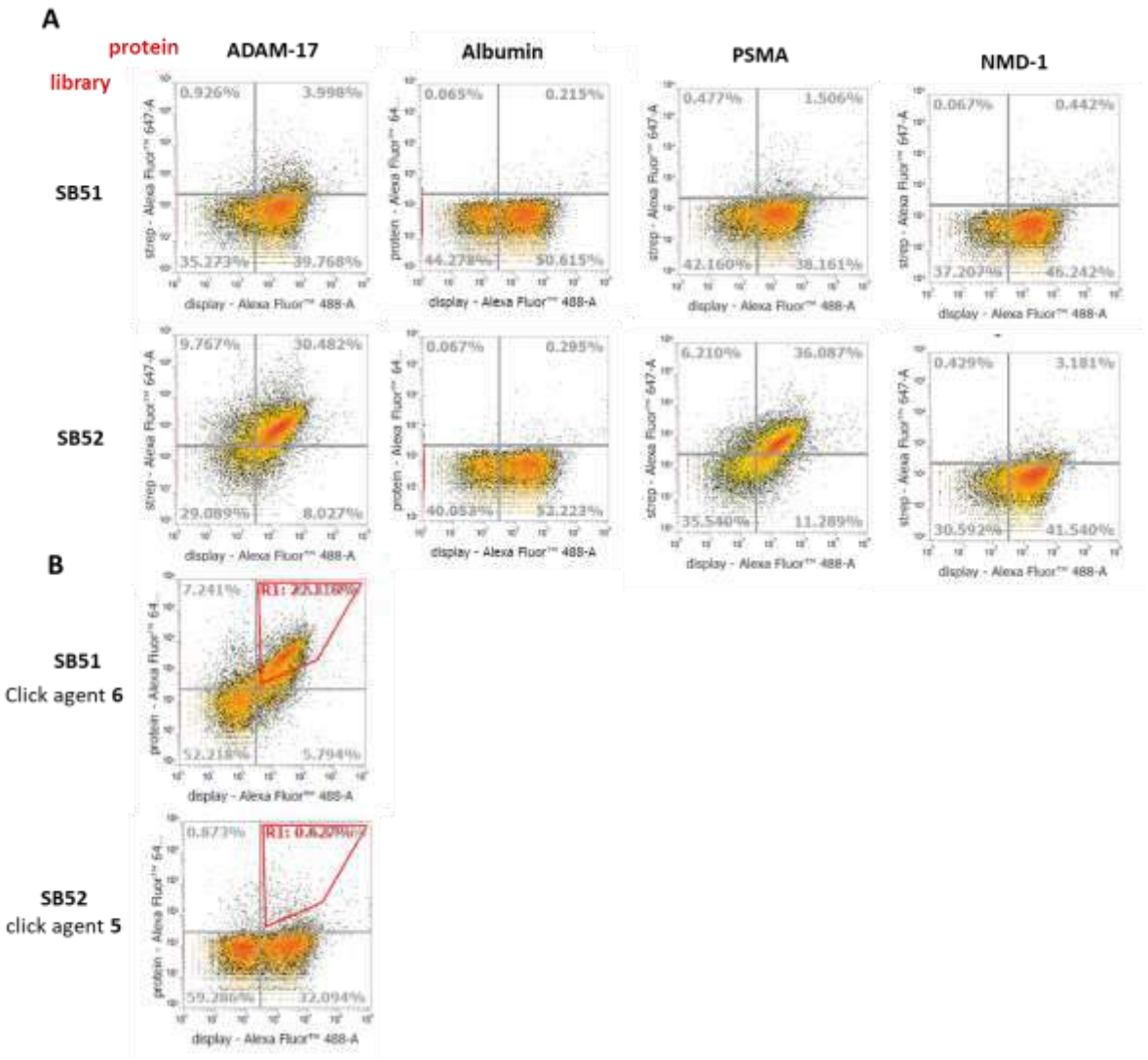

Fig. 49 (**A**) Flow cytometry plots (Alexa Fluor 488 fluorescence vs Strep-647 fluorescence) of (A) SB51 and SB52 libraries treated with ADAM-17, albumin, PSMA, NMD-1 proteins. (**B**) Flow cytometry plots of SB51 library modified with click agent **6** and SB52 library modified with click agent **5** treated with ADAM-17.

Post-translational modified libraries showed different binding properties. Specifically, relevant binding was observed for SB52 library with ADAM-17 and PSMA proteins. In order to understand the contribution of hydroxamic scaffold to the ADAM-17 binding, SB51 library was further modified with click agent **6** and SB52 library was modified with click agent **5** (**Fig.49B**). Results showed that click agent **6** mainly contribute to ADAM-17 binding with negligible contribution of selected peptide library.

For the first time, yeast display screening was coupled to post-translational chemical modification via click chemistry in order to introduce a metal chelating group during a peptide selection of a metalloprotease inhibitor. These results showed that cuAA with click agent **6** significantly increase

the binding property for metalloprotease target, however they confuted the selection of peptide libraries with ncAA. A deeper investigation on the effects of click agents on ADAM-17 interaction was performed with binding and inhibitory assays.

Investigation of ADAM-17 binding and inhibition of click agents and derivatives

The variable of peptide sequence in a yeast display system was removed, using the heptapeptide SSSZSSS, as used for the parameter study. Then, post-translational CuAA was performed with different alkynes and yeast cells were labelled. (**Fig. 50**)

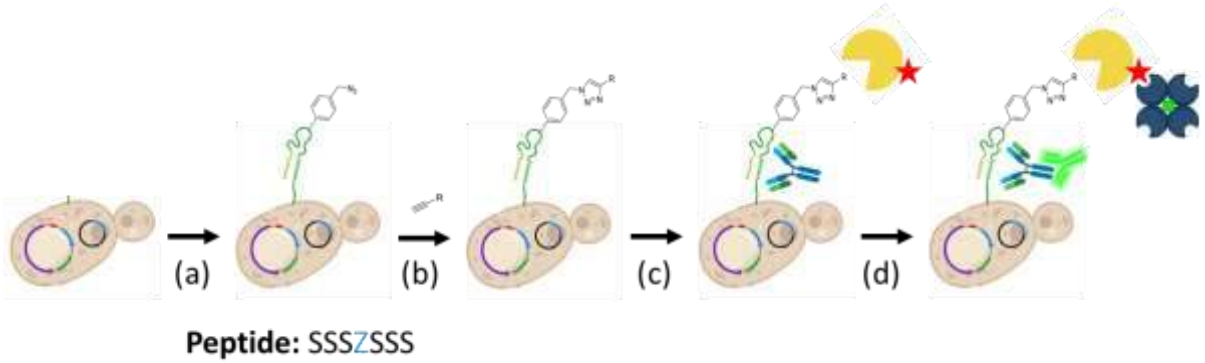

Fig. 50 Schematic representation of (a) heptapeptide with ncAA display, (b) post-translational click modification with alkyne derivatives and labelling with (c) primary (IgG anti-HA, biotinylated ADAM-17) and secondary staining (d) (IgG Alexa Fluor 488, Streptavidin DyLight-647).

Alkyne derivatives and click-products used in binding assay and inhibition assay are reporter in **Fig. 51**.

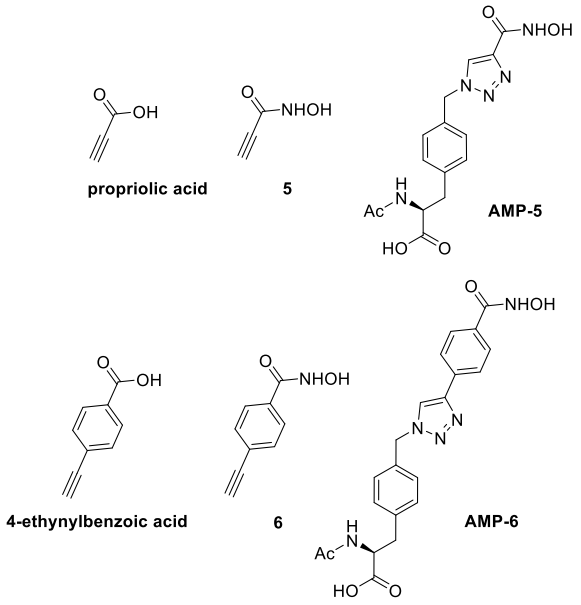

Fig. 51 Structures of tested alkyne derivatives and click-products

Hydroxamates (click agents **5** and **6**) and parent carboxylic acids (propiolic acid and 4-ethynylbenzoic acid) were used in post-translational CuAA of peptide with ncAA and labelling with ADAM-17 was performed at multiple concentrations (**Fig. 52**).

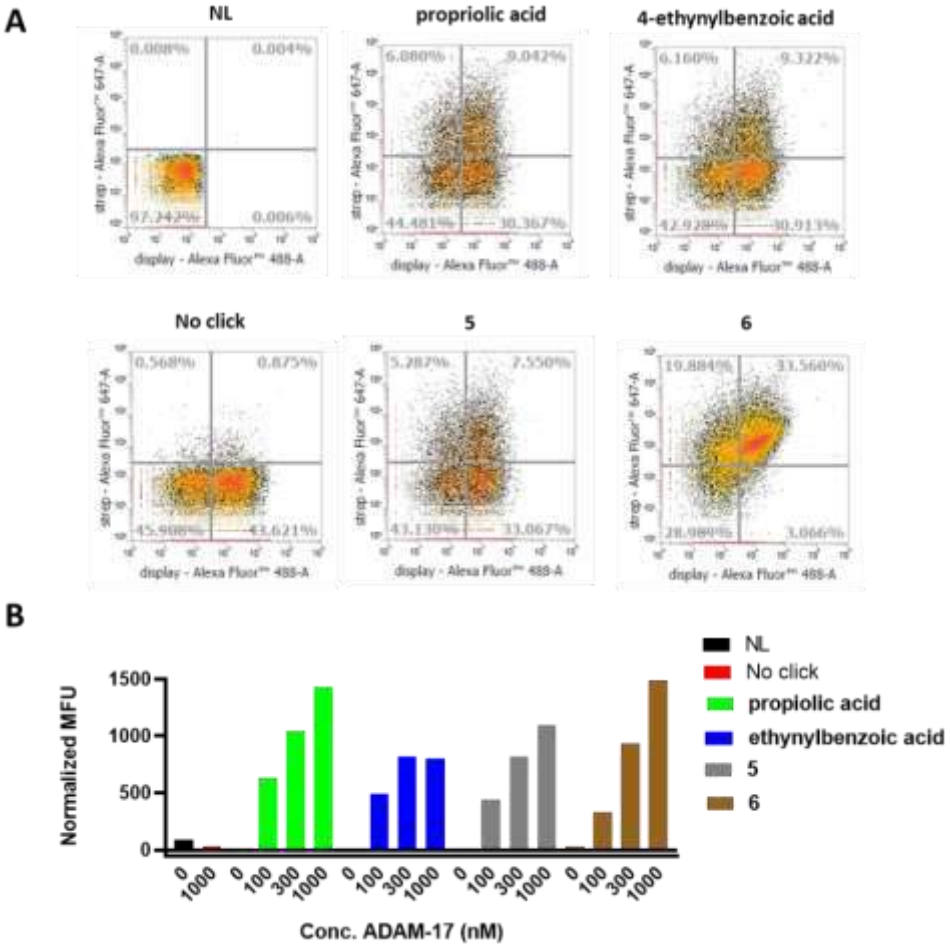

Fig. 52 (**A**) Flow cytometry plots (Alexa Fluor 488 fluorescence vs Strep-647 fluorescence) of yeast cells after post-translational click modification with alkyne derivatives at ADAM-17 conc. 1000 nM. (**B**) Normalized median fluorescence of yeast cells after post-translational modification with alkyne derivatives at different ADAM-17 conc. (0 nM, 100 nM, 300 nM, 1000 nM).

Click-modified samples were analysed with flow cytometry and normalized median fluorescence intensities revealed that click modification affords an important contribution to ADAM-17 binding, compared to not labelled (NL) and not modified (no click) controls. Distributions of population density were different (**Fig. 52A**), however the correlations of fluorescence intensity and target concentration were appreciable for all four alkyne-modified populations (**Fig. 52B**). The difference of metalloprotease binding between the populations with and without click modification was remarkable. Furthermore, binding constants (K_D) of the interaction between post-translational modified peptide and ADAM-17 target were calculated using yeast surface titrations (Angelini et al., 2015). From the sigmodal fitting of plots of median fluorescence intensities and display intensity ratio

vs biotinylated target concentration of four alkyne-modified populations (**Fig. 53A**), binding constants were determined (**Fig. 53C**). Calculated values were in the mid nanomolar range with the strongest binding afforded by the modification with click agent **6**.

Furthermore, the inhibitory potency of alkynes and click-products (**AMP-5** and **AMP-6**) was tested to investigate if these molecules effectively bind the catalytic site with inhibitory effect. (**Fig. 53B, C**) Alkynes were compared with click-products to evaluate the differences after the CuAA modification.

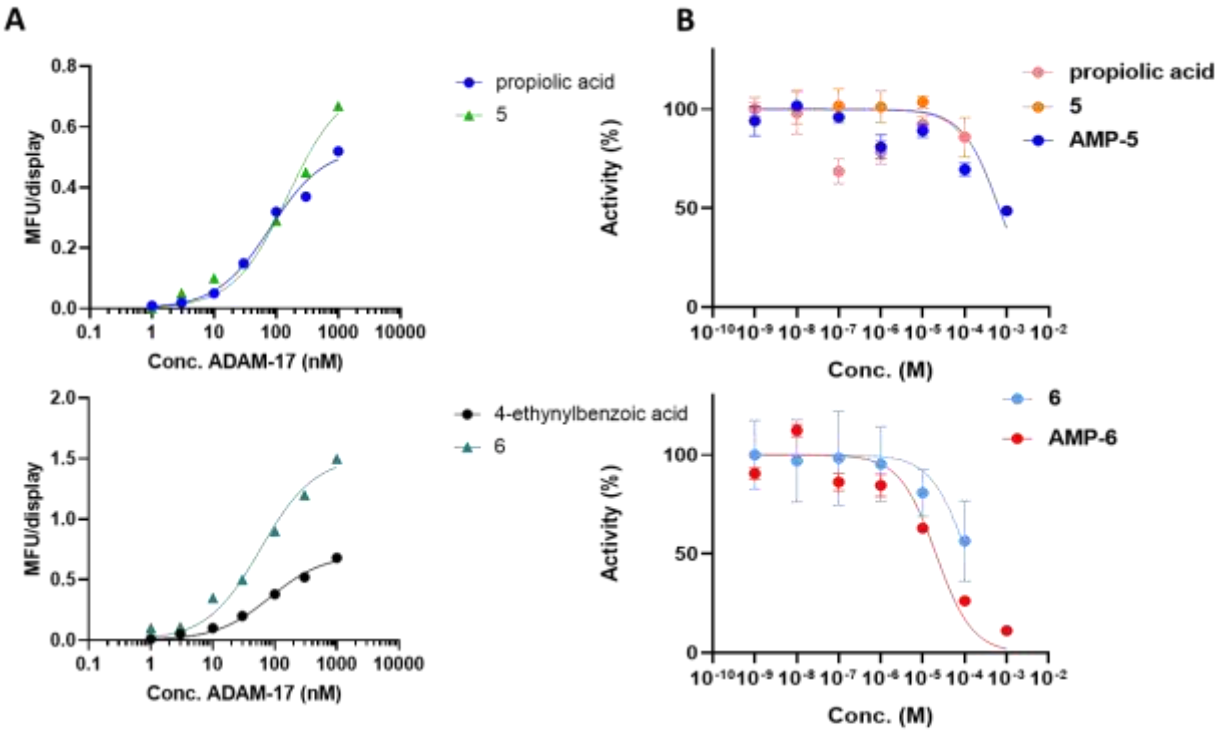

C

Compound	IC_{50} (µM)	K_D (nM)
propiolic acid	> 100	97
5	> 100	189
AMP-5	> 100	-
4-ethynylbenzoic acid	N.D.	114
6	~ 81	71
AMP-6	21	-

Fig. 53 (**A**) Titration curves (ADAM-17 conc. vs median fluorescence/ display ratio) of yeast cells after post-translational click modification with alkyne derivatives (**B**) Inhibition plot of ADAM-17 with alkyne derivatives and click-products (**C**) Table with half inhibitory concentrations and binding constants (N.D. not determinable)

Tested molecules showed absence or low inhibitory potencies in the micromolar range. Specifically, a slight decrease in half-inhibitory concentration was appreciable for click agent **6** after click reaction (**Fig. 53C**). Finally, it was not possible to determine the inhibitory potency of 4-ethynylbenzoic acid due to interference of fluorescence detection in the inhibition assay.

In conclusion, the values of IC_{50} and K_D differ of several orders of magnitude and do not support the hypothesis of an effective binding at the catalytic site. These results may be explained by an aspecific binding of click-modified peptide without effecting the catalytic site.

5.2 Conclusions

In this study, two approaches for the screening of peptide binders of ADAM-17 via yeast surface display were applied. First, a naïve yeast library of 10^9 cyclic peptides with canonical amino acids was sorted and enriched with peptide binders. Selection was performed via magnetic activated cell sorting and fluorescent activated cell sorting.

Although the approach allowed to enrich the population with peptide binders, selected population was not selective towards the metalloprotease target. Five peptide sequences were identified to determine the correspondence with native library. However, selected peptides were no further explored as inhibitors because they lacked the required characteristics of potency and selectivity.

In the second strategy, yeast libraries of peptides with ncAAs were chemically modified with click agents in order to expand the chemical diversity and introduce the hydroxamic moiety.

First, the conditions to perform an efficient post-translational cuAA with click agents **5** and **6** on yeast surface were determined. These conditions were applied on a naïve yeast library of 10^9 cyclic peptides with ncAAs. The peptide library was efficiently produced and screened against metalloprotease target. Selection was performed via magnetic activated cell sorting and fluorescent activated cell sorting. Selected populations were characterized to define the contribution of peptide and hydroxamic scaffold to the binding.

A substantial contribution of the scaffold to the target binding was observed, invalidating the screening and selection steps of peptide library. These results required an investigation on the effects of click agents on ADAM-17 selection. Post-translational modifications of a model peptide were performed with different alkynes. Results of binding and inhibitory assays showed differences of several orders of magnitude. In conclusion, these results may explain an aspecific binding of click-modified peptide without effecting the catalytic site.

5.3 Materials and methods

Yeast Media, Yeast Strains and Plasmids

- Yeast Extract Peptone Dextrose (YPD) media is composed of dextrose (2 % w/v), yeast extract (1 % w/v) and peptone (2 % w/v).

- Synthetic Dextrose medium with CasAmino Acids (SD-CAA) is composed of dextrose (2 % w/v), yeast nitrogen base (0.67 % w/v), casamino acids (−ade, −ura, −trp, 0.5 % w/v), citrate buffer
- Synthetic Dextrose medium without tryptophan, leucine or uracil (SD-CAA −ura, −leu, −trp) is composed of dextrose (2 % w/v), yeast nitrogen base (0.67 % w/v), citrate buffer and synthetic dropout media (1.45 g/L)
- Synthetic Galactose medium with CasAmino Acids (SG-CAA) is composed of galactose (2 % w/v), dextrose (0.2 % w/v), yeast nitrogen base (0.67 % w/v), casamino acids (−ade, −ura, −trp, 0.5 % w/v), phosphate buffer
- Synthetic Galactose medium without tryptophan, uracil (SG-CAA −ura, −trp) is composed of galactose (2 % w/v), dextrose (0.2 % w/v), yeast nitrogen base (0.67 % w/v), phosphate buffer and synthetic dropout media (1.45 g/L)

EBY100 (S. cerevisiae) is a yeast strain derived from BJ5465 (ATCC, MYA-4941) and used for yeast surface display of peptides with canonical amino acids.

RJY100 (S. cerevisiae) was constructed by Van Deventer *et al*. and obtained by the elimination of the amber codon in Trp1/YDR007W gene encoded in strain EBY100 for selection purposes. It was used in yeast surface display of peptides with non-canonical amino acids using the incorporated pRS315LeuOmeRS vector. pRS315LeuOmeRS vector encoding for orthogonal tRNA/aatRNA pair was used for incorporation of -canonical amino acid p-azido-L-methyl phenylalanine in correspondence of a stop codon (Van Deventer et al., 2016). Stalk expression vector is a modified pCT-CON Yeast display vector with HA epitope tag and 649 stalk sequence (Mcmahon et al., 2018) Peptide sequences were coded by custom base oligos and provided by Integrated DNA Technologies. pCT-CON encoding the peptide SSSZSSS is the construct, encoding for the peptide SSSZSSS (S: Ser, Z: p-azide-L-methyl phenylalanine) and is the result of peptide sequence cloning inside the Stalk expression vector.

Vector digestion

The Stalk vector was digested with restriction enzymes (BamHI and NheI) purified by ethanol precipitation.

Peptide library construction

Peptide libraries were constructed following the protocol of Benatuil and coworkers (Benatuil et al., 2010). Briefly, S. cerevisiae cells at logarithmic phase in YPD media were expanded, then collected by centrifugation (3000 rpm for 3 minutes) and washed twice by ice-cold water and ice-cold

electroporation buffer (1 M Sorbitol / 1 mM CaCl2). Yeast cells were conditioned in 0.1 M LiAc/10 mM DTT and shaked at 225 rpm in a culture flask for 30 minutes at 30 °C. Digested vector backbone and DNA insert were combined for electroporation reaction (Gene Pulser Xcell Electroporation Systems). Electroporated cells were grown in 1:1 mix of 1 M sorbitol : YPD media at30°C for 1 hour and then collected and resuspended in SD-UT media, grown for 48 hours at 30°C in shacking and freezed in glycerol stocks. Multiple electroporation steps were followed. Library size was determined via colony counts.

The following peptide display libraries were generated:

Peptide library	**yeast strain**	**Peptide Sequence**	**Theoretical Diversity**	**Experimental Diversity**
LB1	EBY100	CX_7C	1*10^9	4*10^8
LB6	EBY100	CX_9C	5*10^11	2*10^9
LB13	EBY100	CX_3CX_9C	4*10^15	6*10^8
LB14	EBY100	CX_6CX_6C	4*10^15	3*10^8
LB15	EBY100	CX_9CX_3C	4*10^15	5*10^8
LB2	RJY100	$CX\underline{Z}X_5C$	6*10^7	2*10^8
LB3	RJY100	$CX_3\underline{Z}X_3C$	6*10^7	5*10^8
LB4	RJY100	$CX_5\underline{Z}XC$	6*10^7	5*10^8
LB5	RJY100	$\underline{Z}CX_7C$	1*10^9	5*10^8

Yeast library induction with canonical amino acids

Yeast libraries LB1, LB6, LB13, LB14, LB15 (transformed EBY100) were thaw at room temperature and expanded in SD-CAA media with shaking of 250 rpm overnight at 30°C. Then, cells were diluted at OD value of 1 and let grown in SD-CAA media until an OD_{600} value of 2–5 and induced with fresh SG-CAA media. Finally, they were grown at 20 °C with shaking overnight and further used for selection.

Yeast library induction with non-canonical amino acids

Yeast libraries LB2, LB3, LB4, LB5 (transformed RJY100) were thaw at room temperature and expanded in SD-CAA -Ura -Leu -Trp media with shaking of 250 rpm overnight. Then, cells were diluted and let grown in SD-CAA-Ura -Leu -Trp media until OD_{600} value of 2–5 and induced with fresh SG-CAA -Ura -Leu -Trp media in presence of p-azide-L-methyl phenylalanine (1mM). Finally,

they were grown at 20 °C with shaking overnight and further used for post-translational chemical modification with click chemistry reaction.

Magnetic activated cell sorting

Dynabeads biotin binder (10 µL ,Invitrogen) were washed twice with PBSA and incubated with biotinylated ADAM-17 (50 pmol, 1µM) for 1h at 4 °C, then washed twice with PBSA buffer. Freshly induced yeast cells (2.10^9 yeast cells) were precipitated (3,000 × g for 5 min at 4 °C) in 50 mL conical tubes and were incubated with magnetic beads for 2 h at 4°C. Finally, Magnetic beads were washed five times with PBSA (1 mL) and yeast cells were let them grow in SD-CAA overnight at 30°C. Number of replication per hour allowed to estimate the library diversity and beads were removed with the use of a magnet.

Fluorescent activated cell sorting

Yeast cells with a number ten-fold higher than library diversity were pelleted and the supernatant removed by centrifugation (3,000 × g for 5 min at 4 °C). Yeast cells were resuspended in PBSA and washed twice. Then, cells were stained with primary antibody IgG mouse monoclonal anti-HA (1:1000 dilution factor) and biotinylated ADAM-17 with an incubation at room temperature for 1 hour. Cells were pelleted and washed with PBSA. Then, for the secondary staining IgG goat anti-mouse Alexa Fluor 488 (1:200 dilution factor) was used with a 30 minutes incubation in ice bath and shacking at 180 rpm, together with Streptavidin DyLight-647 (1:200 dilution factor) for detection of biotinylated proteins or peptides. Cells were stored as pellet in ice and resuspended in PBSA before the analysis at Flow cytometer (FACSAria™ III Cell Sorter, BD). Collected cells were grown in fresh SD-CAA media overnight. Flow cytometer analyzes cell number and morphology of yeast cells by evaluation of forward side scattering (FSS) and a side scattering (SSC), and absorbance of specific fluorophores used during the staining step.

Analytical cytometry

Freshly induced yeast cells ($2{\cdot}10^6$ cells per sample) were centrifuged (3,000 × g for 5 min at 4 °C) and washed twice with PBSA. Then, biotinylated protein was added at different concentration (with primary IgG mouse anti-HA if necessary) in 40 µL and shacked at room temperature for 1 hour. Subsequently, cells were centrifuged (3,000 × g for 5 min at 4 °C) and washed twice with PBSA. Then, Streptavidin DyLight-647 with 1:200 dilution factor (with IgG goat anti-chicken Alexa Fluor 488 if necessary) was used with a 30 minutes incubation in ice bath and shacking mildly at 180 rpm.

Finally, cells were centrifuged (3,000 × g for 5 min at 4 °C) and washed twice with PBSA before the analysis at Flow cytometer (Attune NxT Flow Cytometer, Thermo fisher).

DNA Plasmid Extraction

DNA plasmid from yeast cells was recovered with a Zymoprep™ Yeast Plasmid Miniprep II Kit (Zymo research) following the instructions reported by the manufacturer. Briefly, yeast cells were lysate with Zymolyase™ and DNA washed and isolated with the use of selective buffers and a mini column.

Bacteria transformation

E. Coli TOP10 cells were used for heat shock transformation. Briefly, chemical competent cells were incubated with plasmid in ice bath for 30 minutes, then placed at 42°C for 1 minute and transferred in ice bath for 1 minute. Subsequently, cells were grown in SOC media at 37°C and plated in LB-selective plates.

DNA sequencing

Purified DNA was sequenced with sequencing Sanger method performed by BMR Genomics S.r.l.

Click chemistry

From a modified protocol of Van Deventer and coworkers (Van Deventer et al., 2016), freshly induced yeast cells ($2 \cdot 10^6$ cells per sample) were centrifuged (3,000 g for 5 min at 4 °C) and washed with PBS. Then, click reaction was performed with addition of aqueous solutions of copper sulphate (75μM), BTTES (375μM), aminoguanidine (1mM) and alkyne-biotin or alkyne derivative (300μM). The sample was mixed and a solution of sodium ascorbate was added (2.5 mM). Sample was incubated at room temperature for 30 minutes, then centrifuged (3,000 rpm for 5 min at 4 °C) and click reaction repeated a second time.

Parameter study of click chemistry

Yield efficiency of post-translational click modification on yeast surface was evaluated following the protocol “Click chemistry” reported above, investigating the parameters:

- Alkyne-biotin concentration (0 μM, 1 μM, 3 μM, 10 μM, 30μM, 100 μM, 300 μM and 1000 μM)
- Solvent (PBS, 10% v/v ACN, 30% v/v MeOH, 20% v/v EtOH)

- Concentration of MeOH (0%, 5%, 10%, 20% and 30% v/v in PBS) and EtOH (0%, 5%, 10%, 20% v/v in PBS).
- Concentration of click agent, **5** and **6** (0 μM, 1 μM, 3 μM, 10 μM, 30μM, 100 μM, 300 μM, 1000 μM) in 0%, 5%, 10%, 20% v/v of MeOH in PBS.
- number of consecutive click reaction (0, 1, 2, 3, 4)

Labelling with Streptavidin DyLight-647 was performed to quantify the conjugation with alkyne-biotin. Streptavidin staining was performed with a 30 minutes incubation in ice bath and shacking at 180 rpm. The cells were centrifuged (3,000 rpm for 5 min at 4 °C) and washed with PBSA twice before the analysis at Flow cytometer (Attune NxT Flow Cytometer, Thermo fisher) for the detection of Streptavidin, Alexa Fluor™ 647 conjugate (Ex 650 nm/Em 668). Assays were performed in triplicate.

Inhibition assay

The enzymatic activity of ADAM-17 was evaluated in the presence of inhibitor (final conc. 10^{-3} – 10^{-9} M) with a 30 min incubation at 37 °C. Then, fluorogenic peptide substrate (Mca-Pro-Leu-Ala-Gln-Ala-Val-Dap(Dnp)-Arg-Ser-Ser-Ser-Arg-NH_2, 48 μM, 4031302, Bachem) was added in 96 well plates (Nunc maxisorp) in buffer 25 mM Tris pH 8, 2.5 μM $ZnCl_2$, and 0.1% v/v Brij-35. Fluorescence was read with a plate reader (Tecan Infinite M200) and the assay was run in triplicate. Plate was read every minute for 30 min at 37 °C and fluorescence slope was calculated with linear fitting. Normalized slope was converted in activity and half inhibitory concentration was determined with sigmoidal fitting. Excitation and emission wavelengths were 355 and 405 nm, correspondingly.

Conclusions and Outlooks

For the development of peptide inhibitors of two metalloproteases involved in OA, chemical modifying agents of peptides were first synthesized and characterized. Subsequently, the strategies of metalloprotease production were explored and lastly the yeast display screenings were performed. The synthesis and characterization of two hydroxamate classes of compounds, thiol-alkylating agents and azido-click coupling agents, for peptide modification have been achieved. Reactivity studies with amino acids and peptides demonstrate their versatility and potentiality. Based on the structure of known dithiol bis-alkylating agents, three novel di-alkylating agents (**2, 3, 4**) have been synthesized and tested, as cyclizing and modifying agent. Di-alkylating agent **2** showed the most interesting properties of reactivity and stability, with remarkable results comparable with known dithiol bis-alkylating agents. Reactivity in a one-pot strategy and chemoselectivity proved the strength and versatility of this agent to produce cyclic peptides functionalized with hydroxamic moiety. Its use for chemical modification of synthetic peptide libraries on high-throughput screenings of metalloprotease inhibitors will be investigated in further studies.

Furthermore, azido-click coupling agents were synthesized and characterized, showing good functionalizing abilities. First, the reactivity of click agents **5** and **6** was investigated with amino acids and synthetic peptide. Subsequently, click agents were used for the first time for site-specific coupling of hydroxamic moiety via post-translational cuAA of peptide libraries with ncAAs on yeast surface.

To produce the metalloprotease targets, a similar strategy was carried out for ADAM-17 and ADAMTS-5. Different constructs of ADAM-17 were initially evaluated and subsequently the target protein was expressed in a large scale. The strategy to produce the recombinant protein afforded good expression yield and biotinylated target was used for screening assay with yeast surface display technology.

With a similar approach, several ADAMTS-5 constructs were evaluated and subsequent protein expression in a medium scale was performed. Active protein and active site mutant were expressed to evaluate the expression yields, catalytic activity and stability. Unfortunately, overall low yield prevented the use of ADAMTS-5 as target for further yeast display screening.

Finally, yeast surface display technology, that enables quantitative screening of large combinatorial libraries of random peptide sequences, was applied for the development of peptide-based inhibitors. A naïve yeast library of 10^9 cyclic peptides with canonical amino acids was sorted and enriched with peptide binders towards ADAM-17 target. Although the approach allowed to enrich the population with peptide binders, selected population was not selective towards the metalloprotease target. Five peptide sequences were identified to determine the correspondence with native library. However,

selected peptides were no further explored as inhibitors because they lacked the required characteristics of potency and selectivity.

In a second attempt, yeast libraries of peptides with ncAAs were chemically modified with click agents in order to expand the chemical diversity and introduce the hydroxamic moiety.

The conditions to perform an efficient post-translational cuAA with click agents **5** and **6** on yeast surface were initially determined with a parameter study.

Selected conditions were used to modify a naïve yeast library of 10^9 cyclic peptides with ncAAs, which was screened against ADAM-17 target. Unfortunately, a substantial contribution of the scaffold **6** to the target binding was observed, invalidating the screening and selection steps of peptide library. In order to clarify the contribution of click agents to ADAM-17 binding, a post-translational modification of a model peptide was performed with different alkynes. The results of binding and inhibitory assays might explain an aspecific binding of click-modified peptide to the protein without effecting the catalytic site. Further studies are necessary to elucidate the contribution of modified peptide to metalloprotease binding.

More investigations are under development in order to apply yeast libraries of peptides with canonicals and non-canonical amino acids for the selection of peptide binders of ADAM-17 metalloprotease.

References

Abbaszade, I., Liu, R. Q., Yang, F., Rosenfeld, S. A., Ross, O. H., Link, J. R., et al. (1999). Cloning and Characterization of ADAMTS11 , an Aggrecanase from the ADAMTS Family. *J. Biol. Chem.* 274, 23443–23450. doi:10.1074/JBC.274.33.23443.

Abramoff, B., and Caldera, F. E. (2020). Osteoarthritis: Pathology, Diagnosis, and Treatment Options. *Med. Clin. North Am.* 104, 293–311. doi:10.1016/j.mcna.2019.10.007.

Amin, A. R. (1999). Regulation of tumor necrosis factor-α and tumor necrosis factor converting enzyme in human osteoarthritis. *Osteoarthr. Cartil.* 7, 392–394. doi:10.1053/JOCA.1998.0221.

Amitai, G., Gez, R., Raveh, L., Bar-Ner, N., Grauer, E., and Chapman, S. (2016). Novel bifunctional hybrid small molecule scavengers for mitigating nerve agents toxicity. *Chem. Biol. Interact.* 259, 187–204. doi:10.1016/j.cbi.2016.04.036.

Andreu, C., and del Olmo, M. (2018). Yeast arming systems: pros and cons of different protein anchors and other elements required for display. *Appl. Microbiol. Biotechnol.* 102, 2543–2561. doi:10.1007/s00253-018-8827-6.

Angelini, A., Chen, T. F., de Picciotto, S., Yang, N. J., Tzeng, A., Santos, M. S., et al. (2015). "Protein Engineering and Selection Using Yeast Surface Display," in *Methods Mol Biol.*, 3–36. doi:10.1007/978-1-4939-2748-7.

Antonczak, A. K., Morris, J., and Tippmann, E. M. (2011). Advances in the mechanism and understanding of site-selective noncanonical amino acid incorporation. *Curr. Opin. Struct. Biol.* 21, 481–487. doi:10.1016/J.SBI.2011.04.004.

Apte, S. S. (2020). "ADAMTS Proteins: Concepts, Challenges, and Prospects," in *Methods in Molecular Biology* (Humana Press Inc.), 1–299. doi:10.1007/978-1-4939-9698-8_1.

Arribas, J., and Borroto, A. (2002). Protein ectodomain shedding. *Chem. Rev.* 102, 4627–4637. doi:10.1021/cr010202t.

Benatuil, L., Perez, J. M., Belk, J., and Hsieh, C. M. (2010). An improved yeast transformation method for the generation of very large human antibody libraries. *Protein Eng. Des. Sel.* 23, 155–159. doi:10.1093/PROTEIN/GZQ002.

Berenbaum, F., Wallace, I. J., Lieberman, D. E., and Felson, D. T. (2018). Modern-day environmental factors in the pathogenesis of osteoarthritis. *Nat. Rev. Rheumatol.* 14, 674–681. doi:10.1038/s41584-018-0073-x.

Boder, E. T., and Wittrup, K. D. (1997). Yeast surface display for screening combinatorial polypeptide libraries. *Nat. Biotechnol.* 15, 553–557. doi: 10.1038/nbt0697-553

Brebion, F., Gosmini, R., Deprez, P., Varin, M., Peixoto, C., Alvey, L., et al. (2021). Discovery of GLPG1972/S201086, a Potent, Selective, and Orally Bioavailable ADAMTS - 5 Inhibitor for the Treatment of Osteoarthritis. *J. Med. Chem.* 64, 2937–2952. doi:10.1021/acs.jmedchem.0c02008.

Cherf, G. M., and Cochran, J. R. (2015). "Applications of Yeast Surface Display for Protein Engineering," in *Yeast Surface Display*, 155–175. doi:10.1007/978-1-4939-2748-7.

Chin, J. W., Cropp, T. A., Anderson, J. C., Mukherji, M., Zhang, Z., and Schultz, P. G. (2003). An expanded eukaryotic genetic code. *Science.* 301, 964–967. doi:10.1126/science.1084772.

Coleman, J. E. (1992). Zinc Proteins: Enzymes, storage proteins, transcription factors, and replication proteins. *Annu. Rev. Biochem.* 61, 897–946. doi:10.1146/annurev.bi.61.070192.004341.

DeGruyter, J. N., Malins, L. R., and Baran, P. S. (2017). Residue-Specific Peptide Modification: A Chemist's Guide. *Biochemistry* 56, 3863–3873. doi:10.1021/acs.biochem.7b00536.

Deng, H., O'Keefe, H., Davie, C. P., Lind, K. E., Acharya, R. A., Franklin, G. J., et al. (2012). Discovery of highly potent and selective small molecule ADAMTS-5 inhibitors that inhibit human cartilage degradation via encoded library technology (ELT). *J. Med. Chem.* 55, 7061–7079. doi:10.1021/jm300449x.

Derda, R., and Jafari, M. R. (2018). Synthetic Cross-linking of Peptides : Molecular Linchpins for Peptide Cyclization. *Protein Pept. Lett.* 25, 1–25. doi:10.2174/0929866525666181120090650.

Di Stasio, E., Lancellotti, S., Peyvandi, F., Palla, R., Mannucci, P. M., and De Cristofaro, R. (2008). Mechanistic studies on ADAMTS13 catalysis. *Biophys. J.* 95, 2450–2461. doi:10.1529/biophysj.108.131532.

Duffy, M. J., McKiernan, E., O'Donovan, N., and McGowan, P. M. (2009). Role of ADAMs in cancer formation and progression. *Clin. Cancer Res.* 15, 1140–1144. doi:10.1158/1078-0432.CCR-08-1585.

Edwards, D. R., Handsley, M. M., and Pennington, C. J. (2009). The ADAM metalloproteinases. *Mol. Aspects Med.* 29, 258–289. doi:10.1016/j.mam.2008.08.001.

El Bakali, J., Gras-Masse, H., Maingot, L., Deprez, B., Dumont, J., Leroux, F., et al. (2014). Inhibition of aggrecanases as a therapeutic strategy in osteoarthritis. *Future Med. Chem.* 6, 1399–1412. doi:10.4155/FMC.14.84.

Farinas, E. T., Bulter, T., and Arnold, F. H. (2001). Directed enzyme evolution. *Curr. Opin. Biotechnol.* 12, 545–551. doi:10.1016/S0958-1669(01)00261-0.

Feldmann, M., and Maini, S. R. N. (2008). Role of cytokines in rheumatoid arthritis: an education in pathophysiology and therapeutics. *Immunol. Rev.* 223, 7–19. doi:10.1111/j.1600-

065X.2008.00626.x.

Fisher, J. F., and Mobashery, S. (2006). Recent advances in MMP inhibitor design. *Cancer Metastasis Rev.* 25, 115–136. doi:10.1007/s10555-006-7894-9.

Fosang, A. (2008). ADAMTS-5: The story so far. *Eur. Cells Mater.* 15, 11–26. doi:10.22203/eCM.v015a02.

Fosang, A. J., and Little, C. B. (2008). Drug Insight: Aggrecanases as therapeutic targets for osteoarthritis. *Nat. Clin. Pract. Rheumatol.* 4, 420–427. doi:10.1038/ncprheum0841.

Fosang, A. J., Rogerson, F. M., East, C. J., and Stanton, H. (2008). ADAMTS-5: The story so far. *Eur. Cells Mater.* 15, 11–26. doi:10.22203/eCM.v015a02.

Fushimi, K., Troeberg, L., Nakamura, H., Ngee, H. L., and Nagase, H. (2008). Functional differences of the catalytic and non-catalytic domains in human ADAMTS-4 and ADAMTS-5 in aggrecanolytic activity. *J. Biol. Chem.* 283, 6706–6716. doi:10.1074/jbc.M708647200.

Gendron, C., Kashiwagi, M., Ngee, H. L., Enghild, J. J., Thøgersen, I. B., Hughes, C., et al. (2007). Proteolytic activities of human ADAMTS-5: Comparative studies with ADAMTS-4. *J. Biol. Chem.* 282, 18294–18306. doi:10.1074/jbc.M701523200.

Georgiadis, D., and Yiotakis, A. (2008). Specific targeting of metzincin family members with small-molecule inhibitors: Progress toward a multifarious challenge. *Bioorganic Med. Chem.* 16, 8781–8794. doi:10.1016/j.bmc.2008.08.058.

Geurink, P., Klein, T., Leeuwenburgh, M., Van Der Marel, G., Kauffman, H., Bischoff, R., et al. (2008). A peptide hydroxamate library for enrichment of metalloproteinases: Towards an affinity-based metalloproteinase profiling protocol. *Org. Biomol. Chem.* 6, 1244–1250. doi:10.1039/b718352f.

Gilbert, A. M., Bikker, J. A., and O'Neil, S. V. (2011). Advances in the development of novel aggrecanase inhibitors. *Expert Opin. Ther. Pat.* 21, 1–12. doi:10.1517/13543776.2011.539204.

Goldring, M. B., and Goldring, S. R. (2007). Osteoarthritis. *J. Cell. Physiol.*, 626–635. doi:10.1002/jcp.21258.

Goto, Y., Katoh, T., and Suga, H. (2011). Flexizymes for genetic code reprogramming. *Nat. Protoc.* 6, 779–790. doi:10.1038/nprot.2011.331.

Griffin, T. M., and Guilak, F. (2005). The role of mechanical loading in the onset and progression of osteoarthritis. *Exerc. Sport Sci. Rev.* 33, 195–200. doi:10.1097/00003677-200510000-00008.

Heinegård, D., and Saxne, T. (2011). The role of the cartilage matrix in osteoarthritis. *Nat. Rev. Rheumatol.* 7, 50–56. doi:10.1038/nrrheum.2010.198.

Heinis, C., Rutherford, T., Freund, S., and Winter, G. (2009). Phage-encoded combinatorial

chemical libraries based on bicyclic peptides. *Nat. Chem. Biol.* 5, 502–507. doi:10.1038/nchembio.184.

Heinis, C., and Winter, G. (2015). Encoded libraries of chemically modified peptides. *Curr. Opin. Chem. Biol.* 26, 89–98. doi:10.1016/j.cbpa.2015.02.008.

Hills, R., Mazzarella, R., Fok, K., Liu, M., Nemirovskiy, O., Leone, J., et al. (2007). Identification of an ADAMTS-4 cleavage motif using phage display leads to the development of fluorogenic peptide substrates and reveals matrilin-3 as a novel substrate. *J. Biol. Chem.* 282, 11101–11109. doi:10.1074/jbc.M611588200.

Hoth, L. R., Tan, D. H., Wang, I. K., Wengender, P. A., Thompson, M. A., Kamath, A. V., et al. (2007). Expression and protein chemistry yielding crystallization of the catalytic domain of ADAM17 complexed with a hydroxamate inhibitor. *Protein Expr. Purif.* 52, 313–319. doi:10.1016/j.pep.2006.10.021.

Huang, Y., Wiedmann, M. M., and Suga, H. (2019). RNA Display Methods for the Discovery of Bioactive Macrocycles. *Chem. Rev.* 119, 10360–10391. doi:10.1021/acs.chemrev.8b00430.

Hunter, D. J., and Bierma-Zeinstra, S. (2019). Osteoarthritis. *Lancet* 393, 1745–1759. doi:10.1016/S0140-6736(19)30417-9.

Huovila, A. P. J., Turner, A. J., Pelto-Huikko, M., Kärkkäinen, I., and Ortiz, R. M. (2005). Shedding light on ADAM metalloproteinases. *Trends Biochem. Sci.* 30, 413–422. doi:10.1016/j.tibs.2005.05.006.

Ingram, R. N., Orth, P., Strickland, C. L., Le, H. V., Madison, V., and Beyer, B. M. (2006). Stabilization of the autoproteolysis of TNF-alpha converting enzyme (TACE) results in a novel crystal form suitable for structure-based drug design studies. *Protein Eng. Des. Sel.* 19, 155–161. doi:10.1093/PROTEIN/GZJ014.

Jacobsen, J. A., Major Jourden, J. L., Miller, M. T., and Cohen, S. M. (2010). To bind zinc or not to bind zinc: An examination of innovative approaches to improved metalloproteinase inhibition. *Biochim. Biophys. Acta - Mol. Cell Res.* 1803, 72–94. doi:10.1016/j.bbamcr.2009.08.006.

Jiang, Y. (2021). Osteoarthritis year in review 2021: biology. *Osteoarthr. Cartil.* doi:10.1016/J.JOCA.2021.11.009.

Jones, I. A., Togashi, R., Wilson, M. L., Heckmann, N., and Vangsness, C. T. (2019). Intra-articular treatment options for knee osteoarthritis. *Nat. Rev. Rheumatol.* 15, 77–90. doi:10.1038/s41584-018-0123-4.

Kelwick, R., Desanlis, I., Wheeler, G. N., and Edwards, D. R. (2015). The ADAMTS (A Disintegrin and Metalloproteinase with Thrombospondin motifs) family. *Genome Biol.* 16, 113. doi:10.1186/s13059-015-0676-3.

Koniev, O., and Wagner, A. (2015). Developments and recent advancements in the field of endogenous amino acid selective bond forming reactions for bioconjugation. *Chem. Soc. Rev.* 44, 5495–5551. doi:10.1039/c5cs00048c.

Könning, D., and Kolmar, H. (2018). Beyond antibody engineering: Directed evolution of alternative binding scaffolds and enzymes using yeast surface display. *Microb. Cell Fact.* 17, 1–17. doi:10.1186/s12934-018-0881-3.

Lawson, G. E., Lee, Y., and Singh, A. (2003). Formation of stable nanocapsules from polymerizable phospholipids. *Langmuir* 19, 6401–6407. doi:10.1021/la034434u.

Lenci, E., Cosottini, L., and Trabocchi, A. (2021). Novel matrix metalloproteinase inhibitors: an updated patent review (2014 - 2020). *Expert Opin. Ther. Pat.* 31, 509–523. doi:10.1080/13543776.2021.1881481.

Li, K., Tay, F. R., and Yiu, C. K. Y. (2020). The past, present and future perspectives of matrix metalloproteinase inhibitors. *Pharmacol. Ther.* 207, 107465. doi:10.1016/j.pharmthera.2019.107465.

Lim, S., Glasgow, J. E., Interrante, M. F., Storm, E. M., and Cochran., J. R. (2017). Dual display of proteins on the yeast cell surface simplifies quantification of binding interactions and enzymatic bioconjugation reactions. *Biotechnol J.* 12, 1–17. doi:10.1002/biot.201600696

Linciano, S., Pluda, S., Bacchin, A., and Angelini, A. (2019). Molecular evolution of peptides by yeast surface display technology. *Medchemcomm* 10, 1569–1580. doi:10.1039/c9md00252a.

Majumdar, M. K., Askew, R., Schelling, S., Stedman, N., Blanchet, T., Hopkins, B., et al. (2007). Double-knockout of ADAMTS-4 and ADAMTS-5 in mice results in physiologically normal animals and prevents the progression of osteoarthritis. *Arthritis Rheum.* 56, 3670–3674. doi:10.1002/ART.23027.

Mammen, M., Choi, S.-K., and Whitesides, G. M. (1998). Polyvalent Interactions in Biological Systems: Implications for Design and Use of Multivalent Ligands and Inhibitors. *Angew. Chemie Int. Ed.* 37, 2754–2794. doi:10.1002/(SICI)1521-3773(19981102)37:20<2754::AID-ANIE2754>3.0.CO;2-3.

Maskos, K., Fernandez-Catalan, C., Huber, R., Bourenkov, G. P., Bartunik, H., Ellestad, G. A., et al. (1998). Crystal structure of the catalytic domain of human tumor necrosis factor-α-converting enzyme. *Proc. Natl. Acad. Sci. U. S. A.* 95, 3408–3412. doi:10.1073/pnas.95.7.3408.

Mcmahon, C., Baier, A. S., Pascolutti, R., Wegrecki, M., Zheng, S., Ong, J. X., et al. (2018). Yeast surface display platform for rapid discovery of conformationally selective nanobodies. *Nat. Struct. Mol. Biol.* 25, 289–296. doi:10.1038/s41594-018-0028-6.

Mead, T. J., and Apte, S. S. (2018). ADAMTS proteins in human disorders. *Matrix Biol.* 71–72, 225–239. doi:10.1016/j.matbio.2018.06.002.

Milla, M. E., Leesnitzer, M. A., Moss, M. L., Clay, W. C., Luke Carter, H., Miller, A. B., et al. (1999). Specific sequence elements are required for the expression of functional tumor necrosis factor-α-converting enzyme (TACE). *J. Biol. Chem.* 274, 30563–30570. doi:10.1074/jbc.274.43.30563.

Mishra, C. B., Tiwari, M., and Supuran, C. T. (2020). Progress in the development of human carbonic anhydrase inhibitors and their pharmacological applications: Where are we today? *Med. Res. Rev.* 40, 2485–2565. doi:10.1002/med.21713.

Mohammad A. Alam (2019). Methods for Hydroxamic Acid Synthesis. *Curr Org Chem.* 23, 978–993. doi:10.2174/1385272823666190424142821.

Morais, M., Nunes, J. P. M., Karu, K., Forte, N., Benni, I., Smith, M. E. B., et al. (2017). Optimisation of the dibromomaleimide (DBM) platform for native antibody conjugation by accelerated post-conjugation hydrolysis. *Org. Biomol. Chem.* 15, 2947–2952. doi:10.1039/c7ob00220c.

Moriki, T., Maruyama, I. N., Igari, A., Ikeda, Y., and Murata, M. (2010). Identification of ADAMTS13 peptide sequences binding to von Willebrand factor. *Biochem. Biophys. Res. Commun.* 391, 783–788. doi:10.1016/j.bbrc.2009.11.138.

Moss, M. L., Jin, S. L. C., Milla, M. E., Burkhart, W., Carter, H. L., Chen, W. J., et al. (1997). Cloning of a disintegrin metalloproteinase that processes precursor tumour-necrosis factor-α. *Nature* 385, 733–736. doi:10.1038/385733a0.

Moss, M. L., and Minond, D. (2017). Recent Advances in ADAM17 Research: A Promising Target for Cancer and Inflammation. *Mediators Inflamm.* 2017. doi:10.1155/2017/9673537.

Moss, M. L., White, J. M., Lambert, M. H., and Andrews, R. C. (2001). TACE and other ADAM proteases as targets for drug discovery. *Drug Discov. Today* 6, 417–426. doi:10.1016/S1359-6446(01)01738-X.

Murumkar, P. R., DasGupta, S., Chandani, S. R., Giridhar, R., and Yadav, M. R. (2010). Novel TACE inhibitors in drug discovery: A review of patented compounds. *Expert Opin. Ther. Pat.* 20, 31–57. doi:10.1517/13543770903465157.

Ochtrop, P., and Hackenberger, C. P. R. (2020). Recent advances of thiol-selective bioconjugation reactions. *Curr. Opin. Chem. Biol.* 58, 28–36. doi:10.1016/j.cbpa.2020.04.017.

Ohtsuka, N., Okuno, M., Hoshino, Y., and Honda, K. (2016). A base-mediated self-propagative Lossen rearrangement of hydroxamic acids for the efficient and facile synthesis of aromatic and aliphatic primary amines. *Org. Biomol. Chem.* 14, 9046–9054. doi:10.1039/c6ob01178k.

Orcutt, K. D., and Wittrup, K. D. (2010). Yeast Display and Selections. *Antib. Eng.*, 207–233. doi:10.1007/978-3-642-01144-3_15.

Passioura, T., and Suga, H. (2017). A RaPID way to discover nonstandard macrocyclic peptide modulators of drug targets. *Chem. Commun.* 53, 1931–1940. doi:10.1039/c6cc06951g.

Peraro, L., Siegert, T. R., and Kritzer, J. A. (2016). *Conformational Restriction of Peptides Using Dithiol Bis-Alkylation*. 1st ed. Elsevier Inc. doi:10.1016/bs.mie.2016.05.035.

Pickens, C. J., Johnson, S. N., Pressnall, M. M., Leon, M. A., and Berkland, C. J. (2018). Practical Considerations, Challenges, and Limitations of Bioconjugation via Azide-Alkyne Cycloaddition. *Bioconjug. Chem.* 29, 686–701. doi:10.1021/acs.bioconjchem.7b00633.

Pillai, V. G., Bao, J., Zander, C. B., McDaniel, J. K., Chetty, P. S., Seeholzer, S. H., et al. (2016). Human neutrophil peptides inhibit cleavage of von Willebrand factor by ADAMTS13: A potential link of inflammation to TTP. *Blood* 128, 110–119. doi:10.1182/blood-2015-12-688747.

Pluda, S., Mazzocato, Y., and Angelini, A. (2021). Peptide-Based Inhibitors of ADAM and ADAMTS Metalloproteinases. *Front. Mol. Biosci.* 8, 678. doi:10.3389/fmolb.2021.703715.

Qiu, Z., Yan, M., Li, Q., Liu, D., Van den Steen, P. E., Wang, M., et al. (2012). Definition of peptide inhibitors from a synthetic peptide library by targeting gelatinase B/matrix metalloproteinase-9 (MMP-9) and TNF-α converting enzyme (TACE/ADAM-17). *J. Enzyme Inhib. Med. Chem.* 27, 533–540. doi:10.3109/14756366.2011.599323.

Reddy, A. S., Kumar, M. S., and Reddy, G. R. (2000). A convenient method for the preparation of hydroxamic acids. *Tetrahedron Lett.* 41, 6285–6288. doi:10.1016/S0040-4039(00)01058-3.

Rostovtsev, V. V., Green, L. G., Fokin, V. V., and Sharpless, K. B. (2002). A stepwise huisgen cycloaddition process: Copper(I)-catalyzed regioselective “ligation” of azides and terminal alkynes. *Angew. Chemie - Int. Ed.* 41, 2596–2599. doi:10.1002/1521-3773(20020715)41:14<2596::AID-ANIE2596>3.0.CO;2-4.

Sako, Y., Goto, Y., Murakami, H., and Suga, H. (2008). Ribosomal synthesis of peptidase-resistant peptides closed by a nonreducible inter-side-chain bond. *ACS Chem. Biol.* 3, 241–249. doi:10.1021/CB800010P.

Santamaria, S. (2020). ADAMTS-5: A difficult teenager turning 20. *Int. J. Exp. Pathol.* 101, 4–20. doi:10.1111/iep.12344.

Santamaria, S., and de Groot, R. (2020). ADAMTS proteases in cardiovascular physiology and disease. *Open Biol.* 10, 200333. doi:10.1098/rsob.200333.

Schaal, J. B., Maretzky, T., Tran, D. Q., Tran, P. A., Tongaonkar, P., Blobel, C. P., et al. (2018). Macrocyclic θ-defensins suppress tumor necrosis factor-α (TNF-α) shedding by inhibition of

TNF-α-converting enzyme. *J. Biol. Chem.* 293, 2725–2734. doi:10.1074/jbc.RA117.000793.

Schaal, J. B., Tran, D. Q., Subramanian, A., Patel, R., Laragione, T., Roberts, K. D., et al. (2017). Suppression and resolution of autoimmune arthritis by rhesus θ-defensin-1, an immunomodulatory macrocyclic peptide. *PLoS One* 12, e0187868. doi:10.1371/journal.pone.0187868.

Schlomann, U., Koller, G., Conrad, C., Ferdous, T., Golfi, P., Garcia, A. M., et al. (2015). ADAM8 as a drug target in pancreatic cancer. *Nat. Commun.* 6, 1–16. doi:10.1038/ncomms7175.

Seegar, T. C. M., and Blacklow, S. C. (2019). Domain integration of ADAM family proteins: Emerging themes from structural studies. *Exp. Biol. Med.* 244, 1510–1519. doi:10.1177/1535370219865901.

Shieh, H. S., Mathis, K. J., Williams, J. M., Hills, R. L., Wiese, J. F., Benson, T. E., et al. (2008). High resolution crystal structure of the catalytic domain of ADAMTS-5 (aggrecanase-2). *J. Biol. Chem.* 283, 1501–1507. doi:10.1074/jbc.M705879200.

Simonetti, L., and Ivarsson, Y. (2020). Genetically Encoded Cyclic Peptide Phage Display Libraries. *ACS Cent. Sci.* 6, 336–338. doi:10.1021/acscentsci.0c00087.

South, K., and Lane, D. A. (2018). ADAMTS-13 and von Willebrand factor: a dynamic duo. *J. Thromb. Haemost.* 16, 6–18. doi:10.1111/jth.13898.

Stanton, H., Rogerson, F. M., East, C. J., Golub, S. B., Lawlor, K. E., Meeker, C. T., et al. (2005). ADAMTS5 is the major aggrecanase in mouse cartilage in vivo and in vitro. *Nature* 434, 648–652. doi:10.1038/nature03417.

Stieglitz, J. T., Kehoe, H. P., Lei, M., and Van Deventer, J. A. (2018). A Robust and Quantitative Reporter System to Evaluate Noncanonical Amino Acid Incorporation in Yeast. *ACS Synth. Biol.* 7, 2256–2269. doi:10.1021/ACSSYNBIO.8B00260.

Supekova, L., Zambaldo, C., Choi, S., Lim, R., Luo, X., Kazane, S. A., et al. (2018). The genetic incorporation of p-azidomethyl-l-phenylalanine into proteins in yeast. *Bioorg. Med. Chem. Lett.* 28, 1570–1573. doi:10.1016/J.BMCL.2018.03.055.

Suzuki, T., Ota, Y., Ri, M., Bando, M., Gotoh, A., Itoh, Y., et al. (2012). Rapid Discovery of Highly Potent and Selective Inhibitors of Histone Deacetylase 8 Using Click Chemistry to Generate Candidate Libraries. *J. Med. Chem.* 55, 9562–9575. doi:10.1021/jm300837y.

Timmerman, P., Beld, J., Puijk, W. C., and Meloen, R. H. (2005). Rapid and quantitative cyclization of multiple peptide loops onto synthetic scaffolds for structural mimicry of protein surfaces. *ChemBioChem* 6, 821–824. doi:10.1002/cbic.200400374.

Tizei, P. A. G., Csibra, E., Torres, L., and Pinheiro, V. B. (2016). Selection platforms for directed evolution in synthetic biology. *Biochem. Soc. Trans.* 44, 1165–1175.

doi:10.1042/BST20160076.

Tornøe, C. W., Christensen, C., and Meldal, M. (2002). Peptidotriazoles on solid phase: [1,2,3]-Triazoles by regiospecific copper(I)-catalyzed 1,3-dipolar cycloadditions of terminal alkynes to azides. *J. Org. Chem.* 67, 3057–3064. doi:10.1021/JO011148J/SUPPL_FILE/JO011148J.

Tortorella, M. D., Burn, T. C., Pratta, M. A., Abbaszade, I., Hollis, J. M., Liu, R., et al. (1999). Purification and cloning of aggrecanase-1: A member of the ADAMTS family of proteins. *Science.* 284, 1664–1666. doi:10.1126/science.284.5420.1664.

Tortorella, M., Pratta, M., Liu, R. Q., Abbaszade, I., Ross, H., Burn, T., et al. (2000). The thrombospondin motif of Aggrecanase-1 (ADAMTS-4) is critical for aggrecan substrate recognition and cleavage. *J. Biol. Chem.* 275, 25791–25797. doi:10.1074/jbc.M001065200.

Van Deventer, J. A., Le, D. N., Zhao, J., Kehoe, H. P., and Kelly, R. L. (2016). A platform for constructing, evaluating, and screening bioconjugates on the yeast surface. *Protein Eng. Des. Sel.* 29, 485–494. doi:10.1093/protein/gzw029.

VanAntwerp, J. J., and Wittrup, K. D. (2000). Fine Affinity Discrimination by Yeast Surface Display and Flow Cytometry. *Biotechnol. Prog.* 16, 31–37. doi:10.1021/bp990133s.

Wallace, I. J., Worthington, S., Felson, D. T., Jurmain, R. D., Wren, K. T., Maijanen, H., et al. (2017). Knee osteoarthritis has doubled in prevalence since the mid-20th century. *Proc. Natl. Acad. Sci. U. S. A.* 114, 9332–9336. doi:10.1073/PNAS.1703856114.

Wang, Z., Wang, L., Fan, R., Zhou, J., and Zhong, J. (2016). Molecular design and structural optimization of potent peptide hydroxamate inhibitors to selectively target human ADAM metallopeptidase domain 17. *Comput. Biol. Chem.* 61, 15–22. doi:10.1016/j.compbiolchem.2015.12.003.

White, C. J., and Yudin, A. K. (2011). Contemporary strategies for peptide macrocyclization. *Nat. Chem.* 3, 509–524. doi:10.1038/nchem.1062.

Whittaker, M., Floyd, C. D., Brown, P., and Gearing, A. J. H. (1999). Design and Therapeutic Application of Matrix Metalloproteinase Inhibitors. *Chem. Rev.* 99, 2735–2776. doi:10.1021/cr9804543.

Wong, A. K., Jacobsen, M. P., Winzor, D. J., and Fairlie, D. P. (1998). Template assembled synthetic proteins (TASPS). Are template size, shape, and directionality important in formation of four-helix bundles? *J. Am. Chem. Soc.* 120, 3836–3841. doi:10.1021/ja971951o.

Wong, E., Cohen, T., Romi, E., Levin, M., Peleg, Y., Arad, U., et al. (2016). Harnessing the natural inhibitory domain to control TNFα Converting Enzyme (TACE) activity in vivo. *Sci. Rep.* 6, 1–12. doi:10.1038/srep35598.

Woolf, A. D. (2015). Global burden of osteoarthritis and musculoskeletal diseases. *BMC*

Musculoskelet. Disord. 2015 161 16, 1–1. doi:10.1186/1471-2474-16-S1-S3.

Yamamoto, K., Santamaria, S., Botkjaer, K. A., Dudhia, J., Troeberg, L., Itoh, Y., et al. (2017). Inhibition of Shedding of Low-Density Lipoprotein Receptor-Related Protein 1 Reverses Cartilage Matrix Degradation in Osteoarthritis. *Arthritis Rheumatol.* 69, 1246–1256. doi:10.1002/art.40080.

Yang, C. Y., Chanalaris, A., and Troeberg, L. (2017). ADAMTS and ADAM metalloproteinases in osteoarthritis – looking beyond the 'usual suspects.' *Osteoarthr. Cartil.* 25, 1000–1009. doi:10.1016/j.joca.2017.02.791.

Yang, F., Zhao, N., Ge, D., and Chen, Y. (2019). Next-generation of selective histone deacetylase inhibitors. *RSC Adv.* 9, 19571–19583. doi:10.1039/c9ra02985k.

Yang, Y., Hu, X.-Q., Li, Q.-S., Zhang, X.-X., Ruan, B.-F., Xu, J., et al. (2015). Metalloprotein Inhibitors for the Treatment of Human Diseases. *Curr. Top. Med. Chem.* 16, 384–396. doi:10.2174/1568026615666150813145218.

Yim, V., Noisier, A. F. M., Hung, K. yuan, Bartsch, J. W., Schlomann, U., and Brimble, M. A. (2016). Synthesis and biological evaluation of analogues of the potent ADAM8 inhibitor cyclo(RLsKDK) for the treatment of inflammatory diseases and cancer metastasis. *Bioorganic Med. Chem.* 24, 4032–4037. doi:10.1016/j.bmc.2016.06.042.

Yiotakis, A., and Dive, V. (2009). Synthetic active site-directed inhibitors of metzincins: Achievement and perspectives. *Mol. Aspects Med.* 29, 329–338. doi:10.1016/j.mam.2008.06.001.

Zeng, W., Corcoran, C., Collins-Racie, L. A., LaVallie, E. R., Morris, E. A., and Flannery, C. R. (2006). Glycosaminoglycan-binding properties and aggrecanase activities of truncated ADAMTSs: Comparative analyses with ADAMTS-5, -9, -16 and -18. *Biochim. Biophys. Acta - Gen. Subj.* 1760, 517–524. doi:10.1016/J.BBAGEN.2006.01.013.

Zhang, E., Yan, X., Zhang, M., Chang, X., Bai, Z., He, Y., et al. (2013). Aggrecanases in the human synovial fluid at different stages of osteoarthritis. *Clin. Rheumatol.* 32, 797–803. doi:10.1007/s10067-013-2171-0.

Zhang, W., Ouyang, H., Dass, C. R., and Xu, J. (2016). Current research on pharmacologic and regenerative therapies for osteoarthritis. *Bone Res.* 4, 15040. doi:10.1038/boneres.2015.40.

Zhang, W., Zhong, B., Zhang, C., Wang, Y., Guo, S., Luo, C., et al. (2018). Structural modeling of osteoarthritis ADAMTS4 complex with its cognate inhibitory protein TIMP3 and rational derivation of cyclic peptide inhibitors from the complex interface to target ADAMTS4. *Bioorg. Chem.* 76, 13–22. doi:10.1016/j.bioorg.2017.10.017.

Zorzi, A., Deyle, K., and Heinis, C. (2017). Cyclic peptide therapeutics: past, present and future.

Curr. Opin. Chem. Biol. 38, 24–29. doi:10.1016/j.cbpa.2017.02.006.

Appendix

Abbreviations

- ACE (Angiotensin Converting Enzyme)
- ACN (Acetonitrile)
- ADAM (A Disintegrin and Metalloproteinase)
- ADAMTS A (A Disintegrin and Metalloproteinase with Thrombospondin)
- AMP (Acetyl p-azide-L-methyl phenylalanine)
- AzM (p-azide-L-methyl phenylalanine)
- CHO (Chinese Hamster Ovary cells)
- CuAA (Copper-catalyzed Azide–Alkyne cycloaddition)
- DCC (DiCyclohexyl Carbodiimide)
- DMF (DiMethyl Formamide)
- ECM (ExtraCellular Matrix)
- FACS (Fluorescent Activated Cell Sorting)
- FSS (Forward Side Scattering)
- FRET (Förster Resonance Energy Transfer)
- HA (Hemagglutinin)
- HPLC (High Performance Liquid Chromatography)
- HysTag (Polyhistidine-tag)
- LC-MS (Liquid chromatography-mass spectrometry)
- MACS (Magnetic Activated Cell Sorting)
- MMP (Matrix Metalloproteinases Protein)
- mSA (mouse Serum Albumin)
- ncAAs (non-canonical Amino Acids)
- NL (Not Labelled)
- NMD1 (New Delhi metallo-beta-lactamase 1)
- OA (Osteoarthritis)
- PBS (Phosphate Buffer Solution)
- PBSA (Phosphate Buffer Solution with 0,1 % w/v bovine serum Albumin)
- POI (Protein or Peptide Of Interest)
- PSMA (Prostate-Specific Membrane Antigen)
- SDS-PAGE (Sodium Dodecyl Sulphate - PolyAcrylamide Gel Electrophoresis)
- SSC (Side Scattering)
- SSPS (Solid Phase Peptide Synthesis)
- SVMP (Snake Venom MetalloProteinases)
- TACE (Tumor necrosis factor-Alpha Converting Enzyme)
- TCEP (tris(2-carboxyethyl)phosphine)
- TEV (Tobacco Etch Virus)
- THP (TetraHydropyranyl ether)
- TIMP-3 (Tissue Inhibitor of MetalloProteinases-3)
- TNF-α (Tumor Necrosis Factor- α)
- TSP-1 (C-terminal ThromboSPondin type-1)
- YSD (Yeast Surface Display)

NMR spectra

4-(bromomethyl)-N-hydroxybenzamide (1)

^{1}H NMR (400 MHz, Acetone-d_6) δ 10.81 (s, 1H), 8.38 (s, 1H), 7.83 (d, J = 8.4 Hz, 2H), 7.55 (d, J = 8.4 Hz, 2H), 4.68 (s, 2H).

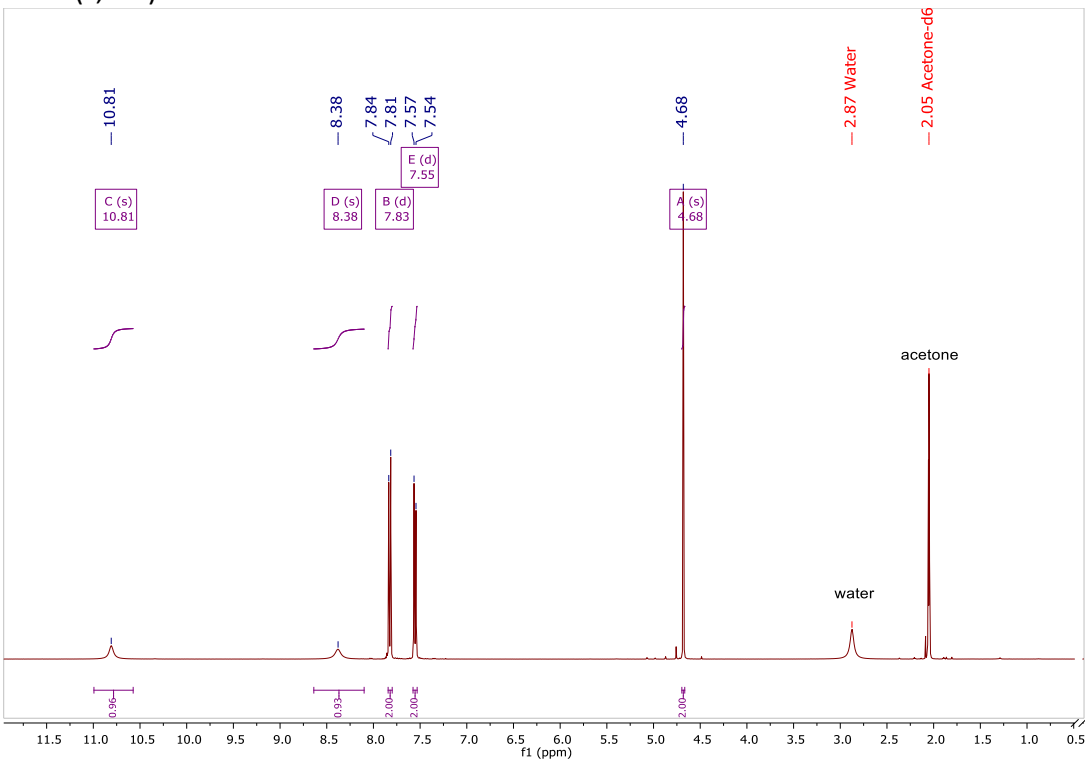

^{13}C NMR (101 MHz, Acetone) δ 165.39, 142.64, 133.06, 130.15, 128.24, 33.33.

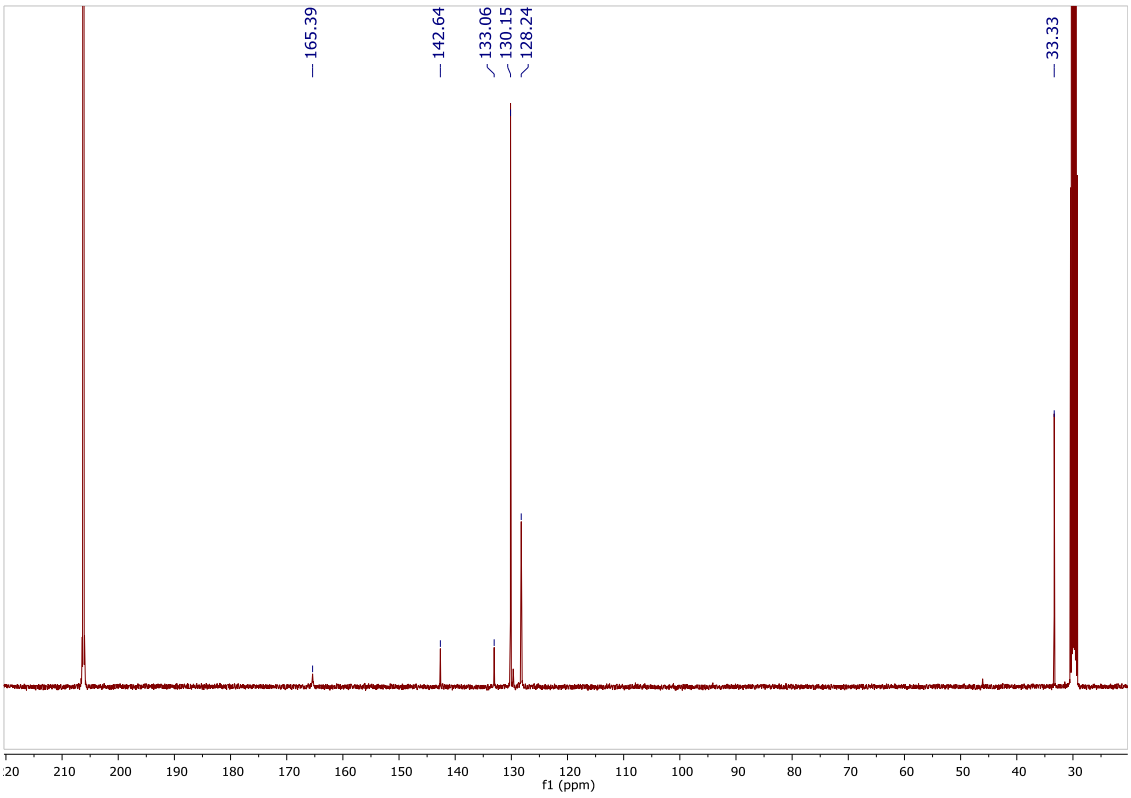

3,5-bis(bromomethyl) benzoic acid

^{1}H NMR (400 MHz, Acetone-d_6) δ 8.06 (s, 2H), 7.82 (s, 1H), 4.74 (s, 4H).

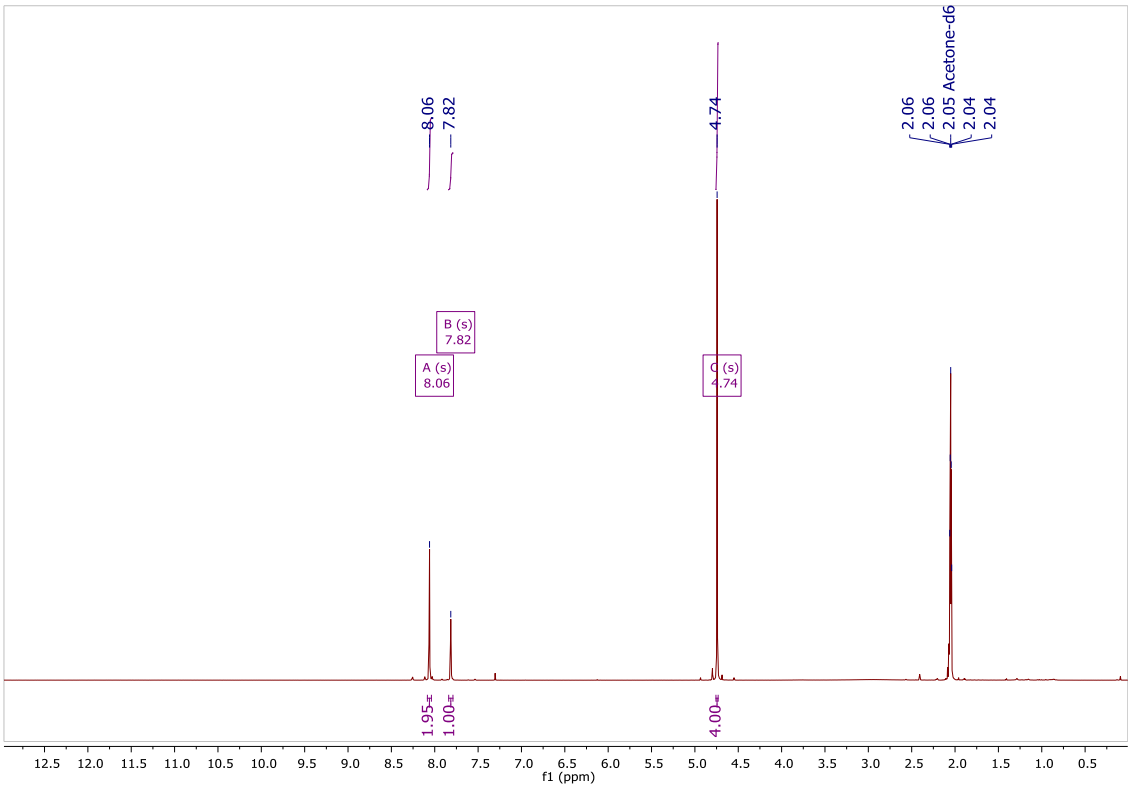

^{13}C NMR (101 MHz, Acetone) δ 166.61, 140.52, 134.94, 132.60, 130.94, 32.97.

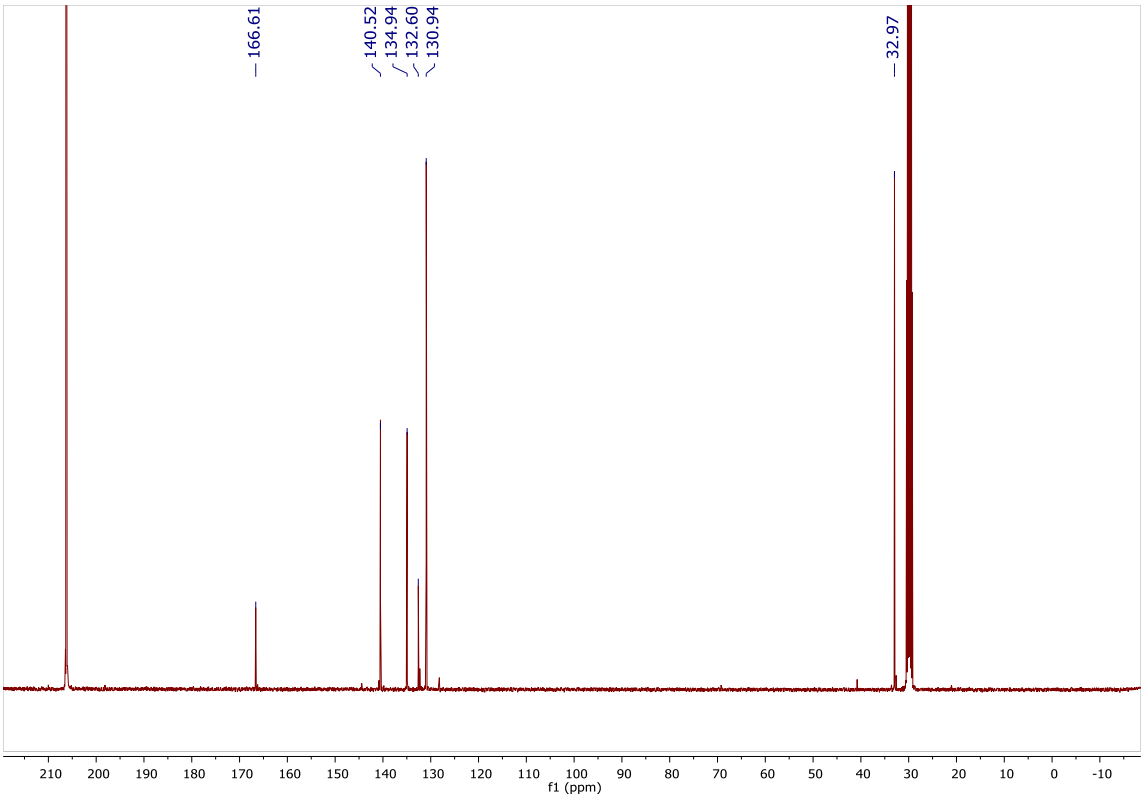

3,5-bis(bromomethyl)-N-hydroxybenzamide (2)

^{1}H NMR (400 MHz, Acetone-d_6) δ 10.91 (s, 1H), 8.31 (s, 1H), 7.85 (d, *J* = 1.7 Hz, 2H), 7.72 (t, *J* = 1.7 Hz, 1H), 4.69 (s, 4H).

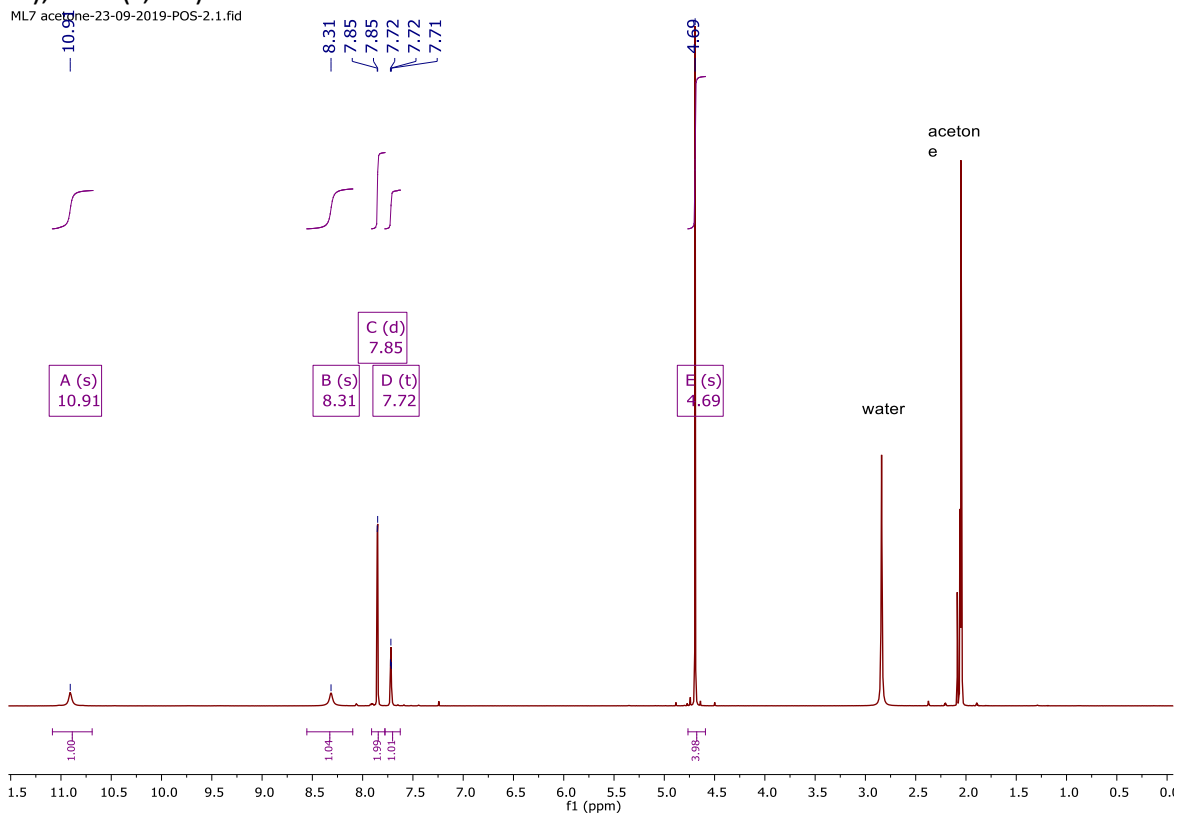

^{13}C NMR (101 MHz, Acetone) δ 163.87, 139.47, 133.59, 132.56, 127.60, 32.21.

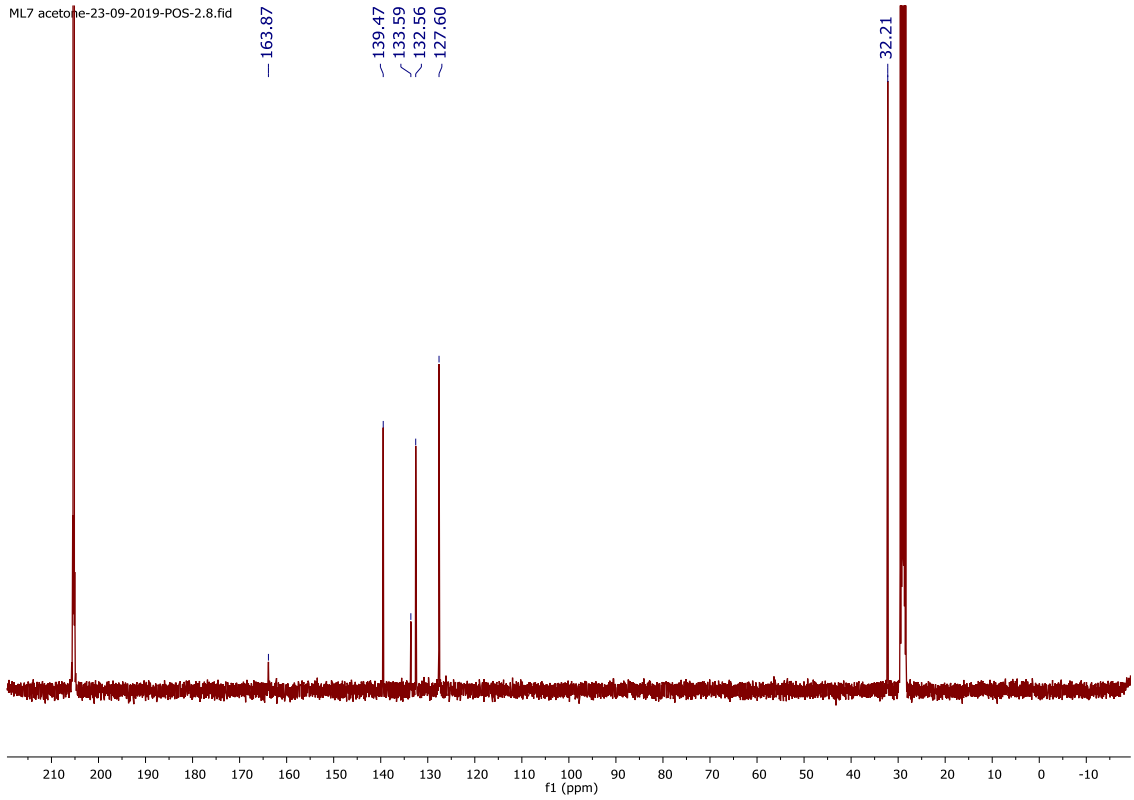

3-(3,4-dibromo-2,5-dioxo-2,5-dihydro-1H-pyrrol-1-yl)propanoic acid

^{1}H NMR (400 MHz, Acetone-d_6) δ 3.87 (dd, J = 7.7, 7.0 Hz, 2H), 2.70 (dd, J = 7.7, 7.0 Hz, 2H).

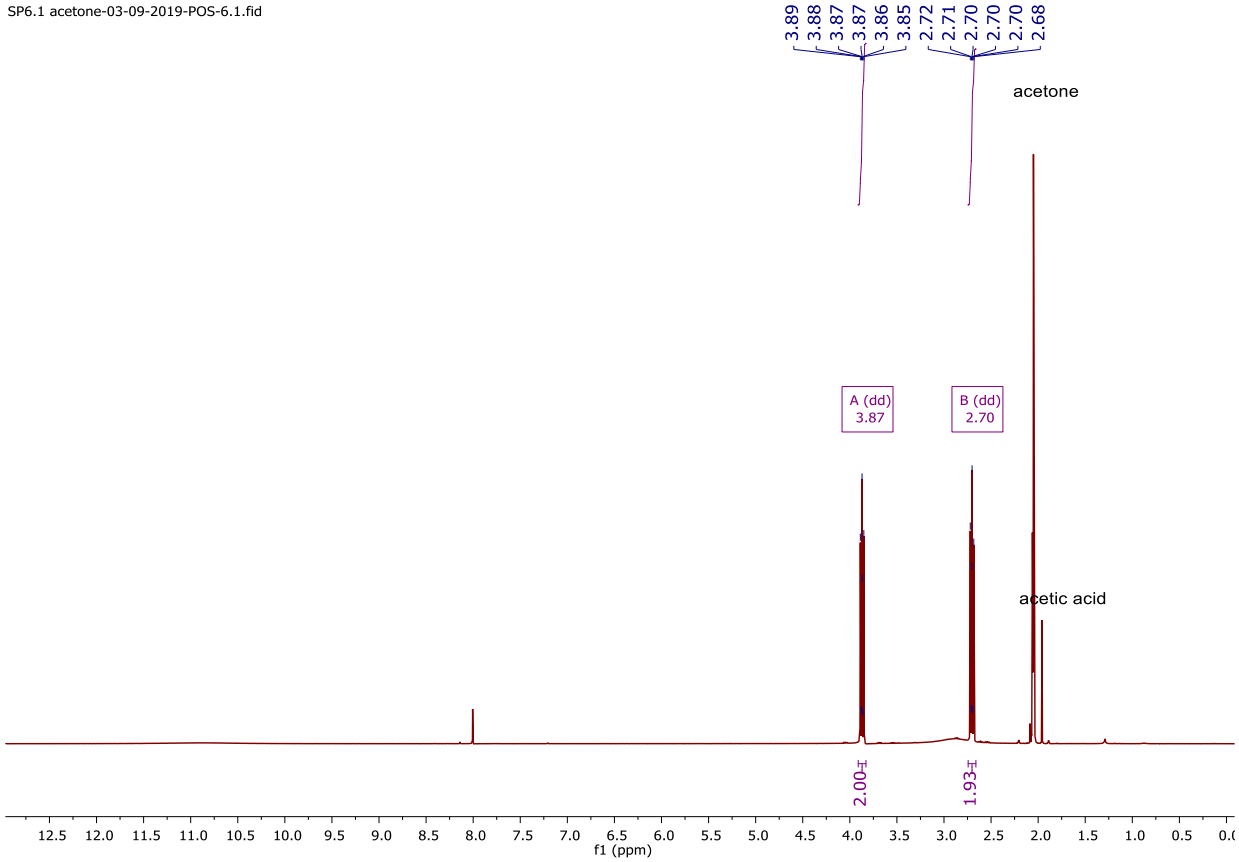

^{13}C NMR (101 MHz, Acetone) δ 171.13, 163.71, 129.23, 35.15, 31.67.

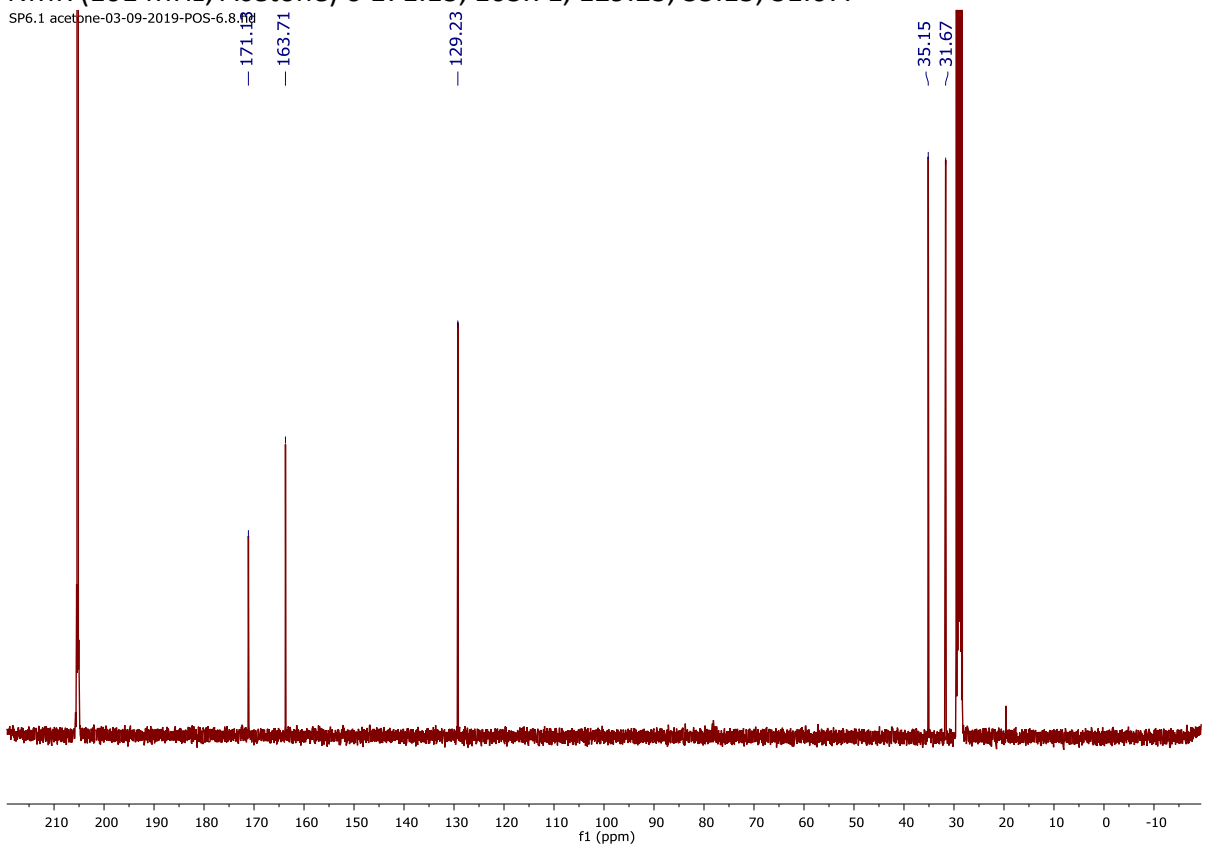

3-(3,4-dibromo-2,5-dioxo-2,5-dihydro-1H-pyrrol-1-yl)-N-hydroxypropanamide (3)

^{1}H NMR (400 MHz, Acetone-d_6) δ 10.07 (s, 1H), 8.08 (s, 1H), 3.87 (t, J = 7.2 Hz, 2H), 2.48 (t, J = 6.8 Hz, 2H).

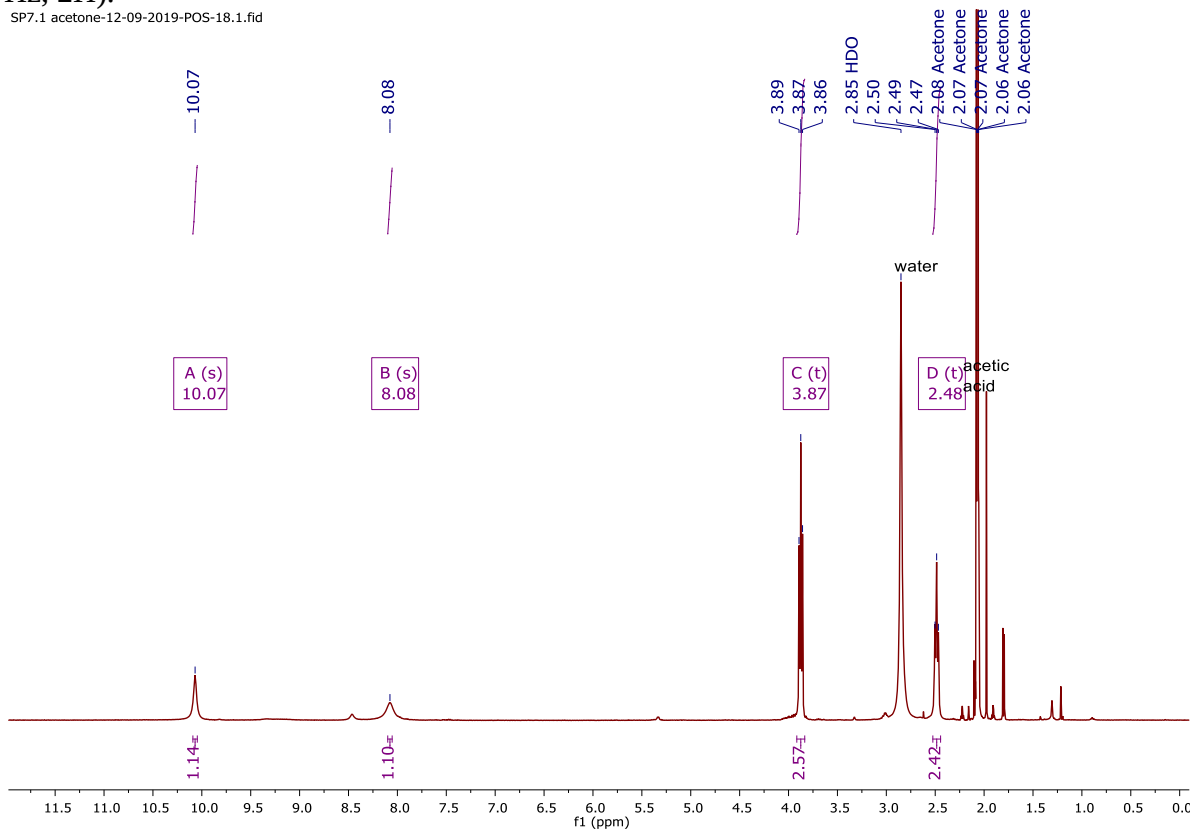

^{13}C NMR (101 MHz, Acetone) δ 166.64, 163.69, 129.23, 35.82, 30.71.

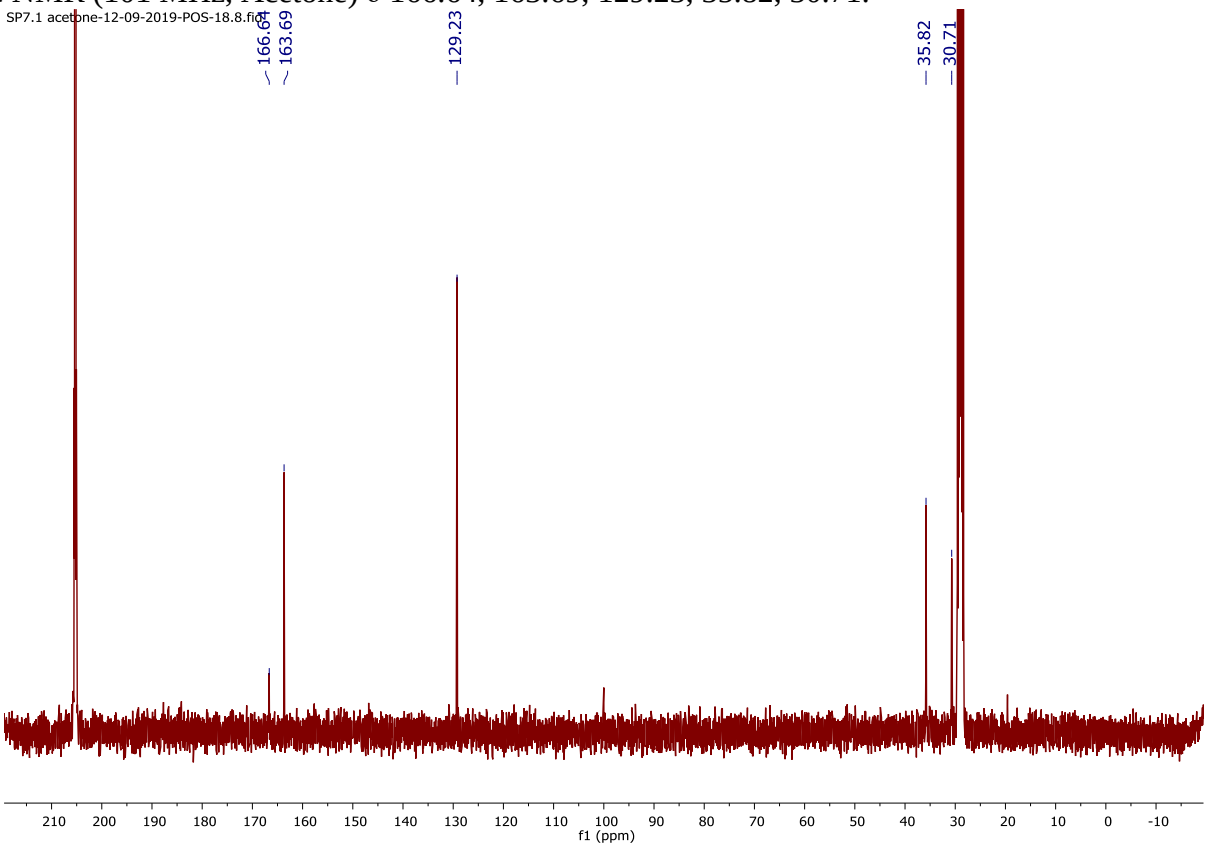

3,5-bis(2-bromoacetamido)benzoic acid

^{1}H NMR (400 MHz, Acetone-d_6) δ 9.77 (s, 2H), 8.28 (t, J = 2.1 Hz, 1H), 8.10 (d, J = 2.0 Hz, 2H), 4.07 (s, 4H).

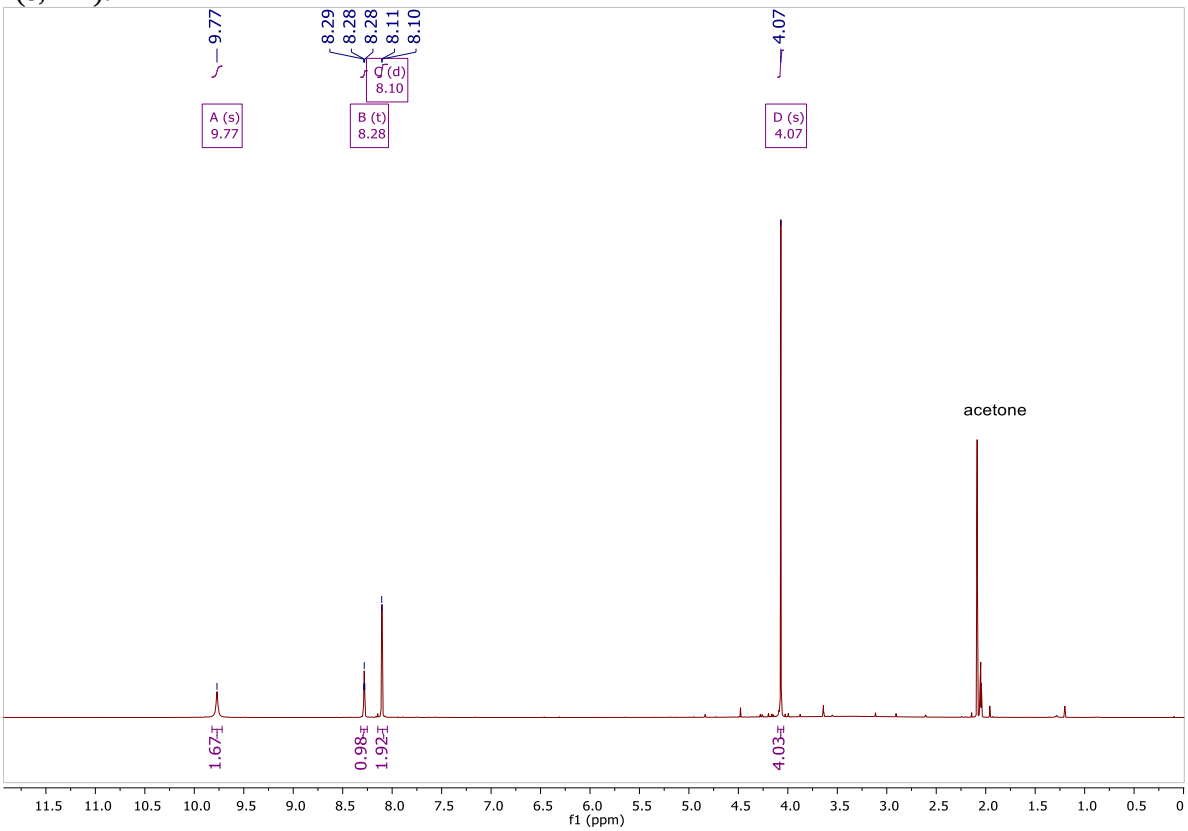

^{13}C NMR (101 MHz, Acetone) δ 167.05, 165.85, 140.33, 132.67, 116.92, 115.18, 30.25.

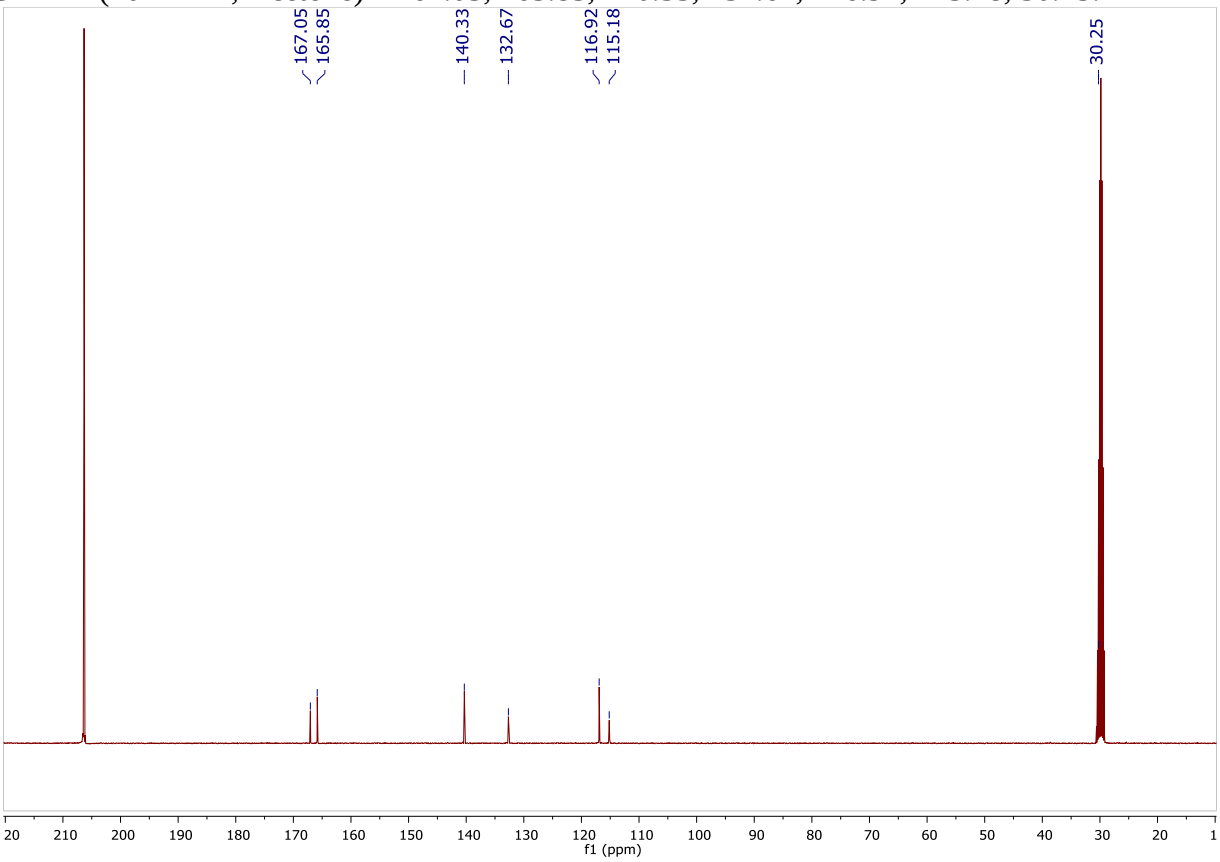

N,N'-(5-(hydroxycarbamoyl)-1,3-phenylene)bis(2-bromoacetamide) (4)

1H NMR (300 MHz, methanol-d4) δ 8.07 (s, 1H), 7.73 (s, 2H), 3.98 (s, 4H).

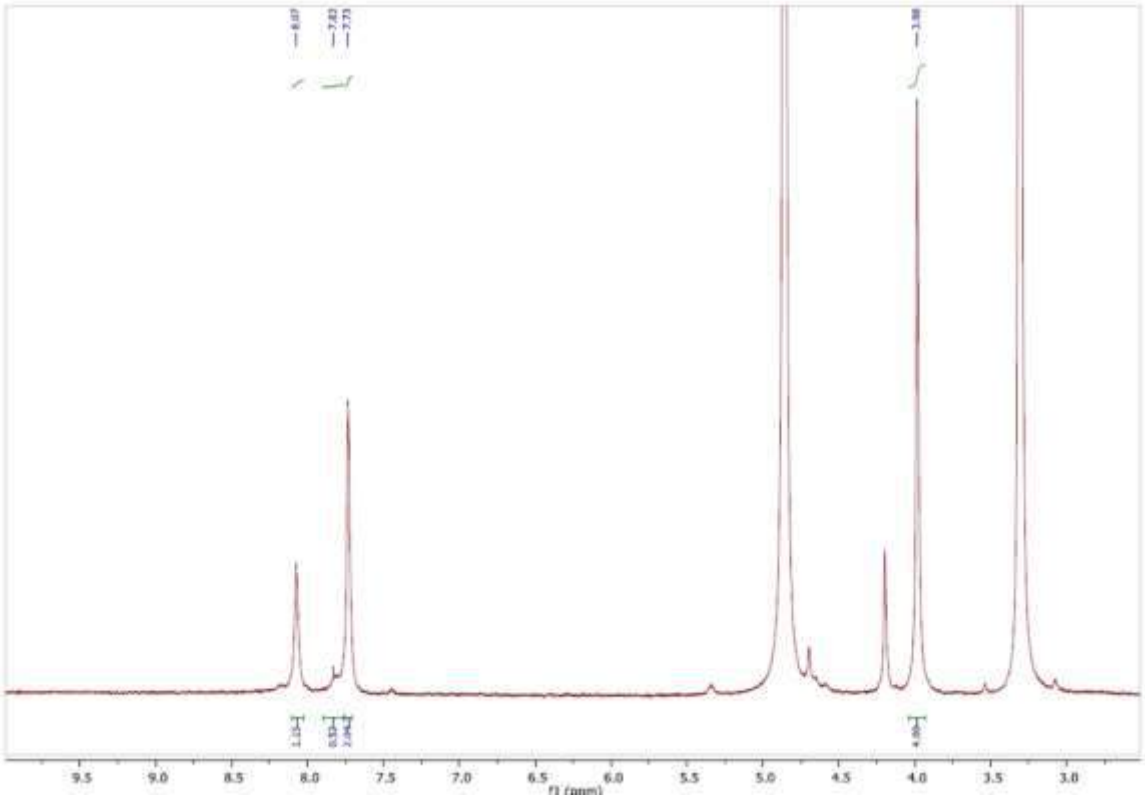

methyl N-acetyl-S-(4-(hydroxycarbamoyl)benzyl)-D-cysteinate (1A)

1H NMR (400 MHz, Acetone-d6) δ 7.80 (d, J = 7.9 Hz, 2H), 7.61 – 7.47 (m, 1H), 7.44 (d, J = 7.8 Hz, 2H), 4.69 (td, J = 7.7, 5.3 Hz, 1H), 3.84 (s, 2H), 3.67 (s, 3H), 2.93 – 2.70 (m, 2H), 1.96 (s, 3H).

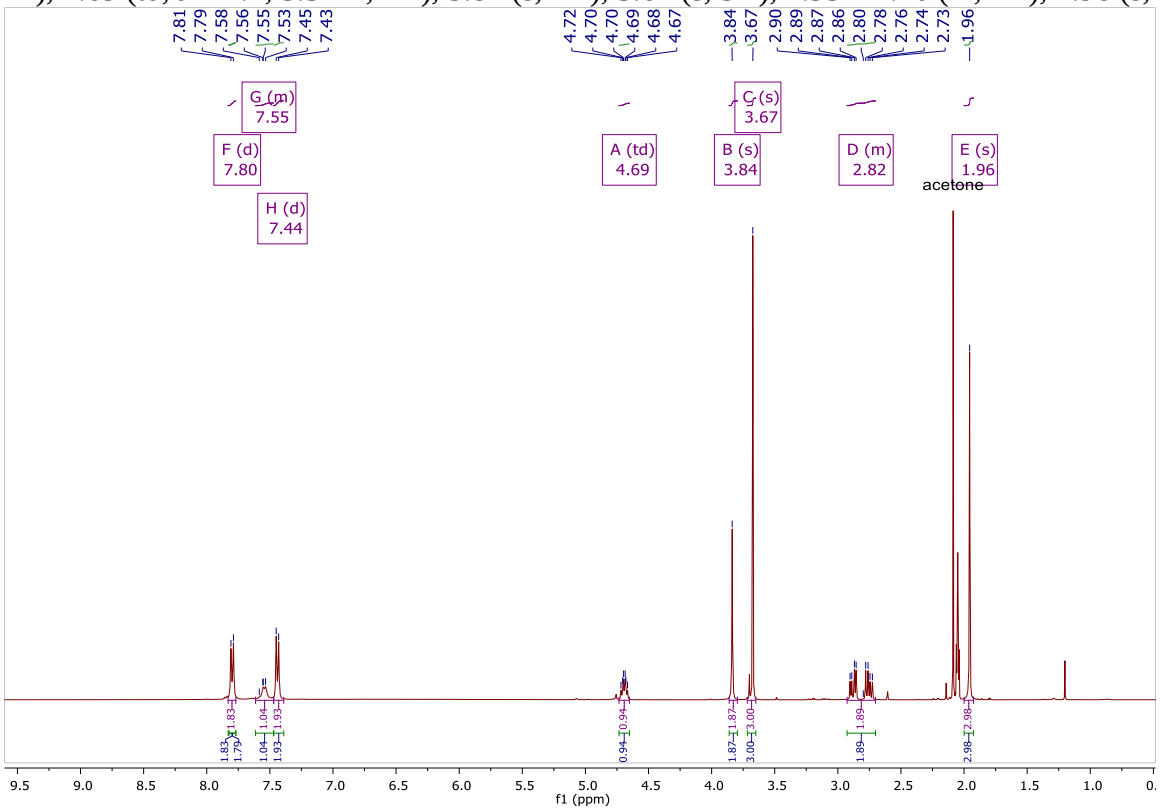

13C NMR (101 MHz, Acetone) δ 171.98, 170.46, 165.67, 143.07, 131.81, 129.98, 128.00, 52.76, 52.51, 36.24, 33.65, 22.62.

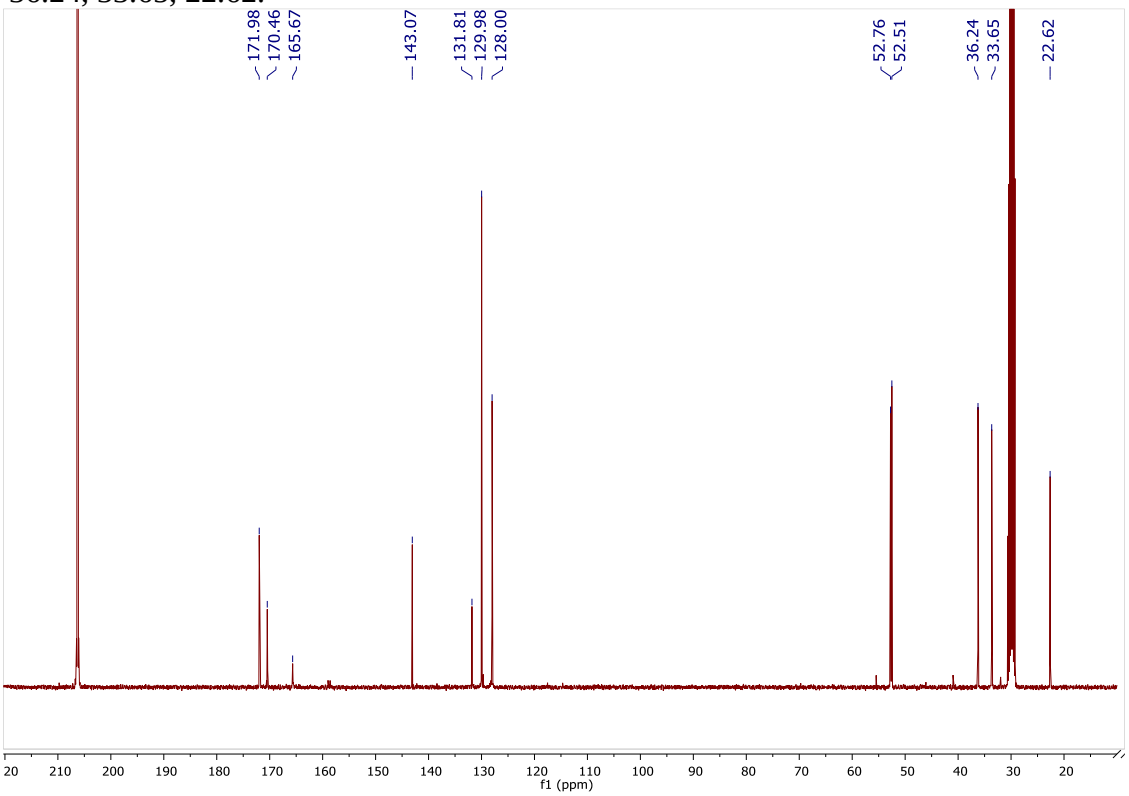

dimethyl 3,3'-(((5-(hydroxycarbamoyl)-1,3-phenylene)bis(methylene))bis(sulfanediyl))(2S,2'S)-bis(2-acetamidopropanoate) (2A)

1H NMR (400 MHz, Acetone-d6) δ 7.70 (s, 2H), 7.60 (d, J = 7.6 Hz, 2H), 7.50 (s, 1H), 4.67 (td, J = 7.7, 5.9 Hz, 2H), 3.84 (s, 4H), 3.68 (s, 6H), 2.91 – 2.68 (m, 4H), 1.97 (s, 6H).

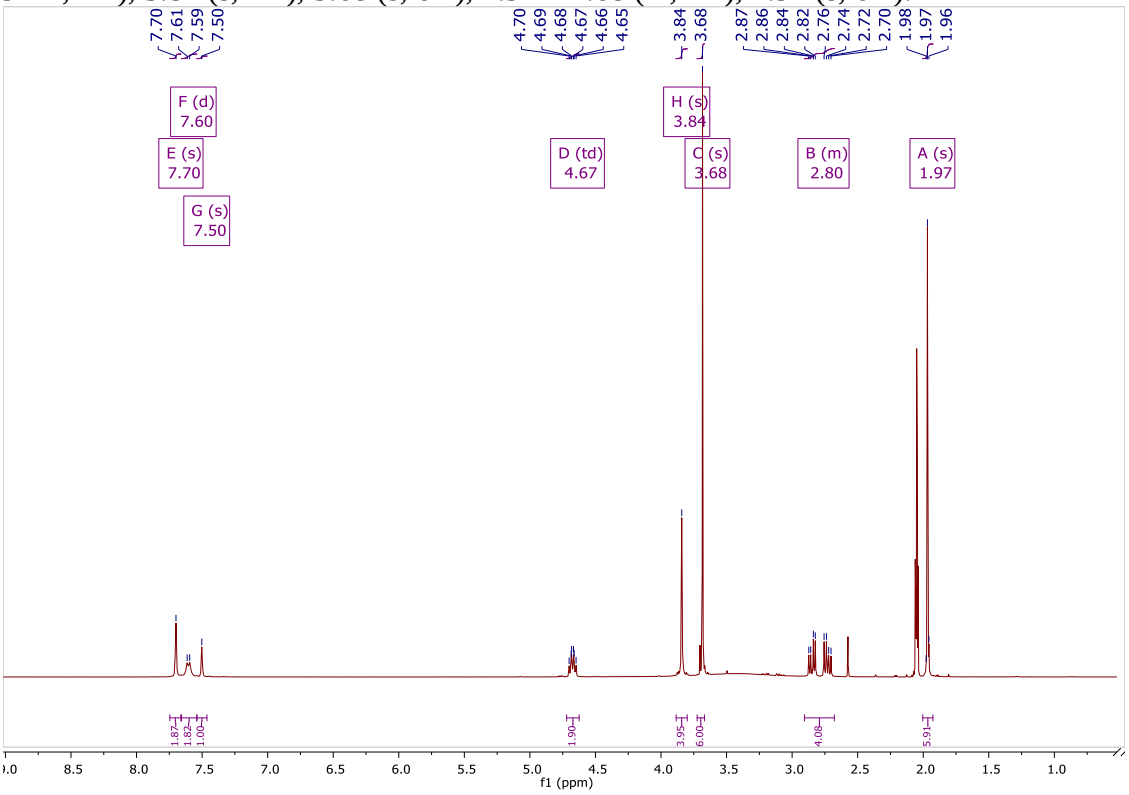

13C NMR (101 MHz, Acetone) δ 171.94, 170.65, 165.45, 140.09, 133.65, 133.45, 127.33, 52.83, 52.55, 36.12, 33.43, 22.71.

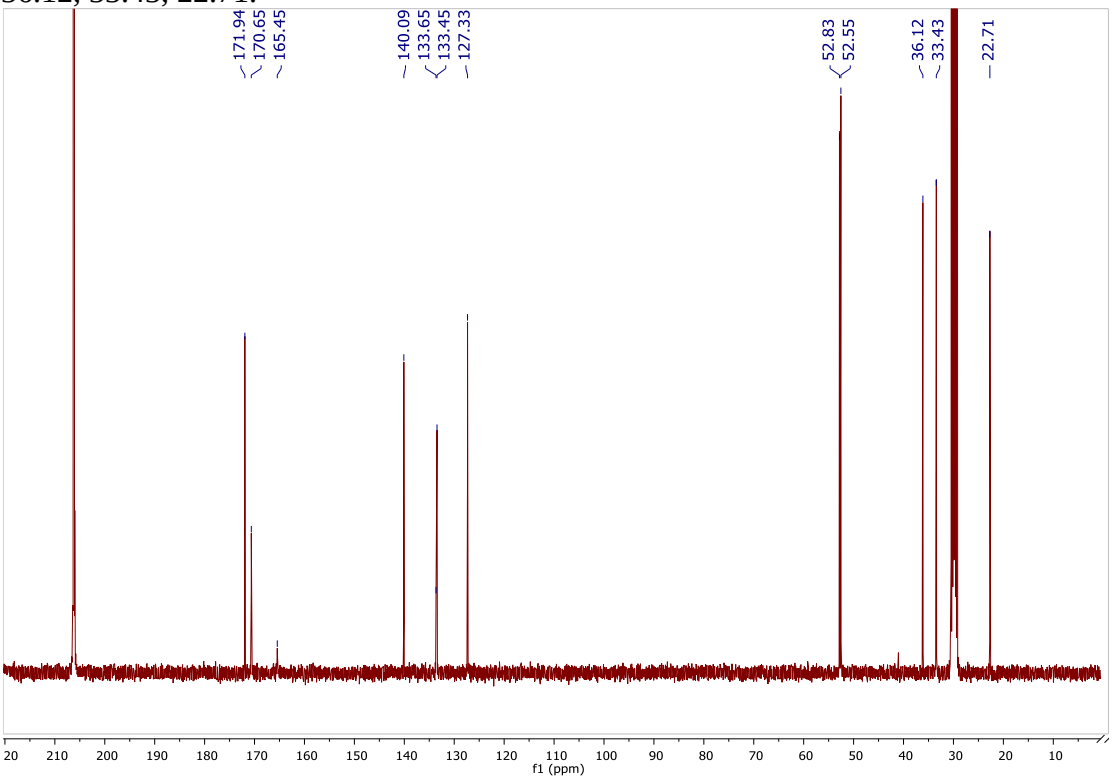

N-((tetrahydro-2H-pyran-2-yl)oxy)propiolamide

1H NMR (400 MHz, Chloroform-d) δ 9.28 (s, 1H), 5.02 – 4.93 (m, 1H), 4.01 – 3.86 (m, 1H),3.70 – 3.56 (m, 1H), 2.89 (s, 1H), 1.86 – 1.71 (m, 3H), 1.69 – 1.46 (m, 3H).

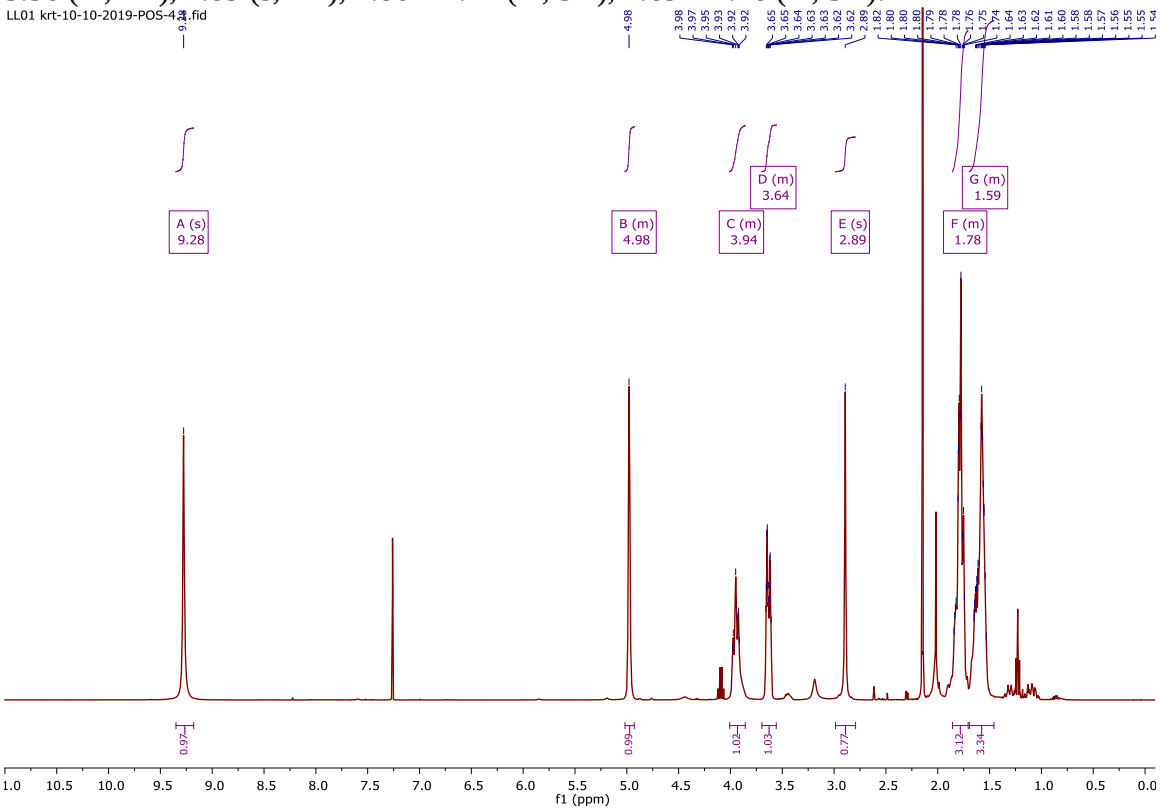

13C NMR (101 MHz, CDCl3) δ 149.97, 102.85, 76.07, 74.66, 62.72, 27.91, 24.93, 18.45.

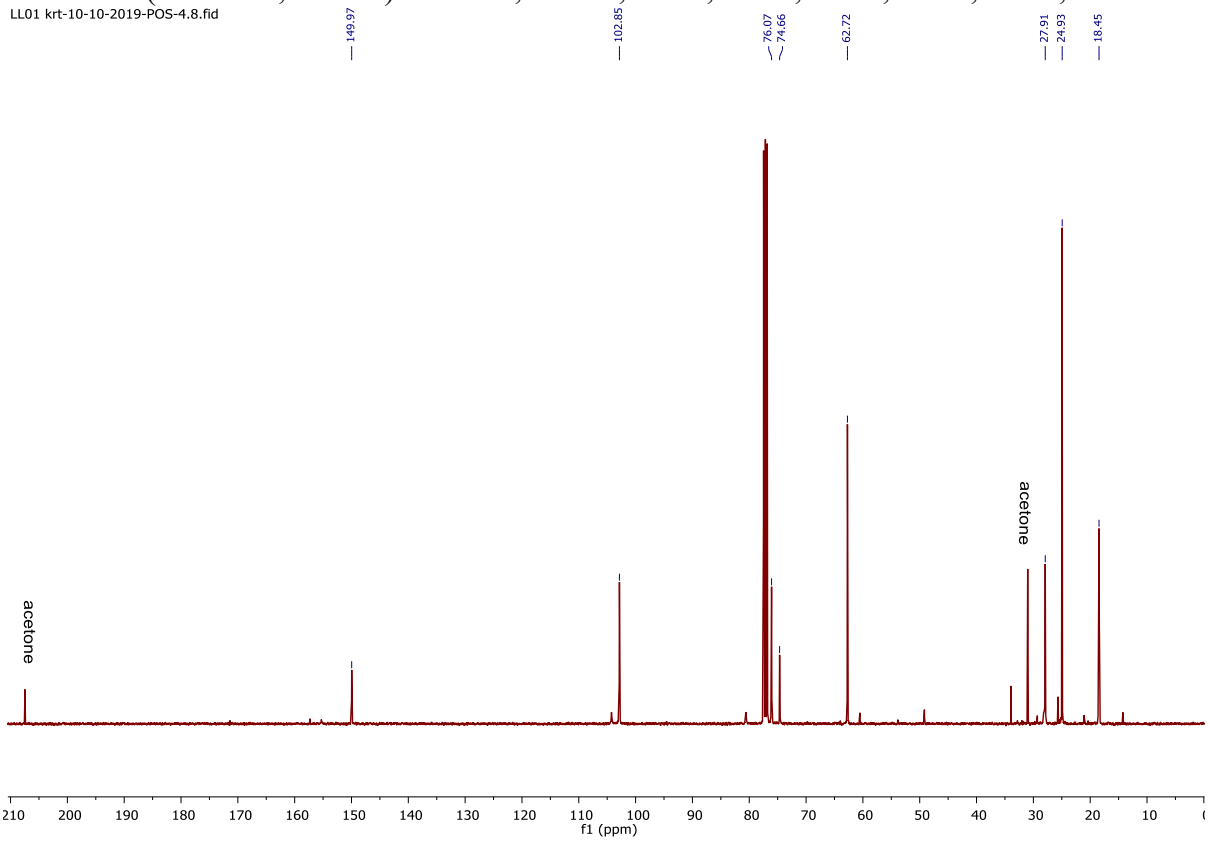

N-hydroxypropiolamide (5)

1H NMR (400 MHz, Acetone-d6) δ 10.59 (s, 1H), 8.57 (s, 1H), 3.63 (s, 1H).

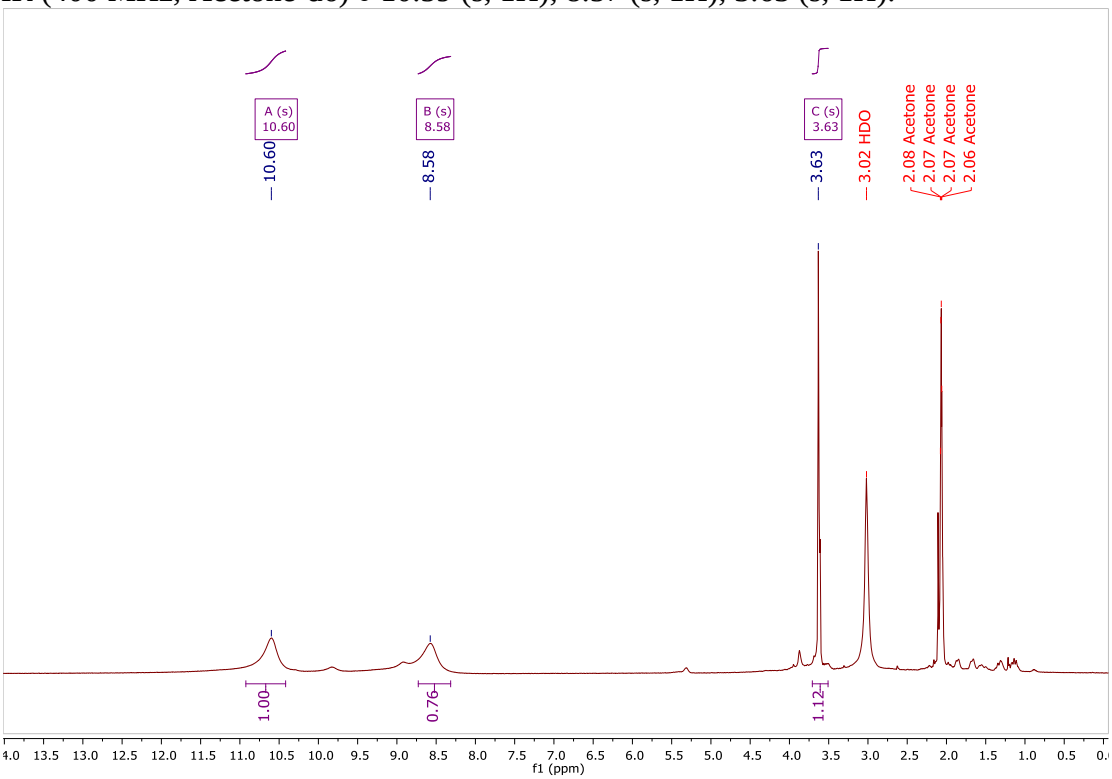

13C NMR (101 MHz, Acetone) δ 149.83, 75.78, 75.27.

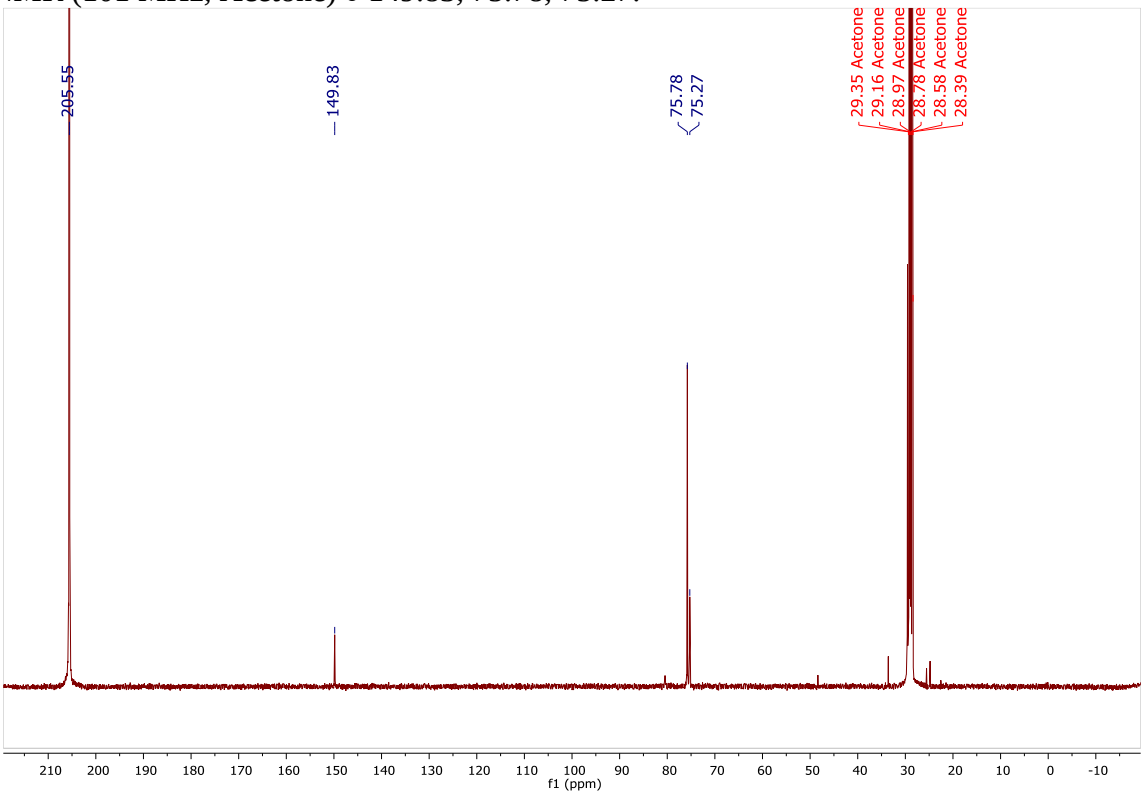

4-ethynyl-N-hydroxybenzamide (6)

1H NMR (400 MHz, DMSO-d6) δ 11.28 (s, 1H), 9.08 (s, 1H), 7.74 (d, J = 7.4 Hz, 2H), 7.54 (d, J = 7.6 Hz, 2H), 4.34 (s, 1H).

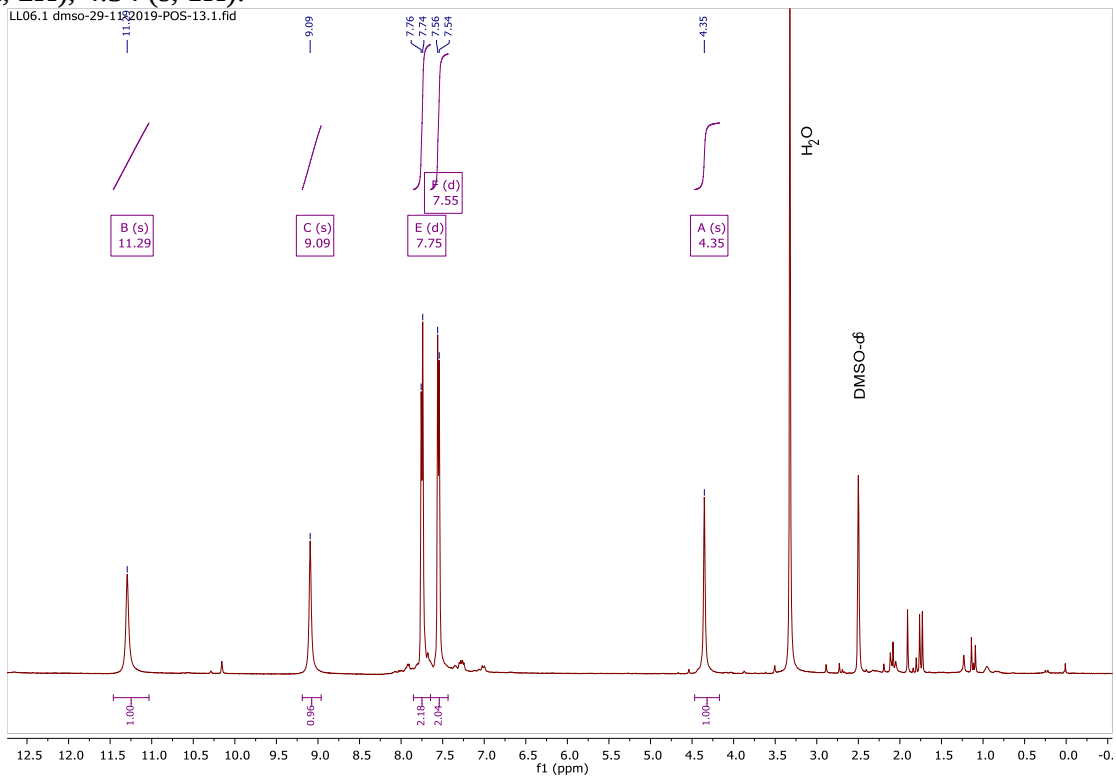

13C NMR (101 MHz, DMSO) δ 163.33, 132.87, 131.70, 127.14, 124.36, 82.82, 82.75.

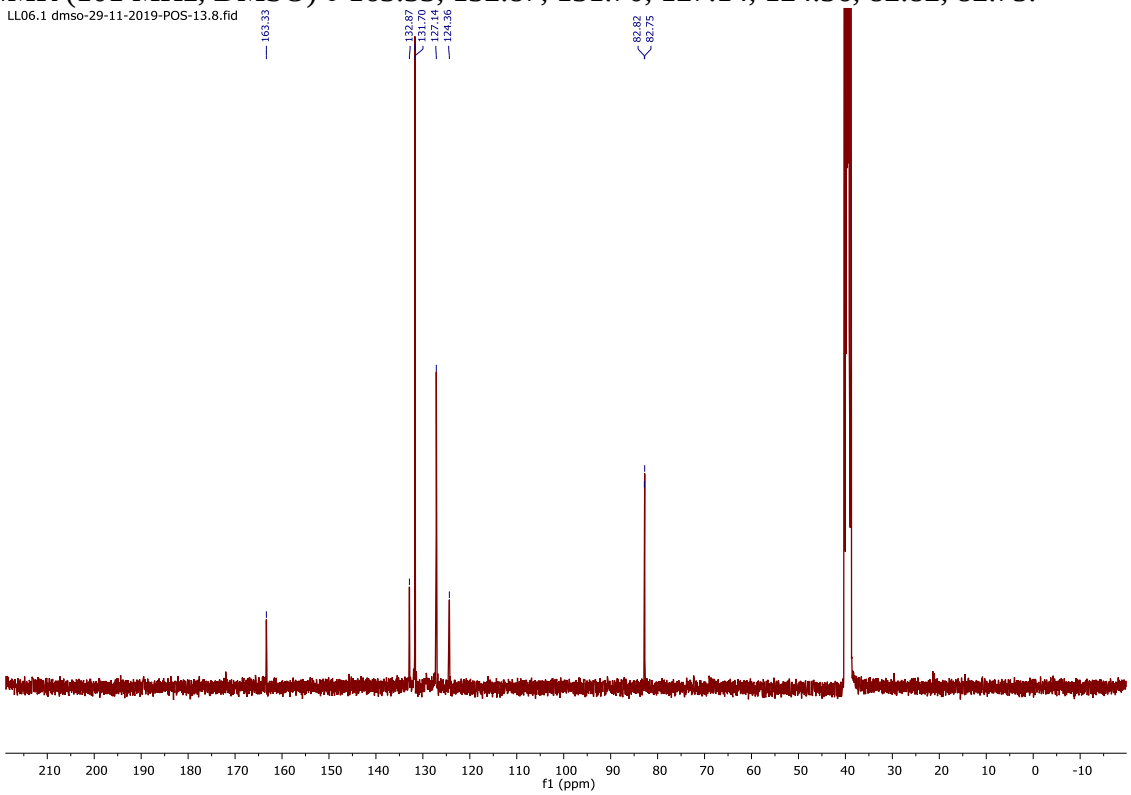

(S)-2-acetamido-3-(4-((4-(hydroxycarbamoyl)-1H-1,2,3-triazol-1-yl)methyl)phenyl)propanoic acid (AMP-5)

1H NMR (400 MHz, DMSO-d6) δ 11.25 (s, 1H), 8.57 (s, 1H), 8.16 (s, 1H), 8.14 (s, 1H), 7.30 – 7.15 (m, 4H), 5.60 (s, 2H), 4.39 (td, J = 8.8, 4.9 Hz, 1H), 3.07 – 2.78 (m, 2H), 1.77 (s, 3H).

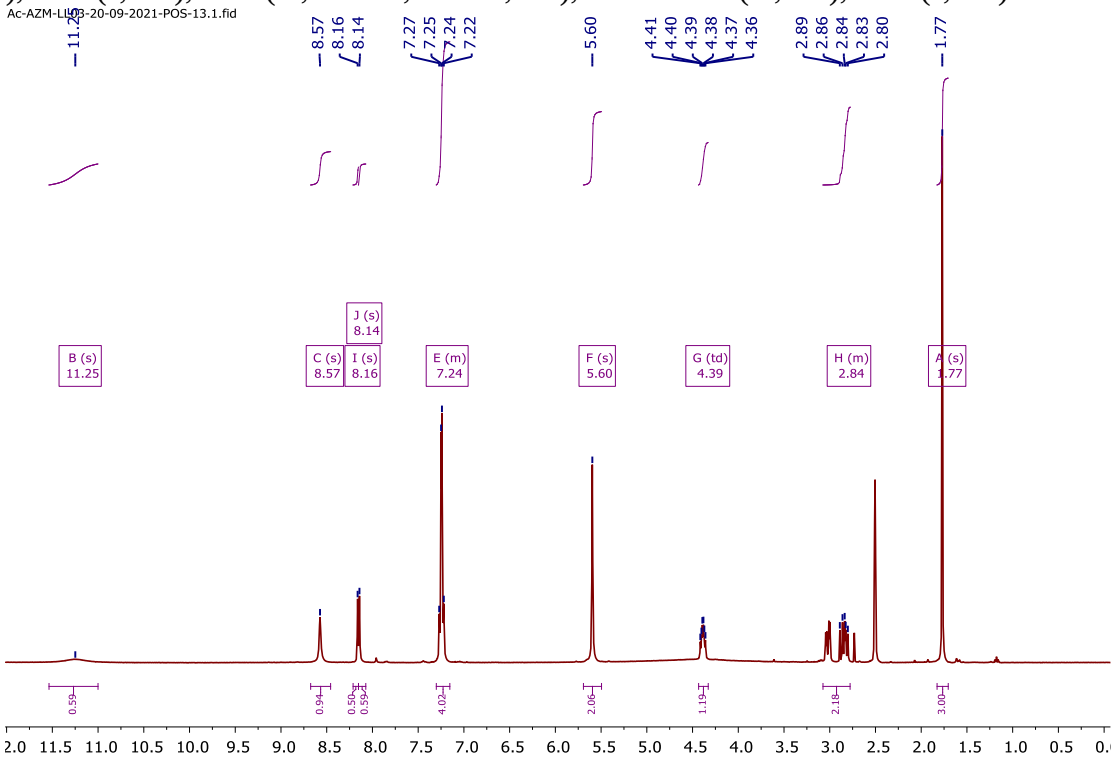

13C NMR (101 MHz, DMSO) δ 173.48, 169.71, 138.37, 134.17, 129.95, 128.39, 126.78, 53.79, 53.26, 36.83, 22.79.

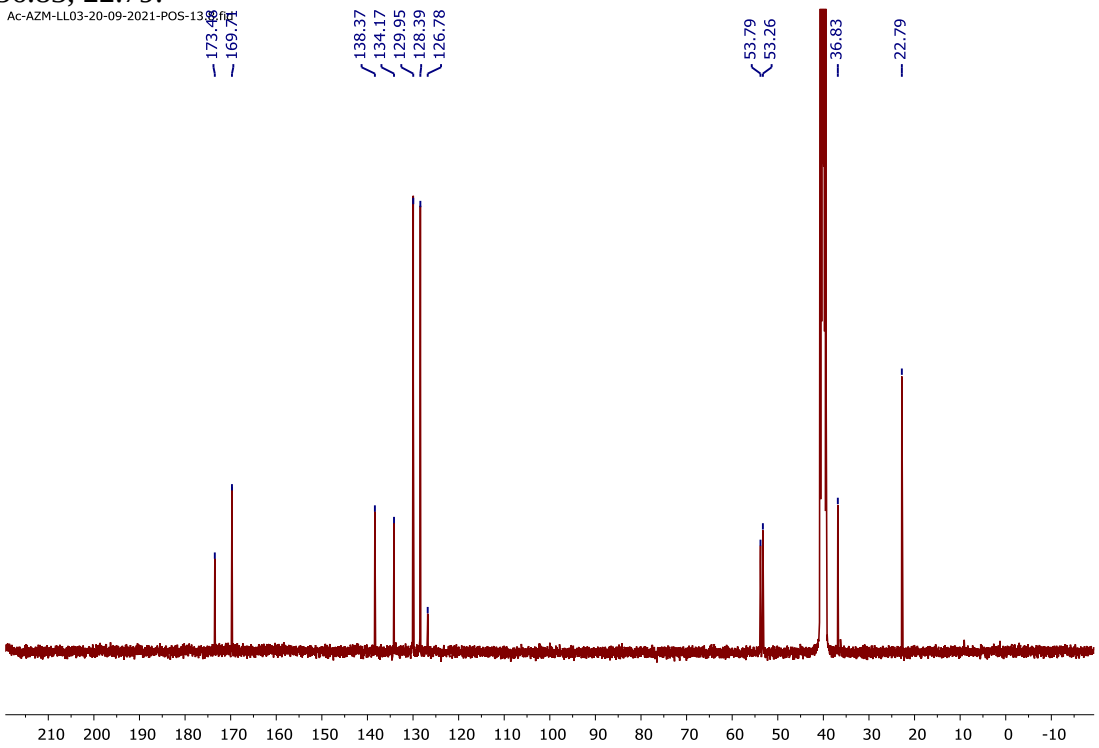

(S)-2-acetamido-3-(4-((4-(4-(hydroxycarbamoyl)phenyl)-1H-1,2,3-triazol-1-yl)methyl)phenyl)propanoic acid (AMP-6)

1H NMR (400 MHz, DMSO-d6) δ 11.24 (s, 1H), 8.71 (s, 1H), 8.17 (s, 1H), 8.15 (s, 1H), 7.87 (dd, J = 42.9, 8.0 Hz, 4H), 7.34 – 7.16 (m, 4H), 5.62 (s, 2H), 4.39 (ddd, J = 9.3, 7.9, 4.9 Hz, 1H), 3.09 – 2.77 (m, 2H), 1.77 (s, 3H).

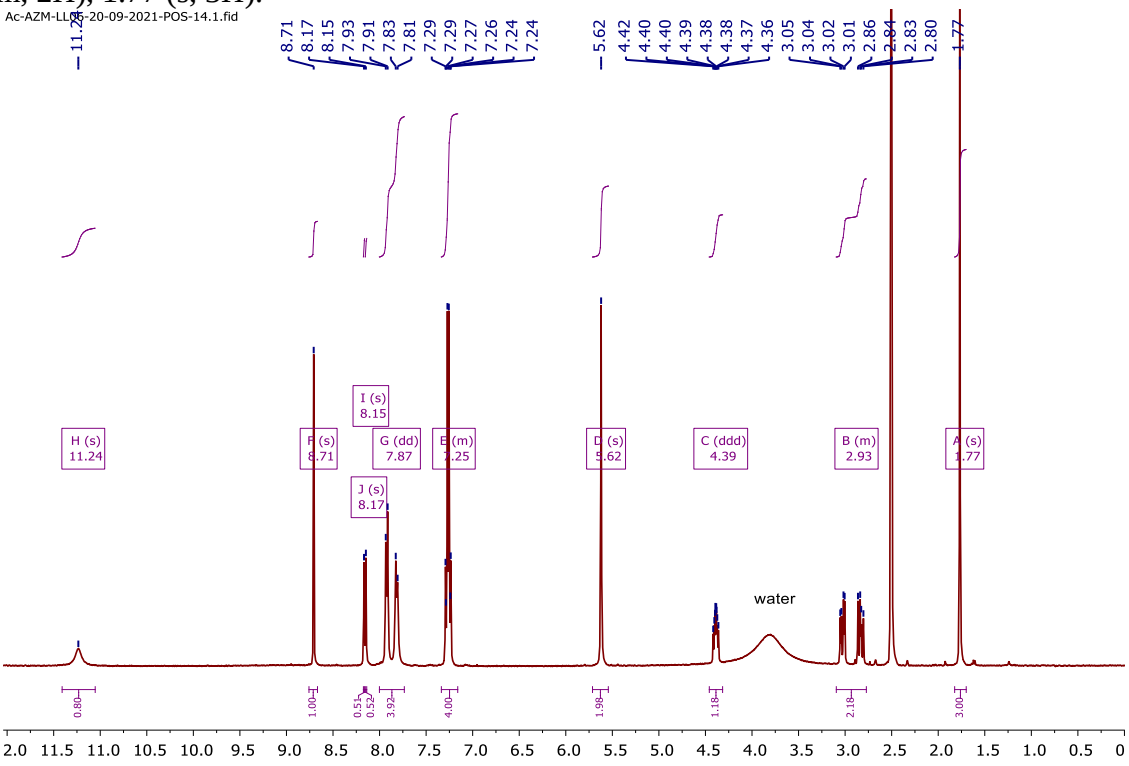

13C NMR (101 MHz, DMSO) δ 173.51, 169.71, 146.33, 138.30, 134.42, 133.71, 129.96, 128.30, 125.43, 122.76, 53.82, 53.32, 36.84, 22.80.

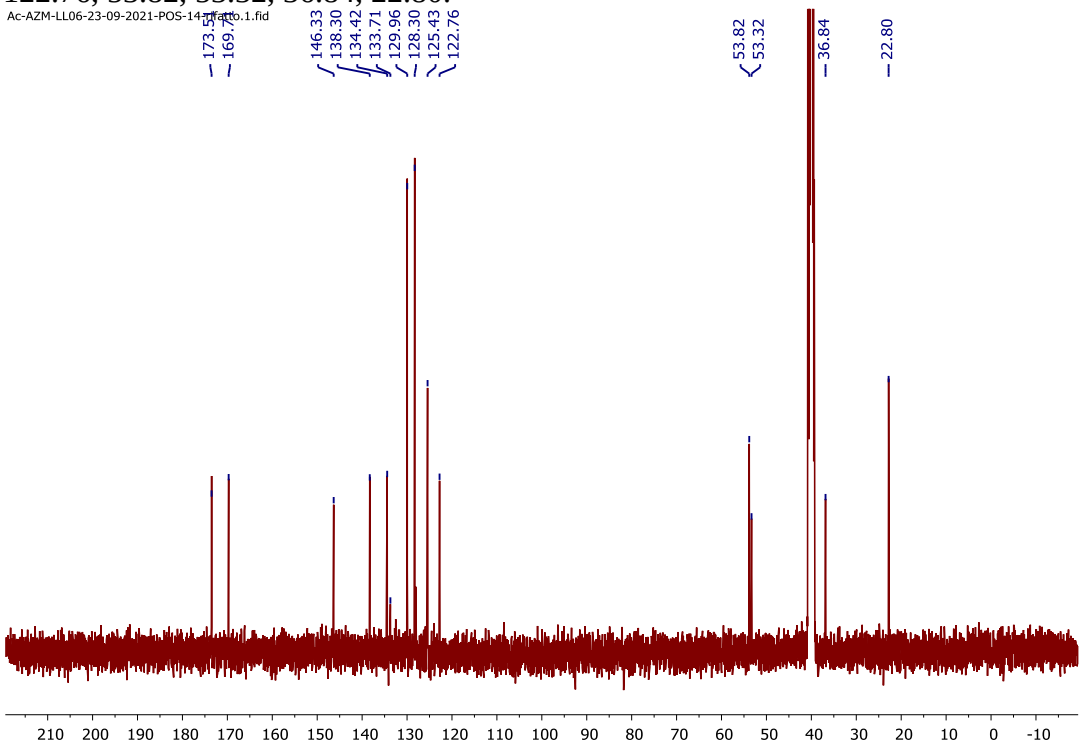

P3

1NMR (400 MHz, Deuterium Oxide) δ 7.57 (dt, *J* = 8.0, 1.1 Hz, 1H), 7.41 (dt, *J* = 8.1, 1.0 Hz, 1H), 7.23 – 7.03 (m, 5H), 7.00 – 6.86 (m, 2H), 4.56 (dd, *J* = 8.0, 6.0 Hz, 1H), 4.44 (t, *J* = 5.6 Hz, 1H), 4.37 (t, *J* = 5.2 Hz, 1H), 4.14 (t, *J* = 7.2 Hz, 1H), 4.02 – 3.79 (m, 3H), 3.78 – 3.68 (m, 5H), 3.28 – 3.05 (m, 2H), 3.03 (d, *J* = 7.3 Hz, 2H).

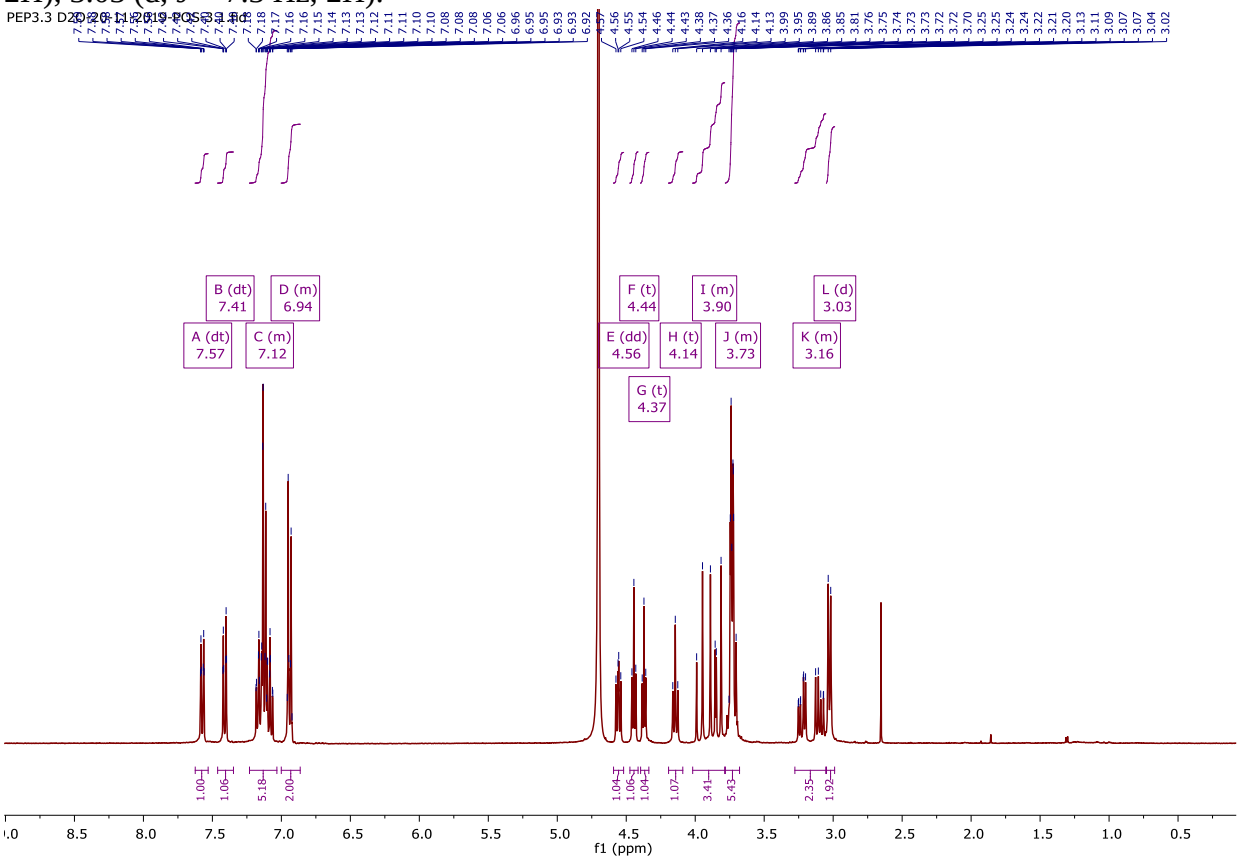

LC-MS spectra

4-(bromomethyl)-N-hydroxybenzamide (1)

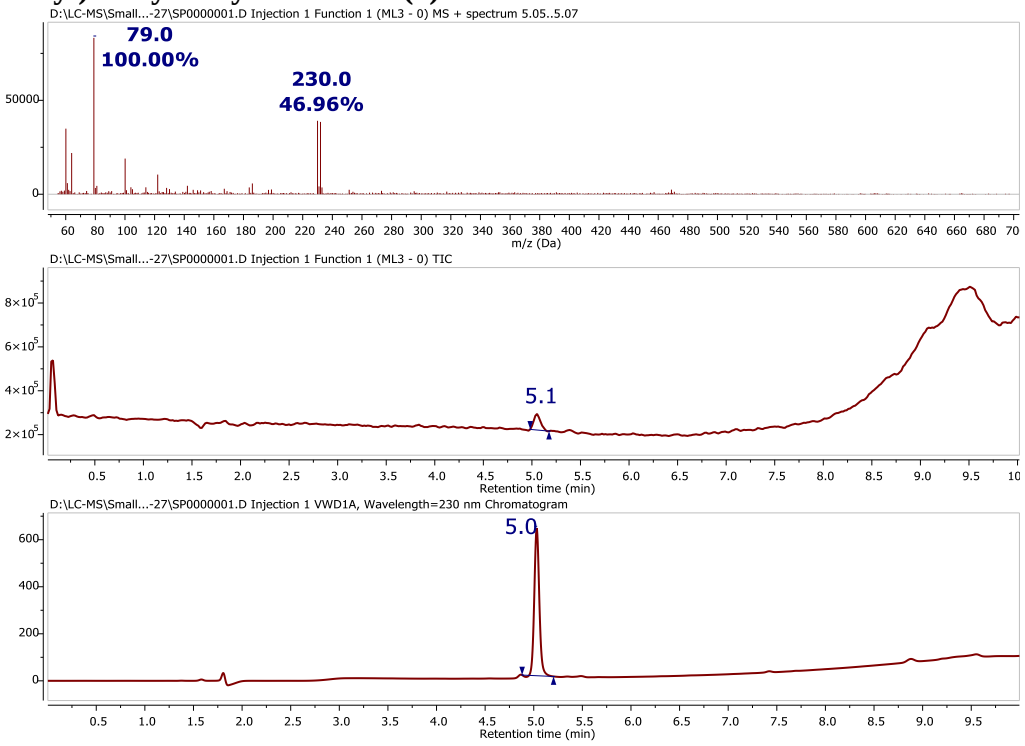

3,5-bis(bromomethyl) benzoic acid

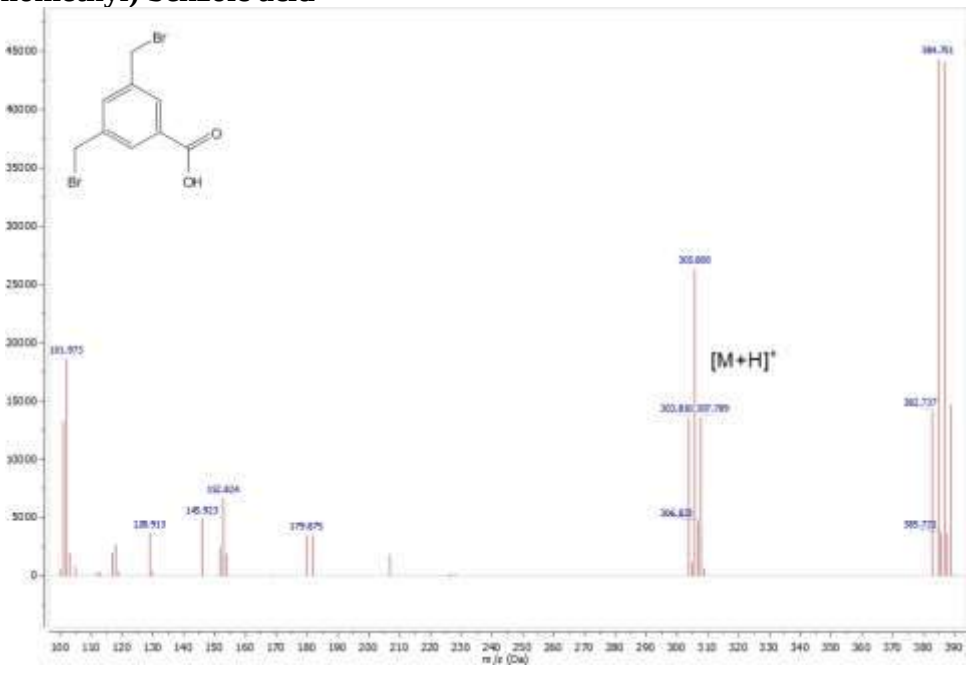

3,5-bis(bromomethyl)-N-hydroxybenzamide (2)

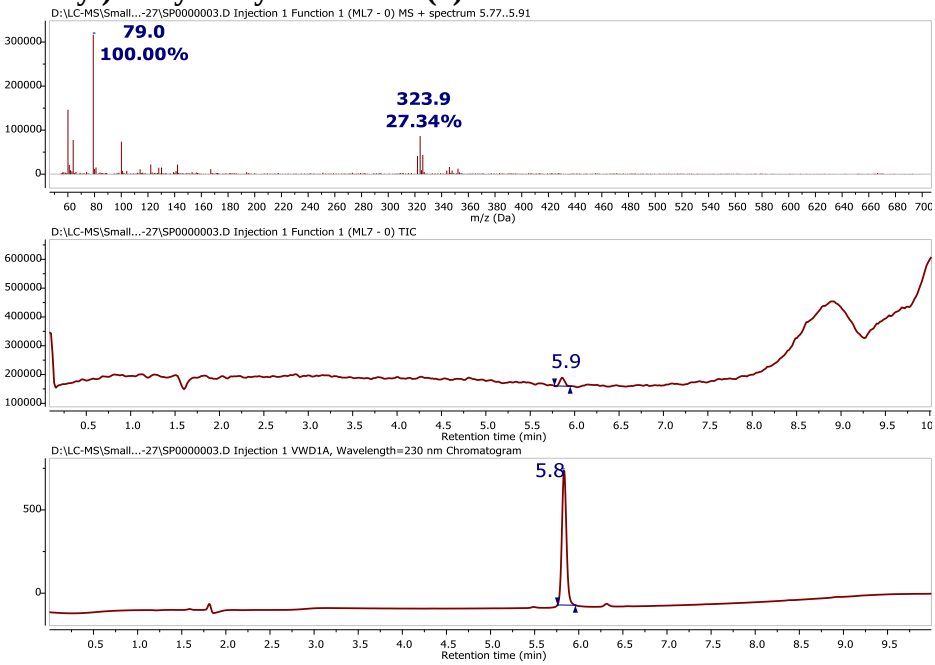

3-(3,4-dibromo-2,5-dioxo-2,5-dihydro-1H-pyrrol-1-yl)-N-hydroxypropanamide (3)

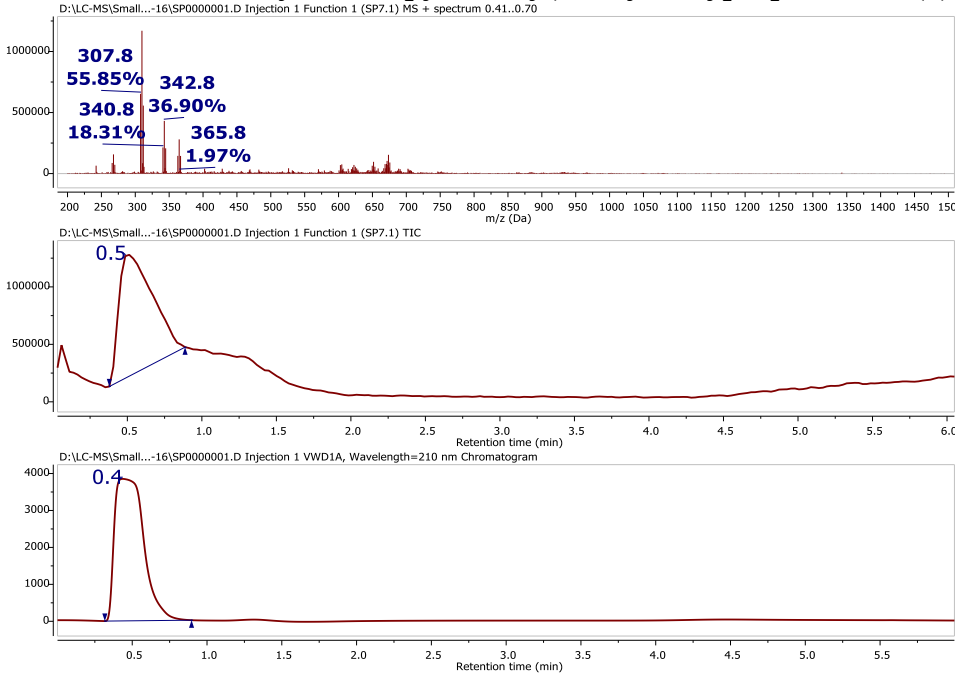

3,5-bis(2-bromoacetamido)benzoic acid

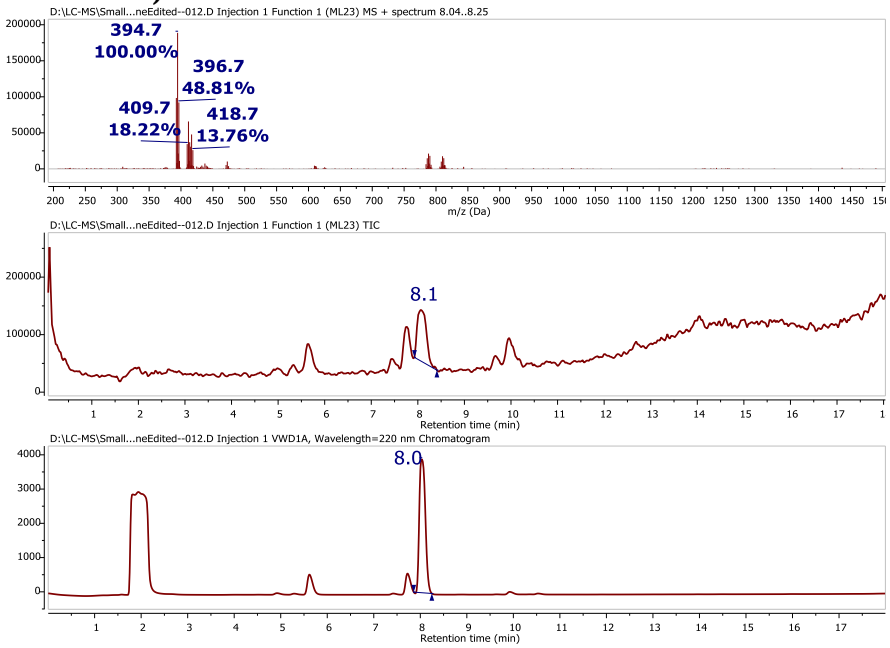

N,N'-(5-(hydroxycarbamoyl)-1,3-phenylene)bis(2-bromoacetamide) (4)

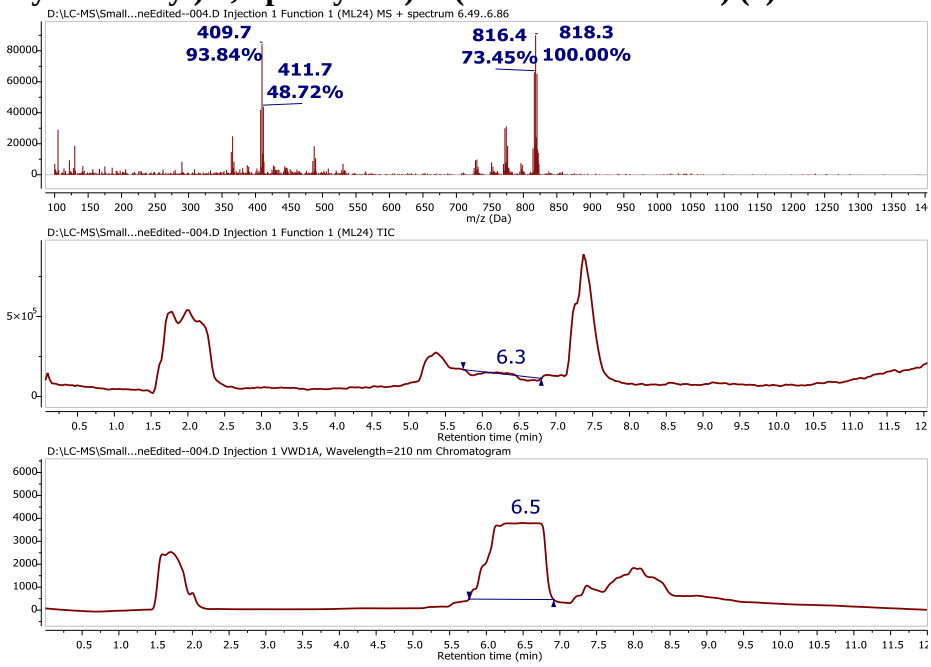

P4

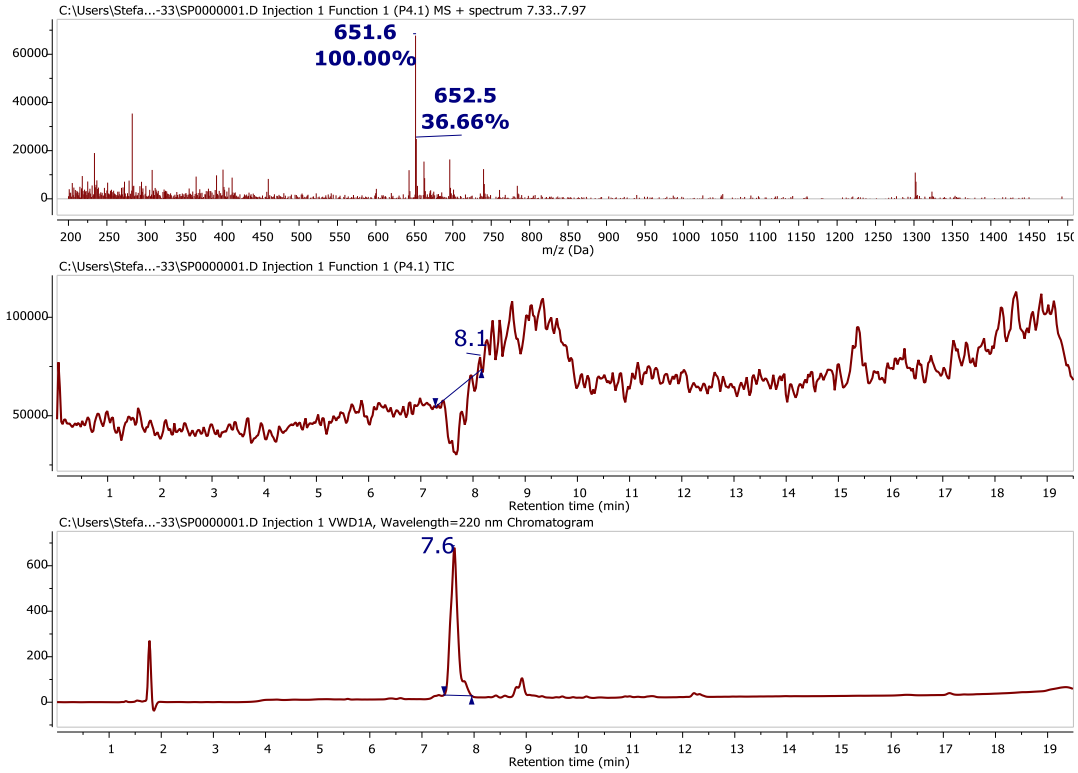
C:\Users\Stefa...-33\SP0000001.D Injection 1 Function 1 (P4.1) MS + spectrum 7.33..7.97
651.6
100.00%
652.5
36.66%
m/z (Da)
C:\Users\Stefa...-33\SP0000001.D Injection 1 Function 1 (P4.1) TIC
8.1
Retention time (min)
C:\Users\Stefa...-33\SP0000001.D Injection 1 VWD1A, Wavelength=220 nm Chromatogram
7.6
Retention time (min)

P4-2

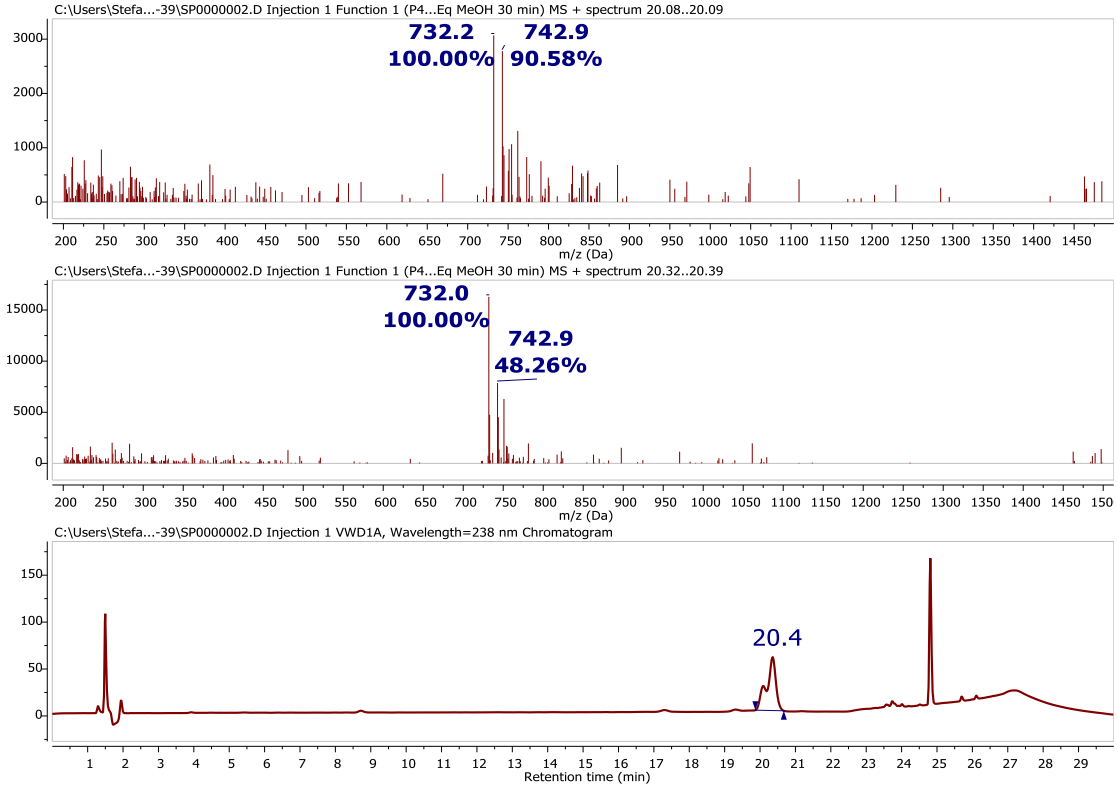
C:\Users\Stefa...-39\SP0000002.D Injection 1 Function 1 (P4...Eq MeOH 30 min) MS + spectrum 20.08..20.09
732.2
100.00%
742.9
90.58%
m/z (Da)
C:\Users\Stefa...-39\SP0000002.D Injection 1 Function 1 (P4...Eq MeOH 30 min) MS + spectrum 20.32..20.39
732.0
100.00%
742.9
48.26%
m/z (Da)
C:\Users\Stefa...-39\SP0000002.D Injection 1 VWD1A, Wavelength=238 nm Chromatogram
20.4
Retention time (min)

P4- 3

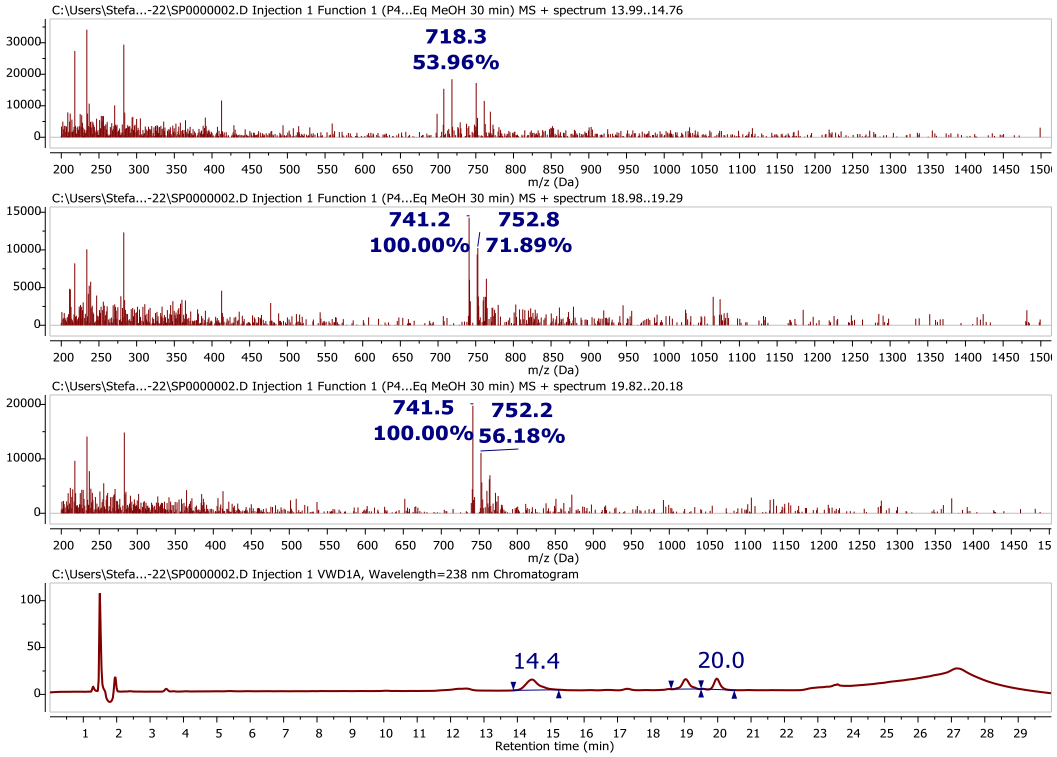
C:\Users\Stefa...-22\SP0000002.D Injection 1 Function 1 (P4...Eq MeOH 30 min) MS + spectrum 13.99..14.76
718.3
53.96%
m/z (Da)
C:\Users\Stefa...-22\SP0000002.D Injection 1 Function 1 (P4...Eq MeOH 30 min) MS + spectrum 18.98..19.29
741.2
100.00%
752.8
71.89%
m/z (Da)
C:\Users\Stefa...-22\SP0000002.D Injection 1 Function 1 (P4...Eq MeOH 30 min) MS + spectrum 19.82..20.18
741.5
100.00%
752.2
56.18%
m/z (Da)
C:\Users\Stefa...-22\SP0000002.D Injection 1 VWD1A, Wavelength=238 nm Chromatogram
14.4
20.0
Retention time (min)

P4- 4

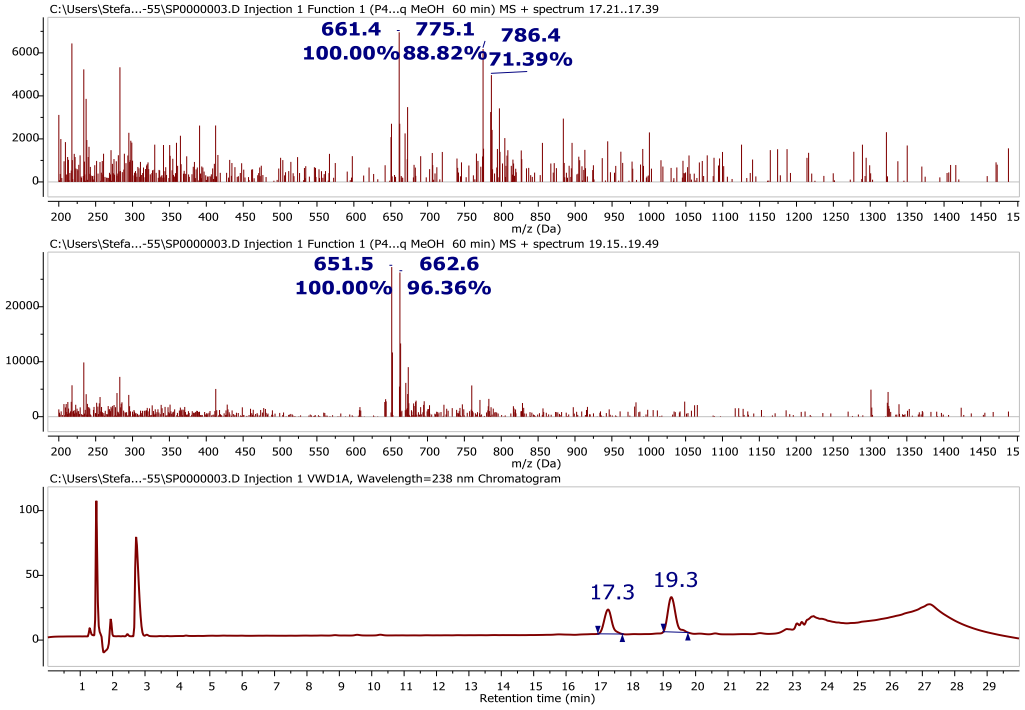
C:\Users\Stefa...-55\SP0000003.D Injection 1 Function 1 (P4...q MeOH 60 min) MS + spectrum 17.21..17.39
661.4
100.00%
775.1
88.82%
786.4
71.39%
m/z (Da)
C:\Users\Stefa...-55\SP0000003.D Injection 1 Function 1 (P4...q MeOH 60 min) MS + spectrum 19.15..19.49
651.5
100.00%
662.6
96.36%
m/z (Da)
C:\Users\Stefa...-55\SP0000003.D Injection 1 VWD1A, Wavelength=238 nm Chromatogram
17.3
19.3
Retention time (min)

methyl N-acetyl-S-(4-(hydroxycarbamoyl)benzyl)-D-cysteinate (1A)

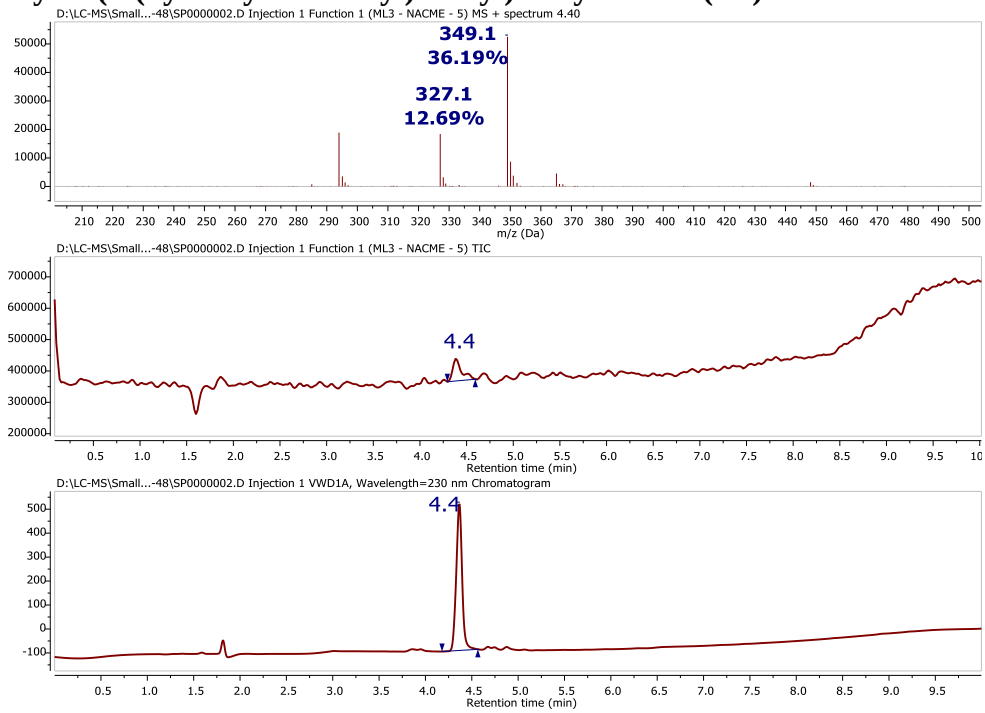

dimethyl 3,3'-(((5-(hydroxycarbamoyl)-1,3-phenylene)bis(methylene))bis(sulfanediyl))(2S,2'S)-bis(2-acetamidopropanoate) (2A)

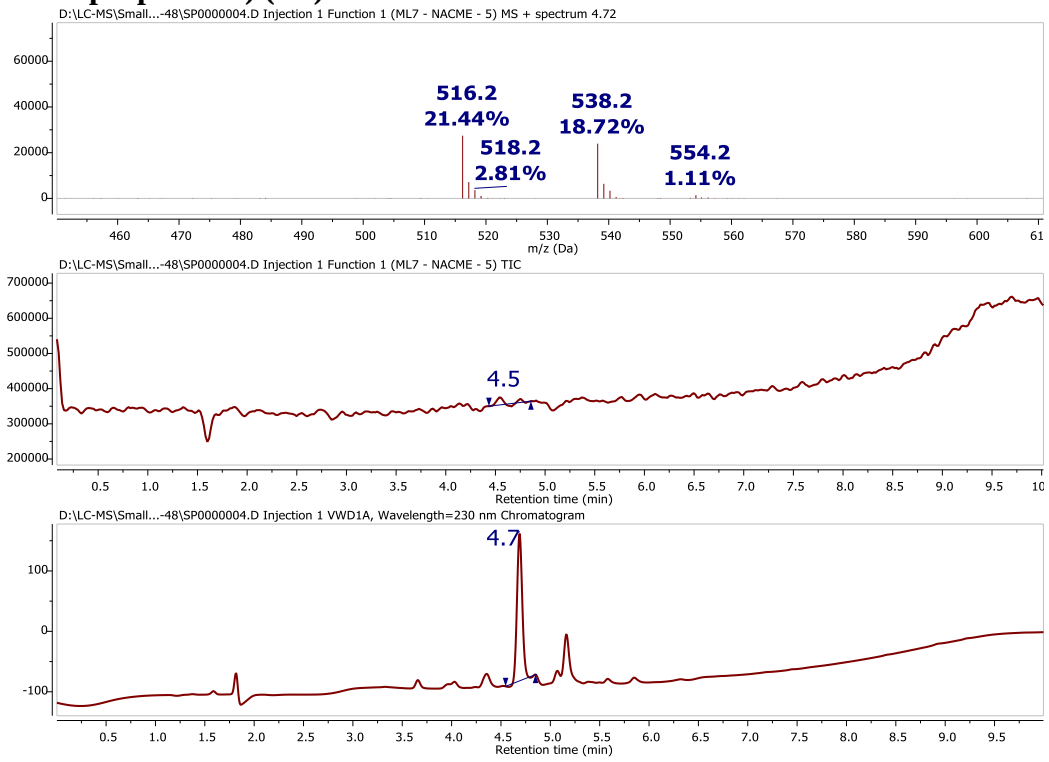

P2.4

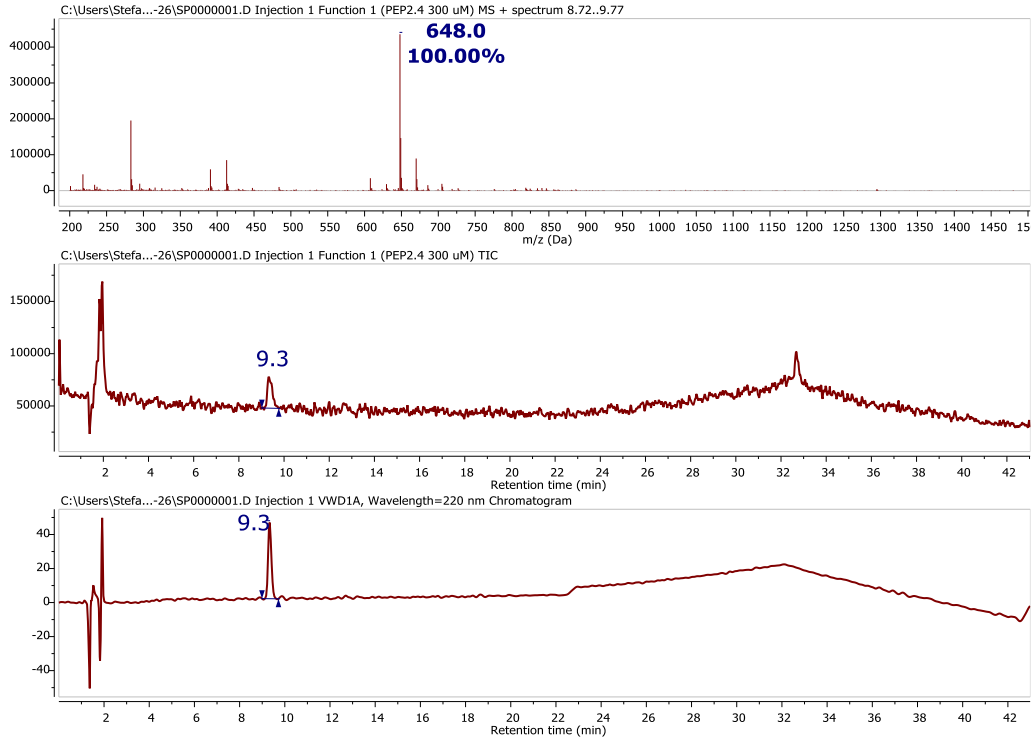
C:\Users\Stefa...-26\SP0000001.D Injection 1 Function 1 (PEP2.4 300 uM) MS + spectrum 8.72..9.77
648.0
100.00%
m/z (Da)
C:\Users\Stefa...-26\SP0000001.D Injection 1 Function 1 (PEP2.4 300 uM) TIC
9.3
Retention time (min)
C:\Users\Stefa...-26\SP0000001.D Injection 1 VWD1A, Wavelength=220 nm Chromatogram
9.3
Retention time (min)

P2.5

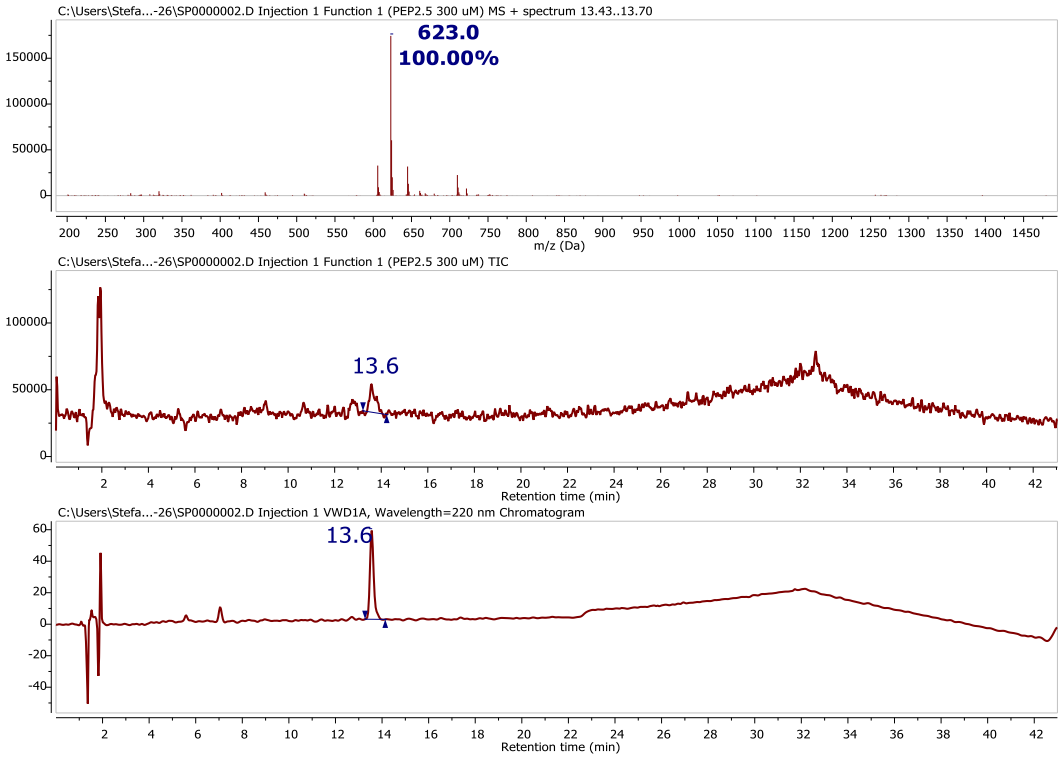
C:\Users\Stefa...-26\SP0000002.D Injection 1 Function 1 (PEP2.5 300 uM) MS + spectrum 13.43..13.70
623.0
100.00%
m/z (Da)
C:\Users\Stefa...-26\SP0000002.D Injection 1 Function 1 (PEP2.5 300 uM) TIC
13.6
Retention time (min)
C:\Users\Stefa...-26\SP0000002.D Injection 1 VWD1A, Wavelength=220 nm Chromatogram
13.6
Retention time (min)

P2.6

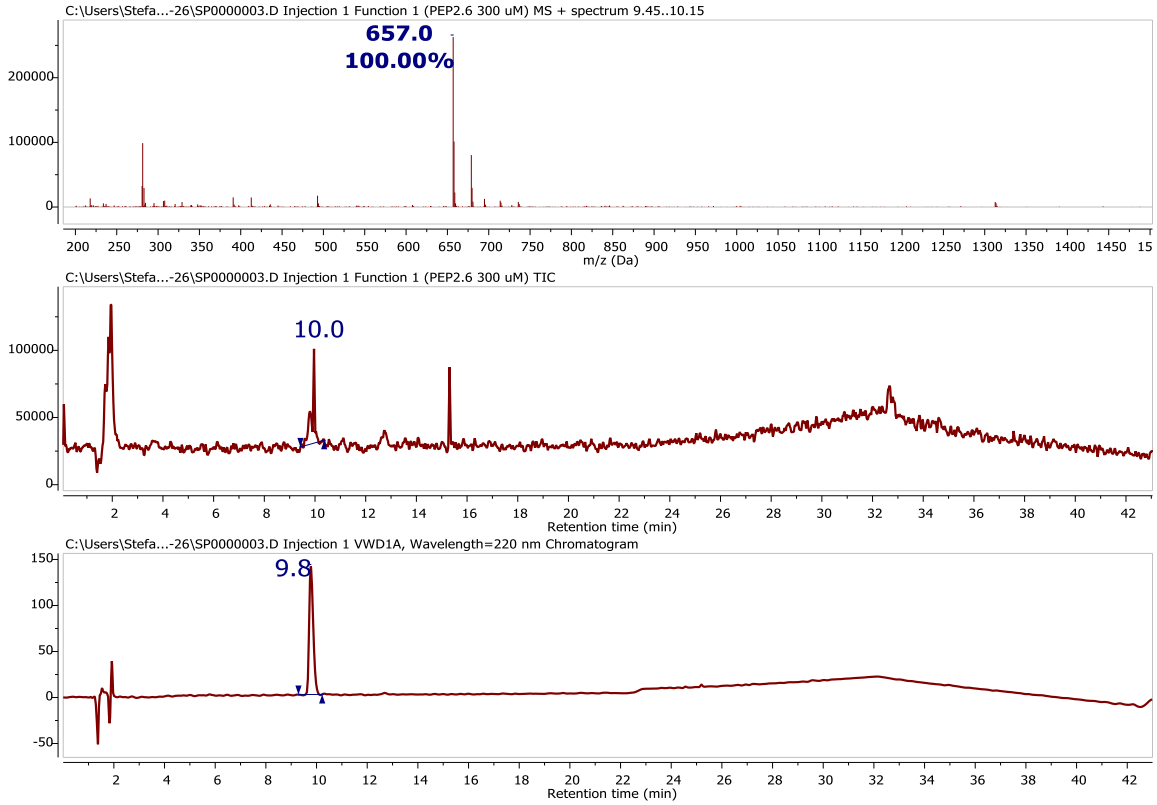
C:\Users\Stefa...-26\SP0000003.D Injection 1 Function 1 (PEP2.6 300 uM) MS + spectrum 9.45..10.15
657.0
100.00%
m/z (Da)
C:\Users\Stefa...-26\SP0000003.D Injection 1 Function 1 (PEP2.6 300 uM) TIC
10.0
Retention time (min)
C:\Users\Stefa...-26\SP0000003.D Injection 1 VWD1A, Wavelength=220 nm Chromatogram
9.8
Retention time (min)

P2.7

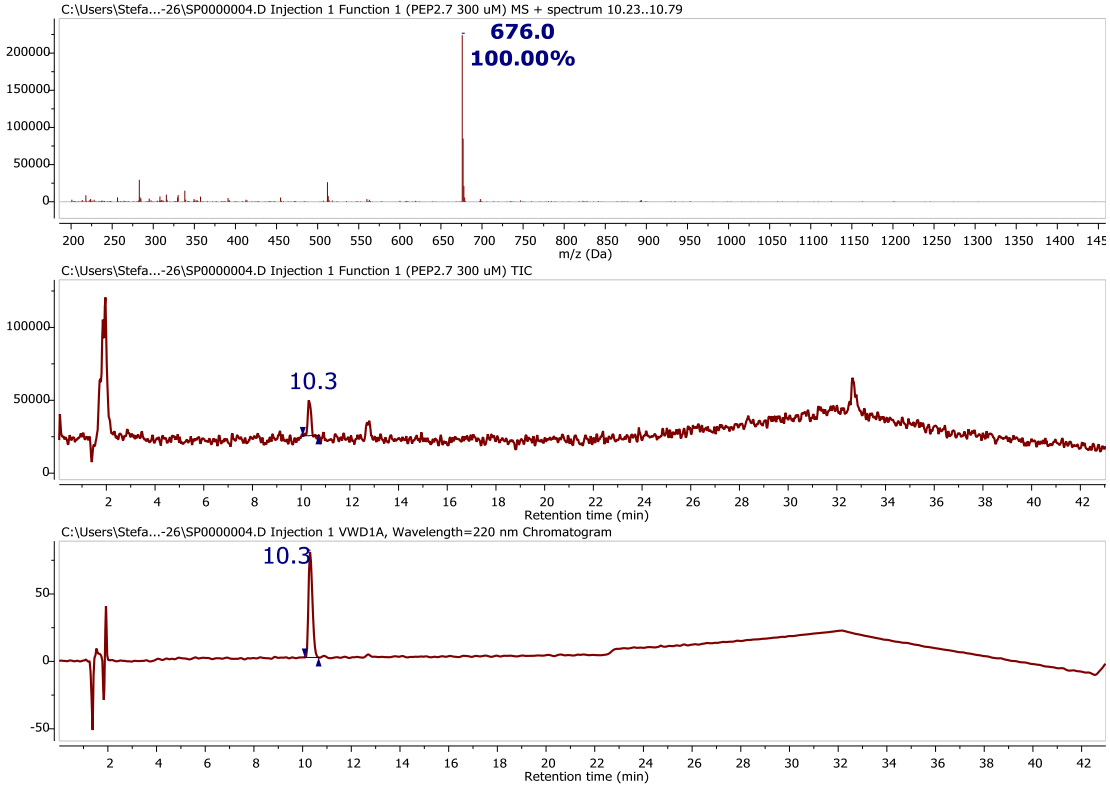
C:\Users\Stefa...-26\SP0000004.D Injection 1 Function 1 (PEP2.7 300 uM) MS + spectrum 10.23..10.79
676.0
100.00%
m/z (Da)
C:\Users\Stefa...-26\SP0000004.D Injection 1 Function 1 (PEP2.7 300 uM) TIC
10.3
Retention time (min)
C:\Users\Stefa...-26\SP0000004.D Injection 1 VWD1A, Wavelength=220 nm Chromatogram
10.3
Retention time (min)

P2.8

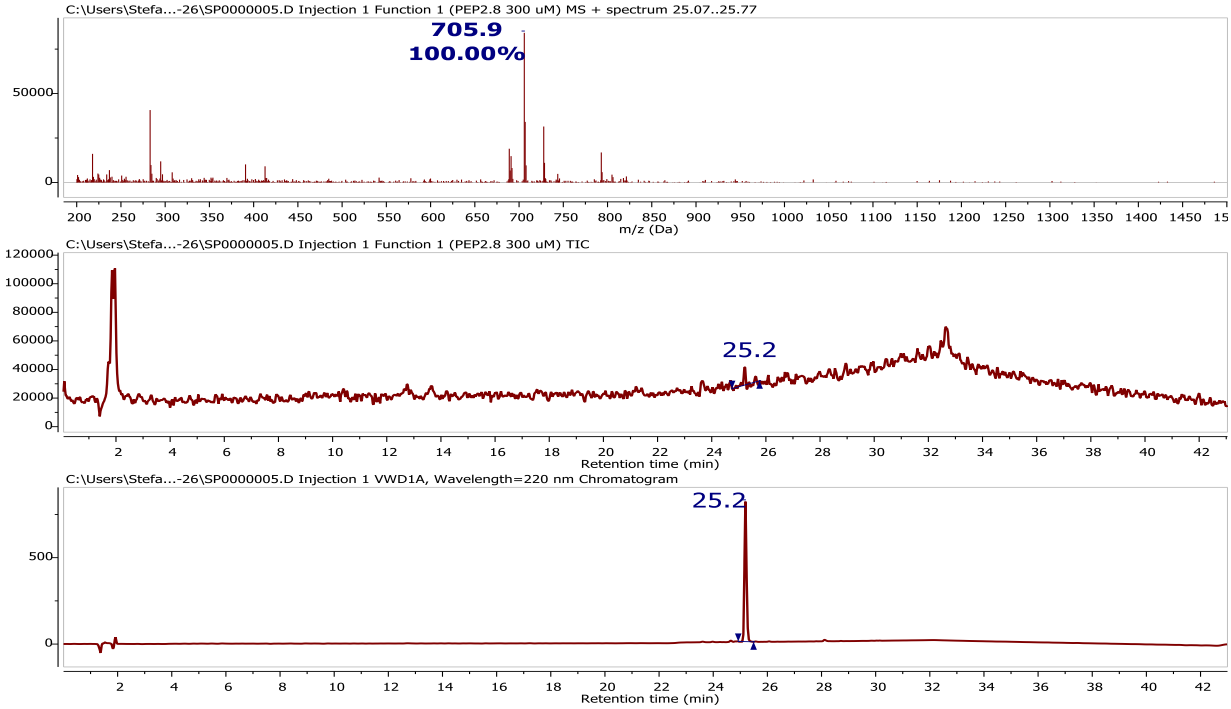
C:\Users\Stefa...-26\SP0000005.D Injection 1 Function 1 (PEP2.8 300 uM) MS + spectrum 25.07..25.77
705.9
100.00%
m/z (Da)
C:\Users\Stefa...-26\SP0000005.D Injection 1 Function 1 (PEP2.8 300 uM) TIC
25.2
Retention time (min)
C:\Users\Stefa...-26\SP0000005.D Injection 1 VWD1A, Wavelength=220 nm Chromatogram
25.2
Retention time (min)

P2.5-2

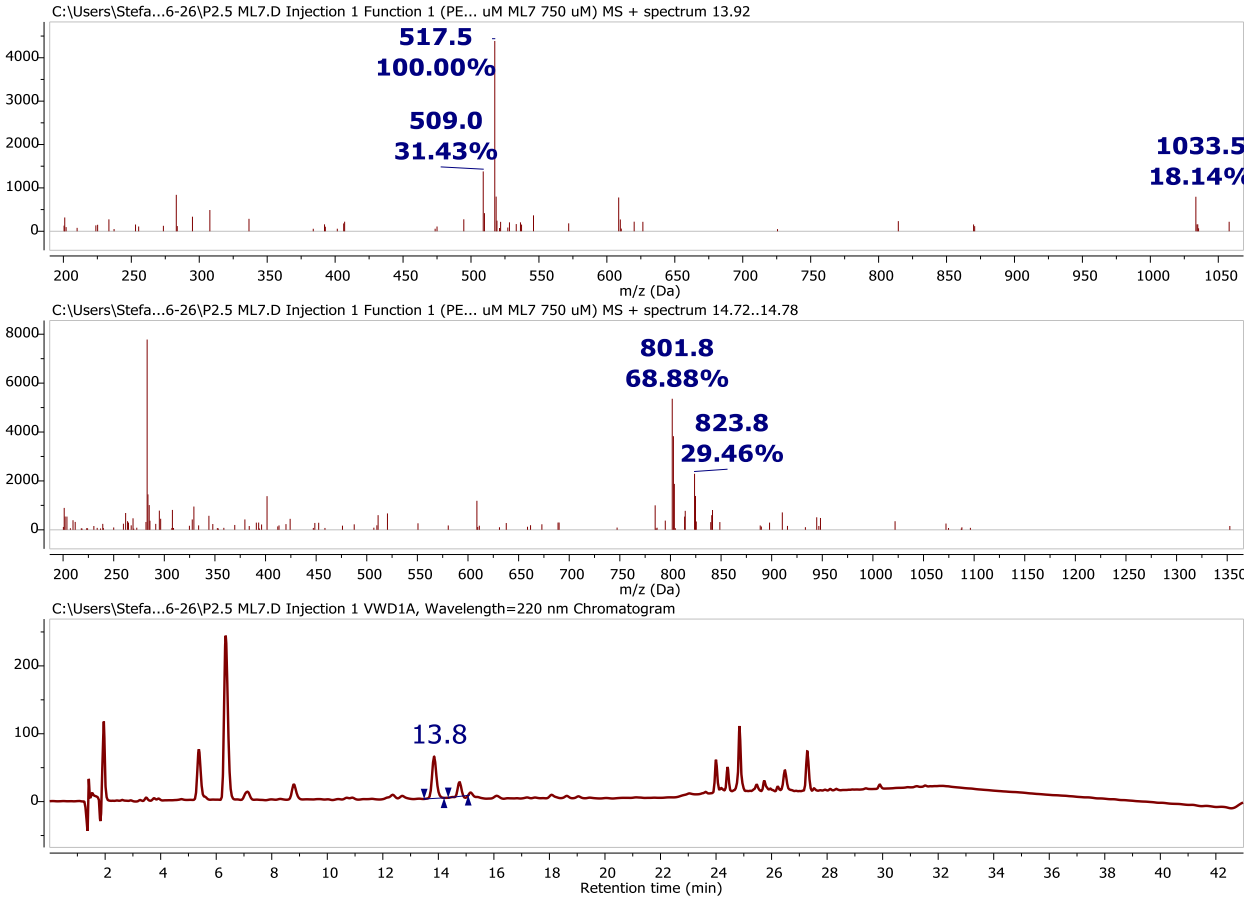
C:\Users\Stefa...6-26\P2.5 ML7.D Injection 1 Function 1 (PE... uM ML7 750 uM) MS + spectrum 13.92
517.5
100.00%
509.0
31.43%
1033.5
18.14%
m/z (Da)
C:\Users\Stefa...6-26\P2.5 ML7.D Injection 1 Function 1 (PE... uM ML7 750 uM) MS + spectrum 14.72..14.78
801.8
68.88%
823.8
29.46%
m/z (Da)
C:\Users\Stefa...6-26\P2.5 ML7.D Injection 1 VWD1A, Wavelength=220 nm Chromatogram
13.8
Retention time (min)

P1.2

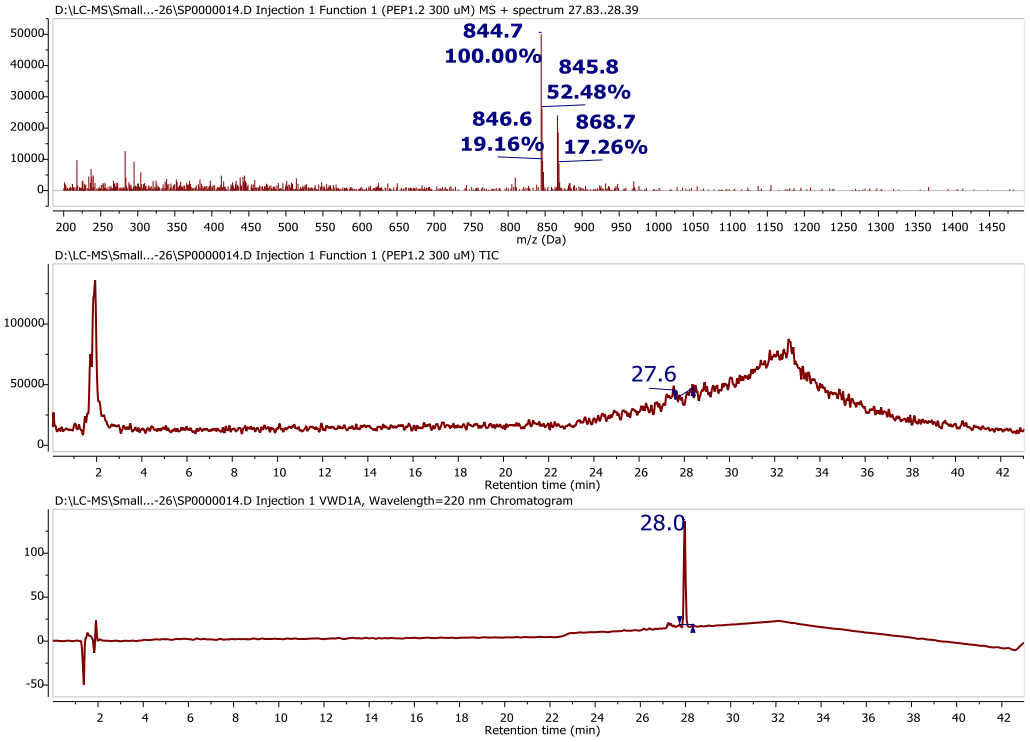
D:\LC-MS\Small...-26\SP0000014.D Injection 1 Function 1 (PEP1.2 300 uM) MS + spectrum 27.83..28.39
844.7
100.00%
845.8
52.48%
846.6
19.16%
868.7
17.26%
m/z (Da)
D:\LC-MS\Small...-26\SP0000014.D Injection 1 Function 1 (PEP1.2 300 uM) TIC
27.6
Retention time (min)
D:\LC-MS\Small...-26\SP0000014.D Injection 1 VWD1A, Wavelength=220 nm Chromatogram
28.0
Retention time (min)

P1.3

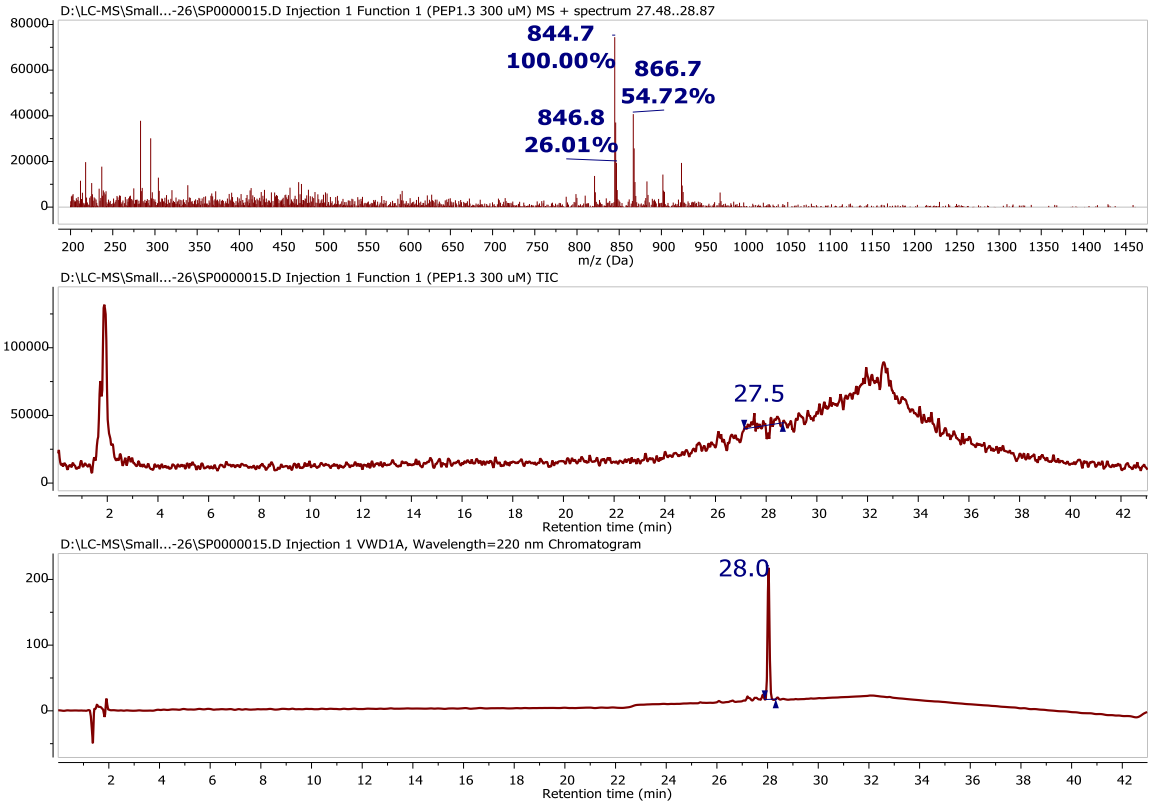
D:\LC-MS\Small...-26\SP0000015.D Injection 1 Function 1 (PEP1.3 300 uM) MS + spectrum 27.48..28.87
844.7
100.00%
866.7
54.72%
846.8
26.01%
m/z (Da)
D:\LC-MS\Small...-26\SP0000015.D Injection 1 Function 1 (PEP1.3 300 uM) TIC
27.5
Retention time (min)
D:\LC-MS\Small...-26\SP0000015.D Injection 1 VWD1A, Wavelength=220 nm Chromatogram
28.0
Retention time (min)

P1.4

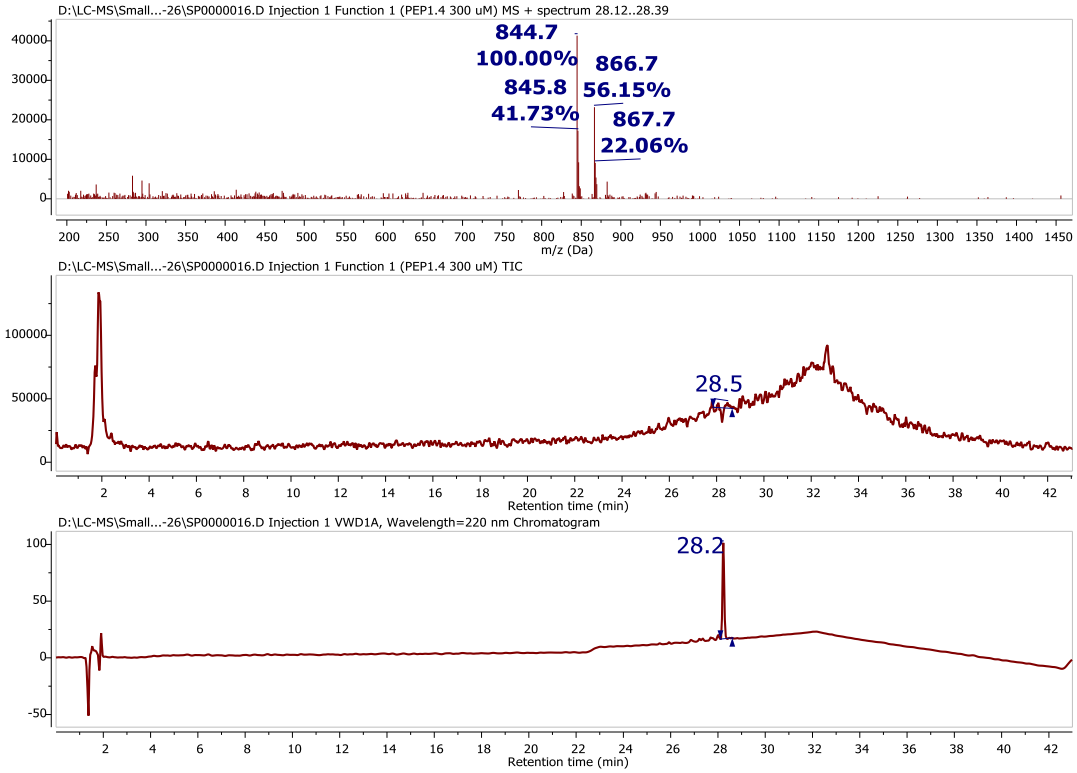
D:\LC-MS\Small...-26\SP0000016.D Injection 1 Function 1 (PEP1.4 300 uM) MS + spectrum 28.12..28.39
844.7
100.00%
866.7
56.15%
845.8
41.73%
867.7
22.06%
m/z (Da)
D:\LC-MS\Small...-26\SP0000016.D Injection 1 Function 1 (PEP1.4 300 uM) TIC
28.5
Retention time (min)
D:\LC-MS\Small...-26\SP0000016.D Injection 1 VWD1A, Wavelength=220 nm Chromatogram
28.2
Retention time (min)

P1.2-2

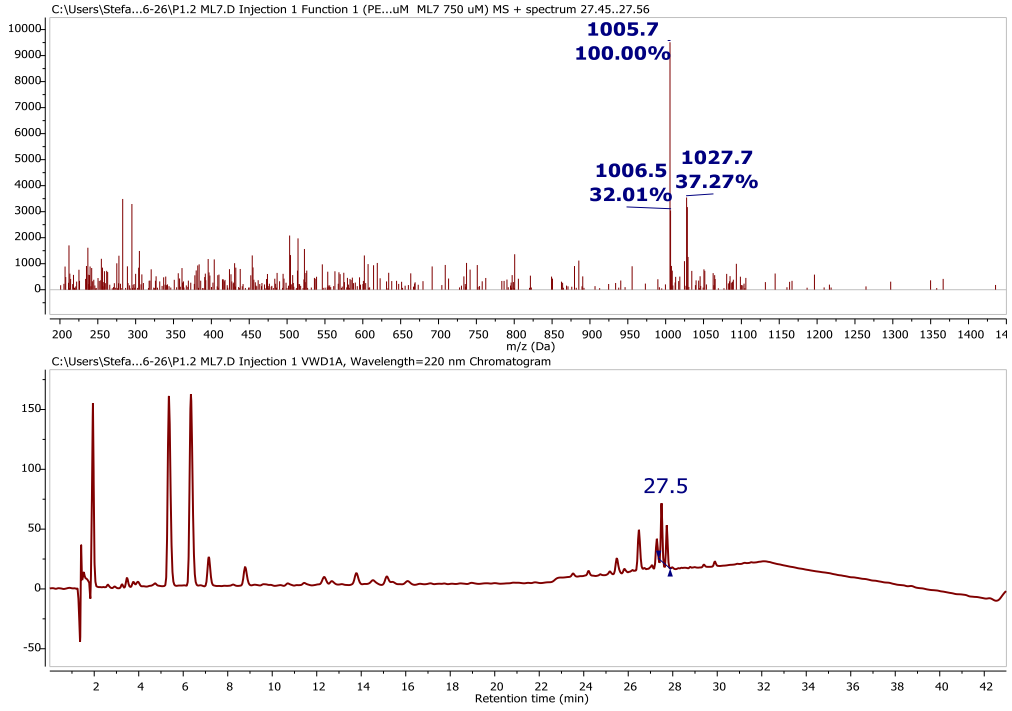
C:\Users\Stefa...6-26\P1.2 ML7.D Injection 1 Function 1 (PE...uM ML7 750 uM) MS + spectrum 27.45..27.56
1005.7
100.00%
1027.7
37.27%
1006.5
32.01%
m/z (Da)
C:\Users\Stefa...6-26\P1.2 ML7.D Injection 1 VWD1A, Wavelength=220 nm Chromatogram
27.5
Retention time (min)

P1.3-2

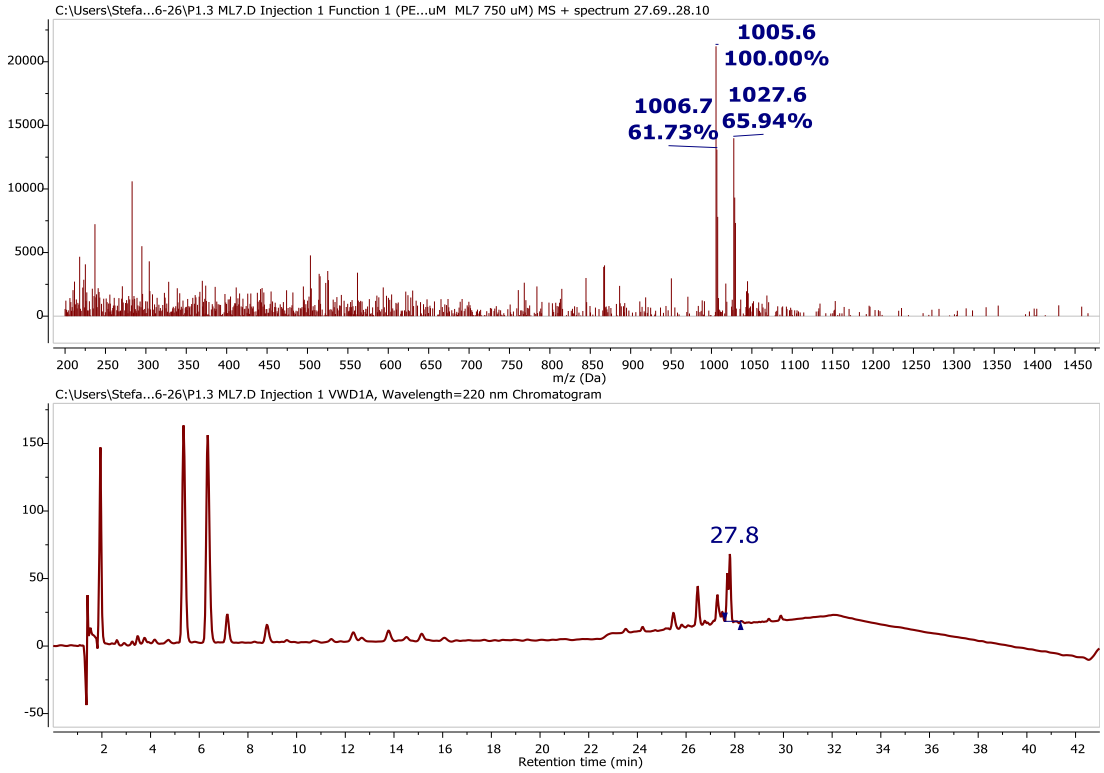
C:\Users\Stefa...6-26\P1.3 ML7.D Injection 1 Function 1 (PE...uM ML7 750 uM) MS + spectrum 27.69..28.10
1005.6
100.00%
1006.7
61.73%
1027.6
65.94%
m/z (Da)
C:\Users\Stefa...6-26\P1.3 ML7.D Injection 1 VWD1A, Wavelength=220 nm Chromatogram
27.8
Retention time (min)

P1.4-2

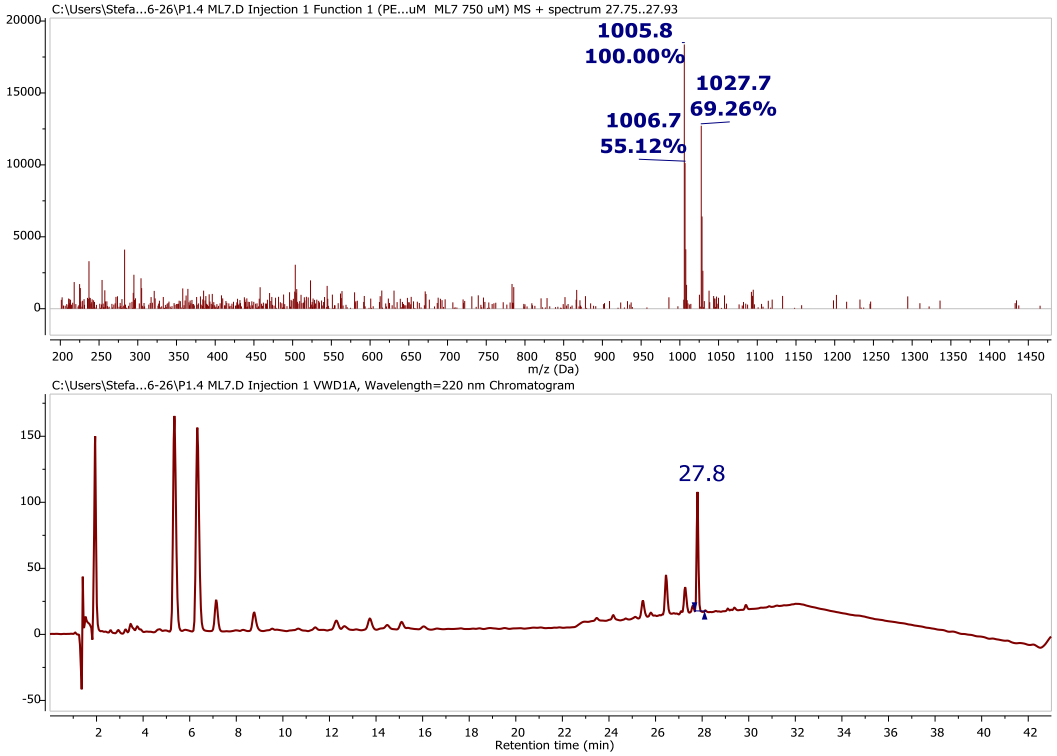
C:\Users\Stefa...6-26\P1.4 ML7.D Injection 1 Function 1 (PE...uM ML7 750 uM) MS + spectrum 27.75..27.93
1005.8
100.00%
1027.7
69.26%
1006.7
55.12%
m/z (Da)
C:\Users\Stefa...6-26\P1.4 ML7.D Injection 1 VWD1A, Wavelength=220 nm Chromatogram
27.8
Retention time (min)

Mca-PLAQAV-Dpa-RSSSR-NH2

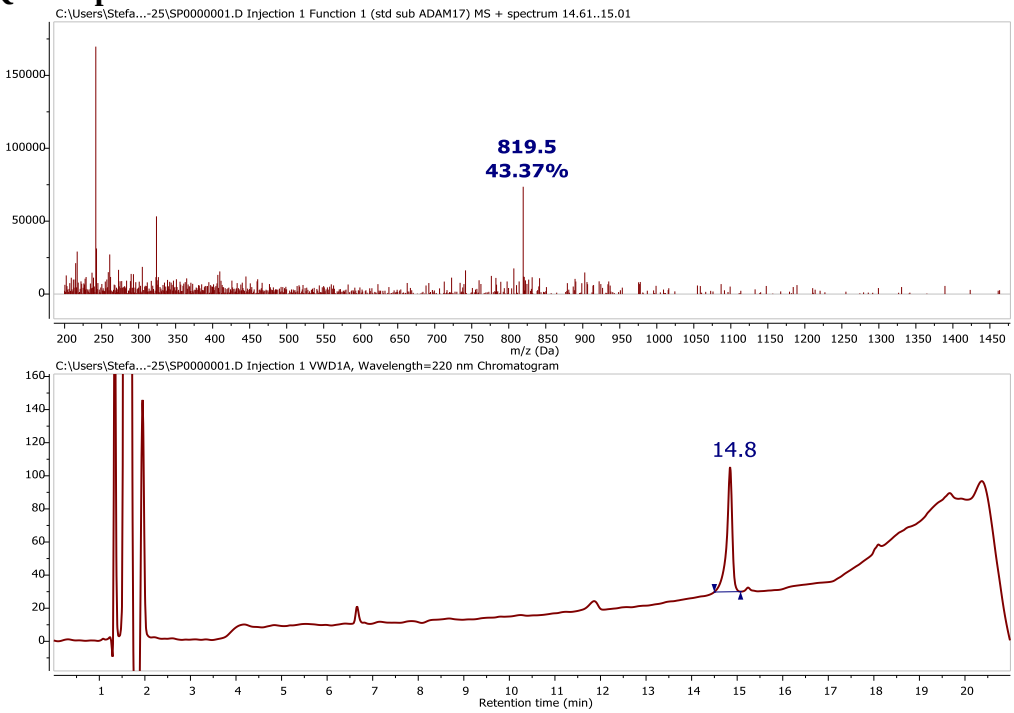

Mca-PLAQA

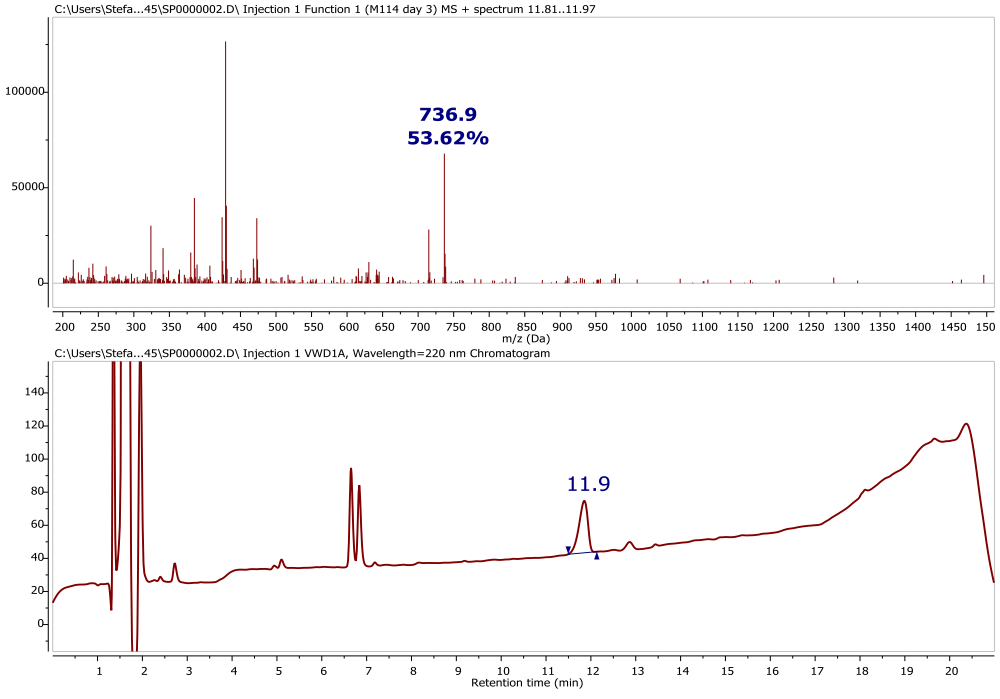

N-((tetrahydro-2H-pyran-2-yl)oxy)propiolamide

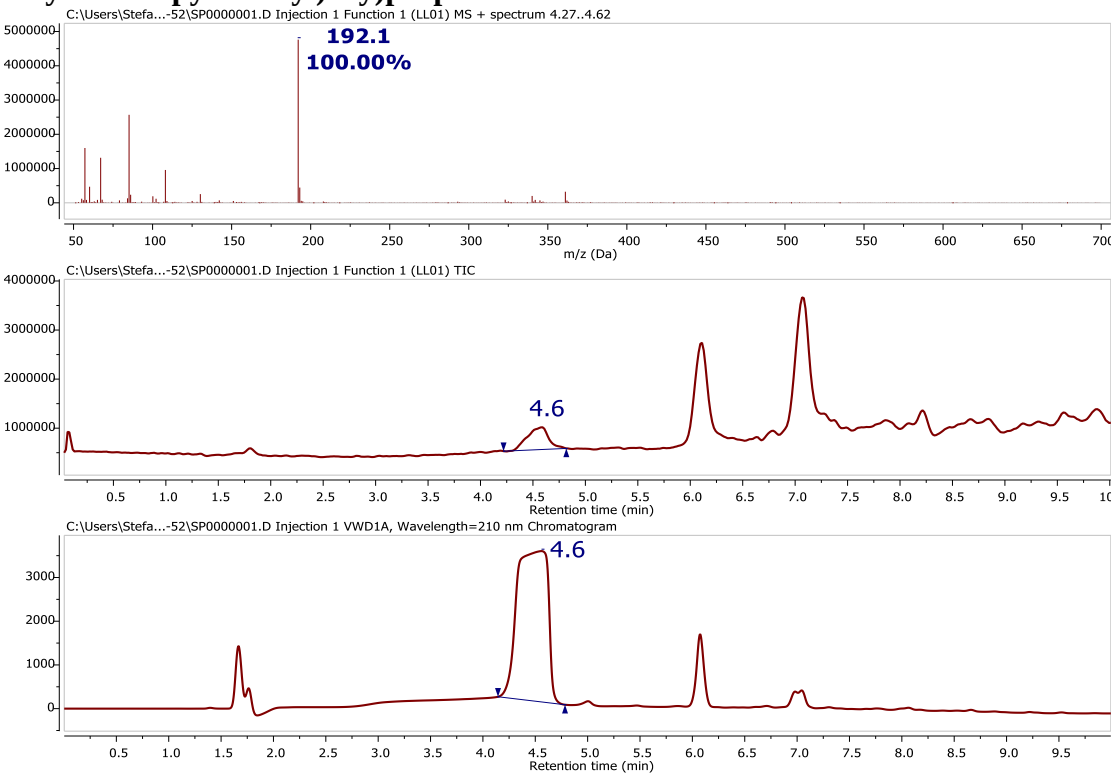

N-hydroxypropiolamide (5)

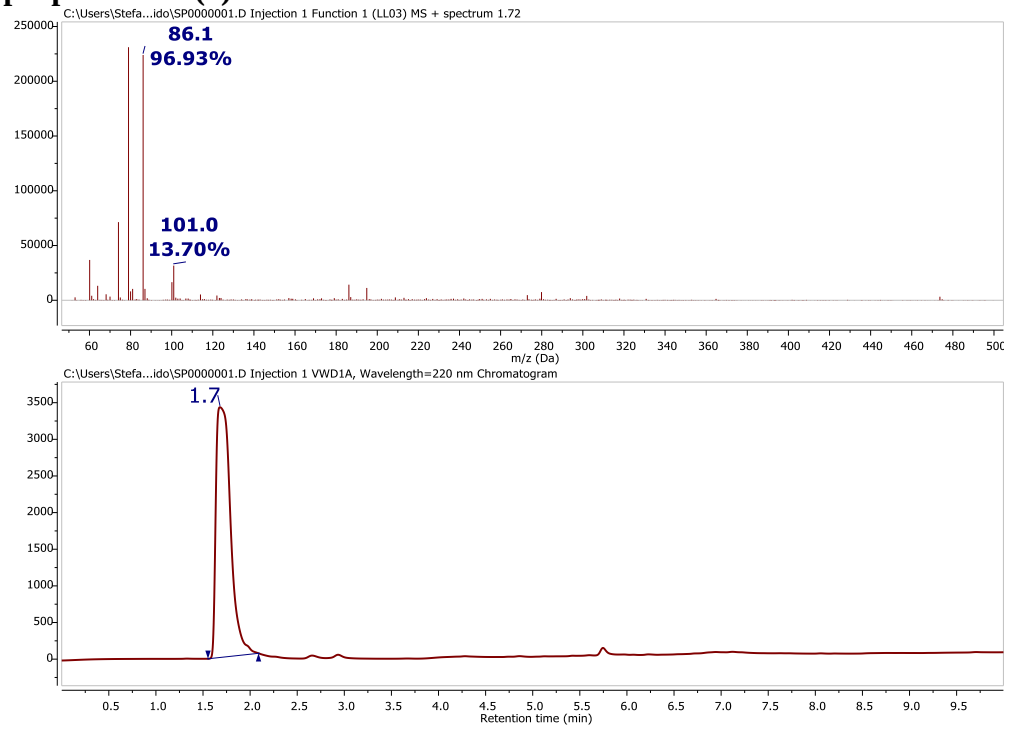

4-ethynyl-N-hydroxybenzamide (6)

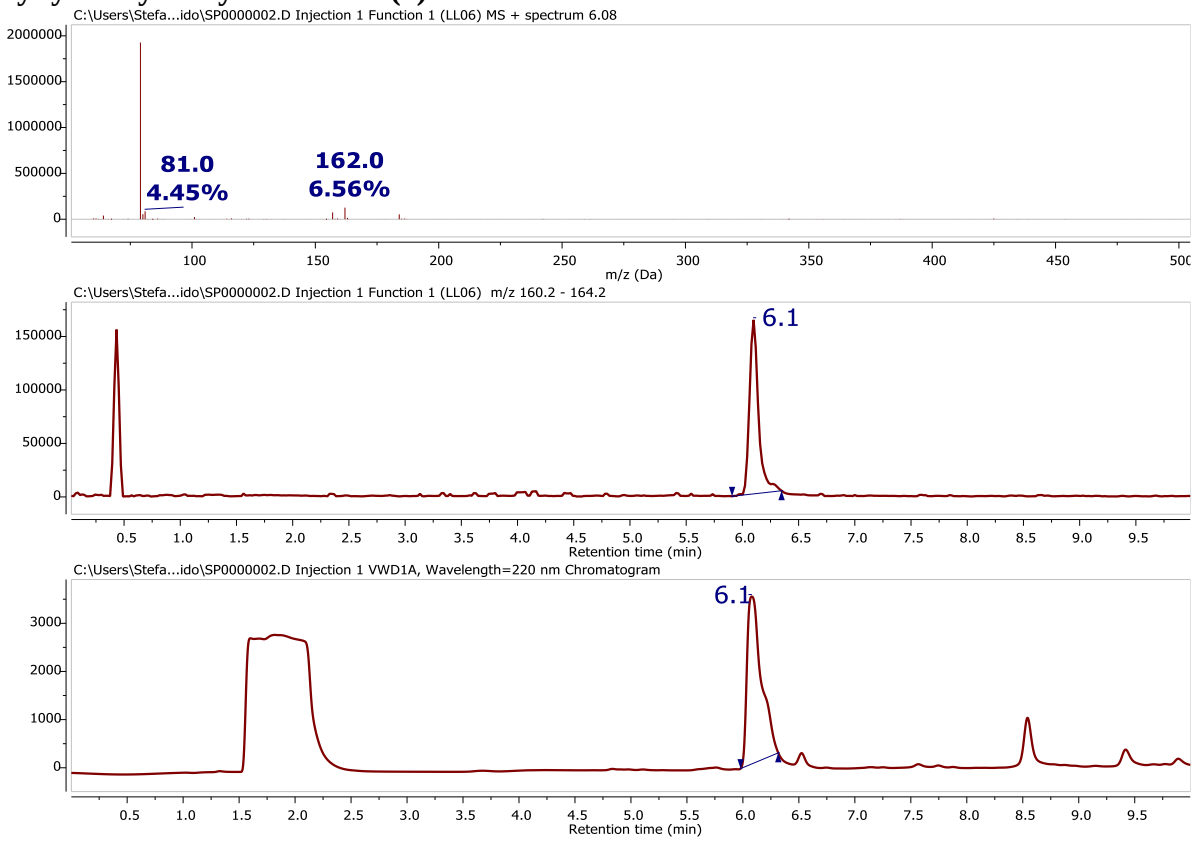

(S)-2-acetamido-3-(4-(azidomethyl)phenyl)propanoic acid (AMP)

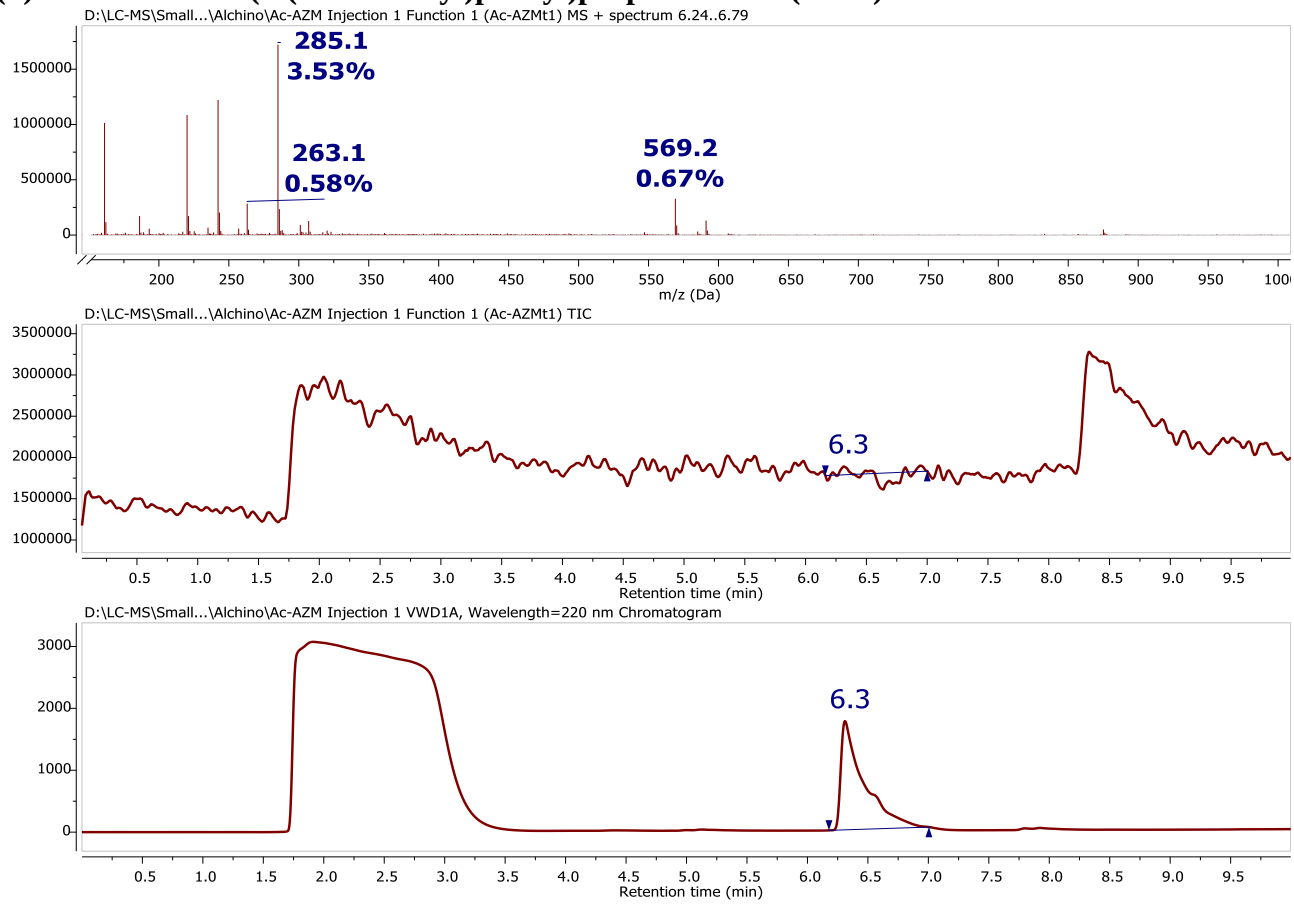

(S)-2-acetamido-3-(4-((4-(hydroxycarbamoyl)-1H-1,2,3-triazol-1-yl)methyl)phenyl)propanoic acid (AMP-5)

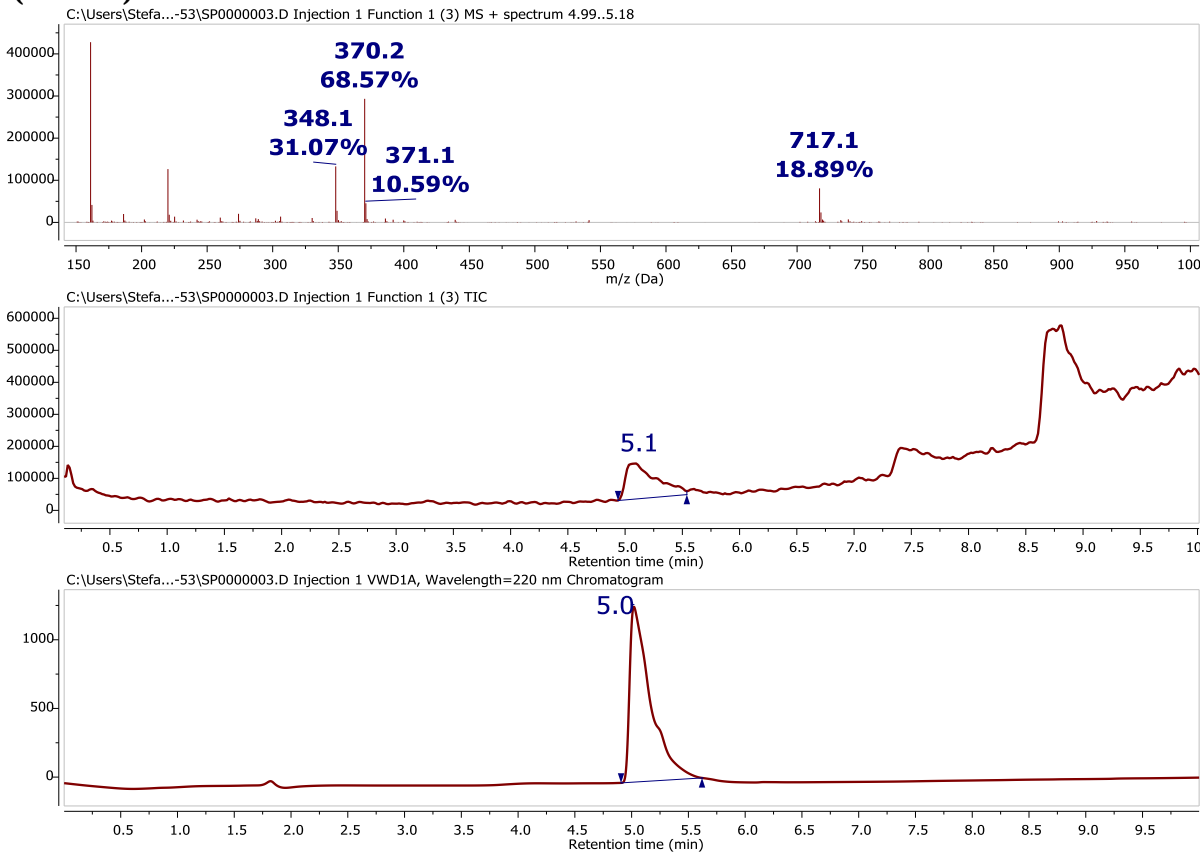

(S)-2-acetamido-3-(4-((4-(4-(hydroxycarbamoyl)phenyl)-1H-1,2,3-triazol-1-yl)methyl)phenyl)propanoic acid (AMP-6)

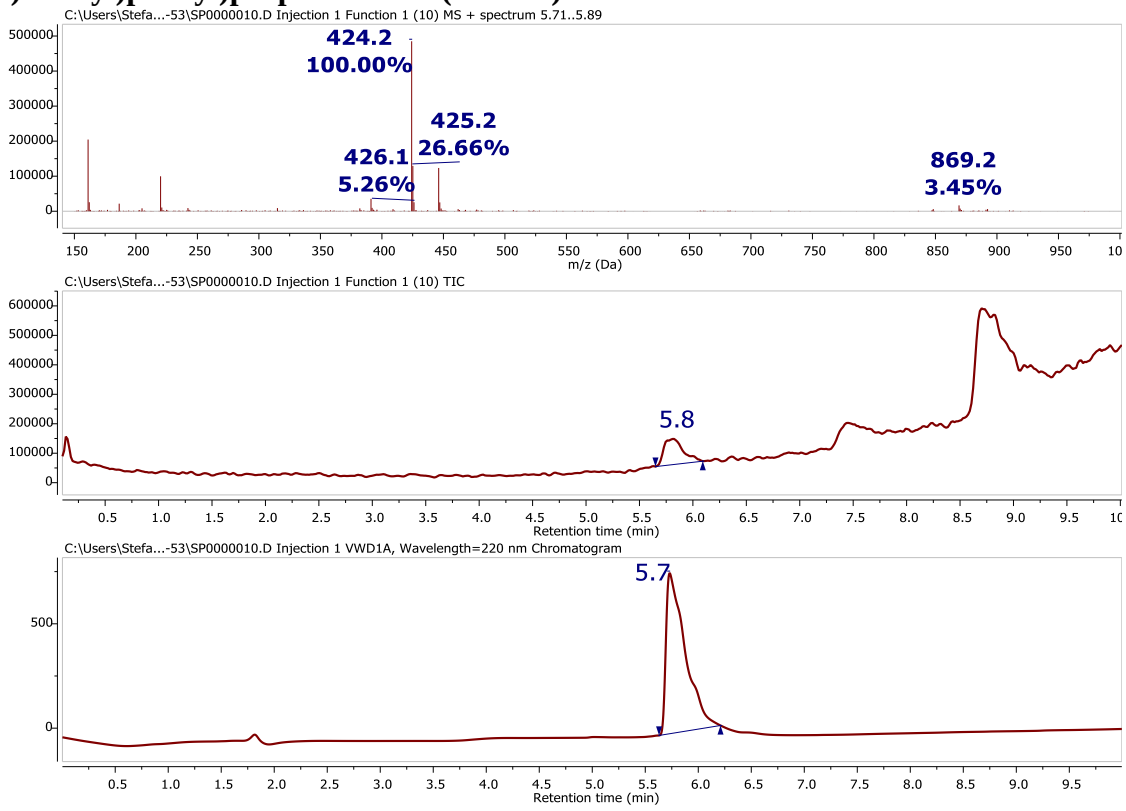

P3

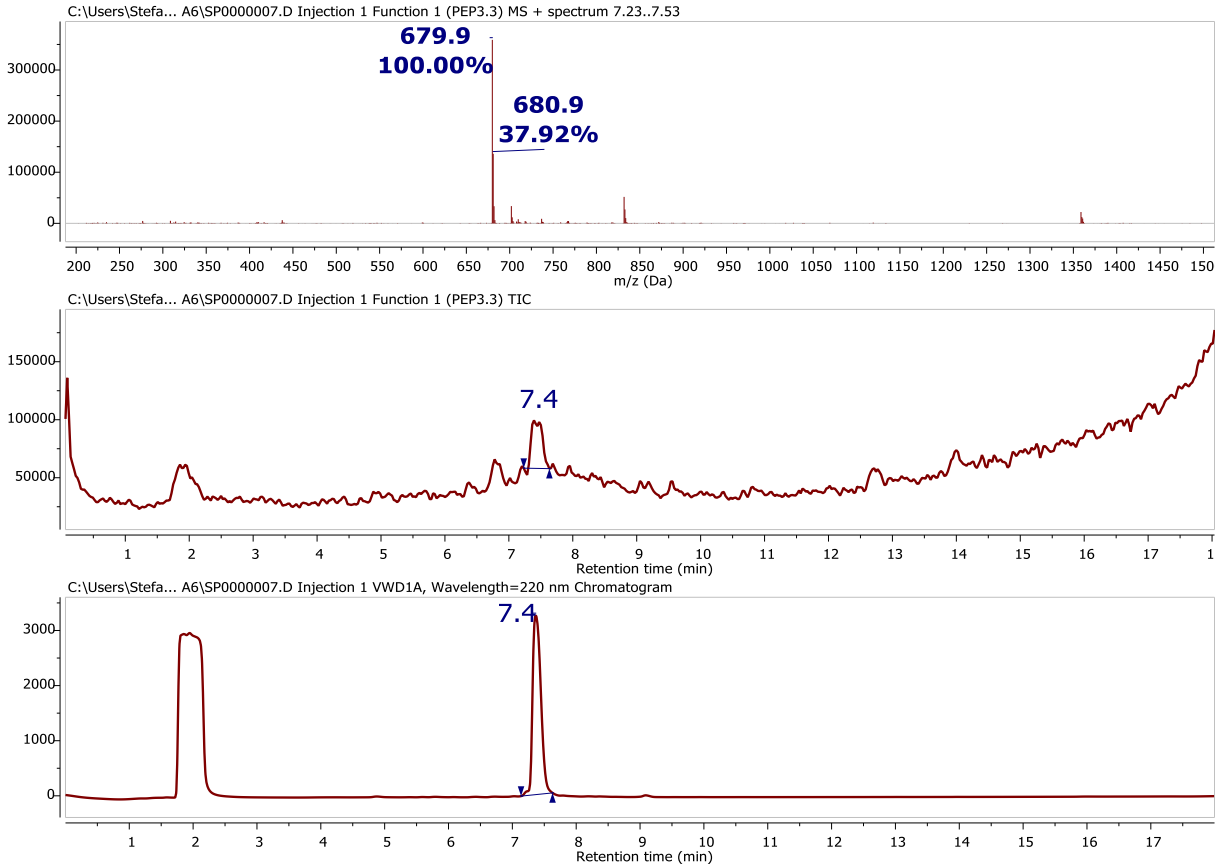
C:\Users\Stefa... A6\SP0000007.D Injection 1 Function 1 (PEP3.3) MS + spectrum 7.23..7.53
679.9
100.00%
680.9
37.92%
m/z (Da)
C:\Users\Stefa... A6\SP0000007.D Injection 1 Function 1 (PEP3.3) TIC
7.4
Retention time (min)
C:\Users\Stefa... A6\SP0000007.D Injection 1 VWD1A, Wavelength=220 nm Chromatogram
7.4
Retention time (min)

P3-5

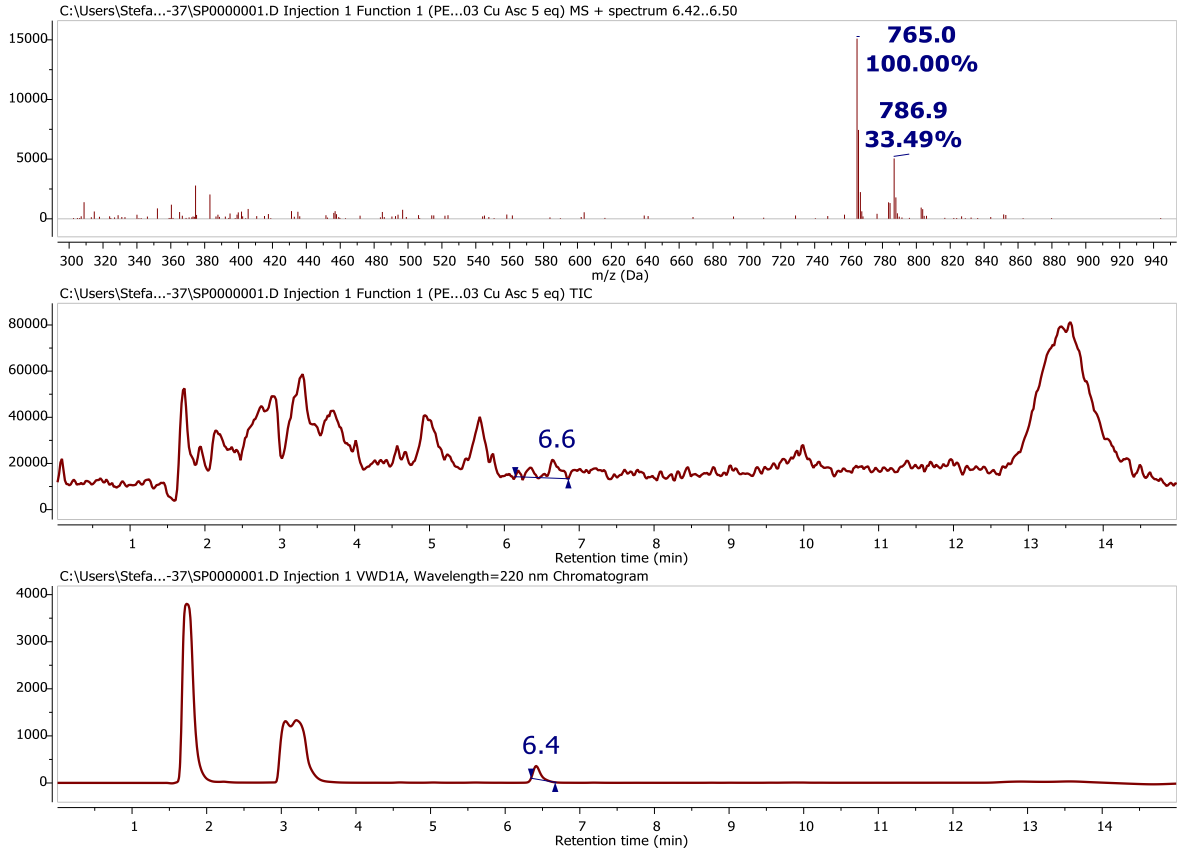
C:\Users\Stefa...-37\SP0000001.D Injection 1 Function 1 (PE...03 Cu Asc 5 eq) MS + spectrum 6.42..6.50
765.0
100.00%
786.9
33.49%
m/z (Da)
C:\Users\Stefa...-37\SP0000001.D Injection 1 Function 1 (PE...03 Cu Asc 5 eq) TIC
6.6
Retention time (min)
C:\Users\Stefa...-37\SP0000001.D Injection 1 VWD1A, Wavelength=220 nm Chromatogram
6.4
Retention time (min)

P3-6

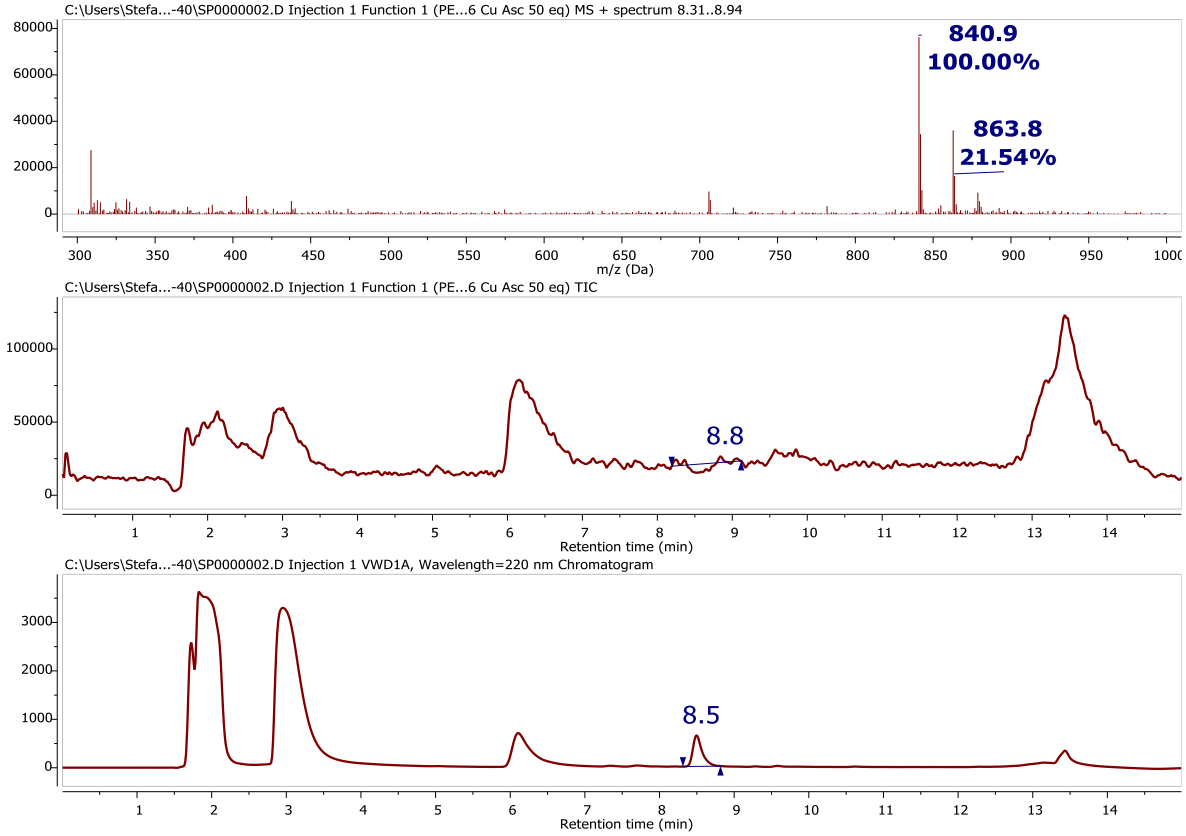
C:\Users\Stefa...-40\SP0000002.D Injection 1 Function 1 (PE...6 Cu Asc 50 eq) MS + spectrum 8.31..8.94
840.9
100.00%
863.8
21.54%
m/z (Da)
C:\Users\Stefa...-40\SP0000002.D Injection 1 Function 1 (PE...6 Cu Asc 50 eq) TIC
8.8
Retention time (min)
C:\Users\Stefa...-40\SP0000002.D Injection 1 VWD1A, Wavelength=220 nm Chromatogram
8.5
Retention time (min)

Primers

Id.	Sequence (5' - 3')	library	Peptide sequence
A211	GGAAGAAGGTGTTCAATTGGACAAGAGAGAAGCTTGTNNKNNKNNKNNKNNKNNKNNKTGTTCCGGTGGTGGTGGCTCTGGTGG	LB1	ACX_7C
A212	GGAAGAAGGTGTTCAATTGGACAAGAGAGAAGCTTGTNNKTAGNNKNNKNNKNNKNNKTGTTCCGGTGGTGGTGGCTCTGGTGG	LB2	$ACXZX_5C$
A205	GGAAGAAGGTGTTCAATTGGACAAGAGAGAAGCTTGTNNKNNKNNKTAGNNKNNKNNKTGTGGTGGTGGTGGCTCTGGTGG	LB3	ACX_3ZX_3C
A213	GGAAGAAGGTGTTCAATTGGACAAGAGAGAAGCTTGTNNKNNKNNKNNKTAGNNKTGTTCCGGTGGTGGTGGCTCTGGTGG	LB4	ACX_5ZXC
A214	GGAAGAAGGTGTTCAATTGGACAAGAGAGAAGCTTAGGGTTGTNNKNNKNNKNNKNNKNNKNNKTGTTCCGGTGGTGGTGGCTCTGGTGG	LB5	$AZGCX_7C$
A215	GGAAGAAGGTGTTCAATTGGACAAGAGAGAAGCTTGTNNKNNKNNKNNKNNKNNKNNKNNKTGTTCCGGTGGTGGTGGCTCTGGTGG	LB6	ACX_9C
A266	GGAAGAAGGTGTTCAATTGGACAAGAGAGAAGCTTGTNNKNNKNNKTGTNNKNNKNNKNNKNNKNNKNNKNNKNNKTGTTCCGGTGGTGGTGGCTCTGGTGG	LB13	ACX_3CX_9C
A267	GGAAGAAGGTGTTCAATTGGACAAGAGAGAAGCTTGTNNKNNKNNKNNKNNKTGTNNKNNKNNKNNKNNKNNKNNKTGTTCCGGTGGTGGTGGCTCTGGTGG	LB14	AC_6C_6C
A268	GGAAGAAGGTGTTCAATTGGACAAGAGAGAAGCTTGTNNKNNKNNKNNKNNKNNKNNKNNKTGTNNKNNKNNKTGTTCCGGTGGTGGTGGCTCTGGTGG	LB15	ACX_9CX_3C

Acknowledgements

First, I would like to thank my academic and industrial supervisors for the opportunity to pursue this research project in an independent and exciting environment. Thank you for the willingness and dedication during this scientific and complicated pathway. I am also grateful for the hospitality during the fruitful experience in the EPFL faculty. University of Ca' Foscari has been instrumental in making my PhD a possibility. I would also like to extend my limitless appreciation for the support I received from my group members. Finally, a special tribute is dedicated to my family for the boundless love and support.